ABSTRACT

Title of dissertation: QUASIPARTICLES IN SUPERFLUIDS AND SUPERCONDUCTORS

Jonathan B. Curtis,
Doctor of Philosophy, 2020

Dissertation directed by: Professor Victor M. Galitski
Department of Physics

Quasiparticle descriptions are a powerful tool in condensed matter physics as they provide an analytical treatment of interacting systems. In this thesis we will apply this tool to theoretically describe two systems: a superconductor interacting with cavity photons and a flowing Bose-Einstein condensate forming a sonic black hole.

First we will consider a two-dimensional s-wave BCS superconductor coupled to microwave cavity photons. We show how a nonequilibrium occupation of the photons can induce a nonequilibrium distribution of superconductor Bogoliubov quasiparticles, yielding an enhancement of the superconducting gap. The analytic dependence of this enhancement is provided in terms of the photon spectral and occupation functions, offering a large parameter space over which enhancement exists.

Next, we analyze the equilibrium properties of a similar superconductor-cavity structure which has strong sub-dominant d-wave pairing interaction. In this case there is a collective mode known as the Bardasis-Schrieffer mode, which is essentially an uncondensed d-wave Cooper pair. We show that by driving an external

supercurrent through the sample the Bardasis-Schrieffer mode can be hybridized with cavity photons, forming exotic Bardasis-Schrieffer-polaritons.

We then turn to consider a flowing Bose-Einstein condensate. In the presence of inhomogeneous flow, the long-wavelength motion of quasiparticles can be mapped onto the kinematics of matter fields in a curved spacetime. This mapping allows for the simulation of a black hole and its interactions with quantum fields via analogy. We show that in the case of a step-like jump in the condensate flow the emission of analogue Hawking radiation is accompanied by evanescent modes which are pinned to the event horizon.

Finally, we generalize this setup to include pseudo-spin half spinor Bose condensates. In this case, we show that the analogue spacetime the quasiparticles experience can be of the exotic Newton-Cartan type. Newton-Cartan gravity – the geometric formulation of Newtonian gravity – is realized when the Goldstone mode disperses quadratically as opposed to linearly. The nature of the analogue spacetime is controlled by the presence or absence of an easy-axis anisotropy in the boson spin-exchange interaction. We conclude by arguing that this Newton-Cartan spacetime can be experimentally realized in current platforms.

QUASIPARTICLES IN SUPERFLUIDS AND SUPERCONDUCTORS

by

Jonathan Bernard Curtis

Dissertation submitted to the Faculty of the Graduate School of the
University of Maryland, College Park in partial fulfillment
of the requirements for the degree of
Doctor of Philosophy
2020

Advisory Committee:
Professor Victor M. Galitski: Chair
Professor Gretchen Campbell
Professor Alexey Gorshkov
Professor Mohammad Hafezi
Professor Jay Deep Sau

Dedication

To my Mom and Dad.

Acknowledgements

There are many more people I would like to acknowledge than space is available, so I will attempt to make this brief.

I would like to begin by thanking my advisor, Victor Galitski, who has not only been an exemplary graduate student advisor, but an excellent physicist and a pleasure to work with. I am especially appreciative of his unwavering support, guidance, and respect.

I would also like to thank Prof. Alexey Gorshkov, who has essentially served as a second advisory and has taught me a great deal, as well as brighten many otherwise lengthy meetings with his enthusiasm. Similarly, I am indebted to Prof. Mohammad Hafezi, from whom I have learned a lot and had many wonderful discussions. Gil Refael, Mohammad Maghrebi, Michael Foss-Feig, Igor Boettcher, Yunxiang Liao, Andrey Grankin, and Colin Rylands also deserve recognition for all of their help and guidance over the years.

Next, I would like to acknowledge my colleagues, especially Zachary Raines, Andrew Allocca, and Justin Wilson. Most, if not all, of the work in this thesis would not have been possible without their help and guidance and I am lucky that they have all been such a pleasure to work with. Tibor Rakovszky, Étienne Lantagne-Hurtubise, Chaitanya Murthy, David Aasen, Steven Torrisi, Hilary Hurst, Aydin Cem Keser, Jeremy Young, Minh Tran, and Andrew Guo also deserve special recognition for their stimulating discussions and friendships.

I would especially like to thank all of my amazing friends who have made my graduate school life about much more than simply physics. Chris Flower, Ananya Sitaram, Noor Shah, Kristin Neil, Jaron Shrock, Kevin Palm, and Nour El Husseini—you have all made my graduate school tenure worth the struggle.

Finally, I cannot thank my family enough. To my parents—I am forever grateful for your love, support, and guidance. From fostering my interest in science at an

early age, to helping me hone my communication and discussion skills, this thesis would not have been possible without all the things you have taught me. To my brother, thank you for being my oldest friend and always inspiring me with your own accomplishments. To my grandparents, thank you for always looking after me and taking interest in my work, and providing me with excellent role-models.

Table of Contents

List of Tables

List of Figures

List of Abbreviations

2DEG 2-Dimensional Electron Gas

AdS Anti-de Sitter space

AMO Atomic, Molecular, and Optical

BCS Bardeen-Cooper-Schrieffer

BdG Bogoliubov-de Gennes

BEC Bose-Einstein-Condensate

BS Bardasis-Schrieffer

CFT Conformal Field Theory

DOS Density of States

FGR Fermi's Golden Rule

GPE Gross-Pitaevskii Equation

NC Newton-Cartan

RPA Random Phase Approximation

List of Publications

This dissertation is based on the following publications

1. J. B. Curtis, Z. M. Raines, A. A. Allocca, M. Hafezi, and V. M. Galitski, "Cavity Quantum Eliashberg Enhancement of Superconductivity", Phys. Rev. Lett. **122**, 167002 (2019), arXiv:1805.01482

2. A. A. Allocca, Z. M. Raines, J. B. Curtis, and V. M. Galitski, "Cavity superconductor-polaritons", Phys. Rev. B **99**, 020504 (2019), arXiv:arXiv:1807.06601v1

3. J. Curtis, G. Refael, and V. Galitski, "Evanescent modes and step-like acoustic black holes", Ann. Phys. **407**, 148–165 (2019), arXiv:1801.01607

4. J. H. Wilson, J. B. Curtis, and V. M. Galitski, *Analogue spacetimes from nonrelativistic Goldstone modes in spinor condensates*, Jan. 2020, arXiv:2001.05496 [quant-gas]

Chapter 1: Introduction

The concept of a quasiparticle is ubiquitous in condensed matter and Atomic, Molecular, and Optical (AMO) physics, owing to its great success in allowing for the treatment of interacting quantum systems. Indeed, many of the phenomena which arise in quantum many-body systems can be explained by invoking a quasiparticle description. This includes such varied examples as Bloch band-theory, Landau-Fermi liquid theory [1], spin-wave descriptions of magnetic order [2], the BCS theory of superconductivity [3], and the Bogoliubov theory of a weakly interacting Bose-Einstein-Condensate (BEC) [1]. Each of these topics, taken on their own, are the subjects of numerous books and research tomes and this thesis is not intended to be a comprehensive authority on any of these phenomena. Nor is it the aim of this thesis to provide an in-depth survey of the foundations of quasiparticle theory or study its (often fascinating) limitations. Rather, it is the aim of this thesis to propose a number of new phenomena in various systems in condensed matter which may be understood easily through a quasiparticle description—in some sense, attesting to the wide applicability and success of the quasiparticle picture.

As this thesis is particularly broad in scope, we will begin by introducing a few basic concepts underlying the systems we will theoretically study. In doing so, we will also introduce and formalise the idea of a quasiparticle and demonstrate how it may be employed to help understand the considered physical systems. Conceptually, this thesis may be roughly split in two, with Chapters 2 and 3 considering a superconductor-cavity microstructure and Chapters 4 and 5 focusing on Bose-Einstein condensed gases of ultra-cold atoms. While each chapter is roughly based on an independent, self-contained publication, we will provide a broad overview of background of each topic given the anticipated disparate audience this thesis is

intended for.

As the first two chapters cover material under the purview of the BCS theory of superconductivity, we will begin by introducing the fundamentals of conventional superconductivity. Then, as the third and fourth chapters focus on the Bogoliubov theory of Bose-Einstein condensates, we will briefly outline the basics of this subject before providing a more detailed treatment in the chapters themselves. Finally, as the subject of these two chapters is "analogue gravity" of BECs, we will introduce some introductory concepts from general relativity, with an emphasis on requiring as little mathematical technology as possible.

As far as conventions are concerned, this thesis will throughout set $\hbar = k_B = 1$ but in general we will retain c and ε_0 as unitfull parameters, unless specifically indicated. We will employ the Einstein summation convention, unless otherwise indicated, and reserve Latin indices (e.g. j, k, l, m) for spatial dimensions while Greek indices (e.g. μ, ν, α, β) are reserved for spacetime. Boldface letters (e.g. $\mathbf{r}, \mathbf{x}, \mathbf{q}$) indicated spatial vectors while italic letters (e.g. r, y, q) will indicate spacetime vectors. For a Minkowski metric, we use the $(-,+,+,+)$ signature. In Fourier space, we use the convention that in d dimensional space

$$\sum_{\mathbf{k}} ... = \text{Vol} \int \frac{d^d k}{(2\pi)^d}$$

is an extensive, unitless sum over momenta, with Vol being the quantization volume in d dimensions. In the Matsubara formalism, we will use

$$\sum_{q} = \sum_{\mathbf{q}} \sum_{i\omega}$$

where the sum over Matsubara frequencies is of the appropriate parity (even for bosons and odd for fermions).

We begin by introducing the BCS theory of superconductivity.

1.1 BCS Theory of Superconductivity

In their pioneering work authors BCS laid out the microscopic mechanism behind conventional electron-phonon superconductivity [3]. This can be understood using the treatment of Bogoliubov and Valatin [1, 4, 5] which emphasizes the quasiparticle description over BCS's original variational calculation. As a simple model, one begins by considering an isotropic Fermi gas of electrons which experience an overall attractive interaction between time-reversal partners [6, 7], presumably originating from exchange of virtual phonon. The Hamiltonian (in d spatial dimensions) can be written in the second-quantized notation as

$$H_{BCS} = \int d^d r \left[\sum_\sigma \hat{\Psi}^\dagger_\sigma(\mathbf{r}) \left(-\frac{\nabla^2}{2m} - E_F \right) \hat{\Psi}_\sigma(\mathbf{r}) - g \hat{\Psi}^\dagger_\uparrow(\mathbf{r}) \hat{\Psi}^\dagger_\downarrow(\mathbf{r}) \hat{\Psi}_\downarrow(\mathbf{r}) \hat{\Psi}_\uparrow(\mathbf{r}) \right]. \tag{1.1}$$

In the second-quantized notation, we indicate the electron field operator $\hat{\Psi}_\sigma(\mathbf{r})$ by a hat, which acts on the many-body wavefunction to annihilate an electron from the system at location $\mathbf{r}$ with spin quantum number σ along the quantization axis. In this simple model, the electrons are taken to have quadratic dispersion with mass m and Fermi energy E_F. The constant $g > 0$ is the attractive BCS interaction constant and here we assume a local interaction between electrons in the singlet channel.

In order to obtain superconductivity, we perform mean-field theory by looking for an order parameter

$$\Delta(\mathbf{r}) = -g \langle \Psi_\downarrow(\mathbf{r}) \Psi_\uparrow(\mathbf{r}) \rangle. \tag{1.2}$$

If this order parameter is non-zero the $U(1)$ global symmetry associated to the conservation of electron number has been spontaneously broken, which characterizes the onset of superconductivity[1] We assume the ground state is characterized by a

[1]Technically, in the presence of a gauged symmetry, as is the case for electrons in a metal, all of these statements require modification, but in the basic mean-field treatment this is a satisfactory stance to take [8–11]. In the case of ultrasmall granular superconductivity, where charge quantization becomes important there are also interesting subtleties [12].

homogeneous order parameter $\Delta(\mathbf{r}) = \Delta$, in which case the mean-field Hamiltonian can be written in real space as

$$H = \int d^d r \left[\sum_\sigma \hat{\Psi}^\dagger_\sigma(\mathbf{r}) \left(-\frac{\nabla^2}{2m} - E_F \right) \hat{\Psi}_\sigma(\mathbf{r}) + \overline{\Delta} \hat{\Psi}_\downarrow(\mathbf{r}) \hat{\Psi}_\uparrow(\mathbf{r}) + \hat{\Psi}^\dagger_\uparrow(\mathbf{r}) \hat{\Psi}^\dagger_\downarrow(\mathbf{r}) \Delta \right]. \tag{1.3}$$

The last two terms describe the interactions of electrons with the "condensate" of Cooper pairs, and allow for the apparent creation and annihilation of electrons in pairs (in reality they are transferring to and from the condensate).

This Hamiltonian is translationally invariant and can be diagonalized in momentum space. In this case it reads

$$H_{\mathrm{BdG}} = \sum_{\mathbf{k}} \sum_\sigma c^\dagger_{\mathbf{k}\sigma} \xi_{\mathbf{k}} c_{\mathbf{k}\sigma} + \overline{\Delta} c_{-\mathbf{k}\downarrow} c_{\mathbf{k}\uparrow} + \Delta c^\dagger_{\mathbf{k}\uparrow} c^\dagger_{-\mathbf{k}\downarrow}, \tag{1.4}$$

where $\xi_{\mathbf{k}} = \frac{\mathbf{k}^2}{2m} - E_F$ is the normal-state electron dispersion relation. This Hamiltonian is solved by means of a Bogoliubov transformation, which is a linear canonical transformation of the fermion operators [1, 4, 5]. We write

$$c_{\mathbf{k}\uparrow} = u_{\mathbf{k}} \gamma_{\mathbf{k},+} + v_{\mathbf{k}} \gamma^\dagger_{-\mathbf{k},-} \tag{1.5a}$$

$$c^\dagger_{-\mathbf{k}\downarrow} = u^*_{-\mathbf{k}} \gamma^\dagger_{-\mathbf{k},+} + v^*_{-\mathbf{k}} \gamma_{\mathbf{k},-}, \tag{1.5b}$$

with $\gamma_{\mathbf{k}\alpha}$ a new set of fermion operators which are indexed by a species quantum number $\alpha = \pm$. Just as the electron operators obey canonical anti-commutation relations, so too do the Bogoliubov quasiparticle operators γ. This imposes a constraint on the coefficients u and v, requiring

$$|u_{\mathbf{k}}|^2 + |v_{\mathbf{k}}|^2 = 1. \tag{1.6}$$

One may view the quasiparticles described by the γ's as a coherent superposition

of electrons and holes. We choose the Bogoliubov coefficients u, v so as to bring the mean-field Hamiltonian to a diagonal form

$$H_{\mathrm{BdG}} = \sum_{\mathbf{k},\alpha} E_{\mathbf{k}} \gamma^{\dagger}_{\mathbf{k},\alpha} \gamma_{\mathbf{k},\alpha} \tag{1.7}$$

with the famous gapped dispersion relation for the quasiparticles of

$$E_{\mathbf{k}} = \sqrt{\xi^2_{\mathbf{k}} + |\Delta|^2}. \tag{1.8}$$

The coefficients u, v can be obtained with some effort and enter in to the calculation of various matrix elements as "coherence factors," which will be required when expressing the electron observables (e.g. charge density, current) in terms of the quasiparticles γ.

Alternatively, one can envision the Bogoliubov-de Gennes (BdG) Hamiltonian (1.4) as describing a collection of two-level pseudo-spin systems, one for each momentum $\mathbf{k}$ [13]. The precise mapping is

$$\hat{S}^z_{\mathbf{k}} = \tfrac{1}{2}\left[c^{\dagger}_{\mathbf{k}\uparrow} c_{\mathbf{k}\uparrow} - c_{-\mathbf{k}\downarrow} c^{\dagger}_{-\mathbf{k}\downarrow}\right] \tag{1.9a}$$

$$\hat{S}^+_{\mathbf{k}} = c^{\dagger}_{\mathbf{k}\uparrow} c_{-\mathbf{k}\downarrow}. \tag{1.9b}$$

If the Kramers pair $(\mathbf{k}\uparrow, -\mathbf{k}\downarrow)$ is occupied then the pseudo-spin for $\mathbf{k}$ is $+\frac{1}{2}$, and if it is empty it is $-\frac{1}{2}$. A superposition of the pair being filled and empty corresponds to a non-zero $\langle \hat{S}^+_{\mathbf{k}} \rangle$, which may be interpreted as the BCS Cooper pair condensate in momentum space. The BdG Hamiltonian (1.4) then becomes

$$H_{\mathrm{BdG}} = \sum_{\mathbf{k}} 2\xi_{\mathbf{k}} \hat{S}^z_{\mathbf{k}} + \Delta \hat{S}^+_{\mathbf{k}} + \bar{\Delta} \hat{S}^-_{\mathbf{k}}$$

which describes a system of pseudo-spins precessing in an effective magnetic field

$\mathbf{B}_\mathbf{k} = (2\xi_\mathbf{k}, \Re\Delta, -\Im\Delta)$. In the disordered phase, $\Delta = 0$ and the stationary states correspond to the pseudo-spins aligning with the z axis, corresponding to a filled Fermi sea. In the ordered phase, $\Delta \neq 0$ and the stationary states require the pseudo-spins to align along the direction of the effective magnetic field, which in general points in a different direction everywhere in momentum space.

The final ingredient in the BCS theory is the self-consistency, or "gap" equation. This ensures that the Δ we use to compute the quasiparticle spectrum indeed satisfies the original definition $\Delta = -g\langle\hat{\Psi}_\downarrow(\mathbf{r})\hat{\Psi}_\uparrow(\mathbf{r})\rangle$. We choose the equilibrium ensemble which implies the density matrix is $\hat{\rho} \propto \exp(-\beta H)$. Thus, the Bogoliubov quasiparticles are distributed according to the Fermi-Dirac occupation function. If we express the order parameter in terms of the Bogoliubov quasiparticles, we obtain the condition

$$\Delta = -\frac{g}{2}\int \frac{d^d k}{(2\pi)^d}\frac{1-2n_F(E_\mathbf{k})}{E_\mathbf{k}}\Delta. \tag{1.10}$$

This always has $\Delta = 0$ as a trivial solution. Below a certain critical temperature, T_c this develops another non-trivial solution (which can be verified to have lower free-energy). This can be manipulated into the simple form

$$\frac{1}{g\nu_F} = \int_\Delta^{\Omega_D} \frac{dE}{\sqrt{E^2-\Delta^2}}(1-2n(E)) \tag{1.11}$$

where ν_F is the density of states at the Fermi level, and Ω_D is the Debye-frequency cutoff on pairing[2]. Here $n(E)$ is the occupation function of the Bogoliubov quasiparticles. The first work of this thesis essentially demonstrates how one can specially tailor the fluctuations of an electromagnetic resonator in order to manipulate the occupation function $n(E)$ away from the equilibrium Fermi-Dirac form and obtain a more favorable solution of Eq. (1.11). This ultimately arises from the fact that in the

[2]More appropriately, in the weak-coupling regime that BCS theory resides in, this acts as a cutoff in momentum space on the attractive part of the effective interaction. However, in the strong-coupling Migdal-Eliashberg framework, this in fact acts as a cutoff in frequency space, which reduces to the momentum space cutoff in the weak-coupling limit [14, 15].

gap equation (1.11), the most detrimental effect on the gap comes from quasiparticle which reside near $E \sim \Delta$, where the density of states is singular. This is shown in Fig. 1.1, which plots the energy dependent Density of States (DOS) around the Fermi level in both the normal state and the superconducting state. Reducing the number of quasiparticles which reside near $E = \Delta$ is therefore the objective to bear in mind when trying to tailor a nonequilibrium occupation function.

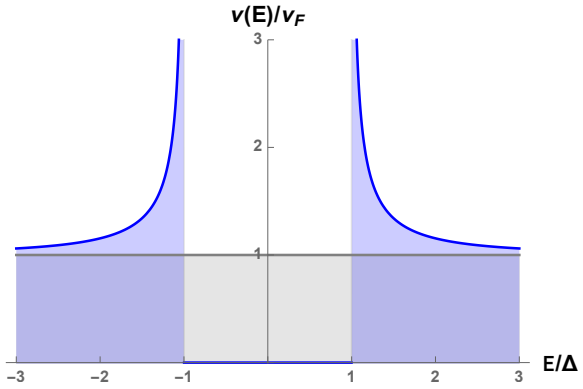

Figure 1.1: Density of states $\nu(E)/\nu_F$ near the Fermi level ($E = 0$) in the normal state (gray curve) and in the BCS superconducting state (blue curve). We see clearly the emergence of a gap and accompanying divergence at $|E| = \Delta$.

1.1.1 Multiple Pairing Channels

The model we have used here qualitatively captures many aspects of BCS superconductors correctly, but in general a more nuanced treatment is required. One such refinement is the inclusion of multiple different pairing channels for the electrons. To see how this is incorporated, we return to the original BCS Hamiltonian (1.1) and focus on the interaction part. In general, the spin-singlet attractive interaction can be written in momentum space as

$$H_{\text{int}} = \sum_{\mathbf{q},\mathbf{k},\mathbf{k}'} c^{\dagger}_{\mathbf{k}'+\frac{1}{2}\mathbf{q},\uparrow} c^{\dagger}_{-\mathbf{k}'+\frac{1}{2}\mathbf{q},\downarrow} V(\mathbf{k},\mathbf{k}';\mathbf{q}) c_{-\mathbf{k}+\frac{1}{2}\mathbf{q},\downarrow} c_{\mathbf{k}+\frac{1}{2}\mathbf{q},\uparrow}. \tag{1.12}$$

In practice, the matrix elements of the interaction $V(\mathbf{k}, \mathbf{k}'; \mathbf{q})$ can be approximated as independent of the total center-of-mass momentum $\mathbf{q}$ of the pair, so that $V(\mathbf{k}, \mathbf{k}'; \mathbf{q}) = V(\mathbf{k}, \mathbf{k}')$. Furthermore, if the interaction between electrons is of the density-density type, then this only depends on the relative momentum exchanged $\mathbf{k} - \mathbf{k}'$. In practice, the interaction is not purely density-density since the phonon interaction matrix elements $M_{\mathbf{p},\mathbf{p}'}$ may depend on both the momenta. Thus, the interaction can in general depend on both relative momenta of each participating pair. We can expand then expand the interaction V in scattering channels depending on the symmetries of the problem and the relative interaction strengths. The lowest harmonic for a singlet-pairing (as we assume here) is the s-wave channel and this is often the dominant interaction. It produces the term $V(\mathbf{k}, \mathbf{k}') = -g_s$, which is simply the interaction we had before, expressed in momentum space.

More generally, we can expand the interaction $V(\mathbf{k}, \mathbf{k}')$ in terms of irreducible representations of the point-group symmetries of the model. In the case of full rotational symmetry, we can use the spherical harmonics to write

$$V(\mathbf{k}, \mathbf{k}') = \sum_{l=0}^{\infty} \sum_{m=-l}^{l} g_l Y_l^{m^*}(\hat{\mathbf{k}}) Y_l^m(\hat{\mathbf{k}}'),$$

expressed as a functions of the unit vectors $\hat{\mathbf{k}}, \hat{\mathbf{k}}'$. In practice, solids don't have the full $SO(3)$ rotational symmetry. Nevertheless, many materials still posses a discrete inversion symmetry. In this case, the next-lowest harmonic allowed (beyond the simple s-wave) should correspond to a remnant of the d-wave pairing channel. If we consider the generic pairing interaction $V(\mathbf{k}, \mathbf{k}')$ we will find a gap equation

$$\Delta_{\mathbf{k}} = -\int \frac{d^d k'}{(2\pi)^d} V(\mathbf{k}, \mathbf{k}') \frac{\Delta_{\mathbf{k}'}}{E_{\mathbf{k}'}} \left[1 - 2n_F(E_{\mathbf{k}'})\right]. \tag{1.13}$$

The solution to this is the gap $\Delta_{\mathbf{k}}$ which in all but the simplest cases is also dependent on the relative momentum $\mathbf{k}$. This in turn leads to a quasiparticle spectrum given

by

$$E_{\mathbf{k}} = \sqrt{\xi_{\mathbf{k}}^2 + |\Delta_{\mathbf{k}}|^2}. \tag{1.14}$$

The quasiparticle dispersion is depicted in Fig. 1.2 for the case of an s wave gap, as well as a $d_{x^2-y^2}$ gap. Notably, the $d_{x^2-y^2}$ gap exhibits nodes where the spectrum for Bogoliubov quasiparticles remains gapless.

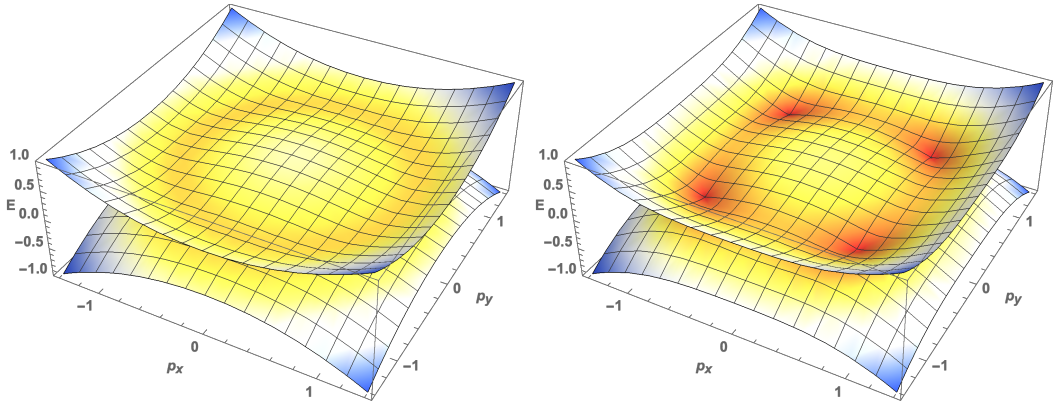

Figure 1.2: (Left) Bogoliubov quasiparticle dispersion relation for two-dimensional Fermi surface with an isotropic s-wave gap, with color indicating the size of the gap (red is smaller, and blue is larger). The two curves are showing the particle-hole symmetric dispersions for the two degenerate species of quasiparticle. (Right) The dispersion relation for the Bogoliubov quasiparticles in the presence of an anisotropic $d_{x^2-y^2}$ gap. We emphasize the four nodes located on the locus of the Fermi surface $\mathbf{p}^2 = p_F^2$ and the pairing nodes $p_x^2 - p_y^2 = 0$. At these points the gap goes to zero, as it must change sign in accordance with the d-wave form factor. All scales are exagerated for clarity.

In Chapter 3, we will consider the effects of competing pairing interactions in a two dimensional electron gas of the form, with the pairing interaction of the form

$$V(\mathbf{k}, \mathbf{k}') = -g_s - g_d 2\cos(2\theta_{\mathbf{k}})\cos(2\theta_{\mathbf{k}'}). \tag{1.15}$$

The first term is assumed to dominate, with an interaction strength $g_s \gg g_d$. The second term describes sub-dominant pairing fluctuations, in this case in the $d_{x^2-y^2}$ channel (because the problem is two-dimensional, the relevant harmonics are not the spherical harmonics but the polar harmonics, corresponding to irreps of $SO(2)$).

We will show how this additional d-wave term can produce higher-angular momentum bound states of Bogoliubov quasiparticles, essentially forming the analogue of excitons in a superconductor [16]. These uncondensed Cooper pairs are essentially precursors to the eventual formation of a d-wave superconductor, which emerges upon increasing the anisotropic pairing to the point where $g_d \gg g_s$. After introducing the Bardasis-Schrieffer mode, we will then show how the collective mode associated to these quasiparticles can be hybridized with photons in an enclosing microcavity, in analogy with exciton-polariton systems involving semiconductor excitons.

As mentioned before, Chapters 2 and 3 of this thesis concern BCS superconductivity, the salient aspects of which have been reviewed here. The remaining two chapters consider the dynamics of ultra-cold atoms which form a BEC. As such, we will review this subject in the next section.

1.2 Bose-Einstein Condensates

In many ways, the theory of Bose-Einstein condensates in ultra-cold atoms is like the BCS theory of superconductivity, but many matters simplify since the constituent degrees of freedom are themselves bosons, whereas in BCS theory they are still fermions. The "standard model" of Bose-Einstein condensation is the dilute Bogoliubov gas, which considers a weakly interacting gas of spinless bosons in d spatial dimensions. In the second quantized notation this is described by the Hamiltonian

$$H = \int d^d r \hat{\Phi}^\dagger(\mathbf{r}) \left[-\frac{\nabla^2}{2m} - \mu + \frac{1}{2} g \hat{\Phi}^\dagger(\mathbf{r}) \hat{\Phi}(\mathbf{r}) \right] \hat{\Phi}(\mathbf{r}) \tag{1.16}$$

with an s-wave density-density interaction of strength $g > 0$. The operator $\hat{\Phi}(\mathbf{r})$ annihilates a spinless boson from location $\mathbf{r}$. Unlike fermions, which have to con-

dense in pairs, bosons can condense individually. This is characterized by an order parameter

$$\phi_0(\mathbf{r}, t) = \langle \hat{\Phi}(\mathbf{r}, t) \rangle \tag{1.17}$$

which, when it is non-zero, spontaneously breaks the $U(1)$ symmetry generated by boson number conservation.

From the full Hamiltonian we can derive Heisenberg equations of motion for the boson field operator $\hat{\Phi}$, which reads

$$\left[i\partial_t + \frac{1}{2m}\nabla^2 + \mu \right] \hat{\Phi}(\mathbf{r}, t) = g\hat{\Phi}^\dagger(\mathbf{r}, t)\hat{\Phi}(\mathbf{r}, t)\hat{\Phi}(\mathbf{r}, t). \tag{1.18}$$

In the simplest approximation, we simply replace the operator $\hat{\Phi}$ by its expectation value ϕ_0, which characterizes the dynamics of the condensate. One thus arrives at the time-dependent Gross-Pitaevskii Equation (GPE)

$$\left[i\partial_t + \frac{1}{2m}\nabla^2 + \mu - g|\phi_0|^2 \right] \phi_0(\mathbf{r}, t) = 0. \tag{1.19}$$

The simplest solution, in the absence of an external potential, is obtained by assuming a time-independent and homogeneous solution. In this case, this reduces to an algebraic equation

$$\left[\mu - g|\phi_0|^2 \right] \phi_0 = 0. \tag{1.20}$$

For $\mu < 0$ this only has a trivial solution of $\phi_0 = 0$ and there is no condensate. For $\mu > 0$ on the other hand, we find a non-trivial solution with $|\phi_0|^2 = \rho = \mu/g$, corresponding to a uniform condensate. This then spontaneously breaks the $U(1)$ symmetry, since only the amplitude is fixed by the saddle-point equation, while the phase remains arbitrary. Since there is a spontaneously broken continuous symmetry, we expect there to be a corresponding gapless Golstone mode, characterizing long-wavelength phase modulations.

To see the emergence of this mode, we must go beyond the saddle-point level. We expand the Hamiltonian around the saddle-point solution, writing

$$\hat{\Phi} = \sqrt{\frac{\mu}{g}} + \hat{\phi}$$

with $\hat{\phi}$ describing quantized fluctuations around the mean-field. Since we are expanding around the saddle-point, terms linear in $\hat{\phi}$ vanish. If we then truncate the expansion to quadratic order, we will obtain a theory of quasiparticles which can be solved exactly.[3]

We obtain the quasiparticle Hamiltonian

$$H^{(2)} = \int d^d r \left[\frac{1}{2m} \nabla \hat{\phi}^\dagger \cdot \nabla \hat{\phi} + g\rho \hat{\phi}^\dagger \hat{\phi} + \frac{1}{2} g\rho \hat{\phi}^\dagger \hat{\phi}^\dagger + \frac{1}{2} g\rho \hat{\phi} \hat{\phi} \right]. \tag{1.21}$$

We note the appearance of the off-diagonal terms $\hat{\phi}^2$ and its conjugate. These again describe the violation of the particle conservation in the presence of a condensate, as we saw for the case of electrons in BCS theory.

We write this in momentum space, with $\hat{\phi} = \sum_{\mathbf{p}} \frac{1}{\sqrt{\text{Vol}}} \hat{a}_{\mathbf{p}} e^{i\mathbf{p}\cdot\mathbf{r}}$. This produces

$$H^{(2)} = \sum_{\mathbf{p}} \hat{a}^\dagger_{\mathbf{p}} \left(\frac{\mathbf{p^2}}{2m} + g\rho \right) \hat{a}_{\mathbf{p}} + \frac{1}{2} g\rho \hat{a}_{\mathbf{p}} \hat{a}_{-\mathbf{p}} + \frac{1}{2} g\rho \hat{a}^\dagger_{\mathbf{p}} \hat{a}^\dagger_{-\mathbf{p}}. \tag{1.22}$$

We again can diagonalize this via a Bogoliubov transformation

$$\hat{a}_{\mathbf{p}} = u_{\mathbf{p}} \hat{b}_{\mathbf{p}} + v_{\mathbf{p}} \hat{b}^\dagger_{-\mathbf{p}}. \tag{1.23}$$

Unlike the BCS case, which had two independent spin species, there is only one species of boson here, so we only need one transformation. More importantly, unlike fermions which obey canonical anti-commutation relations, bosons obey canonical

[3] This assumes that we can neglect interactions between quasiparticles, or at least treat them perturbatively. For bosons, we expect this to occur in the regime of low excitation density, hence the occasional description of this system as a **dilute Bogoliubov gas**.

commutation relations.[4] Thus, in order for the b operators to satisfy the same canonical relations, we must have the coefficients satisfy

$$|u_{\mathbf{p}}|^2 - |v_{\mathbf{p}}|^2 = 1. \tag{1.24}$$

This seemingly innocuous alteration can in fact have dramatic consequences, some of which we will explore later in later chapters. For the problem at hand, we can see that (after some tedious algebra), the Hamiltonian is brought to the diagonal form $H^{(2)} = \sum_{\mathbf{p}} E_{\mathbf{p}} \hat{b}^\dagger_{\mathbf{p}} \hat{b}_{\mathbf{p}}$ with excitation spectrum

$$E_{\mathbf{p}} = \sqrt{\left(\frac{\mathbf{p^2}}{2m} + g\rho\right)^2 - (g\rho)^2} \sim \sqrt{\frac{g\rho}{m}}|\mathbf{p}|, \tag{1.25}$$

with the last equality holding in the long-wavelength expansion. In that case, we see the quasiparticles are in fact describing sound waves which propagate with a speed of sound $c = \sqrt{\frac{g\rho}{m}}$. Thus, through Bogoliubov analysis we have recovered the Goldstone mode.

In Chapter 4 we will examine the case of a spatially-varying mean-field $\phi_0(x)$. This is motivated by the observation, initially due to W.G. Unruh [17], that in some cases the response of quantized sound waves in a flowing (i.e. spatially varying) condensate can be mapped on to the propagation of light rays through an analogue curved spacetime. Even more surprising perhaps, is that it is theoretically possibly to engineer a condensate profile which exhibits an apparent event horizon in the analogue metric. This then allows for the possibility of simulating the kinematics of quantum fields in curved spacetime through laboratory scale experiments on ultra-cold atomic gases. We will now briefly delve into the background of the analogue

[4] While it is beyond the scope of this thesis, this simple fact has very interesting consequences on the eigenvalue structure of bosonic systems which exhibit "pairing" terms $\sim \hat{a}\hat{a},\ \hat{a}^\dagger\hat{a}^\dagger$. In the case of fermions these terms lead to level-repulsion in the Bogoliubov-de Gennes spectrum and formation of superconducting gaps, while for bosons they can lead to level-attraction and dynamical instabilities. See Chapter 4 for a slightly more in depth discussion.

gravity construction for BECs [18–20].

1.2.1 Analogue Gravity in Bose-Einstein Condensates

To see at a simple level how this works, we rewrite the GPE in the Madelung representation, with

$$\phi_0(x) = \sqrt{\rho(x)} e^{i\Theta(x)}. \tag{1.26}$$

We then separate out the real and imaginary parts, obtaining the continuity equation and Bernoulli equation, respectively

$$\frac{\partial \rho}{\partial t} + \nabla \cdot (\rho \mathbf{v}) = 0 \tag{1.27a}$$

$$-\frac{\partial \Theta}{\partial t} + \mu - g\rho(x) - \frac{1}{2} m \mathbf{v}^2 + \frac{1}{2m\sqrt{\rho}} \nabla^2 \sqrt{\rho} = 0. \tag{1.27b}$$

Here we have introduced the velocity field

$$\mathbf{v} = \frac{1}{m} \nabla \Theta. \tag{1.28}$$

In the absence of vorticity, this is incompressible, obeying $\nabla \cdot \mathbf{v} = 0$ and the continuity equation can be rewritten as the Euler equation

$$\left[\frac{\partial}{\partial t} + \mathbf{v} \cdot \nabla \right] \rho = 0. \tag{1.29}$$

Now, consider a slowly varying solution to these equations $\rho_0(x)$ and $\mathbf{v}_0(x) = \frac{1}{m} \nabla \Theta_0$. We then study the behavior of small perturbations around this solution [20–22], writing $\rho = \rho_0 + \delta\rho$ and $\Theta = \Theta_0 + \delta\Theta$. Linearizing these equations in the

perturbations produces two coupled first-order equations

$$\left[\frac{\partial}{\partial t} + \mathbf{v}_0 \cdot \nabla\right] \delta\rho + \frac{(\nabla\rho_0)}{m} \cdot \nabla\delta\Theta = 0 \tag{1.30a}$$

$$\left[\frac{\partial}{\partial t} + \mathbf{v}_0 \cdot \nabla\right] \delta\Theta + g\delta\rho = 0. \tag{1.30b}$$

where we have used the fact that the velocity field (in the absence of vortices) is incompressible and dropped the "quantum pressure" term $\propto \frac{\nabla^2\sqrt{\rho}}{\sqrt{\rho}}$ from the Bernoulli equation. These can be combined in to one second order wave equation for the phase fluctuations

$$\left[(\partial_t + \mathbf{v}_0 \cdot \nabla)^2 - \nabla \cdot c^2\nabla\right] \delta\Theta = 0, \tag{1.31}$$

with the local speed of sound given by $c^2 = g\rho_0(x)/m$. We see that in the case of a stationary ($\mathbf{v}_0 = 0$) and homogeneous ($\nabla c^2 = 0$) medium, the phase fluctuations (phonons) obey the standard relativistic wave equation $\Box\delta\Theta = 0$ with $\Box = \partial_t^2 - c^2\nabla^2$ the usual d'Alembertian operator.

In the case of a non-trivial background, we instead find that this can be mapped on to a wave equation in **curved** spacetime, with form

$$\frac{1}{\sqrt{-g}}\partial_\mu\sqrt{-g}g^{\mu\nu}\partial_\nu\delta\Theta = 0. \tag{1.32}$$

We can read off the components of the inverse metric tensor, up to an overall constant factor. Inverting the matrix, we find the metric tensor is (again up to overall constant factor)

$$g_{\mu\nu}dx^\mu dx^\nu = -(1 - \frac{\mathbf{v}_0^2}{c^2})dt^2 + 2\frac{\mathbf{v}_0}{c^2} \cdot d\mathbf{x}dt + \frac{1}{c^2}d\mathbf{x}^2. \tag{1.33}$$

In the eikonal approximation, the quantized sound waves in the BEC will propagate

as particles along the null geodesics of the metric

$$ds^2 = g_{\mu\nu} dx^\mu dx^\nu = 0. \tag{1.34}$$

Unruh's insight was that, for certain flowing condensates the velocity field $\mathbf{v}_0$ and index of refraction c^2 can be chosen to simulate the metric tensor of a black hole.

The simplest type of black hole is the Schwarzschild black hole, which has mass M and no angular momentum or electric charge. Spacetime around the black hole (which in general relativity is essentially a point mass) is described using the Schwarzschild metric, which reads

$$d\tau^2 = \left(1 - \frac{2GM/c^2}{r}\right) dt^2 - \left(1 - \frac{2GM/c^2}{r}\right)^{-1} \frac{dr^2}{c^2} - \frac{r^2}{c^2} d\Omega^2. \tag{1.35}$$

Here G is Newton's gravitational constant and c is the speed of light, with $d\Omega$ the differential of solid area. In particular, there is an apparent coordinate singularity at $r = R_s = 2GM/c^2$, commonly known as the Schwarzschild radius. While it is known that there is no actual singularity in spacetime at this location (a coordinate transformation exists which renders it locally Minkowski), this does delineate the event horizon, which is a non-local causal partitioning of spacetime.

To see this, consider two points in the vicinity of the horizon, one at r and one at $r + dr$. The proper time interval separating these two points, when the observer time is zero (so that an observer at spatial infinity judges the two events to be simultaneous) is given by

$$d\tau^2 = -\frac{r}{r - R_s} \frac{dr^2}{c^2}. \tag{1.36}$$

This changes sign at the horizon. For two points which are both outside of the horizon this is negative, indicating the two events are space=like separated, as one would expect. On the other hand, for two points on the interior, this is is

positive, indicating a time-like separation. This signifies that the causality requires trajectories on the interior of the horizon eventually flow towards the singularity at $r = 0$.

Classically, black holes only ever increase in size as they consume in falling matter[5]. Remarkably, Hawking showed [24, 25] that this is not necessarily true once one considers the quantum nature of matter. In the presence of quantum fields, a black hole emits Hawking radiation, which is observed by a distant observer as a featureless, outgoing flux of particles distributed according to the thermal distribution. The temperature of the radiation is set by the black hole's mass via the famous Hawking relation

$$T_H = \frac{c^3}{8\pi GM} = \frac{c}{4\pi R_s}. \tag{1.37}$$

While the theoretical basis for this result is relatively sound, it leads to the striking prediction that black holes will eventually radiate their mass away via black body radiation, and evaporate (or perhaps explode, as Hawking suggested in his original manuscript title). Estimates of the Hawking temperature for any astrophysical black hole yield astronomically small numbers, far smaller than the temperature of the cosmic microwave-backgroun radiation. It is in this context that we turn our attention to analogue gravity models. In 1981 W.G. Unruh [17] showed that quantum sound waves in a flowing fluid can be made to propagate as if they were in the spacetime of a Schwarzschild black hole, via the argument we outlined culminating in Eq. (1.31). The exact same principles which lead to Hawking radiation apply to these systems and following this line of reasoning, Unruh predicted that one can engineer an analogue event horizon by producing a fluid flow which breaks the sound barrier in the system. The quantized sound waves will then

[5]This connects to the so-called "second-law" of black hole thermodynamics, which draws an analogy between the surface area of a black hole $A = 4\pi R_s^2 \propto M^2$ and the entropy of a closed system, S both of which may never decrease (classically) [23].

be emitted by the Hawking mechanism and will be thermally distributed with an analogue temperature given by

$$T = \frac{1}{2\pi}\left|\frac{\partial v}{\partial r}\right|_{r_h} \tag{1.38}$$

assuming the velocity field of the fluid $\mathbf{v}$ is spherically symmetric and passes the local speed of sound at the event horizon radius r_h.

In Chap. 4, we investigate corrections to the analogue gravity description due to the non-linear Bogoliubov dispersion relation

$$\omega(\mathbf{k}) = \sqrt{c^2\mathbf{k}^2 + (\mathbf{k}^2/2m)^2}. \tag{1.39}$$

At a characteristic momentum scale of $k_c = mc = \sqrt{mgp}$ the apparent Lorentz invariance, which lead to the effective curved space decsription in terms of Eq. (1.31), is lost. We show one consequence of this is the emergence of evanescent modes, which decay exponentially out of the event horizon and describe a finite depth tunneling of states out from the black hole. Heuristically, this is because the dispersion relation (1.39) is quartic in $\mathbf{k}$. Thus, in determining the solutions to a scattering problem, we are tasked with solving for the allowed $\mathbf{k}$ at a given frequency ω. This becomes an algebraic root-finding problem and since Eq. (1.39) is a quartic polynomial in k, there are four roots over the whole complex plane. One of these is exponentially growing and not permissible by boundary conditions, but the other is evanescent and in general will therefore enter in to the S-matrix for the problem, which is what we emphasize in Chapter 4.

In Chapter 5 we will generalize the treatment above by introducing an internal pseudo-spin degree of freedom. It turns out that the physics becomes much richer when we investigate the analogue gravity of spinor condensates.

1.2.2 Analogue Newton-Cartan geometry

Generically, one might expect the above analogue gravity picture to apply to any Goldstone mode, which will respond to long-wavelength variations in the speed of sound and Doppler shifts in the same way as the Bogoliubov sound mode does in the flowing BEC. However, it turns out this is only the case for so-called "Type I" Goldstone modes, which have dispersion relations of the form $\omega^2 \sim c^2|\mathbf{k}|^2$. In particle physics, Lorentz invariance ensures that this is the only type of Goldstone mode, but in condensed matter physics there are also the "Type II" Goldstone modes [26, 27], which exhibit dispersion relations like $\omega \sim \mathbf{k}^2$. While each Type I Goldstone mode has a one-to-one correspondence with a broken generator of the Lie algebra, each Type-II Goldstone mode corresponds to **two** broken generators, which end up describing the same mode. In Chap. 5 we demonstrate how these modes may arise in more complicated flowing spinor BECs, and find that in the presence of long-wavelength variations in the background condensate, they also propagate in an analogue spacetime. In this case, the analogue spacetime is not like Einstein's theory of gravity, but instead it realizes the Newton-Cartan [28, 29] geometry which arises from gauging Galilean invariance.

Let us briefly outline the idea behind Newton-Cartan (NC) geometry. We start with an action describing a free gapless $U(1)$ charged scalar (Bose) field in a flat spacetime, as might describe the low-energy theory of magnons in a homogeneous ferromagnet.[6] The scalar field $\phi(x)$ is assumed to exhibit Galilean invariance [30], which leads to the action in $d+1$ spacetime dimensions

$$S_{\text{flat}} = \int d^{d+1}x \left(\tfrac{i}{2} \left[\bar{\phi}\partial_t\phi - (\partial_t\bar{\phi})\phi \right] - \tfrac{1}{2m}|\nabla\phi|^2 \right). \tag{1.40}$$

[6] In a Heisenberg ferromagnet, if the spin orders along the $\hat{z}$ axis, there are two modes of spin fluctuation, describing pertubations in the $\hat{x}$ and $\hat{y}$ directions. These two modes are in fact canonically conjugate, and combine together into a single $U(1)$ charged Goldstone mode. This is the essence of the Type-II mode we investigate further in Chapter 5.

We would like to promote this to a theory in the presence of a curved spacetime metric. This is accomplished by introducing the metric tensor $h^{\mu\nu}$, along with the clock one-form n_μ and the velocity field v^μ. These objects are not all independent but must obey the contraints

$$n_\mu h^{\mu\nu} = 0 \tag{1.41a}$$

$$n_\mu v^\mu = 1. \tag{1.41b}$$

Together, these objects make up the Newton-Cartan geometry, which may be interpreted as follows. In NC geometry, spacetime is foliated into spacelike surfaces which are described by the (degenerate) metric tensor $h^{\mu\nu}$, or technically its inverse (when restricted to the non-null directions). These spacelike surfaces are in fact one-forms determined by the clock one-form n_μ. If dx^μ is an infinitesimal displacement between two spacetime events, then $d\tau = n_\mu dx^\mu$ serves as an invariant notion of the elapsed time. The flow of time is essentially determined to be normal to the spacelike surfaces and is locally generated by the velocity vector field v^μ. We therefore see that the causal structure of Newton-Cartan geometry is very different than that of the Einsteinian relativity, and is closer to our naïve notion of "absolute time."

We can use these objects to upgrade the field theory action S_{flat} to the curved space action

$$S_{\text{curved}} = \int d^{d+1}x\sqrt{-g}\left(\tfrac{i}{2}\left[\bar{\phi}v^\mu\partial_\mu\phi - (v^\mu\partial_\mu\bar{\phi})\phi\right] - \tfrac{1}{2m}h^{\mu\nu}\left(\partial_\mu\bar{\phi}\right)\left(\partial_\nu\phi\right)\right). \tag{1.42}$$

Here the determinant $\sqrt{-g}$ is the determinant of the induced metric

$$g_{\mu\nu} = n_\mu n_\nu + h_{\mu\nu} \tag{1.43a}$$

$$h^\nu_\mu = \delta^\nu_\mu - v^\nu n_\mu. \tag{1.43b}$$

The second equation defines the inverse of the degenerate metric $h^{\mu\nu}$ through its projection onto the spacelike hyper-surfaces. The curved space action can then be used to study the behavior of quantum fluctuations in the presence of a non-trivial background metric. Additionally, variations with respect to the Newton-Cartan metric can be used to isolate the energy-current, momentum-density, and stress tensor (momentum current) of the non-relativistic field[7], in the spirit of Luttinger's method [31–34].

In Chap. 5 we will go on to show how one can realize an analogue NC geometry in a flowing spinor BEC by using an extension of Goldstone's theorem for condensed matter systems. We will then present an explicit model which allows to tune the nature of the analogue geometry (at the mean-field level) between the Lorentz-invariant and Newton-Cartan types. We will also use Luttinger's method to isolate the energy and momentum transport quantities for the Goldstone modes in the analogue spacetime.

[7] In a relativistic theory these are all unified into the symmetric stress-energy tensor $T^{\mu\nu}$. In a non-relativistic system, this four-tensor is no longer required to be symmetric and thus the energy-current is no longer equal to the momentum-density.

Chapter 2: Cavity non-equilibrium enhancement of superconductivity

This chapter is based on the publication Curtis, Raines, Allocca, Hafezi, and Galitski [35, © American Physical Society].

2.1 Introduction

The topic non-equilibrium superconductivity is an old and rich subject, dating back to at least the 1960's, when it was found that subjecting a conventional superconductor to strong microwave radiation can lead to an enhancement of superconductivity [36, 37]. The explanation of this effect, sometimes known as the "Wyatt-Dayem effect, "was first provided by Eliashberg *et. al.* [38–40], who showed that the irradiation yields a non-thermal distribution of the Bogoliubov excitations with an effectively colder band edge. This theoretical mechanism was then confirmed experimentally by Klapwijk, *et. al.* [41]. Further theoretical developments include an analysis of the thermodynamic stability of the radiation-enhanced superconducting state [42, 43], and a full kinetic treatment including the non-equilibrium dynamics of the phonons which are responsible for superconductivity in the first place [44]. Recently, there has been renewed interest in this effect including its theoretical application to systems of ultra-cold atoms [45, 46], and a full exploration of the phase diagram using Keldysh path integral methods [47]. A brief, but comprehensive overview of this subject in the context of microwave enhanced superconductivity can be found in Ref. [48].

A large degree of the recent interest stems from a number of remarkable "pump-probe" experiments, which involve subjecting materials to intense THz radiation pulses (the "pump") and studying the subsequent out-of-equilibrium dynamics (the

"probe"). These experiments allow for the experimental study of otherwise elusive non-equilibrium phases and phase transitions [49, 50]. Applying this method to superconductors has uncovered a wide array of elusive and surprising phenomena including the detection of various Higgs modes[1] in superconductors [51–54] and apparent transient superconductivity [55–58] up to very high effective temperatures. Attempts to theoretically understand these experiments have led to wide array of models and calculations, most of which go beyond the the quasiparticle redistribution effect [52, 58–73].

All of these works essentially investigate effects on quantum matter degrees of freedom (e.g. electrons or phonons) due to the presence of external, classical electromagnetic fields. It is the aim of this work to extend some of these results into the regime where quantum and statistical fluctuations of the electromagnetic field become relevant.

Quickly, let us recapitulate why this is an interesting, but challenging regime. Generically, the electromagnetic field can be decomposed in to two contributions. One is from the scalar gauge potential ϕ, while the other is from the vector gauge potential $\mathbf{A}$. We write the electric field $\mathbf{E}$ and magnetic field $\mathbf{B}$ in terms of the gauge potentials as

$$\mathbf{E} = -\nabla\phi - \frac{\partial}{\partial t}\mathbf{A} \tag{2.1a}$$

$$\mathbf{B} = \nabla \times \mathbf{A}. \tag{2.1b}$$

The gauge fields $\phi, \mathbf{A}$ are not directly observable due to gauge invariance. We must impose a gauge constraint in order to use the gauge fields to describe configuration space. Unless otherwise explicitly specified, in this thesis we will use the

[1] This is particularly remarkable because in a superconductor the Higgs mode is both optically inert, as it has no dipole-transition matrix elements, and gapped to twice the quasiparticle gap. It is also damped due to its overlap with the Bogoliubov quasiparticle continuum.

so-called Coulomb gauge[2], which corresponds to choosing $\nabla \cdot \mathbf{A} = 0$, along with the requirement that gauge fields vanish at spatio-temporal infinity.

This naturally partitions the electric field $\mathbf{E}$ into a **longitudinal** part $\mathbf{E}_{\parallel} = -\nabla\phi$, and a **transverse** part $\mathbf{E}_{\perp} = -\frac{\partial \mathbf{A}}{\partial t}$. Application of Gauss' law for electrostatics then reduces to Poisson's equation

$$-\nabla^2 \phi = \frac{1}{\epsilon_0}\rho, \tag{2.2}$$

which shows that the scalar potential can be eliminated in favor of the instantaneous Coulomb interaction (in other words, the scalar potential is slaved to the charge distribution by Gauss' law). In a metal, the static Coulomb interaction is then screened due to the presence of mobile charge carriers, and this remains the case in most superconductors [7, 9, 13, 74]. Furthermore, the longitudinal photon mode does not propagate at frequencies below the plasma frequency, which for a bulk metal is very large. Thus, at low frequencies and long wavelengths, we can essentially neglect the Coulomb interaction.

In a metal, at low frequencies (below the plasma frequency), transverse electromagnetic fields also do not propagate. The primary distinction however is that in a metal there is no screening of the static transverse field, as there is for a static longitudinal field. As such, long-range magnetostatic interactions are still present at low frequencies. However, in metals, which are gapless, the low-frequency excitations feature electrons with a typical velocity of order $v_F \ll c$. Thus, radiative corrections arising from the exchange of virtual photons are expected to be small, as they emanate from magnetic interactions which involve current-current interactions and are thus of order $(v_F/c)^2$.[3] In superconductors, magnetostatic fields **are** screened, due

[2] Also referred to as the radiation or London gauge occasionally.

[3] In principle, gauge-field mediated interactions are important but in real quantum electrodynamics the very small coupling renders them essentially unimportant. However, theories which exhibit emergent gauge fields are not plagued by this problem and in general are quite interesting, albeit complicated to describe [75–78].

to the Meissner effect. As such, we expect we can similarly ignore the transverse interactions, as in this case photons acquire a gap and are irrelevant.

While they are often neglected in solid-state physics, radiative interactions—interactions which involve the exchange of virtual photons—between quantum emitters (such as atoms or ions) are central to the field of AMO physics [79]. In the simplest case, the emitters are characterized by a dipole moment operator $e\hat{\mathbf{r}}$, which couples linearly to the electromagnetic field in the standard way through $H_{\text{int}} = -e\hat{\mathbf{r}} \cdot \mathbf{E}$. Provided that retardation effects can be neglected, it is then straightforward to integrate out the electric field and obtain an effective dipole-dipole interaction between the emitters. For this purpose, the electromagnetic field can often be treated classically. Dating back to seminal work by Purcell [80], Dicke [81], and Jaynes and Cummings [82], a major focus of the field of quantum optics has been the design and study of systems which push the electrodynamics of matter into the quantum realm. Often, resonant electromagnetic cavities are employed in order to increase the light-matter coupling-strength and coherence time-scales. Recently, there has been a great deal of interest in bringing these phenomena into the regime of solid-state physics [83, 84], largely inspired by recent breakthroughs involving systems of exciton-polaritons [85–87].

We will discuss the connection with exciton-polariton systems in more detail in Chap. 3. In this chapter we focus more on non-equilibrium effects in the spirit of the Eliashberg effect.[4] To understand the proposed enhancement mechanism, consider the BCS self-consistency equation for the superconducting order parameter Δ. In its most basic form, this reads

$$\Delta(\mathbf{r}, t) = -g\langle \Psi_{\downarrow}(\mathbf{r}, t)\Psi_{\uparrow}(\mathbf{r}, t)\rangle \tag{2.3}$$

where the correlation function is evaluated in a possibly non-equilibrium state,

[4] Not to be confused with the Migdal-Eliashberg theory for strongly-coupled superconductors.

described by density matrix $\hat{\rho}$, which in turn depends on the order parameter Δ. Here $g > 0$ is the attractive BCS interaction constant. In a homogeneous steady-state this can usually be rewritten in terms of the quasiparticle DOS $\nu_{\rm qp}(E)$ and occupation function $n(E)$ as

$$1 = g \int \frac{dE}{E} \nu_{\rm qp}(E) \left[\tfrac{1}{2} - n(E)\right]. \tag{2.4}$$

In BCS theory for a clean s-wave gap, the density of states is taken as

$$\nu_{\rm qp}(E) = 2\nu_F |E| / \sqrt{E^2 - \Delta^2}\, \theta(|E| - \Delta) \tag{2.5}$$

with ν_F the density of states per spin at the Fermi level[5] and $\theta(x)$ is the Heaviside step-function, which enforces that there are no subgap states. Since $\nu_{\rm qp}$ depends on the gap, Eq. 2.4 is in fact a non-linear equation which essentially defines the gap as a functional of the occupation function, so that $\Delta = \Delta[n(E)]$. In equilibrium, this occupation is simply the Fermi-Dirac distribution, $\frac{1}{2} - n(E) = \tanh \frac{1}{2}\beta E$, and thus the full functional dependence of Δ reduces to a one-parameter dependence on the temperature. The insight of Eliashberg and company [38–40] is that in general the thermal occupation function is not optimal and $\Delta[n]$ can be increased by appropriately choosing a non-equilibrium distribution function.[6]

We will approach the problem as follows. We will first compute the superconducting mean-field state in terms of Bogoliubov quasiparticles for an equilibrium gap $\Delta[n_F]$ with n_F the Fermi-Dirac distribution at a prescribed temperature. Then we will couple the electrons to a fluctuating electromagnetic field and determine

[5] In two dimensions this is explicitly given by $\nu_F = m^*/2\pi$ for the non-interacting Fermi gas, with m^* the effective mass.

[6] However, the gap is still ultimately bounded from above by the zero-temperature occupation function with $n(E) = 0$. Thus, the effect we predict is expected to vanish as we approach zero temperature, as we essentially run out of available unpaired electrons. Other effects which renormalize the coupling constant or density of states may still have an effect at $T = 0$.

how the Bogoliubov quasiparticles are redistributed, computing the correction to the occupation function $\delta n(E) = n(E) - n_F(E)$. We will then use the gap equation to determine the correction to the gap, $\delta\Delta = \Delta[n_F + \delta n] - \Delta[n_F]$. This will be used to diagnose when the cavity is beneficial, or detrimental, to the superconducting gap, assumed to be a proxy variable for observables such as the critical temperature or critical current [41–43]. The remainder of the chapter will be structured similarly. In Sec. 5.3 we will describe the system we consider and in particular, derive the spectral function for our model of electromagnetic cavity. In Sec. 2.3 we will use a kinetic equation to determine the effect that cavity photons have on the occupation function $n(E)$. Then, in Sec. 2.4 we will use this correction to the occupation function to determine the correction to the gap, showing that it can be increased by appropriate tuning of the cavity spectral and occupation function.

2.2 Model

We begin by considering a model of a 2-Dimensional Electron Gas (2DEG) plus attractive BCS interaction described by the Hamiltonian

$$H = \int d^2r \left[\sum_\sigma \hat{\Psi}^\dagger_\sigma(\mathbf{r}) \left(-\frac{\nabla^2}{2m} - \mu \right) \hat{\Psi}_\sigma(\mathbf{r}) - g\Psi^\dagger_\downarrow(\mathbf{r})\Psi^\dagger_\uparrow(\mathbf{r})\Psi_\uparrow(\mathbf{r})\Psi_\downarrow(\mathbf{r}) \right]. \tag{2.6}$$

We will couple this to the radiative electromagnetic field in an enclosing cavity, depicted in Fig. 2.1. This is accomplished by the minimal coupling prescription, which entails upgrading the regular derivative $-i\nabla$ to a covariant derivative $\mathbf{D} = -i\nabla - \mathbf{A}$ where $\mathbf{A}$ is the electromagnetic gauge potential (we set the charge of the electron to unity). We then supplement the Hamiltonian with the Maxwell Hamiltonian for the electromagnetic field [79]. For the moment, we will leave the

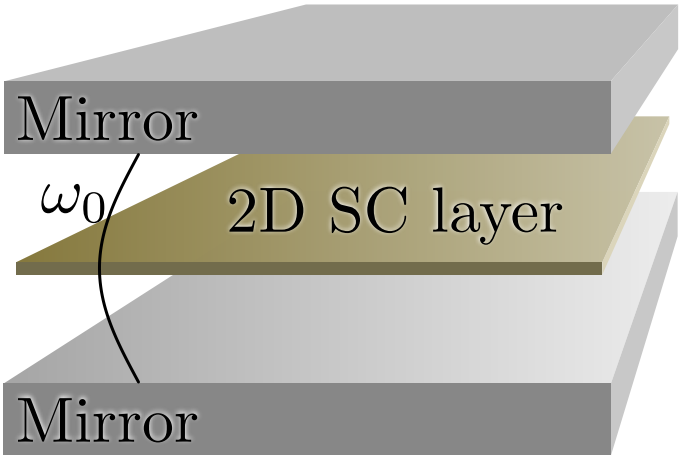

Figure 2.1: Schematic depiction of the system. The superconducting sample itself is oriented in the $x-y$ plane at $z = L/2$ and is of a thickness d which is much less than the length scale L governing the cavity fundamental harmonic. The cavity is modeled by a pair of metallic boundary conditions at $z = 0, L$ and is of an area $A = L_x^2 \gg L^2$ which is large enough to ignore finite-size effects in the transverse direction. The fundamental transverse harmonic is shown, which has an anti-node located $z = L/2$ and frequency $\omega_0 = \pi c/L$.

Maxwell Hamiltonian unspecified, so that the total system Hamiltonian is

$$H = \int d^2r \left[\hat{\Psi}_\sigma^\dagger \left(\frac{\mathbf{D}^2}{2m} - \mu \right) \hat{\Psi}_\sigma - g \hat{\Psi}_\uparrow^\dagger \hat{\Psi}_\downarrow^\dagger \hat{\Psi}_\downarrow \hat{\Psi}_\uparrow \right] + H_{\text{Maxwell}}. \tag{2.7}$$

In this **chapter** we will work with units where the electronic charge $e = 1$. Throughout we will employ the radiation gauge $\nabla \cdot \mathbf{A} = 0$. A detailed solution to Maxwell's equations for the planar cavity geometry and the quantization of the electromagnetic field can be found in Appendix A.

The BCS interaction is decoupled via standard mean-field theory, and the resulting BdG Hamiltonian is diagonalized with a Bogoliubov transformation. In

momentum space, with $\hat{c}_{\mathbf{p},}$ the second-quantized electron operators, we find

$$\begin{pmatrix} \hat{c}_{\mathbf{p},\uparrow} \\ \hat{c}^{\dagger}_{-\mathbf{p},\downarrow} \end{pmatrix} = \begin{pmatrix} u_{\mathbf{p}} & -v_{\mathbf{p}} \\ v_{\mathbf{p}} & u_{\mathbf{p}} \end{pmatrix} \begin{pmatrix} \hat{\gamma}_{\mathbf{p},+} \\ \hat{\gamma}^{\dagger}_{-\mathbf{p},-} \end{pmatrix} \tag{2.8a}$$

$$u_{\mathbf{p}} = \sqrt{\frac{1}{2}\left(1 + \frac{\xi_{\mathbf{p}}}{E_{\mathbf{p}}}\right)} \tag{2.8b}$$

$$v_{\mathbf{p}} = \sqrt{\frac{1}{2}\left(1 - \frac{\xi_{\mathbf{p}}}{E_{\mathbf{p}}}\right)}, \tag{2.8c}$$

where $\hat{\gamma}_{\mathbf{p}\pm}$ are the Bogoliubov quasiparticle annihilation operators, $E_{\mathbf{p}} = \sqrt{\xi_{\mathbf{p}}^2 + \Delta^2}$ is the quasiparticle dispersion, and $\xi_{\mathbf{p}} = \mathbf{p}^2/2m - \mu$ is the normal state electron dispersion.

Likewise, we diagonalize the cavity Hamiltonian, finding the normal modes in the absence of the electrons. The details of this can be found in Appendix A. One important effect the cavity has is that the frequencies of the electromagnetic modes become quantized by finite-size boundary conditions. This leads to a dispersion relation for photons with in-plane momentum $\mathbf{q}$ of

$$\omega_{n,\mathbf{q}} = \sqrt{\left(\frac{n\pi c}{L}\right)^2 + c^2\mathbf{q}^2} \equiv \sqrt{n^2\omega_0^2 + c^2\mathbf{q}^2} \tag{2.9}$$

where $n = 1, 2, 3, ...$ indexes the harmonic of the confined mode.

The interaction between the Bogoliubov quasiparticles and photons is treated perturbatively. To lowest order, the coupling between the two is given by the paramagnetic interaction

$$H^{\text{int}} = -\int d^d r \mathbf{j}(\mathbf{r}) \cdot \mathbf{A}(\mathbf{r}, t) \tag{2.10}$$

where the paramagnetic current is given in terms of the electron fields by

$$\mathbf{j} = \sum_{\sigma} \frac{1}{2m} \hat{\Psi}^{\dagger}_{\sigma} \left[-i \overleftrightarrow{\nabla} \right] \hat{\Psi}_{\sigma}. \tag{2.11}$$

We use the "symmetrized" derivative notation to mean $f \overleftrightarrow{\partial} g = f(\partial g) - (\partial f) g$.

Crucially, the mean-field we evaluate the current matrix elements in is not the Fermi sea background, but the BCS state. As such, the interaction which is diagonal in electron operators is no longer diagonal when written in terms of Bogoliubov quasiparticles. We apply the momentum space rotation matrix from Eq. 2.8 to the momentum-space current in order to obtain the matrix elements in terms of the quasiparticles. This produces the result

$$\begin{aligned} \mathbf{j}_{\mathbf{q}} = \int_{p} \frac{\mathbf{p} - \frac{1}{2}\mathbf{q}}{m} \Big[& \left(u_{\mathbf{p}-\mathbf{q}} u_{\mathbf{p}} + v_{\mathbf{p}-\mathbf{q}} v_{\mathbf{p}} \right) \left(\gamma^{\dagger}_{\mathbf{p}-\mathbf{q},+} \gamma_{\mathbf{p},+} + \gamma^{\dagger}_{\mathbf{p}-\mathbf{q},-} \gamma_{\mathbf{p},-} \right) \\ & + \left(u_{\mathbf{p}-\mathbf{q}} v_{\mathbf{p}} - v_{\mathbf{p}-\mathbf{q}} u_{\mathbf{p}} \right) \left(\gamma^{\dagger}_{\mathbf{p}-\mathbf{q},+} \gamma^{\dagger}_{-\mathbf{p},-} - \gamma_{\mathbf{p},+} \gamma_{-(\mathbf{p}-\mathbf{q}),-} \right) \Big], \end{aligned} \tag{2.12}$$

where we use the shorthand $\int_p \cdots = \int d^2p \cdots / (2\pi)^2$. We see there are three types of matrix element appearing in Eq. (3.7), corresponding to scattering (by both emission and absorption of photons), pair-breaking, and pair-recombination respectively. Through these processes, the fluctuating cavity photon field will induce transitions amongst the quasiparticle eigenstates, resulting in a redistribution of the quasiparticle occupations. In order to calculate the effect of this redistribution, we will use a kinetic equation.

2.3 Kinetic Equation

We are interested in the non-equilibrium occupation of Bogoliubov quasiparticles due to the cavity photons. To model this, we consider a kinetic equation for the occupation function $n_{\mathbf{p}}$. In general, the occupation function is obtained by the

Wigner transform of the two-argument Keldysh Green's function and is function of both space and momentum.

In the absence of collisions, the kinetic equation only has streaming (one-body) terms, which arise from the Liouville equation for conservation of phase-space volume

$$\frac{dn}{dt} \equiv \left[\frac{\partial}{\partial t} + \mathbf{v}_{\mathbf{p}} \cdot \frac{\partial}{\partial \mathbf{r}} - \mathbf{F}_{\text{ext}} \cdot \frac{\partial}{\partial \mathbf{p}}\right] n = 0 \tag{2.13}$$

where $\mathbf{v}_{\mathbf{p}} = \partial_{\mathbf{p}} E_{\mathbf{p}}$ is the quasiparticle group velocity and $\mathbf{F}_{\text{ext}}$ models the external one-body forces.

In addition to the streaming terms, we also model inelastic scattering processes (e.g. due to phonons) by a relaxation-time approximation, with rate $\frac{1}{\tau_{\text{in}}}$, which draws the quasiparticle distribution back towards the equilibrium distribution n_F, held at temperature T_{qp}. Including this term, we get

$$\frac{dn}{dt} = -\frac{1}{\tau_{\text{in}}} (n - n_F) \,. \tag{2.14}$$

The relaxation time approximation used here is the same that was used in the original work of Eliashberg [40–42].

We incorporate the effect of cavity through a collision integral $\mathcal{I}_{\text{cav}}[n]$, which will be calculated using Fermi's Golden Rule (FGR). This produces the full kinetic equation

$$\left[\frac{\partial}{\partial t} + \mathbf{v}_{\mathbf{p}} \cdot \frac{\partial}{\partial \mathbf{r}} - \mathbf{F}_{\text{ext}} \cdot \frac{\partial}{\partial \mathbf{p}}\right] n = \mathcal{I}_{\text{cav}}[n] - \frac{1}{\tau_{\text{in}}} (n - n_F) \,. \tag{2.15}$$

We aim to solve this for a homogeneous steady-state in the absence of external forces. In this case, we can set the $\frac{dn}{dt}$ to zero. In the limit where τ_{in} is small, we can proceed further by perturbatively solving for the deviation from equilibrium

$\delta n = n - n_F$.[7] To lowest order, the correction is

$$\delta n = \tau_{\text{in}} \mathcal{J}_{\text{cav}}[n_F]. \tag{2.16}$$

To compute the cavity-induced collision integral, we rely on FGR, applied to both the pairing/de-pairing and scattering processes implied by the paramagnetic coupling. The result is

$$\begin{aligned}\mathcal{J}_{\text{cav}}[n] = \int_{p'} \Bigg\{ & \Gamma^{\text{pair}}_{\mathbf{p},-\mathbf{p}'} \Big[(1-n_{\mathbf{p}})(1-n_{-\mathbf{p}'}) N(E_{\mathbf{p}} + E_{-\mathbf{p}'}) \\ & \qquad - \left(n_{\mathbf{p}} n_{-\mathbf{p}'} \left(N(E_{\mathbf{p}} + E_{-\mathbf{p}'}) + 1 \right) \right) \Big] \\ & + \Bigg(\Gamma^{\text{scat}}_{\mathbf{p}'\to\mathbf{p}} \Big[n_{\mathbf{p}'} \left(1 - n_{\mathbf{p}}\right) \left(N(E_{\mathbf{p}'} - E_{\mathbf{p}}) + 1 \right) \\ & - \left(1 - n_{\mathbf{p}'}\right) n_{\mathbf{p}} N(E_{\mathbf{p}'} - E_{\mathbf{p}}) \Big] - (\mathbf{p} \leftrightarrow \mathbf{p}') \Bigg) \Bigg\}\end{aligned} \tag{2.17}$$

with the Γ's given by

$$\Gamma^{\text{pair}}_{\mathbf{p},-\mathbf{p}'} = \frac{1}{2\epsilon_0 \omega_{\mathbf{p}-\mathbf{p}'}} \sum_{\alpha} \left| \vec{\epsilon}_{\alpha,\mathbf{p}-\mathbf{p}'} \cdot \left(\frac{\mathbf{p}+\mathbf{p}'}{2m} \right) \right|^2 \times \left(u_{\mathbf{p}} v_{-\mathbf{p}'} - u_{-\mathbf{p}'} v_{\mathbf{p}} \right)^2 \mathcal{A}_{\mathbf{p}-\mathbf{p}'} \left(E_{\mathbf{p}} + E_{-\mathbf{p}'} \right) \tag{2.18a}$$

$$\Gamma^{\text{scat}}_{\mathbf{p}\to\mathbf{p}'} = \frac{1}{2\epsilon_0 \omega_{\mathbf{p}-\mathbf{p}'}} \sum_{\alpha} \left| \vec{\epsilon}_{\alpha,\mathbf{p}-\mathbf{p}'} \cdot \left(\frac{\mathbf{p}+\mathbf{p}'}{2m} \right) \right|^2 \times \left(u_{\mathbf{p}} u_{\mathbf{p}'} + v_{\mathbf{p}'} v_{\mathbf{p}} \right)^2 \mathcal{A}_{\mathbf{p}-\mathbf{p}'} \left(E_{\mathbf{p}} - E_{\mathbf{p}'} \right). \tag{2.18b}$$

These contain the dependence on the cavity mode polarization vectors $\vec{\epsilon}_{\alpha\mathbf{q}}(z = L/2)$,

[7] We require that τ_{in} be small compared to the other relaxational time scales, so that to leading order the solution to the kinetic equation is thermal, with a small correction of $O(\tau_{\text{in}})$. However, we still impose the "Eliashberg" limit, which requires that $\tau_{\text{in}} = 1/\gamma_{\text{in}}$ be large compared to other spectral energy scales. In particular, this is because at $O(A^2)$ there is also a correction to the density-of-states due to depairing energy. In the Eliashberg limit of small γ_{in}, this can be neglected in comparison to the large kinetic effect. See Appendix B or Ref. [41].

the (momentum resolved) photon spectral function

$$\mathcal{A}_{\mathbf{q}}(\omega) = \frac{1/\tau_{\text{cav}}}{(\omega - \omega_{\mathbf{q}})^2 + (1/2\tau_{\text{cav}})^2}, \tag{2.19}$$

with photon lifetime τ_{cav}, and the squares of BCS coherence factors

$$(u_{\mathbf{p}} v_{-\mathbf{p}'} - v_{-\mathbf{p}'} u_{\mathbf{p}})^2 = \frac{1}{2}\left(1 - \frac{\xi_{\mathbf{p}}\xi_{-\mathbf{p}'} + \Delta^2}{E_{\mathbf{p}} E_{-\mathbf{p}'}}\right) \tag{2.20}$$

$$(u_{\mathbf{p}} u_{\mathbf{p}'} + v_{\mathbf{p}} v_{\mathbf{p}'})^2 = \frac{1}{2}\left(1 + \frac{\xi_{\mathbf{p}}\xi_{\mathbf{p}'} + \Delta^2}{E_{\mathbf{p}} E_{\mathbf{p}'}}\right). \tag{2.21}$$

Utilizing the detailed balance properties of thermal equilibrium, we will show that in fact this correction depends only the deviation of the photon occupation function $N(\omega)$ from being in equilibrium with the quasiparticles

$$\delta N_{\text{cav}}(\omega) \equiv N(\omega) - n_B\left(\frac{\omega}{T_{\text{qp}}}\right), \tag{2.22}$$

where $n_B(z) = (e^z - 1)^{-1}$ is the Bose occupation function.

Up until this point we have assumed that the system is translationally invariant, with momentum being a good quantum number. A consequence of this is that in addition to energy conservation, the matrix elements also must obey conservation of momentum. This dramatically restricts the phase space available for interaction. We incorporate impurity scattering within the quasiclassical approximation, essentially following the prescription of Mattis and Bardeen [88]; a more rigorous treatment in terms of the Keldysh Nonlinear σ-Model [47, 89, 90] and related Usadel equation [91] can be found, e.g. in Appendix B. The end result is that we may replace the FGR rates appearing in the collision intergrals with the τ_{el}/ν_F times the Fermi-surface

averaged rates. Explicitly, these read

$$\Gamma^{\text{pair}}(E,E') = \int \frac{d^2q}{(2\pi)^2} \sum_\alpha \frac{\mathcal{A}_{\mathbf{q}}\,(E+E')}{2\epsilon_0\omega_{\mathbf{q}}} \frac{\tau_{\text{el}}}{\nu_F} \overline{\left|\vec{\epsilon}_{\alpha,\mathbf{q}} \cdot \left(\frac{\mathbf{p}+\mathbf{p}'}{2m}\right)\right|^2} \times \frac{1}{2}\left(1 - \frac{\Delta^2}{EE'}\right)^2 \tag{2.23a}$$

$$\Gamma^{\text{scat}}(E,E') = \int \frac{d^2q}{(2\pi)^2} \sum_\alpha \frac{\mathcal{A}_{\mathbf{q}}\,(E-E')}{2\epsilon_0\omega_{\mathbf{q}}} \frac{\tau_{\text{el}}}{\nu_F} \overline{\left|\vec{\epsilon}_{\alpha,\mathbf{q}} \cdot \left(\frac{\mathbf{p}+\mathbf{p}'}{2m}\right)\right|^2} \left(1 + \frac{\Delta^2}{EE'}\right)^2 . \tag{2.23b}$$

Here E, E' are the energies of the participating quasiparticle states (previously labeled by their momenta $\mathbf{p}, \mathbf{p}'$). We have discarded terms in the coherence factors which are odd in ξ, the quasiparticle kinetic energy, as these vanish in the quasiclassical approximation. The overline — indicates an angular averaging of the velocity operator matrix element. Since $\mathbf{q}$, the photon momentum, and $\mathbf{p}, \mathbf{p}'$ the quasiparticle momenta, are decoupled we can easily average this.

The result of this procedure is a collision integral which is a function of the quasiparticle energy only. The integral over the quasiparticle momentum $\mathbf{p}'$ becomes an integral over the quasiparticle energy, weighted by the density of states. We insert the transition rates from Eq. (2.23a) in to Eq.(2.16) to obtain the correction to the occupation function. Evaluating the correction to the quasiparticle distribution function and manipulating the resulting expression, we find

$$\delta n(E) = \tau_{\text{in}} \int_{-\infty}^{\infty} d\Omega J_{\text{cav}}(\Omega) \delta N_{\text{cav}}(\Omega) K(\Omega, E), \tag{2.24}$$

where $K(\Omega, E) = f(\Omega, E) + f(-\Omega, E) - f(-\Omega, -E)$, with

$$f(\Omega,E) = \frac{\nu_{\text{qp}}(E-\Omega)}{\nu_F} \times \frac{1}{2}\left(1 + \frac{\Delta^2}{E(E-\Omega)}\right)\left[n_F\left(\frac{E-\Omega}{T_{\text{qp}}}\right) - n_F\left(\frac{E}{T_{\text{qp}}}\right)\right]. \tag{2.25}$$

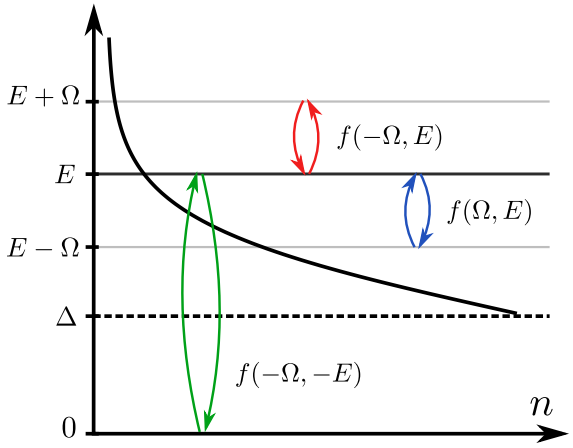

Figure 2.2: Depiction of the three processes taken into account in the occupation function correction in Eq. (2.24). These are shown alongside the equilibrium occupation function $n_F(E/T_{\rm qp})$. The top red arrows correspond to $f(-\Omega, E)$ and describe the absorption of a photon of energy Ω and subsequent scattering **out** of state E and **into** state $E' = E + \Omega$, along with the detailed-balance partner. The middle green arrows correspond to $f(\Omega, E)$ and describe the absorption of a photon of energy Ω and subsequent scattering **into** state E **from** state $E' = E + \Omega$, along with the detailed-balance partner. Finally, there are the blue arrows showing pair breaking processes, corresponding to $f(-\Omega, -E)$. These occur via absorption of a photon of energy $\Omega = E + E' > 2\Delta$, resulting in the population of **both** states E and E', and the detailed balance partner which describes **annihilation** of states E and E' by emission of a photon of energy $\Omega = E + E' > 2\Delta$.

Here $\nu_{\rm qp}$ is the quasiparticle density of states from Eq. (2.5), which includes the Heaviside step-function corresponding to the gap. The three f terms appearing in $K(\Omega, E)$ are depicted schematically in Fig. 2.2, alongside the various processes they describe.

After the Fermi-surface average, the coupling to the cavity is effectively characterized by the coupling function

$$J_{\rm cav}(\Omega) = 4\pi\alpha c D \int \frac{d^2\mathbf{q}}{(2\pi)^2} \frac{\mathcal{A}_{\mathbf{q}}(\Omega)}{2\omega_q} \sum_{\alpha} |\vec{\epsilon}_{\alpha\mathbf{q},\parallel}|^2, \tag{2.26}$$

where $D = v_F^2 \tau_{\rm el}/2$ is the electronic diffusion constant and $\vec{\epsilon}_{\alpha\mathbf{q},\parallel}$ indicates that only the in-plane components of the polarization vector contribute. It is instructive to consider estimating $J_{\rm cav}(\Omega)$ for the case of the planar cavity model (see Appendix A). In this case, we can convert the integral over $\mathbf{q}$ into an integral over the frequency using $qdq = \omega d\omega/c^2$. We approximate the polarization vectors by $\sum_\alpha |\vec{\epsilon}_{\alpha\mathbf{q},\parallel}|^2 \sim \frac{1}{L} \sim \pi\omega_0/c$ with ω_0 the lower cutoff frequency on the cavity. Finally, the integral over the spectral function is essentially a step function $\theta(\Omega - \omega_0)$, consistent with the fact that the density of states of a parabolic band in two dimensions is constant. We ultimately see that

$$J_{\rm cav}(\Omega) \sim \alpha D \omega_0/c^2 \theta(\Omega - \omega_0).$$

All else equal, decreasing the cavity size increases ω_0 and therefore the strength of the effect. However, we also need to take care that ω_0 remains at relevant energy scales.

For a BCS gap of order $\Delta = 10\,\mathrm{K}$ we find a corresponding resonance frequency $\omega_0 \sim 200\,\mathrm{GHz}$. Recently, a number of advances have lead to large enhancements in the strength and tunability of the light-matter coupling strength in this frequency regime, such that $J_{\rm cav}(\Omega)$ may potentially exceed what is expected from our simple

planar cavity model by many orders of magnitude [92–96]. We incorporate this fact by re-scaling the spectral function J by a phenomenological factor X^2, so that $J(\Omega) \to \tilde{J}(\Omega) = X^2 J_{\text{cav}}(\Omega)$.[8]

We illustrate the change in quasiparticle occupation in Fig. 2.3. To compute this, we choose the enhancement factor $X^2 = 133$, corresponding to roughly a 10-fold enhancement of the electric field strength relative to our model, which essentially is to counteract the fine structure constant $\alpha = 1/137$. We use parameters $v_F/c = .02$, $\tau_{\text{el}} T_c = .2$, and $\tau_{\text{in}} T_c = 100.0$. We hold the quasiparticle temperature fixed at $T_{\text{qp}}/T_{\text{cav}} = .95$, and use the Ginzburg-Landau formula for the equilibrium value of the gap of

$$\Delta_0 = \sqrt{\frac{8\pi^2}{7\zeta(3)} T_c (T_c - T_{\text{qp}})}. \tag{2.27}$$

We then study the correction to the occupation function $\delta n(E)$ for two different cavity frequencies ω_0/Δ_0 (indicated), while holding the cavity temperature fixed at $T_{\text{cav}}/T_{\text{qp}} = .5$. For the "multi-mode" case, with J_{cav} described by the planar mirror model, we set $\kappa = 0$ so that the spectral function is essentially a momentum-averaged delta function. This is possible since in the multi-mode case, the effect we predict turns out to not depend strongly on the amount of cavity broadening.

The kinks in $\delta n(E)$ (labeled A,B, and C, see Fig. 2.3) are due to the step-function $\theta(x)$ in the function $f(E, \Omega)$, which in turn reflects the sharp cutoff in the electronic DOS at the gap. In the presence of a finite quasiparticle lifetime (which we have neglected here) this would be smoothed out.

We see that when the cavity frequency ω_0 is too small relative to Δ_0 (orange curve in Fig. 2.3), there is a build-up of low-energy excitations and a corresponding depletion of the higher-lying states. In essence, the quasiparticles are cooled by

[8] The fact that this is X^2 rather than X is largely convention. If we assume that the enhancement comes from the electric field strength being larger than predicted by our model by a factor of X, so that $\mathbf{E}_{\text{actual}} \sim X\mathbf{E}_{\text{model}}$, then we would expect the spectral function J to receive an enhancement factor of X^2, since the spectral function $J \sim \langle EE \rangle$ is related to the auto-correlation function of the electric field.

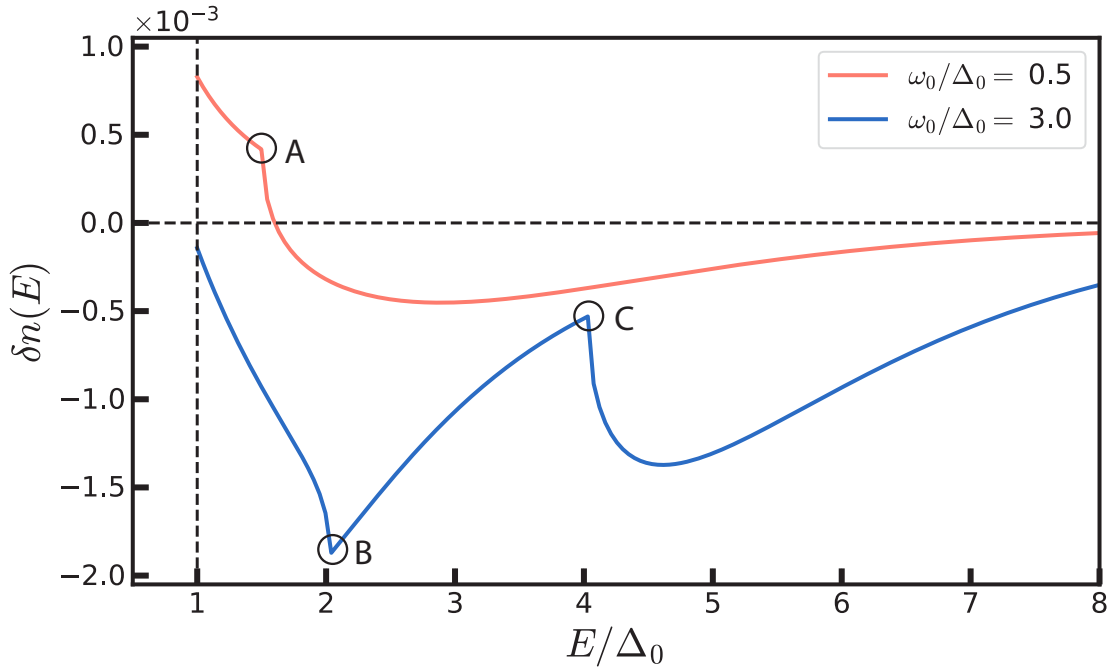

Figure 2.3: Change in quasiparticle distribution function due to cavity photons. This depends on the overall constant $\pi\alpha X^2 D\tau_{\text{in}}/c^2$. We choose parameters $X^2 = 133$, corresponding to roughly a 10-fold enhancement of the electric field strength relative to our model, and set $\pi\alpha D\tau_{\text{in}}T_c^2/c^2 = 9.17 \times 10^{-5}$ with T_c set to unity. The two curves are at the same temperature ($T_{\text{cav}}/T_{\text{qp}} = 0.5$) but different cavity frequencies ω_0/Δ_0. For low cavity frequency (orange), the gap Δ is diminished due to an accumulation of cooler quasiparticles near the gap-edge, due to a down-scattering of particles. For higher cavity frequency (blue), the recombination processes are more dominant and lead to a net reduction in quasiparticles, enhancing the gap Δ. The kink-features labeled A and C reflect the onset of the term $f(\Omega, E)$ in Eqn. (2.24), which is only non-zero for $E > \omega_0 + \Delta_0$. At higher cavity frequencies ($\omega_0 > 2\Delta_0$) an additional kink-feature (located at B) emerges at $E = \omega_0 - \Delta_0$. For $E < \omega_0 - \Delta_0$, the term $f(-\Omega, E)$ (which represents the pair-processes) contributes over the entire integration region of $\Omega > \omega_0$, while for $E > \omega_0 - \Delta_0$ the integral only captures some of the frequencies where this term contributes.

the cavity (which has a lower temperature) primarily through the loss of kinetic energy. Since the number of photons at a given frequency drops off rapidly with energy, most of the photons have energy $\omega \sim \omega_0$, which is not enough to stimulate recombination of Bogoliubov quasiparticles.

On the other hand, for larger cavity frequencies ω_0 relative to Δ_0 (blue curve in Fig. 2.3), the dominant effect is an overall reduction in the number of quasiparticles, especially at low frequencies. In this case, the quasiparticles are cooled primarily through an enhanced recombination rate and subsequent depletion of total quasiparticle number.[9] This reduction in quasiparticle occupation will now be shown to enhance the superconducting gap, as outlined in the introduction and Sec. 2.1.

2.4 Results

In order to simplify the calculation, we will study the system in the Ginzburg-Landau (GL) regime ($T_{\rm qp} \lesssim T_c$), which allows us to expand the gap equation in powers of Δ. Including the non-equilibrium distribution function contribution [42, 43], this results in

$$\left(\frac{T_c - T_{\rm qp}}{T_c} - \frac{7\zeta(3)}{8\pi^2} \frac{\Delta^2}{T_c^2} - 2 \int_\Delta^\infty \frac{dE}{E} \frac{\nu_{\rm qp}(E)}{\nu_F} \delta n(E) \right) \Delta = 0. \tag{2.28}$$

To leading order in the gap change, we obtain the correction to the BCS gap

$$\frac{\delta\Delta}{\Delta_0} = -\frac{T_c}{T_c - T_{\rm qp}} \int_{\Delta_0}^\infty \frac{dE}{E} \frac{\nu_{\rm qp}(E)}{\nu_F} \delta n(E). \tag{2.29}$$

This is plotted in Fig. 2.4(a) as a function of the cavity frequency ω_0 for different photon temperatures relative to the quasiparticle temperature $T_{\rm qp}$. The enhancement is ultimately driven by the enhanced BQP recombination rate which, for a cold

[9] We note that Bogoliubov quasiparticles are not conserved in general, and thus can be annihilated (in pairs). As such, there is no chemical potential to fix their total density.

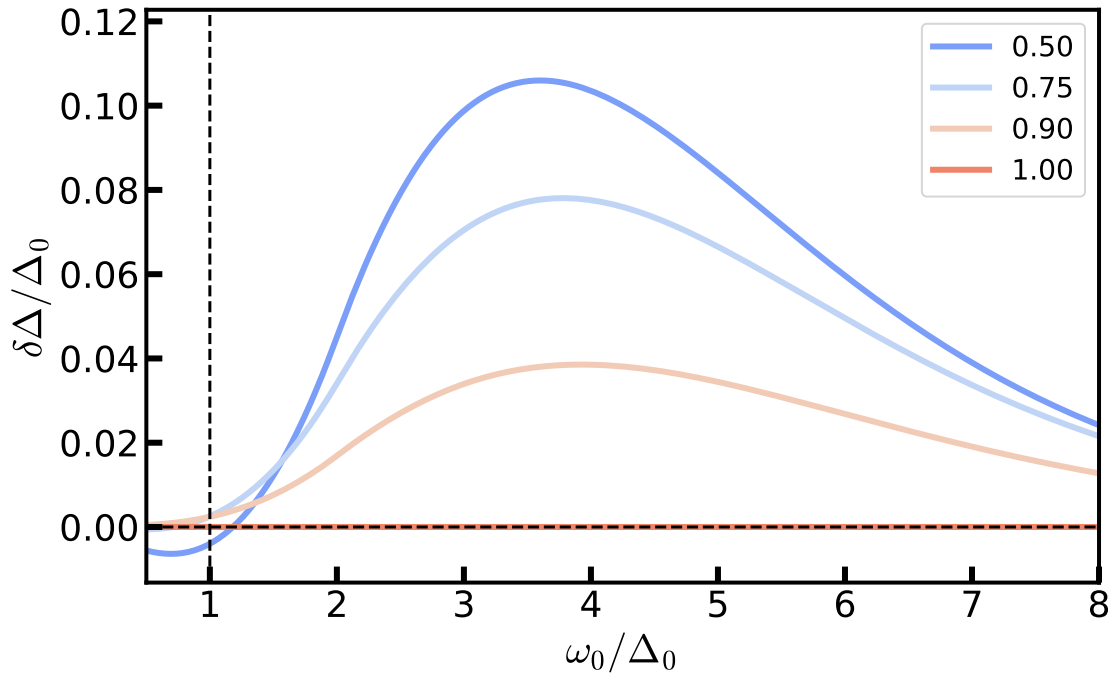

Figure 2.4: Relative enhancement of the gap function as a function of cavity frequency ω_0 for a particular value of the overall scaling constant $\pi\alpha X^2 D\tau_{\text{in}}/c^2$ (we take $X^2 = 133$ and $\pi\alpha D\tau_{\text{in}}T_c^2/c^2 = 9.17 \times 10^{-5}$ with T_c set to unity). Curves are colored and labeled according to the ratio $T_{\text{cav}}/T_{\text{qp}}$, comparing the photon and quasiparticle temperatures. The enhancement is seen set in after the cavity frequency surpasses the pair-breaking energy $2\Delta_0$.

photon reservoir serves to remove detrimental quasiparticles. While the effect we predict here essentially relies on the cooling ability of the cold photon reservoir, we also remark that our formula for $\delta n(E)$, presented in Eq. (2.24), is valid for a wide-variety of photon spectral functions. In particular, we can replace the multi-mode planar cavity, original envisioned in the model and depicted in Fig. 2.1, with a single-mode cavity. The main difference between these two is that the multi-mode spectral function only has a lower-cutoff on frequency, while the single-mode spectral function is peaked around a finite frequency and thus also has an upper-cutoff frequency.

We therefore also calculate the effect on the gap for the case of a single-mode spectral function. The multi-mode cavity spectral function is evaluated in the limit of vanishing cavity line-width $\kappa \to 0$, which gives

$$J_{\text{multi-mode}}(\Omega) = \frac{\alpha D X^2 \omega_0}{\pi c^2} \theta(\Omega - \omega_0) \left(1 + \frac{\omega_0^2}{\Omega^2}\right), \tag{2.30}$$

where we have replaced $1/L$ with $\omega_0/(\pi c)$ and included the phenomenological enhancement parameter X^2 explicitly[10]. We may also consider a single-mode cavity, in which there is finite-size quantization in all three dimensions. If we consider a simple model of a cubic cavity, with linear dimension $L \sim \pi c/\omega_0$, and assume this is larger than the relevant electronic length-scales, then the relevant spectral function J_{cav} will instead be

$$J_{\text{single-mode}}(\Omega) = \frac{4\alpha D X^2 \omega_0^2}{\pi^2 c^2} \frac{2\kappa}{(\Omega - \omega_0)^2 + \kappa^2}, \tag{2.31}$$

where we see that now the cavity linewidth κ is more important as it smoothes the

[10]The last factor, $1 + \omega_0^2/\Omega^2$, varies from 2 at $\Omega = \omega_0$ to 1 at high-frequencies, and essentially counts the number of modes with in-plane polarization. In the planar cavity model, one polarization is always in-plane, while one rotates as a function of momentum from in-plane at low frequencies to out-of-plane at high-frequencies. This will in general be non-universal and model dependent, as it depends on the magnitude of the projection of the electric field onto the sample, which is in general not as simple as the planar-mirror model.

other-wise delta-function resonance into a Lorentzian. Here we have used that the lowest mode of the cubic cavity has a frequency which scales as $\omega_0 = \pi c/L$ (again, this is partially decoupled from the actual volume through the enhancement factor X^2, which is determined by the effective mode-volume).

In particular, switching from a multi-mode planar cavity, where $J_{\text{cav}}(\Omega) \sim \omega_0(1+\omega_0^2/\Omega^2)\theta(\Omega-\omega_0)$ is roughly constant for $\Omega > \omega_0$, to a simpler single-mode cavity, where $J_{\text{cav}} \sim \omega_0^2 \frac{2\kappa}{(\Omega-\omega_0)^2+\kappa^2}$ is peaked at the resonant frequency, will allow for an enhancement in $\delta\Delta$ even when the photon reservoir is hotter than the sample. This is explicitly demonstrated in Fig. 2.5, where we plot $\delta\Delta$ against ω_0 for the case of a single-mode $J_{\text{cav}}(\Omega)$. The enhancement in $\delta\Delta$ due to hot photons is now qualitatively similar to the classical Eliashberg effect, albeit with a narrow spectral broadening applied to the driving. For cold photons, the enhancement is similar to that seen in the multi-mode system and results from the photons cooling the sample via enhanced BQP recombination.

In conclusion, we have generalized the classical Eliashberg effect to include both quantum and thermal fluctuations, as realized by a thermal microwave resonator cavity. In the appropriate parameter regime, we show that the photonic reservoir can be used to drive the quasiparticles into a non-equilibrium state which enhances the superconducting gap Δ. In our calculation, we assumed that the cavity relaxation rate τ_{cav}^{-1} was fast, allowing us to essentially ignore the dynamics and kinetics of the photons themselves, treating them as a quenched reservoir. We should not expect this to remain the case when we go to the limit of a high-quality cavity, in which the relaxation rate τ_{cav}^{-1} is no longer small compared to all the other energy scales in the problem. In the high-quality limit, a more elaborate treatment which treats the joint evolution of fermion-photon system is required. Though potentially much more complicated, the inclusion of photons as a participating dynamical degree of freedom may unveil many new and interesting phenomena. These range from the formation

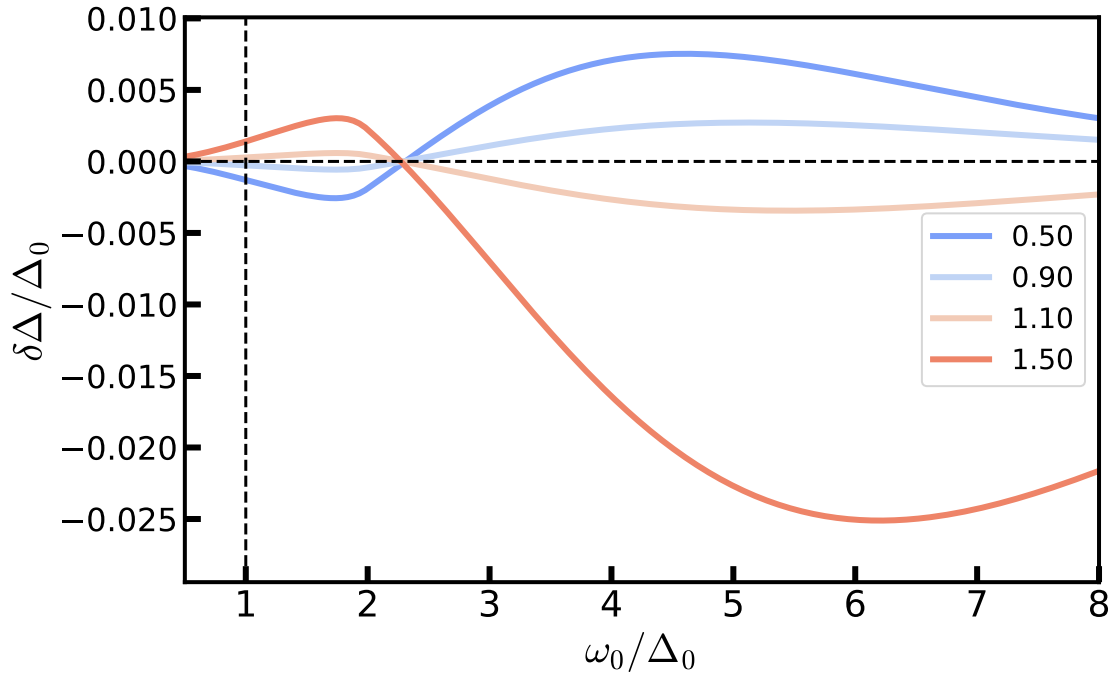

Figure 2.5: Gap enhancement $\delta\Delta_0$ for a single-mode cavity, for both cold and hot photons. The y-axis is determined by the overall scale $\frac{4\pi}{(\pi\sqrt{3})^3}\alpha X^2 \frac{D\tau_{\text{in}}T_c^2}{c^2}$ with the same values chosen for X^2 and $\tau_{\text{in}}, \tau_{\text{el}}, v_F/c$ as in Fig. 2.4. Curves are colored and labeled according to the ratio $T_{\text{cav}}/T_{\text{qp}}$, comparing the photon and quasiparticle temperatures. Here the cavity width is held fixed at $1/2\tau_{\text{cav}} = 10\omega_0$.

of new collective modes (including polaritons) [97, 98], superradiant phases [83, 99], and potentially photon-mediated superconductivity [100]. The prospect of exploring the full breadth of these joint matter-gauge systems is an exciting development in the fields of quantum optics and condensed matter physics.

Chapter 3: Cavity Bardasis-Schrieffer superconducting polaritons

This chapter is based on the publication Allocca, Raines, Curtis, and Galitski [98, © American Physical Society].

3.1 Introduction

Strong light-matter interaction has been a field of continuing interest for many years [101], with exciton polaritons [102] in particular garnering much attention. Formed from strong coupling between microcavity photons and excitons within a semiconductor, exciton-polaritons and their condensation at high temperatures are by now a well-established experimental milestone [86, 103–106]. These systems have recently seen application in the quantum simulation of solid state physics [107–110], acoustic black hole physics [111], and topological properties of quasicrystal states [112].

Recently, there has been some activity in trying to extend the ideas of exciton-polariton systems into the realm of superconducting systems. At a base level, the motivation for this is simple; if one can achieve comparable condensation temperature and superfluidity in a superconductor as one can in exciton-polariton systems, one would effectively have a room-temperature superconductor. Pursuing this line of reasoning, some works have proposed that semiconductor exciton-polariton condensates may be used as the "pairing-glue" for Cooper pairs in a nearby metal [113, 114], while even more recent proposals have raised the possibility of the cavity electromagnetic field directly enabling, or enhancing, superconductivity [35, 83, 97, 100]. However, though there is a superficial similarity between the quasiparticle spectra of semiconducting and (s-wave) superconducting systems, the off-diagonal

order of a superconductor complicates the matter of realizing a direct analogy of exciton-polaritons in superconductor systems.

As it turns out, the existence of exciton-like objects in a superconductor has already been investigated, dating back to work by Bardasis and Schrieffer not long after the development of BCS theory [16]. In this work, the authors found that in general superconductors support collective modes, dubbed BS modes,[1] which can be thought of as Cooper-pairs forming in excited bound-states with respect to the condensate. More precisely, BS modes are un-damped collective modes which reside within the BCS gap, and are due to fluctuations of the superconducting order parameter in a subdominant pairing channel. Furthermore, due to Landau damping, the phase of this collective mode is pinned to $\pi/2$ relative to that of the background condensate.[2] Typically d-wave fluctuations are considered about an s-wave ground state, since these both belong to the same spin multiplet. This is what we will consider in this chapter.

Experimental evidence of the BS mode has been long sought, but historically it has been difficult to detect since it does not linearly couple to the electromagnetic field; only recently has it been observed through Raman spectroscopy in iron-based materials [115–117]. In reality, and in particular in iron-based superconductors, a variety of multiband effects are known to complicate the identification of BS modes [118]. For simplicity, we will neglect these effects.

In this chapter we will instead show how one can use a cavity setup, illustrated in Fig. 3.1, to hybridize photons with these BS modes, realizing the superconducting analogy of exciton-polaritons. In Sec. 3.2 we will introduce the model we study and

[1] While the acronym may imply a degree of skepticism, the physics behind this is very solid.

[2] At zero momentum and zero temperature the Bardasis-Schrieffer collective mode satisfies the linear equation $\left[{g_s}^{-1} - {g_d}^{-1} - \frac{1}{2}\int \frac{dE}{|E|}\nu_{\rm qp}(E)\frac{(\Omega_{BS})^2-2\Delta^2}{(\Omega_{BS})^2-(2E)^2}\right]\Delta^d(\Omega_{BS}) + \Delta^2\int \frac{dE}{|E|}\nu_{\rm qp}(E)\frac{1}{(\Omega_{BS})^2-(2E)^2}\bar{\Delta}^d(-\Omega_{BS}) = 0$, with $\nu_{\rm qp}(E)$ the Bogoliubov quasiparticle density of states. For $g_s^{-1} - g_d^{-1} < 0$, in order for us to find $\Omega_{\rm BS} < \Delta$ (that is, a collective mode which cannot decay in to quasiparticle pairs), we must have $\Delta^d(\Omega_{BS}) + \bar{\Delta}^d(-\Omega_{BS}) = 0$. This fixes the relative phase to $\pi/2$.

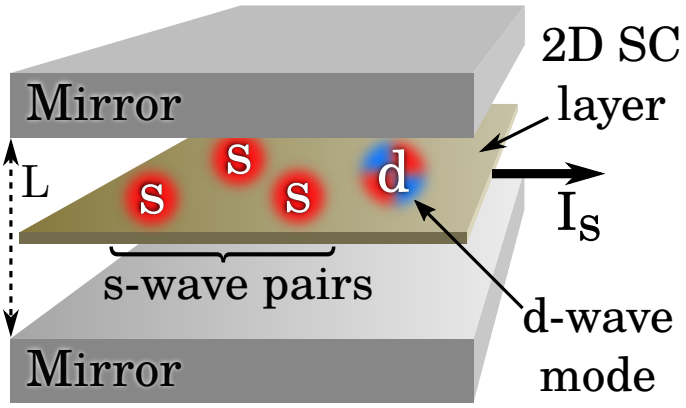

Figure 3.1: Schematic depiction of the cavity-superconductor system. This is similar to the setup used in Chapter 2, but now the superconductor has strong sub-dominant pairing fluctuations in the $d_{x^2-y^2}$ channel, shown in the figure against the s-wave pair condensate. The flowing supercurrent (see Sec. 3.3) is also depicted.

show how Bardasis-Schrieffer modes arise. Then, in Sec. 3.3 we will show how to derive the hybridization and compute the Hamiltonian for the resulting polaritonic system. Finally, we will present an outlook in Sec. 3.4.

3.2 Model

We will begin with a model similar to the one discussed in Chap. 2, but now with the inclusion of a subdominant pairing interaction in the $d_{x^2-y^2}$ channel. We describe the system using a Matsubara action $S[\bar{\Psi}, \Psi]$, with Grassmann fields $\Psi, \bar{\Psi}$ describing the electron fields. The partition function of the system is then given by the functional integral $Z = \int \mathcal{D}[\Psi, \bar{\Psi}] e^{-S}$. The action is most compactly written in momentum space as

$$S = \sum_{p\sigma} \bar{\Psi}_{p\sigma} \left(-i\varepsilon_n + \xi_{\mathbf{p}} \right) \Psi_{p\sigma} - \sum_q \sum_{\ell=s,d} g_\ell \overline{\varphi}_q^\ell \varphi_q^\ell, \tag{3.1}$$

with $p = (i\varepsilon_n, \mathbf{p})$ the fermionic four-momentum[3] of the electron, $q = (i\Omega_m, \mathbf{q})$ is the bosonic four-momentum of what will become the superconducting order parameter, and σ labels the z-projection of the electron spin. Here g_ℓ is the interaction strength of the ac interaction in the ℓ-th channel. We have written the interaction in terms of the bilinears,

$$\varphi_q^\ell = \frac{1}{\sqrt{\beta \mathrm{Vol}}} \sum_k f_\ell(\phi_{\mathbf{k}}) \psi_{-k+\frac{q}{2},\downarrow} \psi_{k+\frac{q}{2},\uparrow}. \tag{3.2}$$

Here we have normalized according to the $2+1d$ spacetime quantization volume $\beta\mathrm{Vol}$.[4] Importantly, following Bardasis and Schrieffer [16] we assume the interaction is sizable in both s-wave and d-wave channels, but a stronger s-wave component, $g_s > g_d$, leads to a purely s-wave superconducting ground state. The form factors are $f_s(\phi_{\mathbf{k}}) = 1$ and $f_d(\phi_{\mathbf{k}}) = \sqrt{2}\cos(2\phi_{\mathbf{k}})$, where $\phi_{\mathbf{k}}$ is the angle the momentum $\mathbf{k}$ makes to the x-axis. This form of the f_d interaction breaks the full rotational symmetry of the Fermi surface by choosing an explicit reference axis from which ϕ_k is measured. This is presumably generated from some anisotropy in the underlying crystal structure of the system—not explicitly present in our continuum model.

We switch to the description in terms of the Nambu spinor $\psi_p = \left(\Psi_{p\uparrow}, \overline{\Psi}_{-p\downarrow}\right)^T$ and decouple the BCS interaction in both angular momentum channels simultaneously with a Hubbard-Stratonovich transformation. The resulting action is written in momentum space as

$$\begin{aligned} S = \sum_k \bar{\psi}_k \left(-i\varepsilon_n + \xi_{\mathbf{k}}\hat{\tau}_3\right)\psi_k + \sum_q \frac{1}{g_s}|\Delta_q^s|^2 + \sum_q \frac{1}{g_d}|\Delta_q^d|^2 \\ + \sum_{k,q} \overline{\psi}_{k+\frac{q}{2}} \sum_\ell \frac{1}{\sqrt{\beta\mathrm{Vol}}} f_\ell(\phi_{\mathbf{k}}) \left[\overline{\Delta}_{-q}^\ell \hat{\tau} + \Delta_q^\ell \hat{\tau}^\dagger\right] \psi_{k-\frac{q}{2}}, \end{aligned} \tag{3.3}$$

[3] We call it the "four-momentum" since it group the energy and spatial momentum together into a single momentum as we would in a $3+1$ dimensional relativistic theory, even though the spatial dimension is 2 and thus only has $3 = 2+1$ components.

[4] In this expression, we have associated $\mathbf{q}/\mathbf{2}$ of the total pair-momentum to each electron. However, this is not a valid procedue for dividing the bosonic Matsubara frequency, which must be associated as $i\omega$ to one or the other electron. This regularization is understood when evaluating the bubble diagrams.

where $\Psi_k = (\psi_{k,\uparrow}, \bar{\psi}_{-k,\downarrow})$ are Nambu spinors, $\hat{\tau}_i$ are the Pauli matrices in Nambu space with $\hat{\tau}_0$ the identity, and Δ_q^ℓ are the complex Hubbard-Stratonovich decoupling fields labeled by angular momentum channel. In fact, such a model has been considered before in, e.g. Ref. [119] as a simplified single-band model of superconductors with competing s- and d-wave instabilities. We now show how to couple these BS modes to the photons in an enclosing cavity.

The cavity is treated as perfectly reflecting boundaries at $z = 0, L$. The action for photons inside the empty cavity is

$$S_{\text{cav}} = \frac{1}{2}\frac{\epsilon_0}{e^2} \sum_{q,n,\alpha} A_{\alpha,n,-q} \left[(i\Omega_m)^2 - \omega_n^2(\mathbf{q}) \right] A_{\alpha,n,q}. \tag{3.4}$$

The discrete quantum numbers are α, which indexes the two cavity polarizations and n, which labels the transverse modes resulting from the finite-size quantization in z, and $\omega_n(\mathbf{q})^2 = \omega_n^2 + c^2\mathbf{q}^2$, with $\omega_n = n\pi c/L$, is the dispersion of photons inside the cavity. We have incorporate the electric charge and dielectric ϵ_0 in to the photon propagator.

We consider just the $n = 1$ mode and drop the index; all other modes are higher in energy and far from the resonance we tune to later. We will therefore suppress the transverse quantum number n, with $\omega_{\mathbf{q}}$ understood as being $\omega_1(\mathbf{q})$, and so on. The vector potential is written in terms of the polarization vectors as $\mathbf{A}_q(z) = \sum_\alpha \vec{\epsilon}_{\alpha,\vec{q}}(z) A_{\alpha,q}$, with $\vec{\epsilon}_{\alpha,\vec{q}}(z)$ the polarization vectors inside the cavity. For a detailed derivation of the solution to Maxwell's equations in the cavity geometry, see Appendix A. The electron system is located in the middle of the cavity, so only $z = L/2$ must be considered. Minimal coupling between the cavity photon and the electron system generates a paramagnetic term proportional to $\mathbf{v}_\mathbf{k} \cdot \mathbf{A}_q$, with the electron velocity operator $\mathbf{v}_\mathbf{k} = \mathbf{k}/m$, and a diamagnetic term proportional to $\mathbf{A}_q^2$. We will henceforth ignore the diamagnetic term for a number of reasons. In

particular, it will not allow for hybridization with the solid-state collective modes at the level of linear response [94], and ultimately only contributes a constant contribution to the photon polarization operator. This constant is fixed by a sum rule and is uninteresting for the finite-frequency and momentum scales we are probing, especially in the presence of any finite amount of disorder [90, 120].

Note that our cavity geometry is chosen for calculation simplicity, but in real microwave cavities the transverse nature of the of photon amplitude envelope is more complicated. The effect of this is to increase the strength of the paramagnetic coupling, which we include via a phenomenological enhancement in the light-matter coupling term [92–96, 100]. Specifically, we will replace $\frac{\epsilon_0}{e^2}$ in the bare electromagnetic photon propagator with

$$\frac{\epsilon_0}{e^2} \to \frac{\epsilon_0}{X^2 e^2}$$

corresponding to an enahncement in the electric field strength of a photon mode due to, e.g. a smaller mode volume.

3.3 Hybridization

In this section we calculate the hybridization energy between the cavity photons and the BS mode of the enclosed superconducting sample. We first argue that in order to generate this coupling, we must run a supercurrent through the sample.

3.3.1 Supercurrent

It turns out that due a number of symmetries[5], the naive linear coupling between photons and the BS mode vanishes. In fact, all of these selection rules can be circumvented by applying a finite supercurrent to the s-wave condensate, a technique

[5]These symmetries include Nambu spin-symmetry, rotational symmetry, and inversion symmetry. Under spatial symmetries, the vector potential A transforms as a vector and is obviously trivial under Nambu-spin rotation. On the other hand, the Bardasis-Schrieffer vertex is off-diagonal in Nambu space and involves a d-wave vertex which does not transform as a vector.

which has already been applied to similar effect in engineering a linear coupling between photons and the Higgs mode of a superconductor [121].

We now include the effect of this external supercurrent by first applying a uniform phase gradient to the s-wave condensate, so that

$$\Delta_s = e^{-2im\mathbf{v}_S\cdot\mathbf{r}}|\Delta_s| \tag{3.5}$$

where $2m$ is the effective mass of the Cooper pair and $\mathbf{v}_S$ is the superfluid velocity in the lab-frame. This phase gradient is gauge equivalent to a uniform background supercurrent, which is seen by applying the unitary transformation $\hat{\mathcal{U}} = e^{-im\mathbf{v}_S\cdot\mathbf{r}\hat{\tau}_3}$ on the Nambu spinors. This essentially implements a Galilean transformation into the frame co-moving with the supercurrent. The action for the electrons (neglecting their interaction with collective modes) then acquires a Doppler shifting term, becoming

$$S_{\text{qp}} = \sum_p \psi_p^\dagger \left(-i\varepsilon_n + \left[\frac{1}{2m} \left(\mathbf{p} + m\mathbf{v}_S\hat{\tau}_3 \right)^2 - \mu \right] \hat{\tau}_3 + \Delta_s\hat{\tau}_1 \right) \psi_p. \tag{3.6}$$

We have ignored fluctuations of the s-wave gap and chosen the phase to be real. Doppler shifting produces two additional terms. One of these, $\frac{1}{2}m\mathbf{v}_S^2$, merely shifts the chemical potential and for $|\mathbf{v}_S| \ll v_F$ this is much smaller than the Fermi energy and will henceforth be ignored. The other term generates a linear coupling between the momentum $\mathbf{p}$ and the superfluid velocity $\mathbf{v}_S$. Notably, this is in the τ_0 channel, and so each species of quasiparticle will see an opposite shifting (similar to a Zeeman splitting would).

In addition to the speed of the supercurrent v_S we can also control the angle the current flows. In particular, an important parameter is the angle $\mathbf{v}_S$ makes with respect to the axis defined by $f_d(\phi_{\mathbf{k}})$, as depicted in the inset in Fig. 3.2. This angle is henceforth denoted θ_S. Later we will show this is another important parameter.

Upon minimal coupling to the electromagnetic vector potential, implemented as

$\mathbf{p} \to \mathbf{p} + \tau_3 \mathbf{A}$, we see the emergence of new photon-interaction vertices due to the Doppler shift.[6] In particular, we find the interaction

$$S_{\psi-A} = \sum_{k,q} \bar{\psi}_{k+\frac{q}{2}} \left(\left(\frac{\mathbf{k}}{m} \hat{\tau}_3 + \mathbf{v}_S \hat{\tau}_0 \right) \cdot \hat{\tau}_3 \frac{\mathbf{A}_q}{\sqrt{\beta \mathrm{Vol}}} \right) \psi_{k-\frac{q}{2}}. \tag{3.7}$$

As mentioned earlier factors of e, the electric charge, as well as the phenomenological electric field strength enhancement factor X [92–96, 100] are absorbed into the photon propagator. Crucially the Nambu structure for the paramagnetic and supercurrent-induced terms are different, since particle and hole velocities are shifted oppositely, ultimately allowing the coupling of the BS mode to light.

3.3.2 Mean-Field Expansion

To proceed, we make the mean-field approximation for the s-wave gap. We then obtain an effective action describing the d-wave fluctuations and their interaction with the cavity photons in terms of the Bogoliubov quasiparticles as

$$S_{\mathrm{eff}} = S_s + S_d + S_{\mathrm{cav}} + S_{\mathrm{qp}} \tag{3.8a}$$

$$S_s = \beta \mathrm{Vol} \times \frac{1}{g_s} \bar{\Delta}^s \Delta^s \tag{3.8b}$$

$$S_d = \sum_q \frac{1}{g_d} \bar{\Delta}^d_q \Delta^d_q \tag{3.8c}$$

$$S_{\mathrm{cav}} = -\frac{1}{2} \frac{\epsilon_0}{e^2 X^2} \sum_{q\alpha} A_{-q\alpha} \left((i\Omega_m)^2 - \omega^2_{\mathbf{q}} \right) A_{q\alpha} \tag{3.8d}$$

$$S_{\mathrm{qp}} = -\sum_k \bar{\psi}_k \hat{G}^{-1}_k \psi_k + \sum_{k,q} \bar{\psi}_{k+\frac{q}{2}} \left(\hat{A}_{k,q} + \hat{\Delta}^d_{k,q} \right) \psi_{k-\frac{q}{2}}, \tag{3.8e}$$

[6] Alternatively, this interaction can be obtained by linearizing the diamagnetic term, which is quadratic in $\mathbf{A} = \mathbf{A}_1 + m\mathbf{v}_S$, about the homogeneous supercurrent. This is because the supercurrent can either be ascribed to the canonical momentum of the Cooper pairs or to a homogeneous gauge potential. Viewed in this way, the linear coupling we generate is essentially a Raman process with a probe field being provided by the twisted boundary conditions of the pair condensate.

with $\hat{G}_k^{-1} = (i\epsilon_n - \mathbf{k}\cdot\mathbf{v}_S)\hat{\tau}_0 - \xi_{\mathbf{k}}^S\hat{\tau}_3 - \Delta^s\hat{\tau}_1$ the inverse Gor'kov Green's function and the d-wave fluctuation and photon vertices

$$\hat{\Delta}_{k,q}^d = \frac{1}{\sqrt{\beta \mathrm{Vol}}} f_d(\phi_k)\left[\hat{\tau}^\dagger \Delta_q^d + \bar{\Delta}_{-q}^d \hat{\tau}\right] \tag{3.9a}$$

$$\hat{A}_{k,q} = \frac{1}{\sqrt{\beta \mathrm{Vol}}} \mathbf{A}_q \cdot \left(\frac{\mathbf{k}}{m}\hat{\tau}_0 + \mathbf{v}_S\hat{\tau}_3\right). \tag{3.9b}$$

In the above we have restricted to the case of a homogeneous, static, real s-wave order parameter, which we treat at the saddle-point level in the absence of $\vec{A}$ and Δ^d but in the presence of the supercurrent, in keeping with the approximation that Δ^s is unaffected by d-wave fluctuations and photons.

We can now integrate out the fermions and expand the resulting "trace log" to second order in $\hat{\Delta}^d$ and $\hat{A}$, giving

$$S_{\text{eff}} = S_d + S_A + S_{d-A}. \tag{3.10}$$

S_d describes the d-wave fluctuations, S_A describes the cavity photons (including the polarization due to the superconductor), and S_{d-A} describes the quasiparticle-mediated interaction between the fluctuations and photons. We now go in to these parts in more detail.

3.3.3 Bardasis-Schrieffer Mode

Since the d-wave fluctuations have much greater kinetic mass than photons, we approximate them with a flat dispersion: their energy in the limit $\vec{q} \to 0$. Additionally, we will evaluate the collective mode dispersion relation within the quasiclassical ξ approximation, which means we neglect energy dependence of the density of states and drop all terms which are odd in ξ. Furthermore, we will split Δ_q^d into its real and imaginary components, $\Delta_q^d = r_q + id_q$ with real fields $r_q = \bar{r}_{-q}$

and $d_q = \bar{d}_{-q}$. The real mode is within the Bogoliubov quasiparticle continuum, and is therefore overdamped [16, 119]. It also remains decoupled from photons despite the supercurrent so we do not consider it further. The imaginary mode d_q is the in-gap Bardasis-Schrieffer mode. We approximate it as a flat band which is described by the effective action at Random Phase Approximation (RPA) level

$$S_d = \sum_q d_{-q} \left[\frac{1}{g_d} + \int \frac{d^2k}{(2\pi)^2} f_d(\phi_{\mathbf{k}})^2 \frac{2\lambda_{\mathbf{k}}\, \delta n_{\mathbf{k}}}{(i\Omega_m)^2 - (2\lambda_{\mathbf{k}})^2} \right] d_q, \tag{3.11}$$

where $q = (i\Omega_m, \mathbf{q})$ is the four-momentum of the collective mode, $\lambda_{\mathbf{k}} = \sqrt{\left(\xi^S_{\mathbf{k}}\right)^2 + \Delta^2}$ is the quasiparticle energy in the co-moving frame, $\delta n_{\mathbf{k}} = n_F(E^-_{\mathbf{k}}) - n_F(E^+_{\mathbf{k}})$, where n_F is the Fermi function, and $E^\pm_{\mathbf{k}} = \mathbf{k}\cdot\mathbf{v}_S \pm \lambda_{\mathbf{k}}$ are the Doppler-shifted locations of the poles for Bogoliubov particles and holes, respectively.

3.3.4 Photon Mode

In addition to the coupling to the Bardasis-Schrieffer mode, the photon also receives a polarization contribution from the superconductor which renormalizes the RPA propagator. The action in this case consists of the of the empty cavity action S_{cav} plus a self-energy term due to the superconductor, so that

$$S_A = -\frac{1}{2} \sum_{q,\alpha,\beta} A_{\alpha,-q} \left[\frac{\epsilon_0}{e^2 X^2} \left((i\Omega_m)^2 - \omega_q^2 \right) \delta_{\alpha\beta} - \Pi_{\alpha\beta}(q) \right] A_{\beta,q}. \tag{3.12}$$

The polarization matrix $\Pi_{\alpha\beta,q}$ encodes the linear response of the superconductor to the electromagnetic field. The detailed structure of this can be found in Appendix C. Importantly, translational invariance implies it is only a function of the photon four-momentum $q = (i\Omega_m, \mathbf{q})$ and since the two polarizations of the photon are linearly independent they form a basis for vectors in the $x-y$ plane. As such, the polarization tensor is a two-by-two matrix in the basis of the polarization vectors.

We note however that the rotational symmetry which is normally present in a 2DEG is absent due to both the d-wave form factor and the orientation of the supercurrent. It turns out that only the component of A along the direction of the supercurrent receives a non-negligible self-energy (see Appendix C). Therefore, it will be convenient to calculate the components of $\Pi_{\alpha\beta}$ in the basis dictated by the orientation of the supercurrent.

3.3.5 Hybridization Term

Finally, we calculate the hybridization between the photon and the BS mode, which is encapsulated in the term in the effective action

$$S_{d-A} = \sum_{q,\alpha} \int \frac{d^2k}{(2\pi)^2} f_d(\phi_{\mathbf{k}}) \frac{i\Omega_m}{(i\Omega_m)^2 - (2\lambda_k)^2} \frac{\delta n_{\mathbf{k}}}{\lambda_{\mathbf{k}}} \left(\mathbf{v}_S \cdot \vec{\epsilon}_{\alpha,q}\right) i\Delta \left(A_{\alpha,q}\, d_{-q} - A_{\alpha,-q}\, d_q\right). \tag{3.13}$$

Note this is linear in the supercurrent $\mathbf{v}_S$, which is consistent with the known result that the BS mode does not normally couple linearly to light. As a consequence, the BS mode only couples to the component of the vector potential parallel to the supercurrent.

The action for all three of the bosonic modes of interest can then compactly be written in terms of a hybrid inverse Green's function

$$S_{\text{eff}} = \frac{1}{2} \sum_q (d_{-q}, A_{\alpha,-q}) \begin{pmatrix} D^{-1}_{\text{BS},q} & g_{\alpha,q}\delta_{\alpha\beta} \\ g^*_{\alpha,q}\delta_{\alpha\beta} & D^{-1}_{\alpha\beta,q} \end{pmatrix} \begin{pmatrix} d_q \\ A_{\beta,q} \end{pmatrix}, \tag{3.14}$$

with sums over repeated indices and with $D^{-1}_{\text{BS},q}$, $D^{-1}_{\alpha\beta,q}$, and $g_{\alpha,q}$ defined implicitly through Eqs. (3.11)–(3.13). A more intuitive description can be obtained by first making a harmonic approximation to the BS action: continue D^{-1}_{BS} to complex frequency, expand around the saddle point solution Ω_{BS}, then restrict back to imaginary frequency. In our clean model Ω_{BS} is purely real, so the BS mode is

undamped. We then expand in terms of BS and photon mode operators, $d_q = (b_q + \bar{b}_{-q})/\sqrt{2K\Omega_{\rm BS}}$ and $A_{\alpha,q} = (a_{\alpha,q} + \bar{a}_{\alpha,-q})/\sqrt{2\omega_q}$, where K is a constant coming from the harmonic expansion. We make the standard approximation of dropping the counter-rotating terms $(aa, \bar{a}\bar{a})$ – an approximation we verify post-hoc – and perform a change of basis from photon polarizations to components parallel and perpendicular to the supercurrent. Inside the coupling and photon terms, we analytically continue to real frequency $i\Omega_m \to \Omega + i0$, then expand around relevant frequencies. The imaginary parts exactly vanish, and the action becomes

$$S_{\rm eff} \approx \sum_q \left(\bar{b}_q, \bar{a}_q^{\parallel}, \bar{a}_q^{\perp}\right) \left(-i\Omega_m \check{\mathbb{1}} + \check{H}_{\mathbf{q}}^{\rm eff}\right) \begin{pmatrix} b_q \\ a_q^{\parallel} \\ a_q^{\perp} \end{pmatrix}, \tag{3.15}$$

now written in terms of an effective Hamiltonian

$$\check{H}_{\mathbf{q}}^{\rm eff} = \begin{pmatrix} \Omega_{\rm BS} & g_{\mathbf{q}} & 0 \\ g_{\mathbf{q}} & \omega_{\mathbf{q}} + \Pi_{\mathbf{q}}^S & 0 \\ 0 & 0 & \omega_{\mathbf{q}} \end{pmatrix}, \tag{3.16}$$

where $q = |\mathbf{q}|$, $\Pi_{\mathbf{q}}^S$ is a self-energy shift of the photon mode which is polarized parallel to the supercurrent, coming from a supercurrent-dependent term in $\Pi_{\alpha\beta,q}$, and

$$g_{\mathbf{q}} = v_S \Delta \sqrt{\frac{2\Omega_{\rm BS}}{LK\omega_{\mathbf{q}}}} \int_{\mathbf{k}} \frac{f_d(\phi_{\mathbf{k}})}{\lambda_{\mathbf{k}}} \frac{\delta n_{\mathbf{k}}}{\Omega_{\rm BS}^2 - (2\lambda_{\mathbf{k}})^2}. \tag{3.17}$$

We keep only to lowest order in $|\mathbf{q}|$. Only one photon mode hybridizes with the BS mode in the Hamiltonian approximation. The photon mode which couples and the BS mode can be made resonant by tuning parameters of the system, most straightforwardly the cavity size L, allowing them to strongly hybridize. For more details about the evaluation of these terms, see Appendix C.

3.4 Results

Having derived the hybridization term between the photons and BS mode, we now present the results and discuss them. Since BS modes are a result of competing s- and d-wave instabilities, they are most prominent in systems with nearly degenerate interactions in the two channels. This is in fact the case in many iron-based superconductors [122–125], where BS modes have been experimentally detected. We thus use these systems as guides in our choice of parameters for calculations.

We set the Fermi energy $\epsilon_F = 100$ meV, the effective mass $m^* = 4m_e$ [7], where m_e is the electron mass, and critical temperature $T_c = 35$ K. We put $1/g_d - 1/g_s = 0.1\nu_F$, where $\nu_F = m^*/2\pi$ is the density of states, and tune the size of the cavity L so that $\omega_0 = \pi/L = 0.96\,\Omega_{\mathrm{BS}}(\theta_S = 0)$, putting photons and the BS mode very near resonance. Finally, we set the phenomenological coupling enhancement to $X = 10$, although enhancements of $X = 10^2$ or greater have been predicted in similar cavity systems [92–96, 100].

We first consider the dependence of coupling strength g_q on temperature, superfluid velocity v_S, and supercurrent angle θ_S, as shown in Fig. 3.2. The coupling is mediated by thermally excited quasiparticles and so vanishes for $T \to 0$. It also vanishes for $T \to T_c$ since $\Delta \to 0$. The result is a unique maximum of $g(T)$ at an intermediate temperature, $T_{\max} \approx 0.42T_c$, which we use for all other computations. Similarly, g vanishes for small v_S — this can be verified by expansion of $\delta n_{\mathbf{k}}$ — and also as v_S approaches a value corresponding to the critical current, where the superconducting state vanishes. We set $v_S = 0.9\Delta(v_S = 0)/k_F$ in our calculations, near the value giving the maximum coupling but not too near the critical value [8].

[7] In the quasiclassical approximation the value of the effective mass cancels everywhere, since only $v_S \propto 1/k_F \propto 1/\sqrt{m^*}$, $K \propto \nu = m^*/2\pi$, and $\sum_{\mathbf{k}} \sim \nu_F \int d\xi$ depend on it. Therefore, the choice of effective mass is mostly unimportant.

[8] The value $\Delta(v_S = 0)/k_F$ yields an approximate critical current consistent with values measured in iron-based systems, though in type II materials the current is limited by vortex pinning rather than condensate depletion [126, 127].

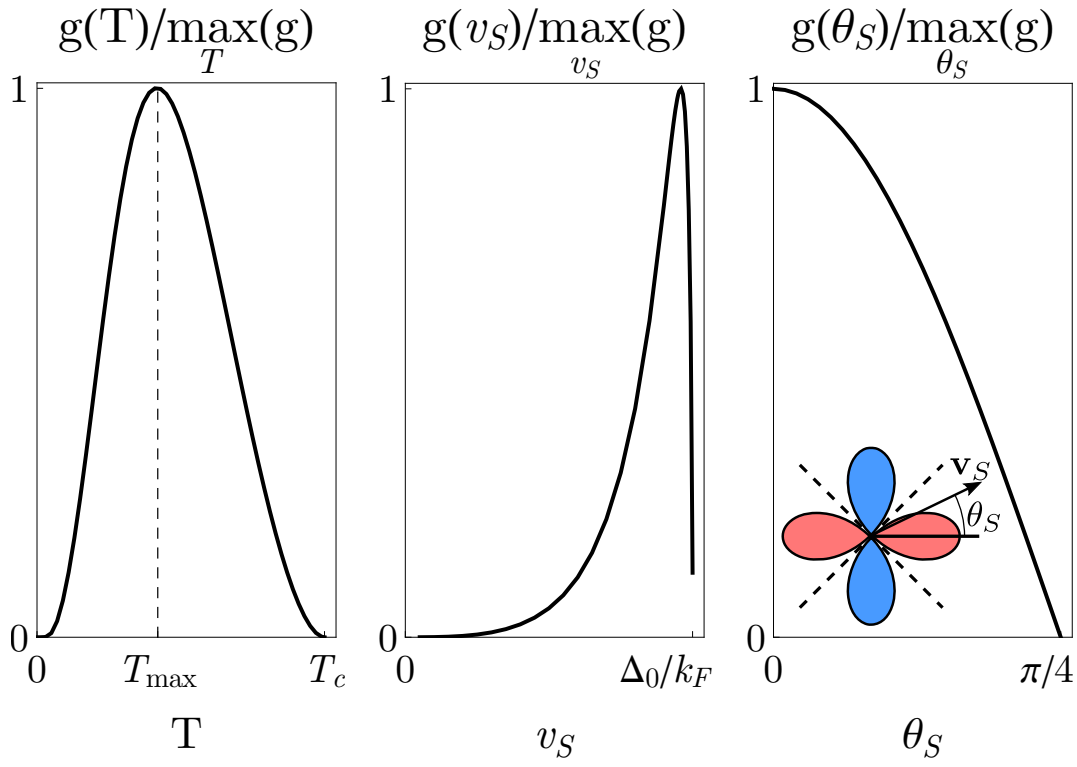

Figure 3.2: The hybridization matrix element g in the effective Hamiltonian as a function of temperature, superfluid velocity, and θ_S, the angle between the direction of the supercurrent and the axis defined implicitly by the d-wave form factor $f_d(\phi_k)$, all scaled by their respective maxima. (Left) $g(T)$ is maximized for a temperature $T_{\max} \approx 0.42T_c$. (Center) $g(v_S)$ is sharply peaked for large superfluid velocity around $v_S \approx 0.96\Delta(v_S = 0)/k_F$. (Note, $\Delta_0 \equiv \Delta(v_S = 0)$.) (Right) $g(\theta_S)$ is maximal for $\theta_S = m\pi/2$, $m \in \mathbb{Z}$, and vanishes when the supercurrent runs along a node of f_d, $\theta_S = (2m + 1)\pi/4$. *Inset* — the orientation of the supercurrent with respect to the d-wave form factor. The color of the lobes gives the relative sign of f_d for different angles, and the dashed lines are the nodes where $f_d = 0$. The plots use $T = T_{\max}$, $v_S = 0.9\Delta(v_S = 0)/k_F$, and $\theta_S = 0$ where applicable, and fixed detuning $\omega_0 = 0.96\Omega_{\mathrm{BS}}$.

Dependence on the supercurrent angle θ_S comes through the d-wave form factor. The coupling is strongest when the supercurrent is along an antinode of the form factor – $\theta_S = m\pi/2$, $m \in \mathbb{Z}$ – and vanishes when the supercurrent is along a node – $\theta_S = (2m+1)\pi/4$. We use $\theta_S = 0$ for all other calculations.

To obtain the polariton modes we both directly solve for the poles of the hybridized Green's function (3.14) and calculate the eigenvalues of the effective Hamiltonian (3.16), which can be diagonalized analytically C. A discussion of the method used to numerically calculate the roots of the dispersion relation can be found in Appendix D. The results of both approaches are in excellent agreement; the dispersions are plotted for both methods in Fig. 3.3. One of the photon modes can be made to strongly hybridize with the BS mode, while the other "dark" photon remains distinct. This is made especially clear by examining the BS component of the eigenvectors of the effective Hamiltonian, as shown in Fig. 3.4. Because the strength of the hybridization is controlled exclusively by g, any of the parameters on which it depends, namely T, v_S, or θ_S, can be used to directly control the strength of the effect.

In this work we have shown that driving a supercurrent through a superconductor in a planar microcavity leads to hybridization of cavity photons with a collective mode of the superconductor. In particular two polariton bands form which have significantly mixed character. This provides a means for observation and control of the Bardasis-Schrieffer mode, and, as for exciton-polaritons, these dispersions could in principle be measured with k-space imaging of the photonic component of the polariton states [86]. The nature of the construction allows for tuning of the hybridization strength, and therefore the polariton states, *in situ* through the externally applied supercurrent.

We speculate that the condensation observed in exciton-polariton systems [104–106] suggests proper driving of these superconductor-polariton modes could lead to

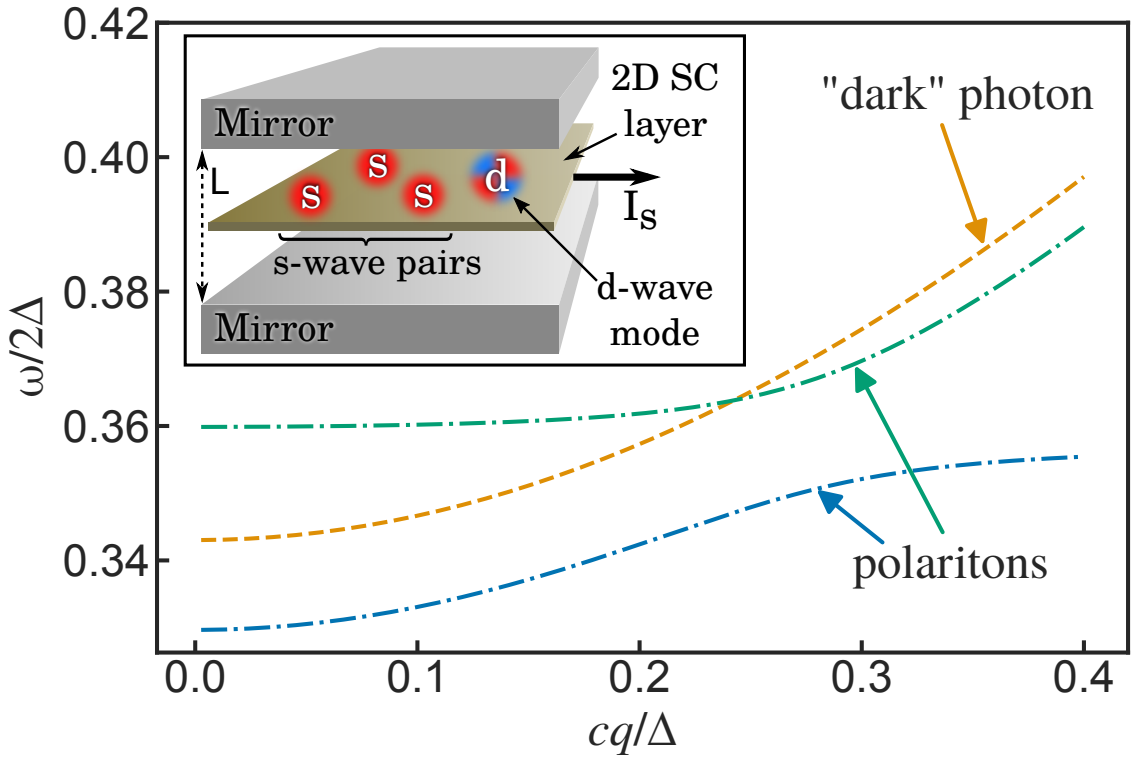

Figure 3.3: The dispersion of the Bardasis-Schrieffer-polariton modes (dot-dashed), calculated both numerically and with a simplified analytic method C – the two give visually identical results. An external supercurrent causes the BS mode and cavity photons to hybridize, and the polariton states have significant overlap with each. The "dark" photon mode (dashed) remains decoupled. The splitting of otherwise degenerate photon modes is a result of a supercurrent-induced self-energy contribution. Temperature and supercurrent angle are chosen to maximize hybridization (see Fig. 3.2). *Inset* — schematic of the system: a 2-dimensional superconductor with an applied supercurrent I_S at the center of a planar cavity.

their condensation and the formation of a non-equilibrium $s \pm id$ superconducting state.[9] There is reason to suspect that condensation is a reasonable prospect; interactions giving thermalization arise at quartic order in perturbation theory, and the polariton lifetime is set by the cavity photon lifetime — the BS mode is in-gap and

[9]In addition to the argument based on Landau damping of the real part of the d-wave mode, we may understand the relative phase of $\pm\pi/2$ as originating from the fact that a mixed gap of the form $s \pm id$ does not break any additional spatial symmetries and has a larger gap, since the two terms add exactly in quadrature to produce $|\Delta_{\mathbf{k}}^{s\pm id}|^2 = |\Delta^s|^2 + |f_{\mathbf{k}}^d|^2|\Delta^d|^2$. On the other hand, in the $s \pm d$ states, the two gap symmetries compete with each other since they add coherently to produce $|\Delta_{\mathbf{k}}^{s\pm d}|^2 = |\Delta^s \pm f_{\mathbf{k}}^d \Delta^d|^2$. This will not only break the C_4 rotational symmetry but will also reduce the effective gap the quasiparticles see. For a more complete treatment, see e.g. Ref. [128]

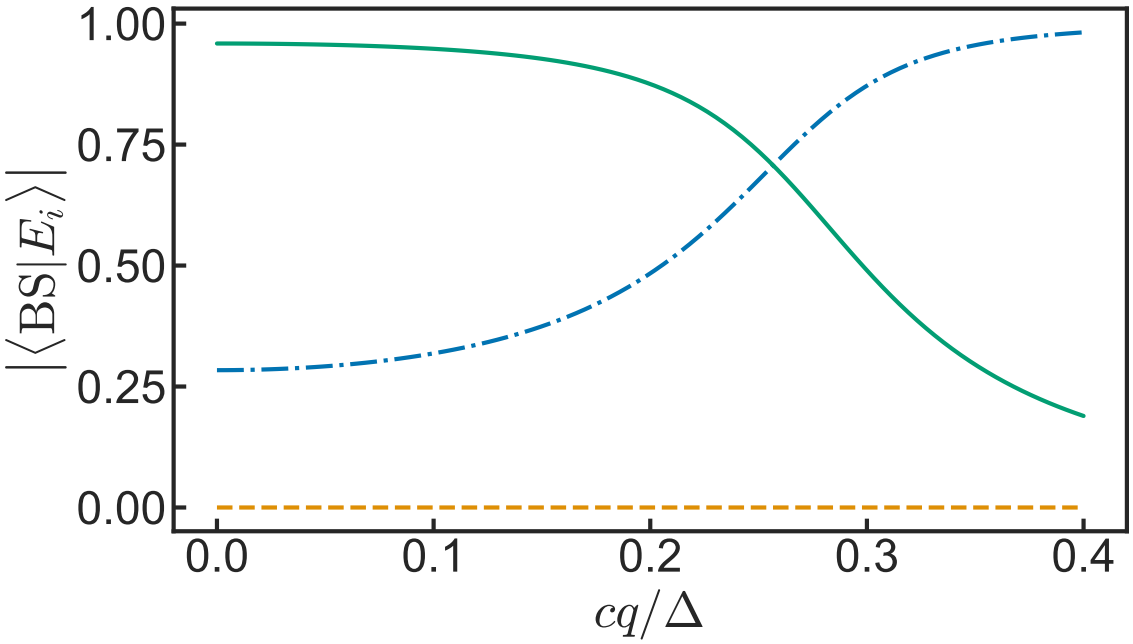

Figure 3.4: The Bardasis-Schrieffer component of the eigenvectors of the effective Hamiltonian, Eq. (3.16) C. The upper (solid) and lower (dot-dashed) polaritons have significant photon and Bardasis-Schrieffer character, indicating strong hybridization between the systems. One can also clearly see the "dark" photon mode (dashed) which does not hybridize with the superconductor's collective mode.

therefore undamped in this clean model. For a high enough Q-factor it is in principle possible for polaritons to thermalize before decaying, allowing for a transient quasi-thermal ensemble. More work must be done, however, before definitive statements can be made about a condensed state, especially regarding spontaneous coherence of the condensate. Finally, we note that finite polariton density with coherence imposed externally, e.g. from a coherent drive, would produce a non-equilibrium state with $s \pm id$ character, which one would expect to be distinct in nature from a thermodynamic $s \pm id$ state.

Chapter 4: Evanescent modes near analogue black-hole horizons in Bose-Einstein condensates

This chapter is based on the publication Curtis, Refael, and Galitski [129].

4.1 Introduction

The existence of black holes was one of the first surprising and novel predictions to emerge from Einstein's geometric theory of gravity. Though initially their existence was a point of contention, it is now well established that black holes exist and play a formative role in the large-scale dynamics of the universe [130]. The interplay between quantum mechanics and these exotic spacetime solutions has uncovered a number of important open problems, with fundamental consequences for theories of quantum gravity an cosmology [131]. Perhaps nowhere is this more evident than in Stephen Hawking's 1974 semiclassical calculation which predicted that black holes constantly emit a flux of thermal quanta [24, 25]. Consequences of this thermal radiation have since raised a number of fundamental questions regarding the interplay of quantum mechanics and gravity, including what is known as the black hole information paradox [132, 133].

Though it is grounded in widely accepted physical principles, observation of astrophysical Hawking radiation seems to be impossible in the near-future at least. In 1981, W.G. Unruh proposed that in lieu of observation of Hawking radiation by an astrophysical black hole, the process of Hawking radiation and black-hole evaporation could be effectively simulated in a laboratory [17]. This proposal, expanded upon extensively by G.E. Volovik as pertaining to superfluid Helium [134], relies on the observation that at long wavelengths sound waves propagating through a fluid are described by the same equations of motion as a scalar boson propagating

through a curved spacetime [20–22, 135]. A simple model which illustrates this physics is that of a BEC, where the condensate flow plays the role of the spacetime metric while the quantum fluctuations (e.g. phonons) are mapped onto matter fields residing in this spacetime. If the condensate velocity exceeds the local speed of sound this effective spacetime develops an event horizon, forming a sonic black/white hole. In exact analogy with Hawking's calculations for an astrophysical black hole, the sonic horizon formed in a condensate should then emit a thermal flux of phonons.

Since Unruh's initial observation, there have been numerous proposals for testing-by-analogy various predictions of semiclassical gravity and cosmology using table-top scale experiments. These employ a range of media including liquid Helium [134, 136, 137], trapped BECs and ultra-cold atoms [18, 135, 138–145], electromagnetic waveguides [146], spintronic materials [147, 148], exciton-polariton condensates [111], non-linear optical media [149, 150], and even water wave-tanks, where signatures of Hawking radiation still manifest themselves through the classical correlation functions [151]. Recent experiments by Jeff Steinhauer have purportedly generated and observed signatures of self-amplifying Hawking radiation [152, 153] and its entanglement [154] in an ultra-cold BEC. Crucially, these experiments do not attempt to detect the Hawking radiation by directly measuring its temperature (which is typically too small to effectively measure), but instead measure non-local density-density correlations which arise due to the Hawking emission [155–157]. These observables, which may be measured in the lab, cannot be measured for real black holes since they involve measuring correlations across the event horizon.

It is an interesting question to consider how all these disparate theories, none exhibiting true Lorentz invariance, differ in their low-energy effective descriptions. Often, the absence of Lorentz invariance at the UV scale manifests itself through the quasiparticle dispersion relations which exhibit either superluminal [158–161] or subluminal propagation at higher momenta [140, 143, 162–168]. At low energies,

all models seem to predict the same thermal occupation function first obtained by Hawking [141, 169–171]. Deviations become apparent only at higher energies/momenta, where departures from this thermal occupation can be observed [141, 160, 163, 170].

In this work we will consider a BEC model of analogue gravity, with the goal being to study how the emergent spacetime responds to regions of large effective spacetime curvature. A major conclusion of ours is that when the background metric varies over a sufficiently abrupt length scale it becomes possible to observe the emergence of evanescent field modes outside the sonic event horizon, which in turn can effect local observables. To motivate this, consider identifying a sonic black hole with an actual astrophysical black hole of equal Hawking temperature. In a Schwarzschild black hole, the temperature T_{astro} (in units with $\hbar = k_B = 1$) is related to the mass M by Hawking's formula

$$T_{\text{astro}} = \frac{c^3}{8\pi G_N M}$$

where c is the speed of light and G_N is the Newton gravitational constant. For a sonic black hole, we invoke Unruh's result [17], whereby we find that the temperature of the sonic black hole T_{sonic} is related to the fluid velocity gradient by

$$T_{\text{sonic}} = \frac{1}{2\pi}\left|\frac{\partial v}{\partial r}\right|_{\text{horizon}}$$

where the derivative is understood as being taken in the direction normal to the event horizon, at the horizon. Thus, identifying these two temperatures implies that the mass of the black hole is related to the inverse of the velocity gradient. If we wish to study the analogue of black holes which are evaporating towards the Planck mass scale, we must understand what happens to the sonic horizon as the velocity gradient increases towards the UV dispersion scale. In the sonic black hole model,

large flow gradients may be modeled most simply by considering a step-like system. In fact, such configurations have been studied before [157, 160, 171], though typically the emphasis is placed on obtaining the form of the universal low-energy Hawking distribution function, which is by now well understood. In this work, we will instead primarily focus on the near-horizon physics, which has seen comparatively little attention due to its generically non-universal nature.

Having motivated the step-like model, the remainder of this paper will be structured as follows. In Section 4.2, we will introduce our model and the associated Bogoliubov-de Gennes formalism used to analyze it. We will then proceed on to consider first the case of a homogeneous flow, presented in Section 4.3. In Section 5.4 we will set up the step-like system and solve it, extracting both the S-matrix and the actual eigenfunctions of the problem, which contain the evanescent modes. We will study the properties of these evanescent modes in more detail in Section 4.5, before moving on to the Conclusion in Sec. 5.6, where we highlight some interesting consequences and potential future avenues of research.

4.2 Formalism

We begin our discussion by considering a model for weakly interacting spinless bosons described by the Hamiltonian

$$\check{H} = \int d^d r \left(\frac{1}{2m} \nabla \check{\Psi}^\dagger \cdot \nabla \check{\Psi} - \mu \check{\Psi}^\dagger \check{\Psi} + \frac{1}{2} g \check{\Psi}^\dagger \check{\Psi}^\dagger \check{\Psi} \check{\Psi} \right), \tag{4.1}$$

where d is the spatial dimension, $g > 0$ is the s-wave interaction constant, and μ is the chemical potential [172]. Here and throughout we use units in which $\hbar = k_B = 1$ and we will distinguish between quantum many-body operators and single-particle differential operators with the use of a check ($\check{}$) and hat ($\hat{}$), respectively. The only

non-trivial equal-time commutator for the boson field operators $\check{\Psi}(\mathbf{r},t)$ is

$$[\check{\Psi}(\mathbf{r},t),\check{\Psi}^\dagger(\mathbf{r}',t)]=\delta^d(\mathbf{r}-\mathbf{r}').$$

The resultant many-body dynamics may be described by the Heisenberg equation of motion

$$\left(i\partial_t+\frac{1}{2m}\nabla^2+\mu-g\check{\Psi}^\dagger\check{\Psi}\right)\check{\Psi}=0. \tag{4.2}$$

Next, we partition the operator field $\check{\Psi}$ into a classical condensate $\psi=\sqrt{\rho}e^{i\Theta}$ and fluctuations about the condensate via

$$\check{\Psi}(\mathbf{r},t)=\psi(\mathbf{r},t)\left(\check{\mathbb{1}}+\check{\phi}(\mathbf{r},t)\right). \tag{4.3}$$

Note the fluctuations are rescaled by the local condensate so that the equal time commutator for the ϕ field reads

$$[\check{\phi}(\mathbf{r},t),\check{\phi}^\dagger(\mathbf{r}',t)]=\frac{1}{\rho(\mathbf{r},t)}\delta^d(\mathbf{r}-\mathbf{r}'). \tag{4.4}$$

Next, we define the superfluid velocity $\mathbf{v}=\frac{1}{m}\nabla\Theta$, in terms of which the mean-field equations of motion become

$$\partial_t\rho+\nabla\cdot(\rho\mathbf{v})=0 \tag{4.5a}$$

$$\mu-\partial_t\Theta-\frac{1}{2}m\mathbf{v}^2-g\rho+\frac{1}{2m\sqrt{\rho}}\nabla^2\sqrt{\rho}=0. \tag{4.5b}$$

We insert the ansatz (4.3) into the Heisenberg equation and apply the mean-field equations of motion (4.5). To linear order in the operator fields $\check{\phi},\check{\phi}^\dagger$ we get the Bogoliubov-de Gennes (BdG) equation

$$\left(i\partial_t+i\mathbf{v}\cdot\nabla+\frac{1}{2m\rho}\nabla\cdot\rho\nabla-g\rho\right)\check{\phi}-g\rho\check{\phi}^\dagger=0. \tag{4.6}$$

This is written compactly in terms of the Nambu spinor $\check{\Phi} = \left(\check{\phi}, \check{\phi}^\dagger\right)^T$ and the Nambu Pauli matrices $\tau^1, \tau^2, \tau^3, \tau^0$ as $\hat{K}_{\text{BdG}}\check{\Phi} = 0$ with the BdG kernel given by

$$\hat{K}_{\text{BdG}} = (i\partial_t + i\mathbf{v}\cdot\nabla)\,\tau^3 - \left(g\rho - \frac{1}{2m\rho}\nabla\cdot\rho\nabla\right)\tau^0 - g\rho\tau^1. \tag{4.7}$$

Additionally, the Nambu spinor has the particle-hole conjugation symmetry

$$\overline{\check{\Phi}}(\mathbf{r},t) \equiv \tau^1\check{\Phi}(\mathbf{r},t)^\dagger = \check{\Phi}(\mathbf{r},t). \tag{4.8}$$

Finally, we have the equal time canonical commutator

$$[\check{\Phi}_\alpha(\mathbf{r},t), \check{\Phi}^\dagger_\beta(\mathbf{r}',t)] = \frac{1}{\rho(\mathbf{r},t)}\delta^d(\mathbf{r}-\mathbf{r}')[\tau^3]_{\alpha\beta} \tag{4.9}$$

where α, β explicitly index the Nambu components. Note that the presence of τ_3 reflects the fact that bosonic BdG dynamics generate symplectic transformations, whereas fermionic dynamics generate unitary dynamics.

We may verify that, provided the background condensate satisfies the continuity equation (4.5), the quasiparticle charge

$$\check{\mathcal{Q}}_{\text{qp}}(t) = \int d^d r\rho(x)(\check{\Phi}^\dagger(x))^T\tau^3\check{\Phi}(x) \tag{4.10a}$$

$$\check{\mathcal{J}}_{\text{qp}}(x) = \rho(x)(\check{\Phi}^\dagger(x))^T\left[\mathbf{v}(x)\tau^3 + \frac{-i}{2m}\overleftrightarrow{\nabla}\right]\check{\Phi}(x) \tag{4.10b}$$

are conserved under the BdG equations of motion (here the left-right over-arrow has the standard definition introduced in previous chapters). Throughout we will carefully distinguish between Hermitian/complex conjugation (which acts element-wise on the spinor components) and Nambu spinor tranposition (which exchanges spinor columns and rows).

We will further restrict our analysis to systems which have time-translational

invariance. In this case, the lab-frame energy ω is a good quantum number and the BdG kernel takes the form

$$\hat{K}_{\mathrm{BdG}}(\omega) = \tau^3 \left(\omega - \hat{\Omega}_{\mathrm{BdG}}\right), \tag{4.11}$$

which effectively defines the BdG Hamiltonian as the linear differential operator

$$\hat{\Omega}_{\mathrm{BdG}} = \tau^3 \left(-\frac{1}{2m\rho}\nabla\cdot\rho\nabla + g\rho\right) + i\tau^2 g\rho - i\mathbf{v}\cdot\nabla. \tag{4.12}$$

In general, the operator $\hat{\Omega}_{\mathrm{BdG}}$ may have complex energy eigenvalues, leading to dynamical instabilities [159, 168, 172, 173]. Though potentially interesting, we will assume that our system does not exhibit these instabilities and that the energy eigenvalues are real.

In order to describe the many-body quantum dynamics of the system, we will first obtain the classical normal modes of the BdG Hamiltonian. To produce an expansion for the operator $\check{\Phi}$ we will then second-quantize these classical modes. Utilizing conservation of the charge defined in Eqn. (4.10), we define a conserved pseudo-inner product [141, 158, 174]

$$(F, G) = \int d^d r \rho(\mathbf{r}) F^{*T}(\mathbf{r}) \tau^3 G(\mathbf{r}), \tag{4.13}$$

where F and G are two c-number spinor fields. This product obeys the properties

$$\begin{aligned}
(F, \tau^1 G) &= -(\tau^1 F, G) \\
(F, \tau^2 G) &= -(\tau^2 F, G) \\
(F, \tau^3 G) &= +(\tau^3 F, G) \\
(F, G)^* &= (G, F) = (F^*, G^*).
\end{aligned} \tag{4.14}$$

Due to the presence of τ^3 this is not a *bona fide* inner product, since we may have

$(F,F) < 0$ for some modes.

The sign of the norm (F,F), as we will now explain, is closely connected to the creation and annihilation of particles. To see this, we construct a time-dependent many-body "wavepacket" operator

$$\check{\mathfrak{a}}_t[F] \equiv \left(F, \check{\Phi}(t)\right) = \int d^d r \rho(\mathbf{r}) F^{*T}(\mathbf{r}) \tau^3 \Phi(\mathbf{r},t) \tag{4.15}$$

from the c-number spinor F. The Hermitian conjugate of this operator may be shown to be

$$\check{\mathfrak{a}}_t^\dagger[F] = \check{\mathfrak{a}}_t[-\tau^1 F^*] = \check{\mathfrak{a}}_t[-\overline{F}]. \tag{4.16}$$

In this sense, the creation operator for wavepacket F is equivalent to the annihilation operator for the conjugate wavepacket $\overline{F}$, up to a minus sign. Similarly, the equal-time commutation relations for two wavepacket operators are

$$\left[\check{\mathfrak{a}}_t[F], \check{\mathfrak{a}}_t^\dagger[G]\right] = (F,G)\,. \tag{4.17}$$

Thus, if $(F,F) > 0$, $\check{\mathfrak{a}}_t[F]$ is a canonical annihilation operator and if $(F,F) < 0$, it is a creation operator.

Evolving these operators in time may now be performed by employing the BdG kernel since

$$i\frac{d}{dt}\check{\mathfrak{a}}_t[F] = \left(F, i\partial_t \check{\Phi}(t)\right) = \left(F, \hat{\Omega}_{\text{BdG}}\check{\Phi}(t)\right).$$

We now observe that with respect to this inner product, the BdG Hamiltonian obeys $\left(F, \hat{\Omega}_{\text{BdG}} G\right) = \left(\hat{\Omega}_{\text{BdG}} F, G\right)$, provided we respect the stationary-flow condition $\nabla \cdot (\rho \mathbf{v}) = 0$. Using this property, we have

$$i\frac{d\check{\mathfrak{a}}_t[F]}{dt} = \check{\mathfrak{a}}_t[\hat{\Omega}_{\text{BdG}} F]. \tag{4.18}$$

In particular, if we consider an energy eigenspinor W_ω with eigenvalue ω, then we can solve Eqn. (4.18) with

$$\check{\mathfrak{a}}_t[W_\omega] = e^{-i\omega t}\check{\mathfrak{a}}[W_\omega] \tag{4.19}$$

from which we may obtain, e.g. the retarded and time-ordered correlation functions.

We may restrict ourselves to looking for only positive-frequency modes $W_{\omega\nu}$ (with ν indexing different degenerate modes) since the BdG Hamiltonian obeys the symmetry

$$\overline{\hat{\Omega}_{\rm BdG}} \equiv \tau^1\hat{\Omega}^*_{\rm BdG}\tau^1 = -\hat{\Omega}_{\rm BdG}. \tag{4.20}$$

Thus up to a linear transformation amongst the degenerate eigenmodes, the mode with eigenvalue $-\omega$ is the conjugate of the mode with eigenvalue $+\omega$. By judiciously choosing the basis elements $W_{\omega\nu}$ in each subspace, we can ensure that

$$W_{-\omega\nu} = -\overline{W}_{\omega\nu} \Leftrightarrow \check{\mathfrak{a}}_t[W_{-\omega\nu}] = \check{\mathfrak{a}}^\dagger_t[W_{\omega\nu}]. \tag{4.21}$$

Rather than continue to analyze the problem at a general, abstract level, it will be beneficial to see how these ideas are applied to specific problems. In particular, we will begin by considering the case of a homogeneous condensate, which may also be solved by means of the standard Bogoliubov transformation [1, 172]. We will then move on to consider cases where the condensate possesses an event horizon.

4.3 Homogeneous Condensate

We begin by consider a translationally invariant stationary condensate. The BdG Hamiltonian is diagonalized in momentum space by the plane wave eigenmodes

$$W_{\mathbf{k}\sigma}(\mathbf{r}) = w_{\mathbf{k}\sigma}e^{i\mathbf{k}\cdot\mathbf{r}}, \tag{4.22}$$

where σ indexes independent modes with the same momentum. The BdG Hamiltonian is now a 2×2 matrix in momentum space which reads

$$\Omega_{\text{BdG}}(\mathbf{k}) = \tau^0 \mathbf{v} \cdot \mathbf{k} + \tau^3 \left(\frac{\mathbf{k}^2}{2m} + g\rho \right) + i\tau^2 g\rho. \tag{4.23}$$

At fixed energy $\omega > 0$ we must solve the equation

$$\left[\tau^0 \mathbf{v} \cdot \mathbf{k} + \tau^3 \left(\frac{\mathbf{k}^2}{2m} + g\rho \right) + i\tau^2 g\rho \right] w_{\mathbf{k}\sigma} = \omega w_{\mathbf{k}\sigma} \tag{4.24}$$

for $\mathbf{k}$ and the corresponding spinor $w_{\mathbf{k}\sigma}$. Setting the determinant to zero produces the well-known Bogoliubov dispersion relation

$$\det \left[\Omega_{\text{BdG}}(\mathbf{k}) - \omega \right] = 0 \Rightarrow (\omega - \mathbf{k} \cdot \mathbf{v})^2 = \frac{g\rho}{m} \mathbf{k}^2 + \left(\frac{\mathbf{k}^2}{2m} \right)^2, \tag{4.25}$$

from which we recognize the speed of sound $c^2 = \frac{g\rho}{m}$. In the long-wavelength limit, Eqn. (4.25) reduces to the Lorentz invariant dispersion $(\omega - \mathbf{v} \cdot \mathbf{k})^2 - c^2 \mathbf{k}^2 \sim 0$.

We will henceforth restrict ourselves to the case of a one-dimensional system. In this case, Eqn. (4.25) becomes a quartic polynomial with roots $k_\nu(\omega)$, which must be real by normalizeability. In solving this equation, it is convenient to introduce the unitless variables

$$\begin{aligned} z &= \frac{k}{mc} \\ \beta &= \frac{v}{c} \\ \lambda &= \frac{\omega}{mc^2} \end{aligned} \tag{4.26}$$

so that the eigenvalue problem now reads

$$\begin{aligned} &\left[\beta z - \lambda + \tau^3 \left(1 + \frac{1}{2} z^2 \right) + i\tau^2 \right] w = 0 \\ &\left(1 + \frac{1}{2} z^2 \right)^2 - 1 = (\lambda - \beta z)^2 . \end{aligned} \tag{4.27}$$

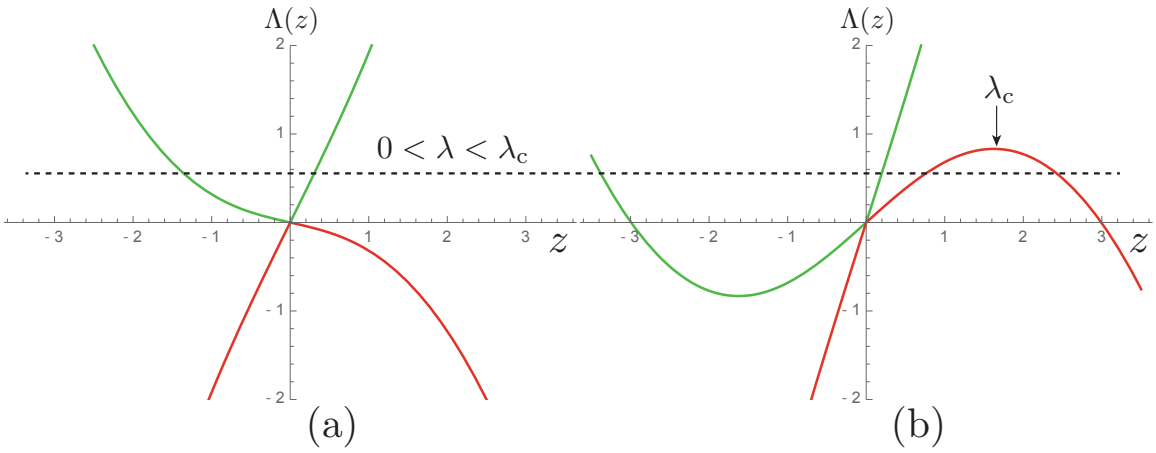

Figure 4.1: Dispersion relations solved graphically at fixed lab-frame energy (dashed line) for (a) subsonic case $\beta = .8$ and (b) supersonic case $\beta = 1.8$. For $\beta^2 > 1$ there is a positive λ_c such that within the window $0 < \lambda < \lambda_c$ there are four real solutions to the dispersion relation. For $\beta^2 > 1$ but $\lambda > \lambda_c$, or when $\beta^2 < 1$ there are only two real roots.

The real roots can be found graphically by plotting the two functions

$$\Lambda_{\pm}(z) = \beta z \pm \sqrt{z^2 + z^4/4} \tag{4.28}$$

and finding their intersections with the prescribed lab-frame energy λ, as depicted in Fig. 4.1. In Eqn. (4.28) the $\pm$ sign determines the sign of the co-moving frequency $\lambda - \beta z$ and, as we will see later, the sign of the norm of the mode as defined in Eqn. (4.13).

For $\beta^2 < 1$ the curve $\Lambda_{\pm}(z)$ is convex, as seen in Fig. 4.1(a). Thus there are only ever two real solutions, $z_{\pm p}$, both of which have positive co-moving frequency/norm but differ in their group velocity. The other two roots ($z_{\pm n}$) are complex conjugates and end up having negative norm (see Appendix E).

In contrast, for $\beta^2 > 1$ the curve $\Lambda_{\pm}(z)$ develops extrema at finite $\pm z_c$, found by

solving the equation $\left.\frac{\partial \Lambda_-(z)}{\partial z}\right|_{z_c} = 0$. For $\beta > 0$ this produces

$$z_c = \sqrt{\frac{\beta^2}{2}\left(1 + \sqrt{1 + \frac{8}{\beta^2}}\right) - 2}. \tag{4.29}$$

As shown in Fig. 4.1(b), for $0 < \lambda < \lambda_c(\beta) \equiv \Lambda_-(z_c)$ there will be four real roots to the dispersion relation. These additional roots are due to the effectively superluminal dispersion, which exhibits a group velocity that increases as momentum increases. These two new roots $z_{\pm n}$ have negative co-moving frequency/norm and are again further labeled by the sign of their group velocity (we use positive for right-movers and negative for left-movers). Generically, one of the negative norm roots also linearly disperses at low energies (for $\beta > 0$ it is z_{+n}), identifying it as the phonon which travels upstream, though now it has been Doppler shifted to such a degree that its lab-frame energy and co-moving energy differ in sign.

We now show that for real momenta the co-moving frequency indeed determines the norm of the mode. First, we obtain expressions for the eigenspinor

$$w_\nu = \begin{pmatrix} u_\nu \\ v_\nu \end{pmatrix} = \frac{1}{\sqrt{|1 - |h_\nu|^2|}} \begin{pmatrix} 1 \\ h_\nu \end{pmatrix}, \tag{4.30}$$

with $h_\nu = \lambda - \beta z_\nu - (1 + z_\nu^2/2)$. We normalize this spinor to the inner product introduced in Eqn. (4.13). When the momentum z is real, this produces the result

$$w_\nu = \frac{1}{\sqrt{2|\lambda - \beta z_\nu|}} \begin{pmatrix} (-h_\nu)^{-\frac{1}{2}} \\ -(-h_\nu)^{+\frac{1}{2}} \end{pmatrix}. \tag{4.31}$$

Explicit calculation then confirms

$$w_\nu^\dagger \tau^3 w_\nu = \text{sign}(\lambda - \beta z_\nu) \tag{4.32}$$

which we recognize is simply the sign of the co-moving frequency, as claimed.

To conclude, we return to the position space eigenmodes and consider the inner product

$$(W_{\omega'\nu'}, W_{\omega\nu}) = \int dx \rho e^{i(k_\nu(\omega) - k_{\nu'}(\omega'))x} w^\dagger_{\omega'\nu'} \tau^3 w_{\omega\nu},$$

which evaluates to a delta function

$$(W_{\omega'\nu'}, W_{\omega\nu}) = 2\pi\rho\delta\left(k_\nu(\omega) - k_{\nu'}(\omega')\right).$$

Note the appearance of the overall factor of the density. This implies the second-quantized operators for these momentum modes have the commutator

$$[\check{\mathfrak{a}}_t[W_{\omega',\nu'}], \check{\mathfrak{a}}^\dagger_t[W_{\omega,\nu}]] = 2\pi\rho\delta\left(k_\nu(\omega) - k_{\nu'}(\omega')\right). \tag{4.33}$$

In order for this to match the canonical commutator we must divide by this factor of the density, so that the appropriately normalized position-space eigenmodes are in fact

$$W_{\omega\nu}(x) = \frac{1}{\sqrt{\rho}} e^{ik_\nu(\omega)x} w_{\omega\nu}. \tag{4.34}$$

This appearance of the factor of the density will prove to be important in the next section, where the density is spatially varying.

4.4 Step-Like Horizon

4.4.1 Set Up

Having examined the homogeneous system, we will now consider the "simplest" generalization; a step-like discontinuity between two otherwise homogeneous regions.

Specifically, the fluid profile considered is

$$v(x) = \begin{cases} v_r & x \geq 0 \\ v_l & x < 0 \end{cases} \tag{4.35a}$$

$$\rho(x) = \begin{cases} \rho_r & x \geq 0 \\ \rho_l & x < 0. \end{cases} \tag{4.35b}$$

Though momentum is no longer a good quantum number, the lab-frame energy still is provided we maintain the stationary-flow condition. In one dimension this requires

$$\partial_x \left(\rho(x)v(x)\right) = 0 \Rightarrow \rho(x)v(x) = \text{constant}.$$

This constrains the step-profile from Eqn. (4.35) to obey

$$\rho_l v_l = \rho_r v_r. \tag{4.36}$$

It will be helpful to rewrite the local density $\rho(x)$ in terms of the local speed of sound $c(x) = \sqrt{g\rho(x)/m}$ which then implies that c obeys

$$c_l^2 v_l = c_r^2 v_r. \tag{4.37}$$

Thus, there are only three independent parameters amongst v_l, c_l, v_r, c_r. We will parameterize these by the two independent unitless variables $\beta_l = v_l/c_l,\ \beta_r = v_r/c_r$ and c_l. This then fixes $c_r = \left(\frac{\beta_l}{\beta_r}\right)^{\frac{1}{3}} c_l$.

The one dimensional BdG Hamiltonian which governs the step system is

$$\hat{\Omega}_{\text{BdG}} = \left(-\frac{1}{2m\rho(x)}\partial_x \rho(x)\partial_x + g\rho(x)\right)\tau^3 + g\rho(x)i\tau^2 - iv(x)\partial_x\tau^0. \tag{4.38}$$

Given the piecewise homogeneous nature of the Hamiltonian, we can solve for the

eigenmodes of Eqn. (4.38) by finding the appropriate plane-wave solutions in each half-space and then gluing them together at the interface, as is done for e.g. a particle reflecting off of a barrier. The appropriate matching conditions may obtained by integrating Eqn. (4.38) across the discontinuity (after multiplying by a factor of the density), and are

$$[W(x)]_{0^-}^{0^+} = 0 \tag{4.39a}$$

$$[\rho(x)\partial_x W]_{0^-}^{0^+} = 0. \tag{4.39b}$$

Each of these in turn produces two equations (recall that W has two components) so that in total, Eqn. (4.39) presents four constraints.

We write the energy eigenmode as

$$W_\nu(x) = \sum_\alpha \begin{cases} \frac{C_\nu^{\alpha l}}{\sqrt{\rho_l}} w_\alpha^l \exp\left(ik_\alpha^l x\right) & x < 0 \\ \frac{C_\nu^{\alpha r}}{\sqrt{\rho_r}} w_\alpha^r \exp\left(ik_\alpha^r x\right) & x \geq 0 \end{cases} \tag{4.40}$$

where α now runs over all four solutions to the half-space homogeneous problem. Crucially, this includes the modes with complex momentum which have negative norm (see Appendix E). Within each half-space one of the complex negative-norm modes will describe an evanescent mode which is allowed by boundary conditions and must be included in order to solve the matching problem [157, 158, 160, 175]. The other complex mode will describe an exponentially growing mode, which is forbidden (it will be formally convenient to include this mode but always set the coefficient to zero).

The coefficients $C_\nu^{\alpha l/r}$ (whose dependence on ω has been suppressed for brevity) must now be chosen to satisfy the matching conditions Eqn. (4.39). We classify the eight C coefficients by whether they are ingoing or outgoing. For modes of real momentum, this is based on whether the lab-frame group velocity is directed

towards or away from the step [170]. For modes of complex momentum, which don't have a group velocity, we instead treat a mode as outgoing if it is evanescent and ingoing if it is growing.

If we hold $\beta_l < 1$ fixed then irrespective of $\omega > 0$, the $+pl, +nl$ modes are ingoing while the $-pl, -nl$ modes are outgoing. Of these, the $+nl$ mode is growing, while the $-nl$ mode is evanescent. As we vary β_r on the other hand, we encounter two cases. The first case applies when either $0 < \beta_r < 1$ or $\beta_r > 1$ but the frequency $\omega > \omega_c$, with

$$\omega_c = mc_r^2 \Lambda_-(z_c(\beta_r)) \tag{4.41}$$

the cutoff frequency in the right half-plane. In this case, the flow is effectively subsonic and the ingoing modes are $-pr, -nr$ while the $+pr, +nr$ modes are outgoing, with $+nr$ evanescent and $-nr$ growing. This case is summarized in Table 4.1.

The second possibility is that $\beta_r > 1$ and $0 < \omega < \omega_c(\beta_l, \beta_r)$. In this case the $\pm nr$ momenta become real and a new scattering channel opens. This regime is summarized in Table 4.2.

Mode	Norm	Left Half-Space	Right Half-Space
$+p$	$+1$	Right-mover (in)	Right-mover (out)
$-p$	$+1$	Left-mover (out)	Left-mover (in)
$+n$	-1	Growing (in)	Evanescent (out)
$-n$	-1	Evanescent (out)	Growing (in)

Table 4.1: Mode classification for step between two effectively subsonic regions at positive energy.

Mode	Norm	Left Half-Space	Right Half-Space
$+p$	$+1$	Right-mover (in)	Right-mover (out)
$-p$	$+1$	Left-mover (out)	Left-mover (in)
$+n$	-1	Growing (in)	Right-mover (out)
$-n$	-1	Evanescent (out)	Left-mover (in)

Table 4.2: Mode classification for step between two subsonic regions at positive energy. Note that in the right-hand side, an "ingoing" growing mode was converted into an ingoing scattering mode with real flux, and the corresponding outgoing evanescent mode was converted into an outgoing scattering mode with real flux.

4.4.2 Solution

We now apply the matching conditions in Eqn. (4.39), which imposes four constraints. This linear system may be written as

$$\mathscr{M}_{\text{out}} \begin{pmatrix} C^{+pr} \\ C^{-pl} \\ C^{+nr} \\ C^{-nl} \end{pmatrix} = \mathscr{M}_{\text{in}} \begin{pmatrix} C^{+pl} \\ C^{-pr} \\ C^{+nl} \\ C^{-nr} \end{pmatrix}, \tag{4.42}$$

with the two matrices defined by

$$\mathscr{M}_{\text{out}} = \begin{pmatrix} \beta_r^{\frac{1}{3}} u_{+pr} & -\beta_l^{\frac{1}{3}} u_{-pl} & \beta_r^{\frac{1}{3}} u_{+nr} & -\beta_l^{\frac{1}{3}} u_{-nl} \\ \beta_r^{\frac{1}{3}} v_{+pr} & -\beta_l^{\frac{1}{3}} v_{-pl} & \beta_r^{\frac{1}{3}} v_{+nr} & -\beta_l^{\frac{1}{3}} v_{-nl} \\ \beta_r^{-\frac{2}{3}} z_{+pr} u_{+pr} & -\beta_l^{-\frac{2}{3}} z_{-pl} u_{-pl} & \beta_r^{-\frac{2}{3}} z_{+nr} u_{+nr} & -\beta_l^{-\frac{2}{3}} z_{-nl} u_{-nl} \\ \beta_r^{-\frac{2}{3}} z_{+pr} v_{+pr} & -\beta_l^{-\frac{2}{3}} z_{-pl} v_{-pl} & \beta_r^{-\frac{2}{3}} z_{+nr} v_{+nr} & -\beta_l^{-\frac{2}{3}} z_{-nl} v_{-nl} \end{pmatrix} \tag{4.43}$$

$$\mathscr{M}_{\text{in}} = \begin{pmatrix} \beta_l^{\frac{1}{3}} u_{+pl} & -\beta_r^{\frac{1}{3}} u_{-pr} & \beta_l^{\frac{1}{3}} u_{+nl} & -\beta_r^{\frac{1}{3}} u_{-nr} \\ \beta_l^{\frac{1}{3}} v_{+pl} & -\beta_r^{\frac{1}{3}} v_{-pr} & \beta_l^{\frac{1}{3}} v_{+nl} & -\beta_r^{\frac{1}{3}} v_{-nr} \\ \beta_l^{-\frac{2}{3}} z_{+pl} u_{+pl} & -\beta_r^{-\frac{2}{3}} z_{-pr} u_{-pr} & \beta_l^{-\frac{2}{3}} z_{+nl} u_{+nl} & -\beta_r^{-\frac{2}{3}} z_{-nr} u_{-nr} \\ \beta_l^{-\frac{2}{3}} z_{+pl} v_{+pl} & -\beta_r^{-\frac{2}{3}} z_{-pr} v_{-pr} & \beta_l^{-\frac{2}{3}} z_{+nl} v_{+nl} & -\beta_r^{-\frac{2}{3}} z_{-nr} v_{-nr} \end{pmatrix}. \tag{4.44}$$

Note we have used the unitless variables introduced in Eqn. (4.26), now given on each half-space (though the continuity relation constrains them, in general). Normalizeability requires the coefficients of the ingoing negative norm modes $(-nr, +nl)$ be set to zero if their momentum is complex. This is always the case for the $+nl$ mode, but for the $-nr$ mode this depends on whether ω is less than the cutoff ω_c or not.

Inverting the $\mathscr{M}_{\text{out}}$ matrix produces

$$\begin{pmatrix} C^{+pr} \\ C^{-pl} \\ C^{+nr} \\ C^{-nl} \end{pmatrix} = \mathcal{A} \begin{pmatrix} C^{+pl} \\ C^{-pr} \\ C^{+nl} \\ C^{-nr} \end{pmatrix}. \tag{4.45}$$

with the $\mathcal{A}$ matrix defined by

$$\mathcal{A} \equiv \mathscr{M}_{\text{out}}^{-1} \mathscr{M}_{\text{in}}, \tag{4.46}$$

which determines the amplitudes of the various outgoing modes present in a particular energy eigenmode, given the initial ingoing amplitudes.

When the step is between two subsonic flows, both the C^{+nl} and C^{-nr} coefficients must be set to zero. Thus, there are only two degenerate eigenmodes which correspond to a modes incident from the left and right. In this sense, the subsonic-subsonic step may be considered as being "adiabatically" connected to the homogeneous system, where the matrix $\mathcal{A}$ becomes a trivial identity map.

For a step between a subsonic flow and a supersonic flow, when the energy is below the cutoff ω_c an event horizon appears and the $\pm nr$ modes become scattering states. These new scattering channels produce a third degenerate eigenmode, increasing the rank of the scattering matrix at this energy from two to three. Because this mode

converts an incident negative norm wave into an outgoing positive norm component, it is responsible for producing Hawking radiation [157, 160]. It would interesting to determine under what general circumstances the rank of the scattering matrix may be related to the presence of event horizons in the spacetime. In addition, the nature of the transition from rank two to rank three may be interesting to study, as it seems impossible for it to occur in a smooth manner. We will leave these questions open for future studies.

Though not our main focus, for completeness we will now explicitly obtain the scattering ($\mathcal{S}$) matrix. This matrix is obtained from the matrix $\mathcal{A}$ by weighting each mode by its asymptotic conserved current, as per equation (4.10). Since the current is defined as the value at spatial infinity, evanescent modes do not carry a well-defined flux, nor do they enter into the unitarity expression. For a scattering mode, the asymptotic current it carries is

$$J^{\alpha} = w_{\alpha}^{\dagger}\left(v\tau^{3} + \frac{k_{\alpha}}{m}\tau^{0}\right)w_{\alpha}. \tag{4.47}$$

It may be shown (see Appendix F) that this current is equal to the group velocity of the mode, weighted by its norm. Thus, the direction of current flow may be determined graphically as well. For the subsonic-subsonic configuration, unitarity requires

$$\begin{aligned}\left|\frac{J^{+pr}}{J^{+pl}}\right||\mathcal{A}^{+pr}_{+pl}|^{2} + \left|\frac{J^{-pl}}{J^{+pl}}\right||\mathcal{A}^{-pl}_{+pl}|^{2} = 1\\ \left|\frac{J^{+pr}}{J^{-pr}}\right||\mathcal{A}^{+pr}_{-pr}|^{2} + \left|\frac{J^{-pl}}{J^{-pr}}\right||\mathcal{A}^{-pl}_{-pr}|^{2} = 1.\end{aligned} \tag{4.48}$$

In Fig. 4.2, the reflection and transmission coefficients are plotted as functions of the lab-frame energy for a mode incident from the left (exterior).

For the subsonic-supersonic configuration (below threshold) we take into account

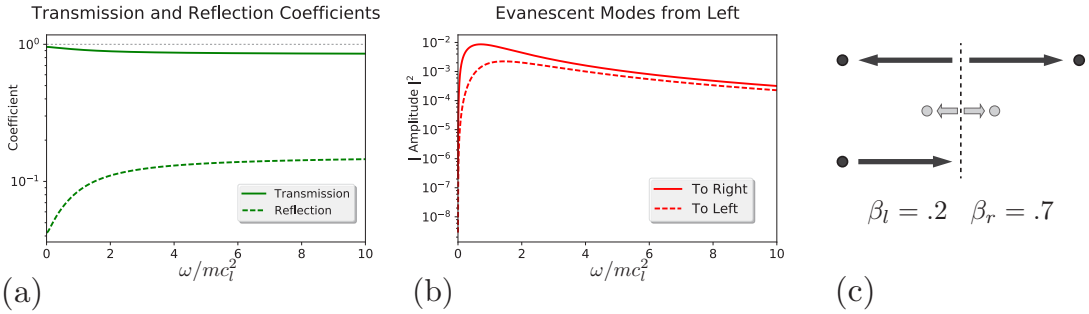

Figure 4.2: (a) Scattering coefficients as functions of energy for a step between two subsonic flows, and the corresponding evanescent mode amplitudes (b). A schematic describing the process (c), with dark arrows representing positive norm modes and light gray arrows representing evanescent modes. The direction of the arrowhead signifies whether the mode is considered ingoing or outgoing.

the additional negative norm scattering modes, producing the unitarity relations

$$\begin{aligned}
\left|\frac{J^{+pr}}{J^{+pl}}\right||\mathcal{A}^{+pr}_{+pl}|^2 + \left|\frac{J^{-pl}}{J^{+pl}}\right||\mathcal{A}^{-pl}_{+pl}|^2 - \left|\frac{J^{+nr}}{J^{+pl}}\right||\mathcal{A}^{+nr}_{+pl}|^2 &= 1 \\
\left|\frac{J^{+pr}}{J^{-pr}}\right||\mathcal{A}^{+pr}_{-pr}|^2 + \left|\frac{J^{-pl}}{J^{-pr}}\right||\mathcal{A}^{-pl}_{-pr}|^2 - \left|\frac{J^{+nr}}{J^{-pr}}\right||\mathcal{A}^{+nr}_{-pr}|^2 &= 1 \quad . \\
\left|\frac{J^{+pr}}{J^{-nr}}\right||\mathcal{A}^{+pr}_{-nr}|^2 + \left|\frac{J^{-pl}}{J^{-nr}}\right||\mathcal{A}^{-pl}_{-nr}|^2 - \left|\frac{J^{+nr}}{J^{-nr}}\right||\mathcal{A}^{+nr}_{-nr}|^2 &= -1
\end{aligned} \tag{4.49}$$

Similar relations have been obtained in, e.g. [157, 159, 170, 171]. Note that the third scattering channel has an overall minus sign, due to the incoming mode having overall negative norm. The presence of the outgoing negative norm states implies that the reflection and transmission coefficients together sum to a value larger than unity, a hallmark of supperradiance.

In Fig. 4.3 we depict the scattering coefficients for each ingoing configuration as a function of energy. Below the cutoff energy there are three ingoing configurations, each scattering into the three possible outgoing channels. Of these three ingoing channels, two have an overall positive norm, while the third describes the Hawking channel and an has overall negative norm. The Hawking radiation spectrum is determined by the transmission coefficient which describes the scattering of this

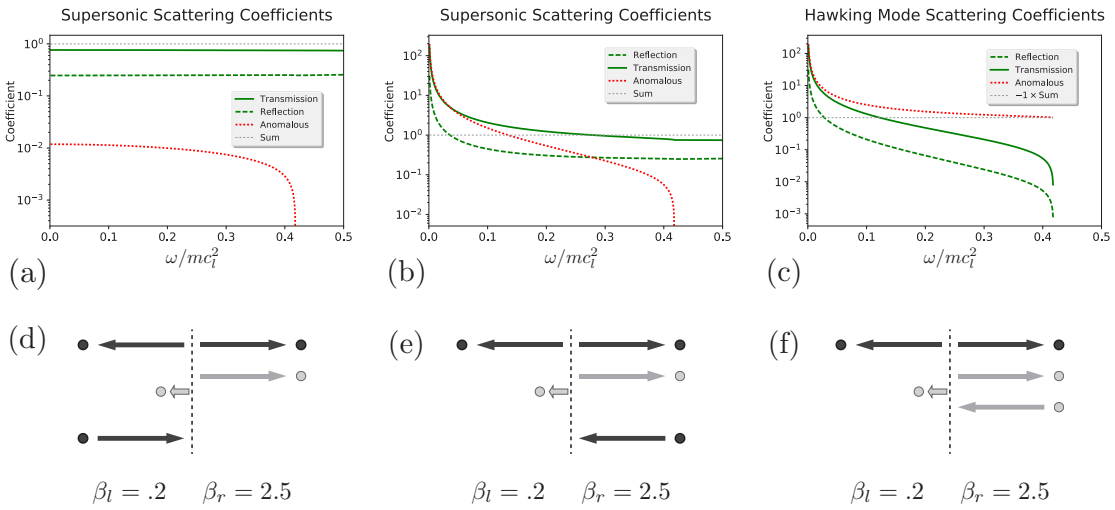

Figure 4.3: Scattering coefficients for subsonic-supersonic step as a function of lab-frame energy. (a) Scattering of a particle incident from the left. The anomalous mode corresponds to conversion into an outgoing negative norm mode. Above the threshold energy, this coefficient goes to zero, as the outgoing channel becomes evanescent. (b) Scattering of a particle incident from the right, a process which can occur due to the superluminal dispersion. (c) The Hawking mode, whereby an incident negative norm mode scatters off of the event horizon. This ingoing channel becomes an exponentially growing mode above the threshold energy, where all the coefficients go to zero. In the schematics (d-f), the large grey arrows indicate the negative norm scattering states.

mode into the outgoing positive norm mode outside the horizon (the $-pl$ mode).

This Hawking flux exiting the black hole is depicted in more detail in Fig. 4.4, where it is also compared to the magnitude of the evanescent mode present in this eigenmode. While the evanescent mode amplitude vanishes at zero energy, the Hawking flux diverges as $1/\omega$ at low frequencies, reflecting its effectively thermal distribution at low energies. As claimed earlier, the distribution function departs from thermality at higher energies before vanishing at the cutoff energy ω_c. We now shift our focus to the evanescent mode, which only exists close to the event horizon.

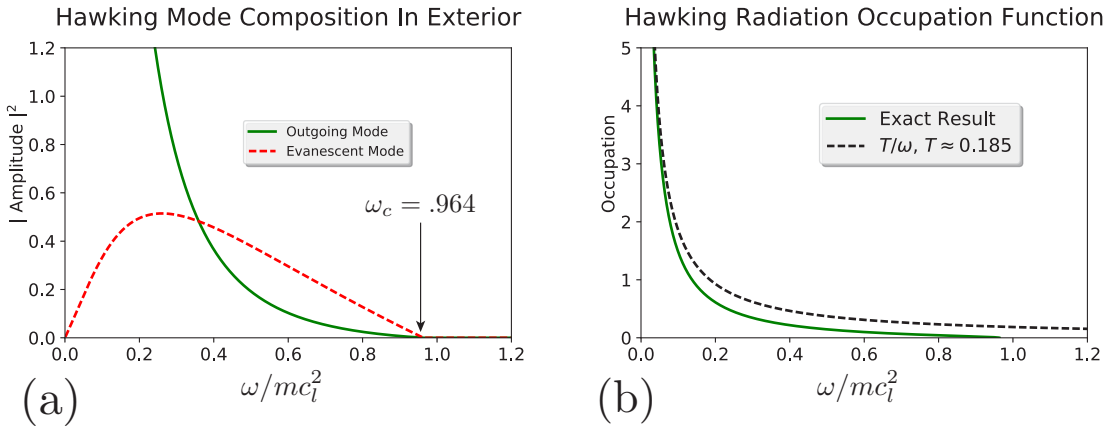

Figure 4.4: (a) The squared-amplitudes of the various modes comprising the Hawking eigenmode for $x < 0$ ($\beta_l = .7, \beta_r = 2.5$). We see that they both go to zero at the cutoff energy, which is also depicted. (b) The computed Hawking flux compared to an approximation by $\sim 1/\omega$, the classical (low energy) approximation to thermal occupation. The proportionality coefficient is extracted and represents (up to an overall greybody absorption factor) the effective black hole temperature. While the two curves agree at low frequencies, they clearly disagree at higher energies.

4.5 Evanescent Modes

In the previous section we argued that evanescent modes do not contribute to the scattering relations since they carry no asymptotic flux. One may then wonder under what conditions they are physically important. We will now demonstrate that if one considers observables which depend on the near-horizon correlation functions [155, 156, 160], the evanescent modes will be important as they will modify quantities measured near the horizon. As a simple example, we consider the norm density of a particular eigenmode, a quantity which is related to the quantum density fluctuations.

Specifically, we will study the Hawking ($-nr$) mode, which only has one scattering mode outside of the horizon. As such, far from the horizon the norm density is a featureless constant, with value $\frac{1}{c_l^2}|\mathcal{A}^{-pl}_{-nr}|^2$. However, near the horizon the evanescent mode is non-zero and can exhibit quantum interference with the outgoing

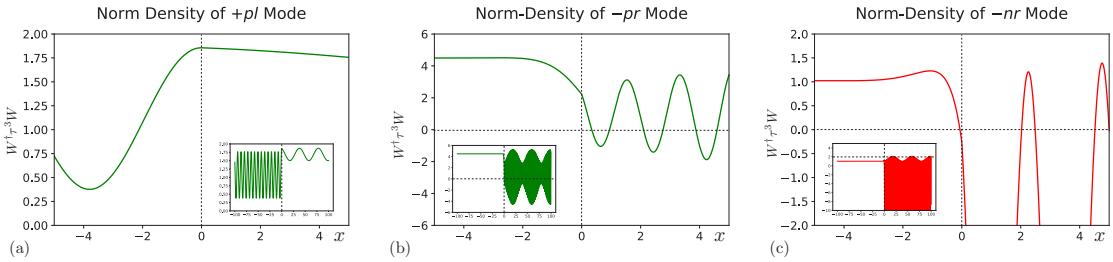

Figure 4.5: Plot of $W^\dagger(x)\tau^3 W(x)$ as a function of x for a particular eigenvalue ($\omega = .260, \beta_l = .7, \beta_r = 2.5$). (a) The near horizon density of the $+pl$ mode, which is incident from the left. The inset of (a) shows the same, but plotted over a larger range of x. (b) The near horizon density of the $-pr$ mode, which is a superluminal positive norm mode incident from right. The inset shows a larger range of x. The evanescent mode is seen as the modulation of the density at $x \lesssim 0$ away from its asymptotic value. (c) The near horizon density of the $-nr$ mode, which is the Hawking mode with a negative norm mode incident from the right. The inset shows a larger range of x. The evanescent mode is again noticeable here as a modulation of the density for $x \lesssim 0$. The horizontal and vertical dashed lines indicate zero for $W^\dagger\tau^3 W$ and x, where the horizon is located, respectively. It should be noted that the true conserved density is $\rho W^\dagger\tau^3 W$, rather than $W^\dagger\tau^3 W$ which has been plotted instead for clarity. Statements made about the evanescent mode are unaffected by this distinction.

Hawking flux, leading to a deviation of the norm density from its value inferred by an observer at spatial infinity. This interference is clearly visible in Fig. 4.5(b),(c) where the density for $x \to -\infty$ is constant and featureless, while the density near $x \lesssim 0$ deviates from this value quite significantly just outside the event horizon.

When considering near-horizon physics, the evanescent modes will have important contributions which would otherwise be overlooked if the horizon curvature is small, or if the observer is sufficiently far from the horizon. Such behavior is not permissible by the equivalence principle, which implies that observers crossing the event horizon experience a locally flat spacetime. It is not surprising therefore that these modes decay over a length scale governed by the scale at which Lorentz invariance is violated. Using the Bogoliubov dispersion relation we find that the

imaginary part of the evanescent mode momentum is related to the real part by

$$(\mathrm{Im}(z_{-nl}))^2 = (\mathrm{Re}(z_{-nl}))^2 + 2(1-\beta_l^2) + \frac{2\beta_l\lambda_l}{\mathrm{Re}(z_{-nl})}. \tag{4.50}$$

The first term and third terms can be shown to be non-negative for $\beta, \lambda > 0$. Thus, we can bound the imaginary part from below by

$$\mathrm{Im}(z_{-nl}) \geq \sqrt{2(1-\beta_l^2)}. \tag{4.51}$$

Replacing units, we find that the evanescent modes are forced to decay over a length scale L_{-nl} such that

$$L_{-nl} \leq \frac{1}{\sqrt{2}mc_l\sqrt{(1-\beta_l^2)}}. \tag{4.52}$$

For any finite subsonic flow this scale is finite and furthermore, as $m \to \infty$ (at fixed c_l), this length scale goes to zero, completely removing the evanescent modes from the spectrum. This is inline with our intuition since the mass m effetively sets the scale at which the superluminal dispersion ruins Lorentz invariance; thus, this limit corresponds to enforcing Lorentz symmetry throughout the entire spectrum. In this case, the equivalence principle requires the evanescent modes to disappear, as they do.

To emphasize the potential importance of these evanescent modes, we recall that in the presence of an event horizon the energy eigenbasis becomes three-dimensional. In this case, we can form the linear combination of ingoing-eigenmodes

$$W_{\text{confined}}(x) \equiv \frac{\mathcal{A}^{-pl}_{-pr}W_{-nr}(x) - \mathcal{A}^{-pl}_{-nr}W_{-pr}(x)}{\mathcal{A}^{-pl}_{-pr}\mathcal{A}^{-nl}_{-nr} - \mathcal{A}^{-pl}_{-nr}\mathcal{A}^{-nl}_{-pr}}, \tag{4.53}$$

which describes a coherent superposition of the Hawking mode and an incident superluminal particle. This particular combination of modes has no flux escaping

the black hole as the two incident amplitudes coherently cancel outside the event horizon. Nevertheless, due to the evanescent modes it is seen to have finite support outside of the event horizon. This is illustrated in Fig. 4.6, which depicts the norm density and individual components of a particular confined eigenmode, indeed confirming that it is exponentially localized to the interior of the black hole. It appears that if we were to extend the black hole interior to include a white hole, this confined mode would represent "half" of a black hole bound state, which are the modes responsible for black-hole-lasing and dynamical instability [152, 159, 165, 168]. Analyzing the stability and evolution of this confined mode with and without the accompanying white hole may uncover interesting instabilities which develop conditioned on the nature of the black hole interior.

4.6 Conclusion

In this work we have systematically studied the step-like horizon formed in a quasi-one dimensional flowing BEC, which we argue serves as a model for acoustic black holes of very large curvature. In addition to computing the scattering coefficients of this system (including the Hawking flux coefficient), we have also highlighted and studied the properties of the evanescent modes which form at the event horizon and result from model's non-linear dispersion. These evanescent modes have been conclusively shown to modify near-horizon observables, despite the fact that they do not affect the scattering relations.

Given that the evanescent modes are effectively negative norm states tunneling across the event horizon, and have no flux out to infinity, it is interesting to speculate on what role, if any, these modes may serve in resolving the black hole information paradox. Through their effect on observables (such as the density and current fluctuations) near the horizon, it is conceivable that they may provide a route for information trapped behind the horizon to escape. In particular, though they cannot

asymptotically carry any information away as they are only a virtual process, it may be possible to retrieve information from the interior via an "external measurement" of the system (e.g. a projective measurement of the density). This is especially important since, in our model we have neglected interactions between the Bogoliubov quasiparticles, truncating the Heisenberg equations to linear order in fluctuations. In the presence of quasiparticle interactions, it is plausible that the system will "self-measure," as the virtual evanescent modes collide and interact with the outgoing Hawking flux, leading to a genuine leakage of information out of the event horizon.

In a similar vein, it is interesting to note that even though the condenate varies in an abrupt step-like manner, the evanescent modes seem to modulate observables on a longer length scale which is comparable to their decay length. If we assume that the quasiparticle correction to the physical boson density behaves similarly, then we should expect that an initially sharp step-like condensate will become dressed by the evanescent modes, smearing it into a less abrupt horizon. This is interesting since it potentially provides an example where the quasiparticle back-reaction on the condensate modifies the event horizon itself. When quasiparticle interactions are included this may generate entanglement between the event horizon and the outgoing Hawking radiation.

Finally, we note that evanescent modes have been seen in other contexts, e.g. the AdS-CFT correspondence [176], where evanescent modes are also seen to emanate from an apparent AdS black hole event horizon. Given that the model we consider only has emergent Lorentz invariance, it is interesting to consider whether it is possible to connect the analogue of the AdS-CFT correspondence for a theory with only emergent Lorentz invariance, i.e. one with a sonic black hole in its bulk and some form of approximate-CFT on the boundary. Similarly, whether it is possible to see these evanescent features in models of quantum gravity with emergent Lorentz invariance (e.g. Hořava gravity [153, 177]) is another interesting avenue of research.

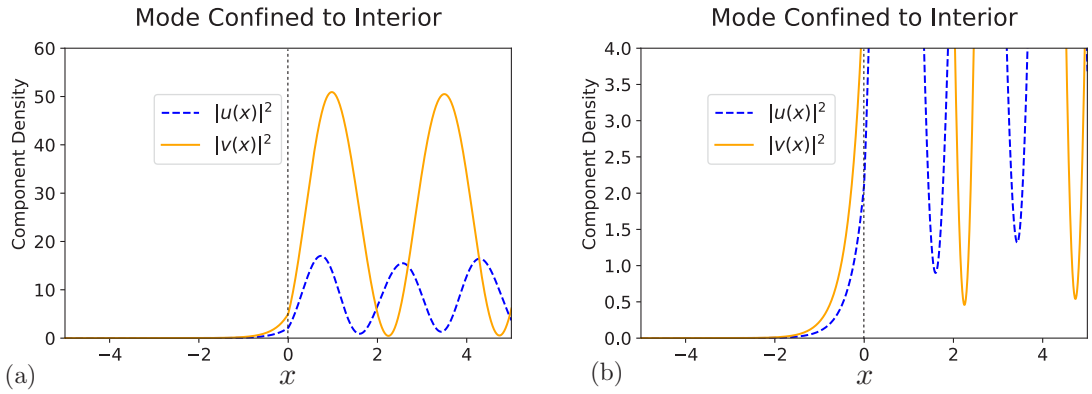

Figure 4.6: Confined mode for horizon with $\beta_l = .7, \beta_r = 2.5$ for a particular eigenenergy ($\omega = .260$). (a) The density (modulus squared) of each component of the mode confined to the interior of the horizon. Note that both components independently decay to zero for $x < 0$ (outside the event horizon). (b) The same quantity, plotted over a smaller y-scale, emphasizing the scale of the decay for $x < 0$.

Chapter 5: Analogue Newton-Cartan spacetime in flowing spinor Bose-Einstein condensates

This chapter is based on the publication Wilson, Curtis, and Galitski [178], which is currently under review.

5.1 Introduction

The marriage of quantum mechanics and general relativity is one of the greatest outstanding problems in modern physics. This is in part due to the fact that this theory would only become truly necessary under the most extreme conditions—the singularity of a black-hole or the initial moments after the big bang. As such, it is extremely difficult to theoretically describe, let alone physically probe.

Despite the seeming intractability, some headway may be made in the understanding of such extreme theories by way of analogy. This idea traces back to Unruh, who in 1981[17] suggested that a flowing quantum fluid could realize a laboratory scale analog of a quantum field theory in a curved spacetime. Access to even the most rudimentary quantum simulator for such a curved spacetime could provide valuable insights into this otherwise inaccessible regime.

Since Unruh's initial proposal, many systems have been advanced as candidates for realizing analog spacetimes [20], including liquid helium [134, 136, 137], Bose-Einstein condensates [18, 19, 22, 138–142, 145, 152, 154], nonlinear optical media [149], electromagnetic waveguides [146], magnons in spintronic devices [148], semi-conductor microcavity polaritons [111], Weyl semi-metals [179, 180], and even in classical water waves [151]. Analog gravity systems are no longer a theoretical endeavor; recent experiments have realized the stimulated Hawking effect [150], and in the case of a Bose-Einstein condensate a spontaneous Hawking effect [152, 154].

Goldstone mode	Dispersion	Analog spacetime	Lagrangian
Type-I	$\omega \sim k$	Einstein-Hilbert	Eq. (5.37)
Type-II	$\omega \sim k^2$	Newton-Cartan	Eq. (5.42)

Table 5.1: Analog spacetimes which appear for the different Goldstone modes in the presence of a background condensate flow. These spacetimes emerge as effective field theories governing the long-wavelength behavior. As we demonstrate in this work, the emergent geometry is determined by the flow profile of the background condensate. This is explicitly demonstrated in Sec. 5.2.4 for the Type-I modes and Sec. 5.2.5 for the Type-II modes, where we also provide an overview of the Newton-Cartan formalism.

In this chapter we will introduce a new kind of analog gravity system, one which exhibits Newton-Cartan geometry [28, 29, 34]. This geometry naturally arises from a full analysis of all Goldstone modes in a flowing spinor (or multicomponent) condensate. Spinor condensates [181] have been studied in the context of analog curved space before [26, 27]; however a full accounting of all gapless modes has not been done to the best of our knowledge. The Goldstone modes which realize the Newton-Cartan geometry exhibit a quadratic $\omega \sim \mathbf{k}^2$ dispersion, known as "Type-II" Goldstone modes [26, 27]. For example, the spin wave excitations about an SU(2) symmetry breaking ferromagnetic mean-field are such a mode. Distinct from the linearly dispersing case (called "Type-I" modes), Newton-Cartan spacetimes implement local Galilean invariance, as opposed to local Lorentz invariance. These results are general and summarized in Table 5.1, where we give a general prescription for separating out all Goldstone modes into either Type-I (linearly dispersing) or Type-II (quadratically dispersing) modes and assigning them either an Einstein-Hilbert or Newton-Cartan spacetime geometry.

Newton-Cartan geometry was developed by Cartan [28, 29] and refined by others [182] as a geometric formulation and extension of Newtonian gravity. It has since found application across different areas of physics, including in quantum Hall systems [32, 34, 183] and effective theories near Lifshitz points [184, 185] with interest to the high-energy community with implications for quantum gravity [186, 187]. We extend

these applications here to flowing condensates for the case of Type-II Goldstone modes.

Heuristically, one may view the quadratic dispersion relation $\omega \sim |\mathbf{k}|^2 + ...$ as the limit of a linear dispersion relation $\omega \sim v|\mathbf{k}| + ...$ with vanishing group velocity $v \to 0$. In terms of the analog spacetime, this corresponds to an apparent vanishing of the speed of light. As such, the formation of event horizons and their corresponding Hawking radiation ought to be ubiquitous in such spacetimes; however our results contradict this intuition. Specifically, we find that fields propagating in Newton-Cartan geometries exhibit an additional conservation law which precludes the emission of Hawking radiation.

The immediate implication of this is that any Type-I mode can have an effective event horizon and therefore a Hawking effect (similar things have been noticed for specific other Type-I modes), and further, no Hawking effect can occur for Type-II modes, at least not without introducing quasiparticle interactions (which corresponds to going being a quadratic treatment of fluctuations).

Finally, we discuss the relationship between transport phenomena and gravitational metrics in our theory [31–34]. Specifically, we obtain the stress-tensor, energy flux, and momentum density for theories both with the Einstein-Hilbert and Newton-Cartan geometries. In particular, we relate the energy-momentum tensor calculated in an analog Einstein-Hilbert geometry to its nonrelativistic counterparts through the use of Newton-Cartan geometry. This helps identify how the analog Hawking effect results in nontrivial energy and momentum currents in the underlying nonrelativistic system.

The outline of the remaining sections are as follows. Section 5.2 shows that in the presence of a flowing background condensate Type-I and -II Goldstone modes couple to Einstein-Hilbert (Section 5.2.4) and Newton-Cartan (Section 5.2.5) geometries respectively. In Section 5.3, we present a minimal model for these space-times and

the phase transition that connects them. In Sec. 5.3.1 we develop the Bogoliubov-de Gennes framework which we then use to analyze this system. In Sec. 5.4 we apply this to a specific step-like flow geometry and show the effect of the geometry on the emitted Hawking radiation. We then discuss transport of energy and momentum in these different analog spacetimes systems in Sec. 5.5. We conclude the chapter in Section 5.6. Our two appendices include Appendix G where we put the full fluctuation calculation of the Lagrangian and Appendix H where we review the Hawking calculation for the phonon problem.

5.2 Relationship between spacetime and Goldstone's theorem

In this work we consider models of ultra-cold bosonic spinor quantum gases described by an N-component field variable $\Psi(\mathbf{r},t) = [\Psi_1, \Psi_2, \dots, \Psi_N]^T$ residing in d spatial dimensions (we do not make the distinction between "spinor" and higher multiplet fields in this work). The Lagrangian describing this system is taken to be of the general form

$$\mathcal{L} = \tfrac{i}{2}(\Psi^\dagger \overrightarrow{\partial_t} \Psi - \Psi^\dagger \overleftarrow{\partial_t} \Psi) - \tfrac{1}{2m} \nabla\Psi^\dagger \cdot \nabla\Psi - V(\Psi^\dagger, \Psi), \tag{5.1}$$

where m is the mass of the atoms in the gas and $V(\Psi^\dagger, \Psi)$ is a general potential energy function that includes interactions with an external potential as well as local inter-particle interactions. Such a system may be realized by cold-atoms, where in addition to the inter-particle interactions external potentials such as a harmonic trap, optical lattice, or magnetic field may be present. For a comprehensive review regarding the theory and experimental realization of spinor condensates see Ref. [181].

We consider the case where the Lagrangian exhibits invariance under an internal symmetry described by a Lie group G, according to which Ψ transforms via a linear unitary representation $\mathcal{R}(G)$ such that the action $\mathcal{S} = \int \mathcal{L}\, d^{d+1}x$ remains invariant.

That is,

$$\Psi(x) \to U\Psi(x) \Rightarrow \mathcal{S} \to \mathcal{S} \quad \forall U \in \mathcal{R}(G). \tag{5.2}$$

Recall that a Lie group G is generated by its corresponding Lie algebra $\mathfrak{g}$, and this has a representation of $\mathcal{R}(\mathfrak{g})$ when acting on the field Ψ. For ease of calculations, we use the mathematical convention that Lie algebras consist of anti-Hermitian elements. Hence, if A is an element of $\mathcal{R}(\mathfrak{g})$, then $A = -A^\dagger$ and the corresponding group element is $e^A = ((e^A)^{-1})^\dagger$.

We pursue a semi-classical analysis of our system by first obtaining the classical equations of motion (i.e. the saddle-point of the action). Then we linearize the action around the saddle-point, obtaining a description of the symmetry-broken phases in terms of their Goldstone modes. The primary point of our work is that this linearized action admits a simple description in terms of different emergent analog spacetimes and depending on the nature of the saddle-point, this analog spacetime may develop non-trivial curved geometry.

The rest of this section is organized as follows. We perform a quadratic fluctuation analysis in Section 5.2.1. In Section 5.2.2 we review the proof of the Goldstone theorem in non-relativistic settings [26, 27] and show how this allows us to classify Goldstone modes into Type-I and Type-II. Section 5.2.3 then presents the full Lagrangian for the Goldstone modes while Sections 5.2.4 and 5.2.5 make explicit the connection to curved space geometry.

5.2.1 Saddle-Point Expansion

We begin by looking for saddle-points of the Lagrangian Eq. (5.1), the spinor Gross-Pitaevskii equation

$$i\partial_t \Psi = -\frac{1}{2m}\nabla^2\Psi + \frac{\partial V}{\partial \Psi^\dagger}. \tag{5.3}$$

Suppose that we have found a mean-field solution to this equation $\Psi_0(\mathbf{r},t) \equiv \langle \Psi(\mathbf{r},t) \rangle$ which describes the dynamics of a mean-field condensate (neglecting fluctuation back-reaction); for a general out-of-equilibrium system, the space-time dependence of $\Psi_0(\mathbf{r},t)$ may be non-trivial [22, 181, 188].

The presence of a non-zero mean-field solution Ψ_0 spontaneously breaks the internal symmetry group G down to a subgroup $H \subset G$. Let $\mathfrak{h}$ be the Lie algebra that generates the subgroup H. This is defined by the set of generators

$$\mathfrak{h} = \{\hat{\tau} \in \mathfrak{g} \mid \hat{\tau}\Psi_0 = 0\}. \tag{5.4}$$

We can form a complete basis for $\mathfrak{h} = \text{span}\{\tau_k\}$. The original Lie algebra then separates into two sub-spaces; $\mathfrak{g} = \mathfrak{h} \oplus \mathfrak{h}^c$, where $\mathfrak{h}^c$ is simply the complement of $\mathfrak{h}$. It is useful to form an explicit basis for $\mathfrak{h}^c \equiv \text{span}\{\sigma_l\}$ so that $\mathfrak{g} = \text{span}\{\tau_k\} \cup \{\sigma_l\} = \text{span}\{\sigma_l, \tau_k\}$. Formally, $\mathfrak{h}^c$ is isomorphic to the quotient algebra $\mathfrak{g}/\mathfrak{h}$, and the basis elements σ_l are isomorphic to coset spaces.

It is important to emphasize that, although in general the mean-field $\Psi_0(x)$ may break the symmetry group G down to different subgroups $H = H(x)$ at each spacetime point, we do not consider this in full generality since it leads to a very complicated (but interesting) structure involving a non-Abelian connection on the spacetime. However, we later consider *flowing* condensates which inhomogeneously break the $U(1)$ subgroup of G.

We now examine the quadratic fluctuations of the field Ψ about the mean-field by expanding the Lagrangian in powers of $\delta\Psi(x) = \Psi(x) - \Psi_0(x)$. This separates into two distinct contributions; the massless Goldstone modes $\theta_l(x)$ which correspond to spontaneously broken symmetries, and massive fields $\beta_n(x)$ which describe all the remaining modes. Each Goldstone mode corresponds to a broken generator $\sigma_l \in \bar{\mathfrak{h}}$ acting on the mean-field condensate $\Psi_0(x)$. These contribute to the fluctuation

action as

$$(\delta\Psi(x))_{\text{Goldstone}} = \sum_l \theta_l(x)\sigma_l\Psi_0(x) \equiv \hat{\sigma}(x)\Psi_0(x), \tag{5.5}$$

which serves to define the Goldstone matrix field $\hat{\sigma}(x)$. The remaining degrees of freedom are generically massive and are not amenable to a description in terms of the Lie algebra's generators. It is advantageous to parameterize the fluctuations $\delta\Psi$ in terms of real fields with massive terms orthogonal to the massless terms in the sense described below. Within the quadratic theory, this implies the fluctuations reside within a real vector space $\mathbb{R}^{2N} \sim \mathbb{C}^N$. The Goldstone modes $\sigma_l\Psi_0(x)$ form a subspace of this manifold while the remaining basis elements are generically massive and are written as $\xi_n(x)$. We note that in general the basis elements are spacetime dependent simply because the mean-field is also spacetime dependent.

In order to make the notion of orthogonality precise we lift the standard complex ($\mathbb{C}^N$) inner product onto our real vector space $\mathbb{R}^{2N}$ to obtain the *real* inner product g defined by

$$g(\xi, \chi) \equiv \tfrac{1}{2}(\xi^\dagger\chi + \chi^\dagger\xi). \tag{5.6}$$

In terms of the Goldstone manifold and its complement, the variation $\delta\Psi(x)$ takes the compact form

$$\delta\Psi(x) = \hat{\sigma}(x)\Psi_0(x) + \xi(x), \tag{5.7}$$

where we have defined the massive modes by

$$\xi(x) = \sum_n \beta_n(x)\xi_n(x). \tag{5.8}$$

We proceed to the expansion of the Lagrangian in terms of the variation $\delta\Psi$. First, we consider the potential. It is locally invariant under under G, so we can write

$$V(\Psi^\dagger, \Psi) = V(\Psi^\dagger e^{\hat{\sigma}(x)}, e^{-\hat{\sigma}(x)}\Psi). \tag{5.9}$$

Furthermore, we can use our expansion of $\Psi(x)$ to obtain

$$\begin{aligned} e^{-\hat{\sigma}}\Psi &\approx e^{-\hat{\sigma}}[\Psi_0 + \hat{\sigma}\Psi_0 + \xi] \\ &\approx (1 - \hat{\sigma} + \tfrac{1}{2}\hat{\sigma}^2)[\Psi_0 + \hat{\sigma}\Psi_0 + \xi] \\ &\approx \Psi_0 + \xi - \hat{\sigma}\xi - \tfrac{1}{2}\hat{\sigma}^2\Psi_0, \end{aligned} \tag{5.10}$$

keeping terms up to quadratic order in fluctuations. This allows us to expand the potential energy up to quadratic order (dropping the terms constant and linear in the variation)

$$\begin{aligned} V(\Psi^\dagger, \Psi) = -\left[\frac{\partial V}{\partial \Psi} \cdot \left(\tfrac{1}{2}\hat{\sigma}^2\Psi_0 + \hat{\sigma}\xi\right) + \text{c.c.}\right] \\ + \frac{1}{2}\xi^*\xi^* \cdot \frac{\partial^2 V}{\partial\Psi^\dagger\partial\Psi^\dagger} + \xi^* \cdot \frac{\partial^2 V}{\partial\Psi^\dagger\partial\Psi} \cdot \xi + \frac{1}{2}\frac{\partial^2 V}{\partial\Psi\partial\Psi} \cdot \xi\xi, \end{aligned} \tag{5.11}$$

where all derivatives of the potential are understood as being evaluated at the mean-field. The terms quadratic in ξ, ξ^* represent massive terms, and the first line of Eq. (5.11) drops out when combined on-shell with similar terms from the kinetic part of the Lagrangian. Deriving the full fluctuation Lagrangian is not instructive, and has been relegated to Appendix G; the final result is given below.

Focusing on the Goldstone modes, written in terms of the "angle fields" $\theta_l(x)$, the resulting Lagrangian for fluctuations is given by

$$\begin{aligned} \mathcal{L}_{\text{fluc}} = \theta_m P^\mu_{mn}(\partial_\mu\theta_n) + \beta_m Q^\mu_{mn}(\partial_\mu\theta_n) \\ + (\partial_j\theta_n)T^{jk}_{mn}(\partial_k\theta_n) + \mathcal{L}_{\text{mass}}(\beta_m, \partial_\mu\beta_m), \end{aligned} \tag{5.12}$$

where we have instituted the Einstein summation convention. In this and the following, Roman indices $i, j, k, ...$ run over spatial dimensions while Greek indices $\mu, \nu, ...$ run over both temporal and spatial dimensions (with $\mu = 0 = t$ the temporal index). The Roman indices $n, m, ...$ enumerate the different Goldstone modes or

massive modes and are similarly summed. The terms P^{μ}_{mn}, Q^{μ}_{mn}, and T^{jk}_{mn} depend on both space and time, and are given by

$$\begin{aligned}
P^{t}_{mn} &= \tfrac{i}{2}\Psi_0^\dagger[\sigma_n,\sigma_m]\Psi_0,\\
P^{j}_{mn} &= \tfrac{1}{4m}(\partial_j\Psi_0^\dagger[\sigma_m,\sigma_n]\Psi_0 - \Psi_0^\dagger[\sigma_m,\sigma_n]\partial_j\Psi_0),\\
Q^{t}_{mn} &= i(\Psi_0^\dagger\sigma_n\xi_m + \xi_m^\dagger\sigma_n\Psi_0),\\
Q^{j}_{mn} &= \tfrac{1}{2m}(\xi_m^\dagger\sigma_n\partial_j\Psi_0 - \partial_j\Psi_0^\dagger\sigma_n\xi_m\\
&\qquad\qquad + \Psi_0^\dagger\sigma_n\partial_j\xi_m - \partial_j\xi_m^\dagger\sigma_n\Psi_0),\\
T^{jk}_{mn} &= \tfrac{1}{2m}\delta^{jk}\Psi_0^\dagger\sigma_n\sigma_m\Psi_0.
\end{aligned} \tag{5.13}$$

As mentioned previously, it is also important to keep track of the massive modes in the full Lagrangian and we offer that full analysis in Appendix G.

5.2.2 Proof of the nonrelativistic Goldstone theorem

Before proceeding to simplify the Lagrangian and derive the curved space analogues, we need to understand and make use of the nonrelativistic Goldstone theorem [26, 27], providing a complementary proof in the process.

We consider the following ansatz for the mean-field

$$\Psi_0(x) = \sqrt{\rho(x)}e^{i\vartheta(x)}\chi, \quad \chi^\dagger\chi = 1, \quad \partial_\mu\chi = 0. \tag{5.14}$$

Importantly the spinor structure given by χ is independent of space and time. The global $U(1)$ symmetry implies the phase and density obey a continuity relation which can be conveniently written as

$$\partial_\mu J^\mu = 0, \tag{5.15}$$

with the condensate four-current given by $J^\mu = \rho v_s^\mu$, where the superfluid four-

velocity field is $v_s^\mu = (1, \frac{1}{m}\nabla\vartheta)$. This simplifies the term

$$P^\mu_{mn} = -\tfrac{i}{2} J^\mu \chi^\dagger [\sigma_n, \sigma_m] \chi, \tag{5.16}$$

which dictates which real fields θ_n are canonically conjugate to each other. In non-relativistic systems, the relationship between broken symmetry generators and Goldstone modes is not one-to-one. Instead, we must separate out our modes into Type-I and Type-II Goldstone modes, which is done by going to the preferred basis of the matrix P^μ_{mn}.

To understand this, we return to the *real* vector space defined by the Goldstone mode manifold, which we label $\mathcal{A}_\mathbb{R}$. That is,

$$\mathcal{A}_\mathbb{R} = \mathrm{span}_\mathbb{R}\{\sigma_l \Psi_0(x)\}. \tag{5.17}$$

The real dimension $D_\mathbb{R}$ of this subspace is simply equal to the number of broken generators. We can complexify this vector space by allowing for complex-valued coefficients

$$\mathcal{A}_\mathbb{C} \equiv \mathrm{span}_\mathbb{C}\{\sigma_n \Psi_0\}. \tag{5.18}$$

It may be the case that two generators which are linearly independent under real coefficients are linearly dependent when multiplied by complex coefficients. For this reason, this vector space has an associated *complex* dimension $D_\mathbb{C} \leq D_\mathbb{R}$. The essence of the Goldstone mode theorem is that $D_\mathbb{R}$ is the number of broken generators and $D_\mathbb{C}$ is the number of modes, and these two quantities can be formally related by classifying each basis element $\sigma_l \Psi_0(x) \in \mathcal{A}_\mathbb{R}$ due to whether $i\sigma_n \Psi_0 \in \mathcal{A}_\mathbb{R}$ or not.

To establish this we need to return to our real inner product $g(\cdot,\cdot)$. We can use the operation of multiplication by i to define a symplectic bilinear form $\omega(\cdot,\cdot)$ by

$$\omega(\eta, \xi) \equiv g(i\eta, \xi) = \tfrac{i}{2}(\xi^\dagger \eta - \eta^\dagger \xi). \tag{5.19}$$

The multiplication by i (acting on the basis vectors $\sigma_l \Psi_0(x)$) can be restricted to the real vector space $\mathcal{A}_{\mathbb{R}}$, which we define by the notation

$$i|_{\mathcal{A}_{\mathbb{R}}} \equiv I : \mathcal{A}_{\mathbb{R}} \to \mathcal{A}_{\mathbb{R}}. \tag{5.20}$$

Similarly, we define $\operatorname{range} I \equiv \mathcal{A}_{\mathrm{II}} \subset \mathcal{A}_{\mathbb{R}}$ as the range of I. The null space of I is then defined to be $\mathcal{A}_{\mathrm{I}}$ and represents states $\eta \in \mathcal{A}_{\mathbb{R}}$ which leave the real vector space upon multiplication by i. As a simple example, consider unit vectors $\hat{e}_1 = (1,0)^T$ and $\hat{e}_2 = (i,0)^T$. As elements of a real vector space these are linearly independent, however $i\hat{e}_1 = \hat{e}_2$ and so these are not linearly independent in a complex vector space. In this case, we have $D_{\mathbb{R}} = 2,\ D_{\mathbb{C}} = 1$ and $\operatorname{range} I = \mathcal{A}_{\mathbb{R}},\ \operatorname{null} I = 0$. However, if $\hat{e}_1 = (1,0)^T$ and $\hat{e}_2 = (0,1)^T$ then $D_{\mathbb{R}} = 2 = D_{\mathbb{C}}$ and $\operatorname{range} I = 0,\ \operatorname{null} I = \mathcal{A}_{\mathbb{R}}$.

The classification of basis elements may be accomplished by taking the real inner product of $i\eta$ with the other elements of $\mathcal{A}$—if this vanishes, then η is in the kernel of I. But this is exactly given by the symplectic bilinear form defined above so that

$$\mathcal{A}_{\mathrm{I}} \equiv \operatorname{null} I = \{\eta \in \mathcal{A}_{\mathbb{R}} \mid \omega(\eta, \chi) = 0, \forall \chi \in \mathcal{A}\}. \tag{5.21}$$

This condition can be simplified into a matrix condition if we note that we can let $\eta = \sum_n a_n \sigma_n \Psi_0$ and $\chi = \sum_m b_m \sigma_m \Psi_0$, so that

$$0 = \omega(\eta, \chi) = -\tfrac{i}{2} a_n \Psi_0^\dagger [\sigma_n, \sigma_m] \Psi_0 b_m. \tag{5.22}$$

This relates the null-space of I to the null-space of the matrix $\Psi_0^\dagger [\sigma_n, \sigma_m] \Psi_0 \propto P^\mu_{mn}$, the term appearing in our Lagrangian which determines the canonically conjugate pairs of modes. Using the rank-nullity theorem, we have

$$\mathcal{A}_{\mathbb{R}} = \mathcal{A}_{\mathrm{I}} \oplus \mathcal{A}_{\mathrm{II}}. \tag{5.23}$$

Since the matrix given by elements $-\frac{i}{2}\Psi_0^\dagger[\sigma_n,\sigma_m]\Psi_0$ is real and antisymmetric, we can block-diagonalize the matrix with a special orthogonal transformation. Going to this basis and using our ansatz for the flowing mean-field $\Psi_0 = \sqrt{\rho}e^{i\vartheta}\chi$, the result is

$$-\tfrac{i}{2}\Psi_0^\dagger[\sigma_n,\sigma_m]\Psi_0 = -\tfrac{i}{2}\rho\chi^\dagger[\sigma_n,\sigma_m]\chi \quad = \rho \left(\begin{array}{cccc|cc} \overbrace{\begin{array}{cccc} 0 & \lambda_1 & 0 & 0 \\ -\lambda_1 & 0 & 0 & 0 \\ 0 & 0 & 0 & \lambda_2 \\ 0 & 0 & -\lambda_2 & 0 \end{array}}^{\mathcal{A}_{\mathrm{II}}} & \begin{array}{c} \cdots \\ \cdots \\ \\ \\ \ddots \end{array} & & \overbrace{\begin{array}{c} \\ \\ \\ \\ \end{array}}^{\mathcal{A}_{\mathrm{I}}} \\ \hline \begin{array}{cccc} & 0 & & \\ & \vdots & & \end{array} & & & \begin{array}{cc} 0 & \\ & \ddots \end{array} \end{array}\right) \tag{5.24}$$

with $\lambda_j > 0$. This defines a preferred basis for the broken generators $\{\sigma_l\}$ which we henceforth assume is the basis we are in. Note that in this basis $\mathcal{A}_{\mathrm{II}}$ takes the form of a direct sum of decoupled symplectic forms.

This matrix provides a natural way to break up the generators. First, we can define σ_n^{II} and its conjugate generator $\overline{\sigma_n^{\mathrm{II}}}$ via $-\frac{i}{2}\Psi_0^\dagger[\sigma_n^{\mathrm{II}},\overline{\sigma_n^{\mathrm{II}}}]\Psi_0 = \rho\lambda_n$. This implies that $\overline{\sigma_n^{\mathrm{II}}}\Psi_0 = i\sigma_n^{\mathrm{II}}\Psi_0$ (however $\overline{\sigma_n^{\mathrm{II}}} \neq i\sigma_n^{\mathrm{II}}$). Let n_{II} be the number of λ_j's, so that $\dim(\mathcal{A}_{\mathrm{II}}) = 2n_{\mathrm{II}}$. As the coefficient of the temporal derivative term in the Lagrangian, this matrix tells us that the two Goldstone fields described by $\sigma_n^{\mathrm{II}}\Psi_0(x)$ and $\overline{\sigma_n^{\mathrm{II}}}\Psi_0(x)$ are canonically conjugate to each other and therefore describe the **same mode**, a Type-II Goldstone mode. Finally, let $\dim(\mathcal{A}_{\mathrm{I}}) = n_{\mathrm{I}}$ be dimension of the null-space of I. This is the number of Type-I Goldstone modes; they represent modes which are canonically conjugate to a massive mode. It is evident by the rank-nullity result that

$$2n_{\mathrm{II}} + n_{\mathrm{I}} = D_{\mathbb{R}} \tag{5.25}$$

is the number of broken generators, while

$$n_{\mathrm{II}} + n_{\mathrm{I}} = D_{\mathbb{C}} \tag{5.26}$$

is the number of Goldstone modes in the system.

With this particular grating into n_{II} basis elements $\sigma_n^{\mathrm{II}}\Psi_0$ and n_{I} basis elements $\sigma_n^{\mathrm{I}}\Psi_0$, we can rewrite our real vector space

$$\mathcal{A}_{\mathbb{R}} = \mathrm{span}\{\sigma_n^{\mathrm{II}}\Psi_0, \overline{\sigma_n^{\mathrm{II}}}\Psi_0, \sigma_n^{\mathrm{I}}\Psi_0\}, \tag{5.27}$$

and similarly, we can write the complexified vector space in two equivalent ways

$$\begin{aligned} \mathcal{A}_{\mathbb{C}} &= \mathrm{span}_{\mathbb{C}}\{\sigma_n^{\mathrm{II}}\Psi_0, \sigma_n^{\mathrm{I}}\Psi_0\}, \\ \mathcal{A}_{\mathbb{C}} &= \mathrm{span}\{\sigma_n^{\mathrm{II}}\Psi_0, \overline{\sigma_n^{\mathrm{II}}}\Psi_0, \sigma_n^{\mathrm{I}}\Psi_0, i\sigma_n^{\mathrm{I}}\Psi_0\}. \end{aligned} \tag{5.28}$$

The modes represented by $i\sigma_n^{\mathrm{I}}\Psi_0$ are exactly the massive modes conjugate to $\sigma_n^{\mathrm{I}}\Psi_0$ (by definition, they are not in $\mathcal{A}$ and are thus not associated with a broken generator).

At low energies (below the relevant mass gaps), massive modes that are not conjugate to Goldstone modes can be trivially integrated out and do not contribute in the IR. This then leaves the Goldstone modes, which are gapless, and a few massive modes which are canonically conjugate to the Type-I Goldstone modes. These massive modes cannot be trivially integrated out and they are to be included in the low-energy theory. Doing so amounts to adding the basis elements $i\sigma_n^{\mathrm{I}}\Psi_0$ to our fluctuation manifold.

5.2.3 Lagrangian for Goldstone Modes

We now employ this classification into Type-I and -II modes to our benefit by using it to simplify the fluctuation Lagrangian. Recall that in this work we restrict

ourselves to flowing condensates which have a spatial texture to the phase mode (and thus inhomogeneously break the global $U(1)$ part of the symmetry group), but have a homogeneous and static spinor texture. For instance, one may consider a condensate of pseudo-spin-$\frac{1}{2}$ atoms in its ferromagnetic phase which has a definite homogeneous magnetization $\langle S_z \rangle = \chi^\dagger S_z \chi = \frac{1}{2}$ but a non-zero density and phase profile. As remarked earlier, this flow produces a non-zero spatial component for the Noether current $J_\mu(x)$. Going to the preferred basis of P^μ_{mn}, obtained in Sec. 5.2.2 then yields the partitioning into the Goldstone modes given by $\{\sigma^{\rm II}_n \Psi_0, \overline{\sigma^{\rm II}_n}\Psi_0, \sigma^{\rm I}_n \Psi_0\}$. Let us remind the reader that Type-I modes are those for which $i\sigma_n \Psi_0$ cannot be written as a broken generator $\sigma'_n \Psi_0$ and therefore, the associated real field comes with a massive term in the Lagrangian.

The basis elements $\{\sigma^{\rm II}_n \Psi_0, \sigma^{\rm I}_n \Psi_0\}$ have the property that they are orthogonal in the conventional sense (e.g. $\eta^\dagger \chi = 0$). As a result of this,

$$\begin{aligned} \Psi_0^\dagger \sigma^{\rm I}_n \sigma^{\rm II}_m \Psi_0 &= 0, \\ -\Psi_0^\dagger \sigma^{\rm II}_n \sigma^{\rm II}_m \Psi_0 &= \lambda_n \delta_{nm} \rho(x), \\ -\Psi_0^\dagger \sigma^{\rm I}_n \sigma^{\rm I}_m \Psi_0 &= \mu_n \delta_{nm} \rho(x), \end{aligned} \tag{5.29}$$

where we have defined $\mu_n \equiv -\chi^\dagger (\sigma^{\rm I}_n)^2 \chi > 0$ and used the fact that $\lambda_n = -\chi^\dagger (\sigma^{\rm II}_n)^2 \chi > 0$.

In this basis, the field variation $\delta\Psi(x)$ may be described by three real Goldstone fields θ_n, $\bar{\theta}_n$, and ϕ_n along with the real massive field β_n via

$$\begin{aligned} \hat{\sigma} &= \sum_{n=1}^{n_{\rm II}} \left(\theta_n \sigma^{\rm II}_n + \bar{\theta}_n \overline{\sigma^{\rm II}_n} \right) + \sum_{n=1}^{n_{\rm I}} \phi_n \sigma^{\rm I}_n, \\ \xi &= \sum_{n=1}^{n_{\rm I}} \beta_n i \sigma^{\rm I}_n \Psi_0 + \cdots, \end{aligned} \tag{5.30}$$

where "$\cdots$" represents other massive modes that can be trivially integrated out. In

this basis, the coefficient P^{μ}_{mn} simplifies to

$$P^{\mu}_{mn} = \delta_{n\bar{m}}\lambda_n \rho(x) v^{\mu}_s, \tag{5.31}$$

where $\bar{m}$ is defined as the index of the conjugate field to the field labeled by m. Similarly, we may simplify Q^{μ}_{mn} which connects Type-I Goldstone modes to their conjugate massive fields. We indeed find

$$Q^{\mu}_{mn} = 2\delta_{nm}\mu_n \rho(x) v^{\mu}_s, \tag{5.32}$$

where the massive field with index m is indicated by the basis element $i\sigma^{\mathrm{I}}_m \Psi_0$. Lastly, we have the kinetic energy term which we can separate out into its contribution to Type-I and Type-II fields

$$\begin{aligned} T^{jk}_{mn}|_{\mathrm{I}} &= -\tfrac{1}{2m}\delta^{jk}\rho(x)\mu_n\delta_{mn} \\ T^{jk}_{mn}|_{\mathrm{II}} &= -\tfrac{1}{2m}\delta^{jk}\rho(x)\lambda_n\delta_{mn} \end{aligned} \tag{5.33}$$

Notice that λ_n or μ_n multiplies all elements in the Lagrangian where that field (or its conjugate) appears, so we can simply absorb this constant into a re-definition of θ_n, $\bar{\theta}_n$, ϕ_n, and β_n. Then, substituting the form of our fluctuations, the Lagrangian is

$$\begin{aligned} \mathcal{L}_{\mathrm{fluc}} = &\sum_{n=1}^{n_{\mathrm{I}}} \rho(x)\left[-2\beta_n v^{\mu}_s(x)\partial_\mu\phi_n - \tfrac{1}{2m}[(\nabla\phi_n)^2 + (\nabla\beta_n)^2] - 2mc_n^2(x)\beta_n^2\right] \\ &+ \sum_{n=1}^{n_{\mathrm{II}}} \rho(x)\left\{-v^{\mu}_s(x)(\bar{\theta}_n\overrightarrow{\partial_\mu}\theta_n - \bar{\theta}_n\overleftarrow{\partial_\mu}\theta_n) - \tfrac{1}{2m}[(\nabla\theta_n)^2 + (\nabla\bar{\theta}_n)^2]\right\}. \end{aligned} \tag{5.34}$$

Since the basis for Type-I modes is not uniquely fixed by the canonical conjugate structure of Eq. (5.24), this leaves us free to diagonalize the mass tensor produced by the variation of the potential in Eq. (5.11). Doing so produces the effective chemical

potential terms, $mc_n^2(x)$.

We end this section with a note about the validity of this fluctuation Lagrangian: it can be seen that the overall size of this action is set by the condensate density $\rho(x)$, which uniformly multiplies all terms. Thus, the condensate density $\rho(x)$ acts to enforce the saddle-point in the sense that if it is large, the fluctuation contribution from $\mathcal{L}_{\text{fluc}}$ is suppressed. This tells us that our approach ought not be valid if either the condensate density is strongly fluctuating or vanishing all-together, as might happen at finite temperatures or near e.g. the core of a vortex. Additionally, there may be breakdowns in smaller dimensional systems, where long-range order is prohibited by Mermin-Wagner [189–191]. Barring these considerations, we proceed on to study the properties of the effective field theory described in Eq. (5.34). We first consider the case where the Goldstone mode is Type-I, and then we study the case of a Type-II mode.

5.2.4 Type-I Goldstones: Relativistic Spacetime

Consider an isolated Type-I Goldstone mode, with Lagrangian

$$\mathcal{L}_{\text{I}} = \rho(x)[-2\beta v_s^\mu(x)\partial_\mu\phi - \tfrac{1}{2m}[(\nabla\phi)^2 + (\nabla\beta)^2] - 2mc^2(x)\beta^2], \tag{5.35}$$

we assume that $mc^2(x)$ is large enough to dominate over the kinetic energy for β, so that β can be easily integrated out via $mc^2(x)\beta = -2v_s^\mu\partial_\mu\phi$. We get the resulting Lagrangian, valid at long wavelengths and times

$$\mathcal{L}_{\text{I}}^{\text{eff}} = \frac{\rho(x)}{2m}\left[\left(\frac{v_s^\mu(x)\partial_\mu\phi}{c(x)}\right)^2 - (\nabla\phi)^2\right]. \tag{5.36}$$

This describes a scalar field propagating along geodesics of an emergent space-time metric $\mathcal{G}_{\mu\nu}$ with

$$\mathcal{L}_{\text{I}}^{\text{eff}} = \tfrac{1}{2}\sqrt{-\mathcal{G}}\mathcal{G}^{\mu\nu}\partial_\mu\phi\partial_\nu\phi, \tag{5.37}$$

and $\mathcal{G}^{\mu\nu}$ given by the line-element

$$ds^2 = \frac{\rho}{c}[c^2dt^2 - (d\mathbf{x} - \mathbf{v}dt)^2] = \mathcal{G}_{\mu\nu}dx^\mu dx^\nu. \tag{5.38}$$

This was first observed by Unruh in Ref. [17] where he showed that metrics of the form given above can possess non-trivial features including event-horizons. Indeed, the metric for a Schwarschild black hole can take a very similar form in certain coordinate systems. One of the central results of this chapter is the extension of this analog to include the Type-II modes, which do not have emergent Lorentz invariance. This is shown below.

5.2.5 Type-II Goldstones: Non-relativistic Spacetime

We focus on a single Type-II Goldstone mode, for which there is no massive field to integrate out. We are left with the fluctuation Lagrangian

$$\mathcal{L}_{\text{II}} = \rho(x)\left[-v_s^\mu(x)\left(\bar{\theta}\partial_\mu\theta - \theta\partial_\mu\bar{\theta}\right) - \tfrac{1}{2m}[(\nabla\theta)^2 + (\nabla\bar{\theta})^2]\right]. \tag{5.39}$$

To simplify things, we group the two real fields into one complex field $\psi = \theta + i\bar{\theta}$ so that we have

$$\mathcal{L}_{\text{II}} = \rho[\tfrac{i}{2}v_s^\mu(\psi^*\overrightarrow{\partial_\mu}\psi - \psi^*\overleftarrow{\partial_\mu}\psi) - \tfrac{1}{2m}|\nabla\psi|^2]. \tag{5.40}$$

It turns out this too has a simple geometric description in terms of an emergent curved space-time. However, instead of being an "Einsteinian" geometry, the resulting description is in terms of a Newton-Cartan geometry [28, 29, 32–34, 183].

Newton-Cartan geometry consists of three key objects: $(n_\mu, v^\mu, h^{\mu\nu})$. These are not all independent, but rather must satisfy the constraints

$$n_\mu v^\mu = 1, \quad n_\mu h^{\mu\nu} = 0. \tag{5.41}$$

Also note that the indices on these objects are given as covariant and contravariant specifically and cannot be freely raised/lowered without the definition of a metric tensor (which we describe how to construct in Sec. 5.5).

To understand the geometry these objects encode, we begin with the fundamental object that enforces time's special status within a nonrelativistic theory: n_μ. As a one-form, n_μ (colloquially, we call it the "clock" one-form) can be imagined as a series of surfaces (foliations), and when a spacetime displacement vector is contracted with it, it gives the elapsed time in a covariant manner. In conjunction with the clock one-form, we have the velocity field v^μ, which must go forward a unit of time (hence the constraint $n_\mu v^\mu = 1$) as a four-velocity; flow along v^μ causally connects spatial surfaces. Lastly, the spatial metric $h^{\mu\nu}$ is degenerate ($n_\mu h^{\mu\nu} = 0$) since it solely describes the geometry confined to the d-dimensional spatial foliations. While in what follows we describe $h^{\mu\nu}$ emerging from intrinsic properties of the fluid flow, it can also inherit extrinsic contributions (i.e. if the fluid is flowing on an actual curved manifold).

In the presence of this curved Newton-Cartan geometry, the Lagrangian for a massless scalar field takes the form

$$\mathcal{L} = n_0\sqrt{h}[\tfrac{i}{2}v^\mu(\psi^*\overrightarrow{\partial_\mu}\psi - \psi^*\overleftarrow{\partial_\mu}\psi) - \tfrac{h^{\mu\nu}}{2m}\partial_\mu\psi^*\partial_\nu\psi] \tag{5.42}$$

where $h = (|\det h^{ij}|)^{-1}$.

The Lagrangian of a Type-II Goldstone mode may be brought into this form. Relating Eq. (5.40) to Eq. (5.42), we can extract the geometric objects n_μ, v^μ, and $h^{\mu\nu}$. We see that in our systems $h^{00} = 0 = h^{0i}$, and that $h^{ij} = h^{-1/d}\delta^{ij}$ in d spatial

dimensions. Therefore, we know $n_i = 0$; hence, $n_0 v^0 = 1$. Relating terms, we have

$$\begin{aligned} \sqrt{h} &= \rho, \\ n_0 \sqrt{h} v^i &= \rho v_{\mathrm{s}}^i, \\ n_0 h^{(d-2)/(2d)} &= \rho. \end{aligned} \tag{5.43}$$

This gives us the geometric quantities

$$h = \rho^2, \quad n_0 = \rho^{2/d}, \tag{5.44}$$

and hence

$$\begin{aligned} n_\mu &= [\rho^{2/d}, 0], \\ v^\mu &= \rho^{-2/d} v_s^\mu, \\ h^{ij} &= \rho^{-2/d} \delta^{ij}. \end{aligned} \tag{5.45}$$

One important aspect of Newton-Cartan geometry is the notion of "torsion" [192]. Regarded as a differential form, the clock one-form $n = n_\mu dx^\mu$ is in general not an exact differential. This is seen by taking the exterior derivative, which defines the "torsion tensor" $\omega = dn$. Explicitly,

$$\omega_{\mu\nu} = \partial_\mu n_\nu - \partial_\nu n_\mu. \tag{5.46}$$

It is straightforward to see that in general, the torsion tensor in our geometry is non-zero;

$$\omega_{0j} = \partial_j n_0 = \partial_j \rho^{2/d}. \tag{5.47}$$

Were the torsion zero, we could define an absolute time coordinate T, from which we would get the clock one-form as $n = dT$. While the non-zero torsion implies there is

no such absolute time, we may confirm that the more general condition

$$n \wedge dn = 0 \tag{5.48}$$

is satisfied. This is a necessary and sufficient condition for the foliation of spacetime into "space-like" sheets which are orthogonal to the flow of time [192]. As such, there is still a notion of causality in this geometry.

We conclude by commenting that the Newton-Cartan geometry we find here is in fact intimately related to the gravitational field first considered by Luttinger in the context of calculating heat transport [31]. In that limit $n_\mu \propto [e^\Phi, 0]$, and so the gravitational potential (up to scale factor in the logarithm) would be

$$\Phi = \frac{2}{d} \log(\rho). \tag{5.49}$$

Using this connection, quantities like energy current and the stress-momentum tensor can be calculated as we discuss in Sec. 5.5. First, we explore a minimal realization of these geometries and the associated quantum phases in Sec. 5.3 as well as the fate of the Hawking effect across such a transition in Sec. 5.4.

5.3 Minimal Theoretical Model

In this section, we introduce a minimal model which exhibits a transition between an Einstein-Hilbert and Newton-Cartan spacetime. We begin by analyzing the ground state within mean-field theory. Once this is understood, we study the behavior of fluctuations about the mean-field by employing a BdG description.

The model is that of a pseudospin $\frac{1}{2}$ bosonic field $\Psi(x) = \big(\Psi_\uparrow(x), \Psi_\downarrow(x)\big)^T$ with

the following Lagrangian density

$$\mathcal{L} = \Psi^\dagger \left(i\partial_t + \frac{1}{2m}\nabla^2 + \mu \right) \Psi - \frac{1}{2} g_0 \left(\Psi^\dagger \Psi \right)^2 - \frac{1}{2} g_3 \left(\Psi^\dagger \sigma_3 \Psi \right)^2 \quad (5.50)$$

where σ_j are the Pauli matrices for the pseudo-spin and μ is the chemical potential, which controls the conserved density of the bosons, $\rho = \Psi^\dagger \Psi$. The coupling $g_0 > 0$ describes a $U(2) = U(1) \times SU(2)$ invariant repulsive density-density contact interaction, as may be expected in a typical spinor BEC, while the g_3 parameter introduces anisotropy into the spin exchange interaction. The g_3 coupling explicitly breaks the $SU(2)$ symmetry down to $U(1) \otimes \mathbb{Z}_2$ comprised of rotations of the Bloch vector by any angle about the z axis and reflections of the Bloch vector through the xy mirror plane. Note that stability requires that $g_3 > -g_0$.

Let us briefly comment that, while Lagrangian (5.50) is a perfectly valid model, a more natural set-up may be realized by the more experimentally available spin-1 systems such as condensed ^{7}Li, ^{23}Na, or ^{87}Rb. All of these atoms are bosons which have a total hyperfine spin $F = 1$ manifold [181]. In this case, the phase transition is between two phases which both respect the full $SU(2)$ spin-rotation symmetry—the ferromagnetic phase and polar (nematic) phase [188, 193, 194]. In this case, rather than being driven by anisotropy, the transition is driven by the overall sign of the spin-exchange interaction. It turns out that the different ground-state phases have different types of Goldstone modes and therefore exhibit different analog spacetimes for the spin waves once condensate flow is introduced. The relevant coupling constant is the spin-exchange coupling c_2, which is given in terms of the scattering lengths by

$$c_2 = \frac{4\pi}{m} \frac{a_2 - a_0}{3}.$$

For ^{7}Li and ^{87}Rb,$c_2 < 0$ while for ^{23}Na $c_2 > 0$ [181]. Thus, all else equal we can realize both the polar (nematic) phase (which occurs for $c_2 > 0$) as well as the ferromagnetic phase ($c_2 < 0$) by using two different species of trapped atom. All this is to say that, while Eq. (5.50) is not as easily realized experimentally, there may be more experimentally feasible models which realize the same physics. We now move on to the analysis of the technically simpler model proposed above.

The mean-field ground state of Eq. (5.50) is identified as the homogeneous minimum of the energy density

$$V = \frac{1}{2}g_0 \left(\Psi^\dagger \Psi\right)^2 + \frac{1}{2}g_3 \left(\Psi^\dagger \sigma_3 \Psi\right)^2 - \mu \Psi^\dagger \Psi.$$

For $\mu < 0$ the ground state is trivial and there is no condensate. For $\mu > 0$ there is Bose-Einstein condensation and the ground state is a BEC with a uniform condensate density which obeys the equation of state

$$\rho = \Psi^\dagger \Psi = \begin{cases} \frac{\mu}{g_0}, & g_3 > 0, \\ \frac{\mu}{g_0 - |g_3|}, & -g_0 < g_3 < 0. \end{cases}$$

A non-zero condensate density always spontaneously break the overall $U(1)$ phase symmetry. The corresponding Goldstone mode corresponds to the broken generator $i\sigma_0 = i\mathbb{1}$ where $\mathbb{1}$ is the 2×2 identity matrix.

Depending on the value of g_3, additional symmetries may be broken, resulting in the phase diagram illustrated in Fig. 5.1. We write the condensed Ψ in the density-phase-spinor representation as

$$\Psi = \sqrt{\rho} e^{i\Theta} \chi, \quad \chi^\dagger \chi = 1 \tag{5.51}$$

where χ yields the local magnetization density. It may be parameterized in terms

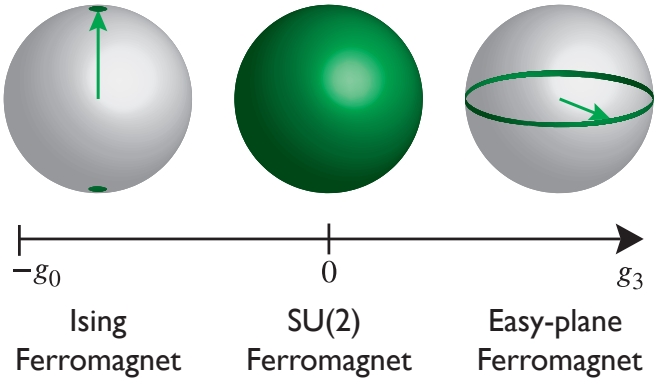

Figure 5.1: Illustration of the different ground-state Bloch-vector manifolds as the parameter g_3 is tuned. For $g_3 < 0$ the ground state manifold consists of the north and south poles and thus the system realizes an Ising ferromagnet, spontaneously breaking the $\mathbb{Z}_2$ symmetry while maintaining the $U(1)$ symmetry. For $g_3 = 0$ the full $SU(2)$ symmetry is realized and the ground-state manifold consists of the entire Bloch sphere. Thus, the system is a Heisenberg ferromagnet which spontaneously breaks the full $SU(2)$ down to $U(1) \subset SU(2)$. Finally, for $g_3 > 0$ the ground state manifold consists of the equatorial plane, rendering the system an XY (easy-plane) ferromagnet. Thus, the initial symmetry is $U(1)$ which is spontaneously broken to the trivial group.

Phase	Sound waves	Spin waves
Ising Ferromagnet	$\omega \sim k$	Gapped
SU(2) Ferromagnet	$\omega \sim k$	$\omega \sim k^2$
Easy-plane Ferromagnet	$\omega \sim k$	$\omega \sim k$

Table 5.2: Goldstone modes associated to each phase shown in Fig. 5.1. All phases have a Type-I Goldstone mode associated to the spontaneous breaking of the global $U(1)$ phase, corresponding to the conventional sound mode. Additionally, there may also be Goldstone modes associated with spontaneous breaking of spin symmetries, leading to spin waves. In the Ising phase, the broken symmetry is discrete and there are no Goldstone modes. In the SU(2) invariant Heisenberg phase there is a Type-II Goldstone mode describing transverse fluctuations of the magnetization, while in the XY easy-plane phase there is a Type-I Goldstone describing equatorial fluctuations of the magnetization.

of one complex parameter ζ via

$$\chi = \frac{1}{\sqrt{2(1+|\zeta|^2)}} \begin{pmatrix} 1+\zeta \\ 1-\zeta \end{pmatrix}, \quad \zeta \in \mathbb{C}. \tag{5.52}$$

Alternatively, it may be represented in the more canonical Euler angle representation as

$$\chi = \begin{pmatrix} \cos\frac{\theta}{2} \\ \sin\frac{\theta}{2} e^{i\varphi} \end{pmatrix}, \quad \varphi \in [0, 2\pi) \quad \theta \in [0, \pi).$$

We use both of these representations throughout. In terms of ζ and θ, φ the anisotropic interaction is

$$V = \frac{1}{2} g_3 \rho^2 \frac{(\zeta + \zeta^*)^2}{(1+|\zeta|^2)^2} = \frac{1}{2} g_3 \rho^2 \cos^2\theta.$$

We now proceed to study the mean-field phase diagram of the ground state.

Ising phase.—We begin by considering the case of $g_3 < 0$, i.e. the "Ising ferromagnet" phase. The interaction has a $U(1) \times \mathbb{Z}_2$ symmetry generated by $\frac{i}{2}\sigma_3$ composed with inversion of the z component of the magnetization. In this case it is energetically favorable for the Bloch vector to align with the z axis. This breaks the $\mathbb{Z}_2$ symmetry and preserves $U(1)$ so the ground state manifold is the symmetric space $U(1) \times \mathbb{Z}_2/U(1) \sim \mathbb{Z}_2$. This is depicted in the left-most panel of Fig. 5.1, which shows the ground-state manifold for the spinor χ for various couplings. The Goldstone modes associated with the broken-symmetry ground-state, along with their dispersions are shown in Table 5.2. As the ground-state manifold is discrete there is no additional Goldstone mode in this phase and we no longer consider this portion of the phase diagram in this work.

Heisenberg phase.—When $g_3 = 0$ the interaction term is isotropic and the model has the full $SU(2)$ invariance. The ground state then spontaneously break the $SU(2)$

symmetry down to $U(1)$ so that the ground state manifold is the symmetric space $SU(2)/U(1) \sim S^2$—the full Bloch sphere. This is illustrated in the middle panel of Fig. 5.1. Without loss of generality, we take the ground state magnetization to point along the positive x direction. Thus, $\zeta = 0$ and $\chi = \frac{1}{\sqrt{2}}(1,1)^T$. Then the unbroken generators are $\{\frac{i}{2}(\sigma_1 - \mathbb{1})\}$ and the broken generators are $\{\frac{i}{2}(\sigma_1 + \mathbb{1}), \frac{i}{2}\sigma_2, \frac{i}{2}\sigma_3, \}$. Using the formalism from Sec. 5.2, we find that the P matrix appearing in the Goldstone mode Lagrangian is

$$P^t = \rho \begin{pmatrix} 0 & 0 & 0 \\ 0 & 0 & \frac{1}{4} \\ 0 & -\frac{1}{4} & 0 \end{pmatrix}, \tag{5.53}$$

where the columns refer, in order, to the generators $\{\frac{1}{2}i\sigma_0 + \frac{1}{2}i\sigma_1, \frac{1}{2}i\sigma_2, \frac{1}{2}i\sigma_3\}$. In this case, we have one Type-II Goldstone mode associated with the two generators $\{\frac{1}{2}i\sigma_2, \frac{1}{2}i\sigma_3\}$ which exhibits a quadratic dispersion relation and hence realize the Newton-Cartan geometry in the presence of inhomogeneous condensate flow. This is summarized in Table 5.2.

XY phase.—We now move on to the case where $g_3 > 0$. In this case there is an energy penalty associated with a non-zero z component of the magnetization and thus the ground state lies in the manifold defined by $\cos\theta = 0 \Rightarrow \theta = \pi/2$. Thus, the ground state breaks the $U(1)$ symmetry but remains invariant under reflections through the $z = 0$ plane. As such, the ground state resides in the symmetric space $U(1) \times \mathbb{Z}_2/\mathbb{Z}_2 = U(1) \sim S^1$, as depicted in the right panel of Fig. 5.1. Without loss of generality we again take the Bloch vector to lie along the $+x$ direction. Thus, only two generators remain unbroken in the Lagrangian $\{i\mathbb{1}, \frac{1}{2}i\sigma_3\}$ and the mean-field breaks both of them. We again refer to Eq. (5.24) to obtain

$$P^t_{mn} = 0. \tag{5.54}$$

Thus, there are no Type-II Goldstone modes in this system, but instead two Type-I modes which are linearly dispersing and therefore exhibit an analog Einstein-Hilbert spacetime, summarized in Table 5.2.

5.3.1 Bogoliubov-de Gennes Analysis

We now proceed to examine the fluctuations about the mean-field by obtaining and diagonalizing the Bogoliubov-de Gennes equations of motion. To see how the analog spacetime emerges we consider a mean-field condensate ψ_0 which is inhomogeneous, but has a constant magnetization density. Taking the spin to point in the $+x$ direction, we obtain

$$\psi_0 = \sqrt{\rho(x)}e^{i\Theta(x)}\chi_0 = \sqrt{\rho(x)}e^{i\Theta(x)}\begin{pmatrix}\frac{1}{\sqrt{2}}\\ \frac{1}{\sqrt{2}}\end{pmatrix}. \tag{5.55}$$

In this case, the mean-field describes a flowing condensate with superfluid density $\rho(x) = \psi_0^\dagger(x)\psi_0(x)$ and superfluid velocity $\mathbf{v}_s = \frac{1}{m}\nabla\Theta(x)$. Fluctuations about this mean-field can be fully parameterized in terms of the two complex fields ϕ and ζ as

$$\delta\Psi = (\phi\sigma_0 + i\zeta\sigma_2)\,\psi_0. \tag{5.56}$$

To quadratic order, the Lagrangian from Eq. (5.50) decouples into two quadratic BdG Lagrangians

$$\mathcal{L}_\phi = \rho\left[\tfrac{i}{2}(\phi^* D_t\phi - \phi D_t\phi^*) - \tfrac{|\nabla\phi|^2}{2m} + \tfrac{1}{2}g_0\rho(\phi+\phi^*)^2\right] \tag{5.57a}$$

$$\mathcal{L}_\zeta = \rho\left[\tfrac{i}{2}(\zeta^* D_t\zeta - \zeta D_t\zeta^*) - \tfrac{|\nabla\zeta|^2}{2m} + \tfrac{1}{2}g_3\rho(\zeta+\zeta^*)^2\right] \tag{5.57b}$$

with $D_t = \partial_t + \mathbf{v}_s\cdot\nabla$ the material derivative in the frame co-moving with the superfluid flow. These two Lagrangians are specific examples of the more general

Eq. (5.34). In particular, for $g_3 > 0$ at long wavelengths we can apply the analysis of Sec. 5.2.4 to obtain the relativistic analog spacetime. If on the other hand, $g_3 = 0$, then at long wavelengths we can apply the analysis of Sec. 5.2.5 to obtain the nonrelativistic Newton-Cartan analog spacetime. Nevertheless, it is instructive to instead follow Ref. [129, 170], and directly employ the BdG equations when determining the consequences of the changing spacetime structure. This is because the BdG equations provide us with a single unified description with which we may capture both phases, as well as the transition between them.

The BdG equations are obtained as the Euler-Lagrange equations of Lagrangians $\mathcal{L}_\phi, \mathcal{L}_\zeta$ and are most transparently expressed in terms of the Nambu spinors

$$\Phi_0 = \begin{pmatrix} \phi \\ \phi^* \end{pmatrix}, \quad \Phi_3 = \begin{pmatrix} \zeta \\ \zeta^* \end{pmatrix} \tag{5.58}$$

for condensate and spin wave fluctuations, respectively. We then find the BdG equations $\hat{K}_0\Phi_0 = 0$, and $\hat{K}_3\Phi_3 = 0$, with the BdG differential operators

$$\hat{K}_0 = \tau_3 \left(i\partial_t + i\mathbf{v}_s \cdot \nabla\right) + \frac{1}{2m\rho}\nabla \cdot \rho\nabla\tau_0 - g_0\rho\left(\tau_0 + \tau_1\right) \tag{5.59a}$$

$$\hat{K}_3 = \tau_3 \left(i\partial_t + i\mathbf{v}_s \cdot \nabla\right) + \frac{1}{2m\rho}\nabla \cdot \rho\nabla\tau_0 - g_3\rho\left(\tau_0 + \tau_1\right), \tag{5.59b}$$

written in terms of the Nambu particle-hole Pauli matrices τ_a. Let us emphasize that the only difference between $\hat{K}_0$ and $\hat{K}_3$ is the coupling constant appearing in front of the $\tau_0 + \tau_1$ term. For sound waves it is g_0, while for the spin waves it is g_3. Thus, both Goldstone modes end up coupling to the same background condensate density and velocity, albeit with different speeds of sound. Sound waves end up propagating with the local group velocity $c_0(x) = \sqrt{\frac{g_0\rho(x)}{m}}$ while the spin waves have the local group velocity $c_3(x) = \sqrt{\frac{g_3\rho(x)}{m}}$. Thus, we see that the coupling g_3 allows us to independently tune the two speeds of sound relative to each other.

For generic values of $g_3 > 0$ and arbitrary condensate flows we cannot find quantum numbers with which we can diagonalize $\hat{K}_3$. However, at the $SU(2)$ symmetric point $g_3 = 0$ we observe that the BdG kernel for spin waves obeys

$$\hat{K}_3 = \tau_3 \left(i\partial_t + i\mathbf{v} \cdot \nabla \right) + \frac{1}{2m\rho} \nabla \cdot \rho \nabla \tau_0 \Rightarrow \left[\tau_3, \hat{K}_3 \right] = 0. \tag{5.60}$$

Since τ_3 now commutes with the kernel, the two components of the BdG spinor decouple and each independently obeys a Galilean-invariant dispersion relation. This also results in an additional $U(1)$ symmetry generated by τ_3 which imposes a selection rule for the allowed Bogoliubov transformations. In particular, there is no matrix element which scatters a "particle-like" Bogoliubov quasiparticle into a "hole-like" particle. this process is the one responsible for Hawking radiation and as such we find, counter-intuitively, that it is impossible to generate Hawking radiation in the Newton-Cartan spacetime despite the fact that all flow velocities $\mathbf{v}_s$ are now supersonic. This is explicitly demonstrated for the case of a step-like horizon, which we analyze in the following section.

5.4 Step-Like Horizon

In order to get a more quantitative understanding of how the changing spacetimes affect observable physics, we imagine a specific flow profile and use the BdG equations to solve for the spin-wave scattering matrix. We imagine a quasi-one-dimensional stationary condensate flow with a superfluid density and velocity which obeys $\partial_t \rho = \partial_t v_s = 0$. The continuity equation for the condensate then implies

$$\partial_x (\rho v_s) = 0 \Rightarrow \rho(x) v_s(x) = \text{const.} \tag{5.61}$$

The local speed of sound for the spin-waves (henceforth simply written as c) is therefore $c(x) = \sqrt{g_3 \rho(x)/m}$.

To further simplify calculations, we consider the case of a step-like profile for $\rho(x), v(x)$ of the form

$$\rho(x) = \begin{cases} \rho_l & x < 0 \\ \rho_r & x \geq 0 \end{cases} \tag{5.62a}$$

$$v(x) = \begin{cases} -|v_l| & x < 0 \\ -|v_r| & x \geq 0. \end{cases} \tag{5.62b}$$

Note that continuity requires $v_l \rho_l = v_r \rho_r \Leftrightarrow v_l c_l^2 = v_r c_r^2$. In this work we adopt the convention that v is negative, so that the condensate flows from the right to the left. With this set-up, we can employ the BdG techniques usually used for phonon modes to these spin waves [129, 170].

This step-like potential has the advantage that away from the jump, momentum eigenstates solve the BdG equations, and the scattering matrix reduces to a simple plane-wave matching condition at the boundary. The details of this procedure may be found, e.g. in Appendix H. Here we simply discuss the results of the calculation. We start by considering $g_3 > 0$ to be large and then decrease down to zero. As we do so, while keeping the flow profile fixed, we pass through three regimes.

The first regime occurs for large g_3 so that $c_l > |v_l|$ and $c_r > |v_r|$. Thus, there is no sonic horizon and no Hawking radiation.

Eventually as we continue decreasing g_3 we enter the regime where $|v_r| < c_r$ but $c_l < |v_l|$. This exhibits a sonic horizon at $x = 0$ and is thus accompanied by Hawking radiation.

Finally, we reach the regime where $|v_l| > c_l$ and $|v_r| > c_r$. This is a novel regime wherein both the interior and exterior of the jump are supersonic. However, due to the non-linear Bogoliubov dispersion, there are still some short-wavelength modes for which one or both sides of the flow are not supersonic (this is due to

the convex dependence of the group-velocity on momentum). Thus there is still Hawking radiation, however we find that as we decrease g_3 further, the total "flux" of modes which are emitted decreases until we recover the result that at $g_3 = 0$ there is no radiation at all.

To see this, we define the "total number of Hawking modes" at a given frequency to be $N(\omega)$ (see Eqs. (H.20) and (H.22)). This is obtained by calculating the "Hawking" element of the scattering matrix for the BdG equations. From $N(\omega)$ we can then define the total "luminosity" [162] leaving the horizon by

$$L_{\mathrm{H}} = \int_0^\infty d\omega \, \frac{\omega}{2\pi} N(\omega). \tag{5.63}$$

Note that in the conventional black hole case, $N(\omega)$ is the number of photons at frequency ω seen at asymptotic infinity and thus this is simply the number flux per unit frequency of the radiation.

The upshot is given by Fig. 5.2 which plots L_{H} as a function of $(c_r/v_r)^2 = g_3\rho_r/mv_r^2$. Thus, for fixed flow density and velocity, this is essentially plotting as a function of the control parameter g_3. We see the three distinct regions and importantly at $g_3 = 0$ we see the Hawking effect vanish.

To understand this effect, we consider the dispersion relation of the waves away from the horizon, for which momentum is a good quantum number. In the right and left half-spaces we have the relations

$$(\omega - v_\alpha k)^2 = c_\alpha^2 k^2 + \frac{k^4}{4m^2}, \tag{5.64}$$

where $\alpha = l, r$ for the left and right regions respectively. This relates the lab-frame frequency of a wave ω to the lab-frame momentum k. This dispersion relation is plotted in Figs. 5.3 and 5.4. Due to the presence of a discontinuity at $x = 0$ modes with different momenta mix and only ω can be fixed globally. Thus, the dispersion

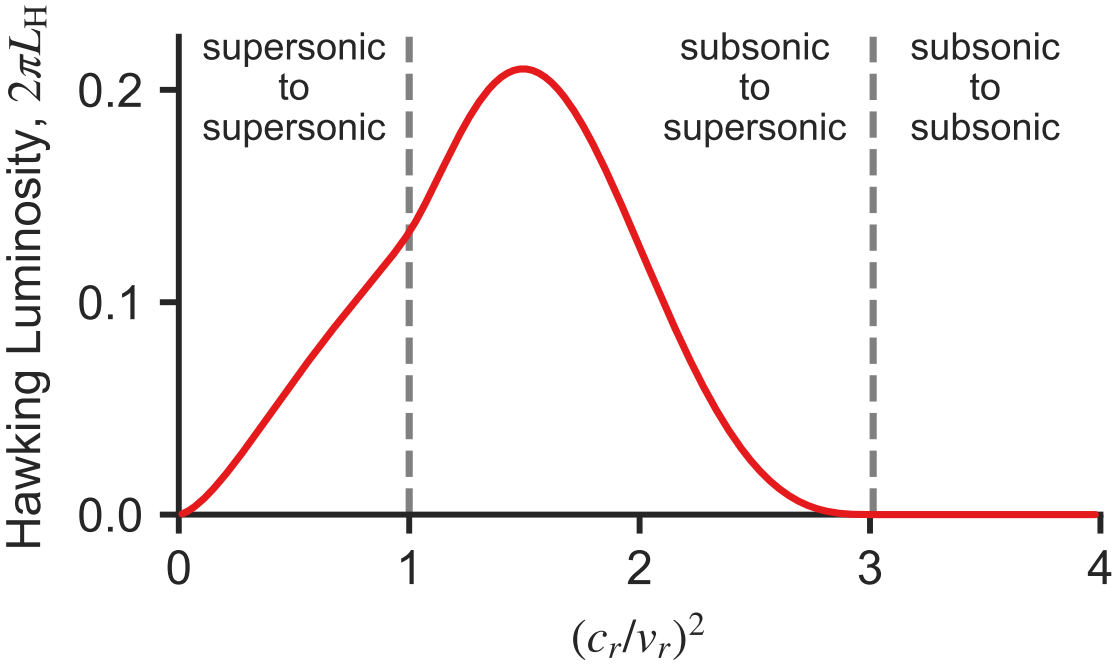

Figure 5.2: The total luminosity due to the Hawking radiation for a fixed density profile $\rho(x)$ and velocity profile $v(x)$. We see that there is no Hawking radiation when c_r is sufficiently large so that $c_l > v_l$ (recall these are constrained by the continuity equation). When $c_l < v_l$ but $c_r > v_r$ we get a region of subsonic flow that flows into a supersonic region and we begin seeing traditional Hawking radiation. As we further tune g_3, c_r drops below v_r and both regions become supersonic at low frequencies. Evidently, there is still a channel for Hawking radiation emission as seen by the non-zero integrated flux. However, as c_r drops to zero this channel closes, vanishing precisely at the quantum phase transition into the Newton-Cartan geometry ($c_r = 0 = g_3$). In this plot, $v_l = 1.3$, $v_r = 0.9$, $m = 10$, and $\rho(x)v(x) = 1$.

relation is to be solved by finding the allowed momenta at each fixed lab-frame frequency. This amounts to finding the roots of a quartic polynomial with real coefficients, and as such there are always four solutions (which are either real or complex conjugate pairs). The real momenta represent propagating modes while we later find that the complex roots describe evanescent modes localized around the horizon.

5.4.1 Subsonic-Supersonic Jump

First, we consider the case of a jump between a subsonic and supersonic flow, depicted graphically in Fig. 5.3. In this case, we recover the well-known result that there is Hawking radiation emitted. The dispersion relation in each half-plane is plotted and intercepts with a constant $\omega > 0$ are found. These intercepts yield the momenta of the propagating modes in each region for the given frequency. Each curve is depicted with a color indicating the sign of the group velocity in the **co-moving** frame, which is what is used to distinguish between "particle-like" (red) and "hole-like" (blue), in accordance with the BdG norm (see Appendix H and in particular Eq. (H.3) for definition). We see that the outgoing Hawking mode (combined with an evanescent piece at the horizon) is connected to three incoming waves, one of which is a negative norm state originating from the interior of the horizon. This particle-hole conversion processes is the origin of the Hawking effect, as this induces a Bogoliubov transformation which connects the vacuum of the asymptotic past to a one-particle state in the asymptotic future (and vice-versa).

We see that due to the convex non-linear Bogoliubov dispersion relation, there is a maximum frequency of the emitted Hawking radiation obtained by finding the local maximum of the negative norm dispersion relation. Above this frequency, the flow is no longer supersonic since the group velocity of modes depends non-trivially on the frequency.

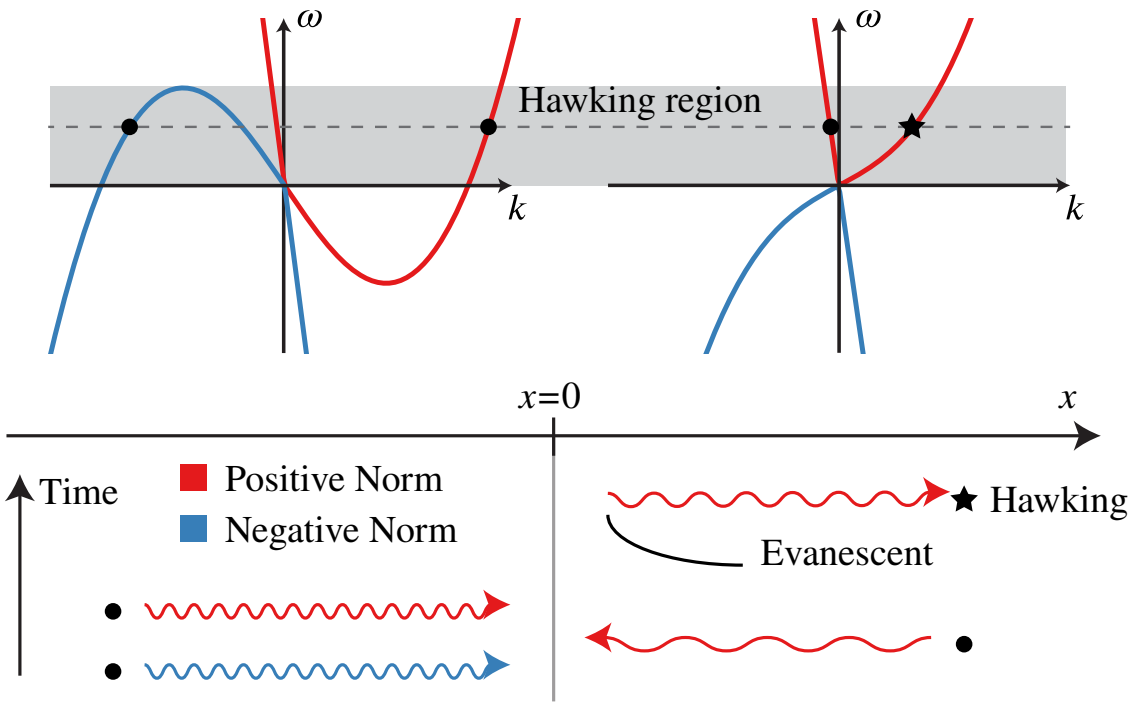

Figure 5.3: The Hawking effect for g_3 such that $c_r > v_r$ and $c_l < v_l$ (sub-sonic to super-sonic). In this situation, one side (left) flows faster than the speed of some excitations, and the other side (right) flows slower than the speed of any excitation. The dashed line represents the constant lab frame energy ω. The mode that carries away energy from the horizon is the "Hawking mode," shown by the star marker. Tracing this mode back in time (bottom of figure), we find that it comes from a scattering process that includes positive (red) and negative (blue) norm states. It is the negative norm state to the left of the horizon that is responsible for particle creation in the Hawking channel. Notice that for frequencies larger than those in the labeled "Hawking region," there is no Hawking effect due to lack of negative energy modes to have scattered from at earlier times.

5.4.2 Supersonic-Supersonic Jump

As we decrease g_3 beyond a critical value the system enters a parameter regime where both sides of the jump are supersonic flows. In this case, the dispersion relation still exhibits a Hawking-like region, as we see in Fig. 5.4. However, we also see a new region emerge at low energies (labeled "super-Hawking" in the figure) in which now both a positive and negative norm mode can be scattered into. This opens a new channel in the scattering matrix which leads to a reduction in the amplitude for scattering into the Hawking channel, as per generalized unitarity constraints. This is seen in Fig. 5.5, which compares $N(\omega)$ for the case of a subsonic-supersonic (red) and supersonic-supersonic jump (blue). Both curves are qualitatively similar at high frequencies, corresponding to the "Hawking" region of frequencies in Figure 5.4. On the other hand, we see that at low ω, when we have subsonic-to-supersonic flow, $N(\omega)$ diverges in the universal thermal manner, while in the supersonic-to-supersonic regime, there is a noticeable change in behavior between the Hawking and super-Hawking regimes, cutting off this low ω divergence.

There are two effects occurring which are responsible for decreasing the Hawking luminosity L_{H}. First, in the Hawking region the incoming negative norm states now begin to more strongly backscatter into their corresponding negative norm state, occupying the evanescent mode on the right side of the horizon. Second, in this super-Hawking region, the appearance of an outgoing negative-norm mode provides an opportunity for the ingoing negative norm channel to avoid scattering into the positive norm channel. We indeed find that the two channels begin to decouple from each other, diminishing the amount of Hawking radiation that can be produced.

5.4.3 Absence of Hawking Radiation for Type-II modes

This takes us directly into the point where $g_3 = 0$, which exhibits the new Newton-Cartan spacetime geometry. One might expect that there should be something akin

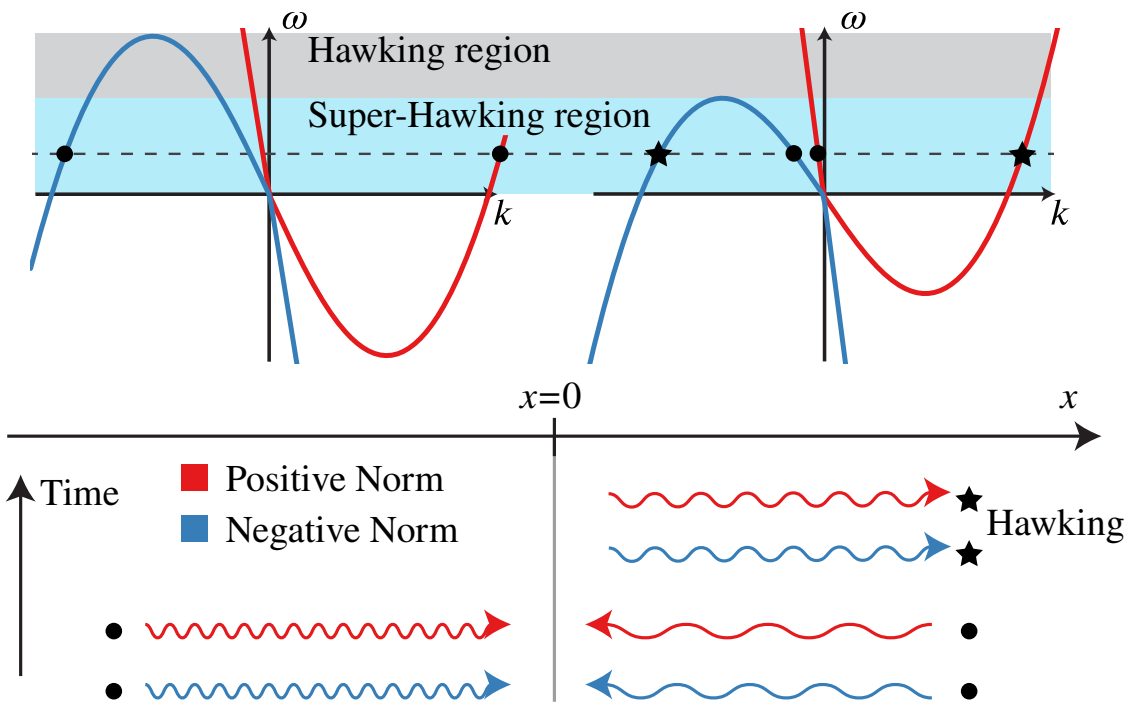

Figure 5.4: The Hawking effect for g_3 such that $c_r < v_r$ and $c_l < v_l$ (super-sonic to super-sonic). With both regions flowing faster than the speed of excitations (relative to the horizon), we still have a Hawking region, but now we also have a "Super-Hawking" region where the positive and negative normalization modes from both regions can scatter between one another.

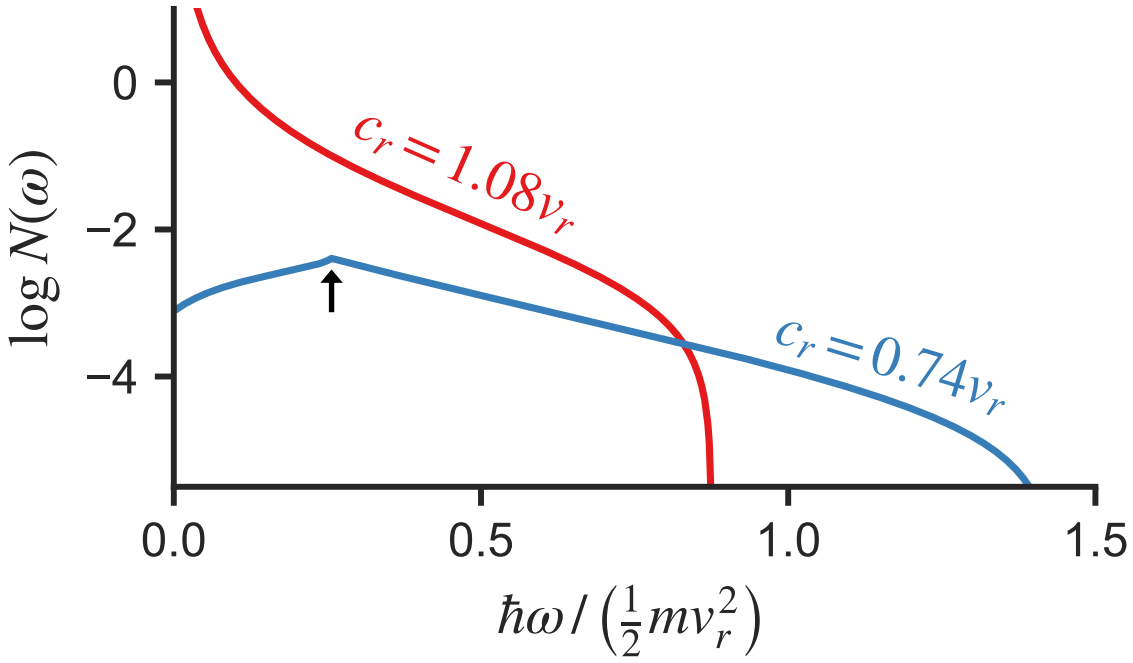

Figure 5.5: Hawking flux $N(\omega)$ as a function of frequency for the subsonic-to-supersonic case (red) and the supersonic-to-supersonic case (blue). As we approach the Heisenberg symmetric point $g_3 = 0$, we find the Hawking flux disappears both in its overall magnitude and singular behavior. The black arrow indicates the onset of the "super-Hawking region" responsible for the absence of the singular distribution.

to a Hawking effect since some modes "see" a horizon for any difference in $|v_l|$ and $|v_r|$. However, this horizon does not translate into a Hawking effect. As explained earlier, at this point the BdG kernel $\hat{K}_3$ commutes with τ_3. In terms of the BdG Lagrangian of Eq. (5.57), we find that there is now a new global $U(1)$ symmetry $\zeta \to e^{i\vartheta}\zeta$. We can see explicitly from the BdG analysis that this conserved charge density is given by

$$Q_{\text{BdG}} = \int d^3x\, \rho|\zeta|^2.$$

On the other hand, by applying Noether's theorem directly on the general Newton-Cartan action of Eq. (5.42), in the limit where n_0 is the only nonzero component of n_μ and the Lagrangian is independent of the x^0, we find

$$Q_{\text{BdG}} = \int d^3r\sqrt{h}|\psi|^2. \tag{5.65}$$

If we identify $\psi = \zeta$ and use the results of Eq. (5.45) we find that these two indeed match each other. In particular, Eq. (5.65) describes a conserved charge for the field ψ on a curved manifold given by $h^{\mu\nu}$.

Since, unlike the charge in Eq. (H.3), this density is positive definite it can be genuinely interpreted as the number of BdG quasiparticles. This symmetry then imposes a selection rule on the scattering matrix which prohibits the scattering processes responsible for the Hawking process, which leads to a creation of BdG quasiparticles. This is evident if we see that when $g_3 = 0$,

$$\left[i\left(\partial_t + \mathbf{v}\cdot\nabla\right) + \frac{1}{2m\rho}\nabla\cdot\rho\nabla\right]\zeta = 0, \tag{5.66}$$

and hence ζ and ζ^* do not mix. Indeed, as Fig. 5.6 illustrates, though Hawking radiation is permissible by conservation of energy and momentum, as seen by the dispersion relation in Fig. 5.6, there is no permissible matrix element for any scatter-

ing process which mixes positive and negative norm modes. Thus, at low frequencies (below the cutoff frequency on the right), negative norm modes may be transmitted across the horizon but only as outgoing negative norm modes. This is analogous to the "super-Hawking" regime earlier, but since there is no conversion between positive and negative norm modes, there is no Hawking radiation effect.

Above the cutoff frequency on the right (in what we refer to as the "regular Hawking regime"), all negative norm modes incident from the interior of the horizon must be reflected back. Even in this case, there is still a finite penetration of the negative norm state across the event horizon in the form of an evanescent mode which is decaying away from the horizon, as originally predicted in Ref. [129]. In fact, this evanescent tail is also present when $g_3 > 0$, but now it is not accompanied by any other outgoing mode. Again, let us emphasize that this evanescent mode is associated with a negative norm mode and therefore does not couple to positive norm modes. Thus, it cannot be spontaneously excited from the ingoing vacuum. Ultimately, as the negative norm mode must be reflected, all the amplitude which initially went into the outgoing positive norm states when $g_3 > 0$ is now transferred into the reflected negative norm state and the evanescent tail.

5.5 Transport in Newton-Cartan Geometry

In this section we take up the issue of energy transport in systems exhibiting Newton-Cartan geometry. Building on Luttinger's work on computing heat transport via coupling to a gravitational field [31], there has been a well-established method of coupling systems to Newton-Cartan geometry in order to extract their heat transport properties [32–34, 183]. With these methods, we can begin with the results in Sec. 5.2.5 and find the stress tensor $T^{\mu\nu}$, energy current ϵ^{μ}, and momentum density p_{μ}. However, as we have mentioned previously, we can also reformulate the relativistic Lagrangian in Sec. 5.2.4 in terms of a Newton-Cartan geometry with an

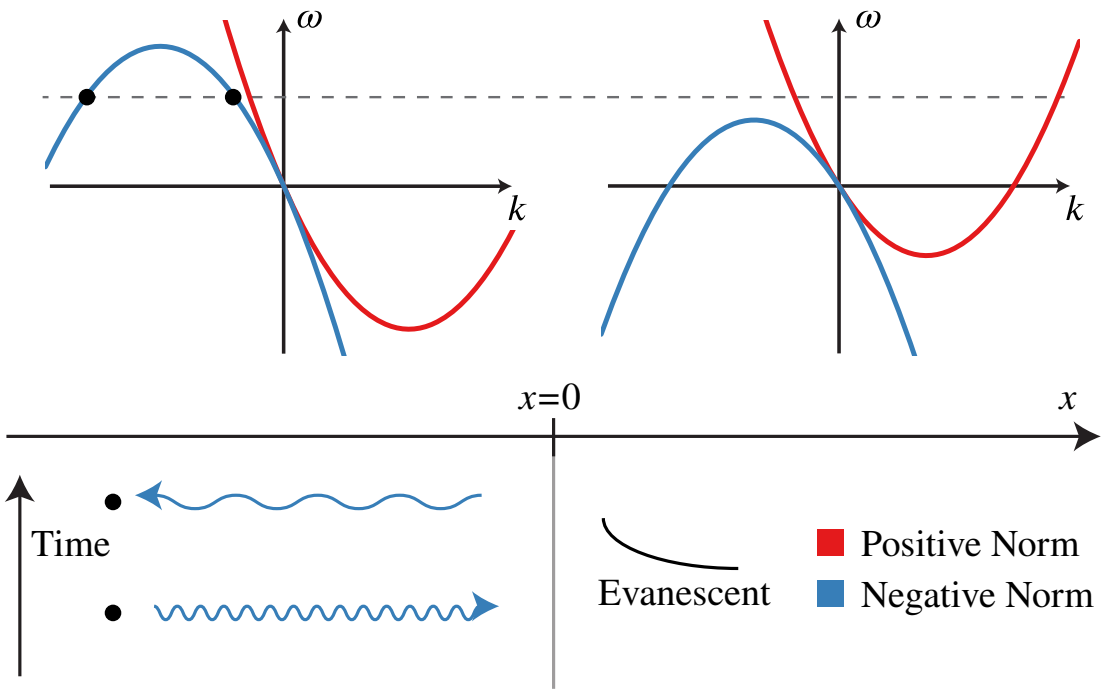

Figure 5.6: For $g_3 = 0$ in the Newton-Cartan geometry there is an excitation number conservation that protects negative norm states from scattering into positive norm states and as a result, if we scatter a negative norm state in what used to be the "Hawking region," we find it fully back scatters into a negative norm state and leaks past the horizon only with an evanescent tail characteristic to a "classically forbidden" region.

additional external field. Therefore, in the bulk of this section, we make that precise and use the energy transport machinery to relate the relativistic stress-energy tensor of Type-I modes to its non-relativistic counterparts.

We begin by noting that the variations in the geometry are not independent as they must satisfy the constraints imposed by Newton-Cartan geometry that $n_\mu v^\mu = 1$ and $n_\mu h^{\mu\nu} = 0$. Parameterizing the variations so as to respect these constraints is done by introducing the perturbations δn_μ, δu^μ and $\delta\eta^{\mu\nu}$ such that

$$\begin{aligned} \delta v^\mu &= -v^\mu v^\lambda \delta n_\lambda + \delta u^\mu, \\ \delta h^{\mu\nu} &= -(v^\mu h^{\nu\lambda} + v^\nu h^{\mu\lambda})\delta n_\lambda - \delta\eta^{\mu\nu}, \end{aligned} \tag{5.67}$$

where $n_\mu \delta u^\mu = 0$, and $n_\mu \delta\eta^{\mu\nu} = 0$ so that δu^μ and $\delta\eta^{\mu\nu}$ are orthogonal to the clock one-form n_μ.

To find the full Lagrangian it is useful to formally define a non-degenerate metric in the full spacetime by

$$g^{\mu\nu} \equiv v^\mu v^\nu + h^{\mu\nu}. \tag{5.68}$$

Note that unlike relativistic metrics, this Newton-Cartan has no invariant distinction between space-like and time-like separations (simultaneity is a global concept imposed by n_μ). As $g^{\mu\nu}$ is non-degenerate, we may proceed to take the inverse which is defined by

$$g_{\mu\alpha} g^{\alpha\nu} = \delta^\nu_\mu, \tag{5.69}$$

where δ^ν_μ is the usual Kronecker delta. This also serves to define the inverse of the degenerate metric $h^{\mu\nu}$ by

$$g_{\mu\nu} \equiv n_\mu n_\nu + h_{\mu\nu}. \tag{5.70}$$

Note that the constraints on the geometry then imply $h_{\mu\nu}$ obeys

$$h^{\mu\sigma} h_{\sigma\nu} = \delta^\mu_\nu - v^\mu n_\nu. \tag{5.71}$$

The right hand side essentially acts to project onto the manifold upon which $h^{\mu\nu}$ is not degenerate. These are the "spatial" three-surfaces which are in some sense "iso-temporal."

Introducing g is helpful in particular because we then find that if take the determinant $g = \det(g_{\mu\nu})$, we find that $\sqrt{g} = n_0\sqrt{h}$ [1]. This is exactly the volume measure of the Lagrangian Eq. (5.42). This assists in taking the variation

$$\delta[\sqrt{g}] = \sqrt{g}[v^\mu \delta n_\mu + \tfrac{1}{2} h_{\mu\nu}\delta\eta^{\mu\nu}]. \tag{5.72}$$

We can then use the variations to find the stress tensor $T_{\mu\nu}$, energy current ϵ^μ, and momentum density p_μ via [33]

$$\delta S = \int d^{d+1}x\sqrt{g}\left(\tfrac{1}{2}T^{\mu\nu}\delta\eta_{\mu\nu} - \epsilon^\mu \delta n_\mu - p_\mu \delta u^\mu\right). \tag{5.73}$$

Due to the constraints on δu^μ and $\delta\eta_{\mu\nu}$, these values of p_μ and $T^{\mu\nu}$ are not unique. In fact, we can make any substitution $p_\mu \to p_\mu + a n_\mu$ or $T^{\mu\nu} \to T^{\mu\nu} + b^\mu v^\nu + b^\nu v^\mu$. We impose uniqueness by requiring $p_\mu v^\mu = 0$ and $T^{\mu\nu}n_\nu = 0$. Lastly, one can derive continuity equations for these quantities by considering how these objects change under a diffeomorphism (see Ref. [33]).

We now compute these quantities for both the Type-I and Type-II modes. It is worth noting that these models describe the free propagation of Goldstone modes and thus are in a sense "non-interacting." By this, we mean there are no additional terms due to interactions [195]. For Type-II modes, the resulting transport quantities are known [32, 34, 183]. We briefly recapitulate this calculation here.

[1] This is derived more directly using g^{-1} defined by $g^{\mu\nu}$. If one locally takes $n_\mu = (n_0, \mathbf{0})$, then $g^{00} = (v^0)^2 \equiv A^{00}$, $g^{0i} = g^{i0} = v^0 v^i \equiv B^{0i}$ and $g^{ij} = v^i v^j + h^{ij} \equiv D^{ij}$. One can take the Schur complement of this inverse metric g^{-1}/A to compute the determinant; then $1/g = \det(g^{-1}) = \det(A)\det(D - B^T A^{-1} B) = 1/(n_0^2 h)$.

5.5.1 Energy transport for Type-II modes

We proceed to vary the Newton-Cartan geometry in action Eq. (5.42). This straightforwardly yields the momentum density as

$$p_\mu = -\tfrac{i}{2}\left[\bar{\psi}(\partial_\mu - n_\mu v^\alpha \partial_\alpha)\psi - \psi(\partial_\mu - n_\mu v^\alpha \partial_\alpha)\bar{\psi}\right]. \tag{5.74}$$

The limit works out as expected: if we let $n_\mu = (1, \mathbf{0})$ and $v^\mu = (1, \mathbf{0})^T$, only the spatial components survive and we obtain the momentum current for a non-relativistic theory with conserved density $|\psi|^2$. Next, we compute the stress tensor, which describes the momentum flux. We find

$$T^{\mu\nu} = -\tfrac{i}{4}v^\alpha\left[\bar{\psi}\partial_\alpha\psi - \psi\partial_\alpha\bar{\psi}\right]h^{\mu\nu} + \tfrac{1}{4m}\partial_\alpha\bar{\psi}\partial_\beta\psi(h^{\alpha\mu}h^{\beta\nu} + h^{\alpha\nu}h^{\beta\mu} - h^{\mu\nu}h^{\alpha\beta}) \tag{5.75}$$

and the energy current as

$$\epsilon^\mu = -\tfrac{1}{2m}(\partial_\alpha\bar{\psi})(\partial_\beta\psi)\left[v^\alpha h^{\beta\mu} + v^\beta h^{\alpha\mu} - v^\mu h^{\alpha\beta}\right]. \tag{5.76}$$

Both have sensible flat-space limits as well.

5.5.2 Energy transport for Type-I modes

For Type-I modes, an analog relativistic theory emerges from a nonrelativistic theory, and in both the cases, we can compute energy densities, momentum densities, and the stress-tensor. The objective of this section is to compute how the quantities in the analog relativistic system are related to their nonrelativistic counterparts, motivated by the spacetime relations derived in Sec. 5.2.

We have shown the Type-I modes can be thought of as residing in a relativistic analog spacetime, equipped with an analog metric tensor $\mathcal{G}_{\mu\nu}$. If we vary with respect to this tensor, we obtain a Lorentz-invariant stress-energy-momentum tensor, $\mathcal{T}^{\mu\nu}$.

Note Lorentz invariance constrains this to be symmetric, relating the energy current and momentum densities to each other.

On the other hand, we have shown that one can obtain the Type-I modes by gapping out one of the generators of a Type-II mode. Thus, we can also consider varying the Newton-Cartan geometry that the Type-II mode resides in before including a mass gap. This yields for us the Newton-Cartan stress tensor, momentum density, and energy current and provide for us a general relationship between the relativistic energy-momentum tensor and the non-relativistic counterparts.

First, we return to Eq. (5.36) and rewrite the Lagrangian in terms of the Newton-Cartan geometry *prior* to integrating out the massive mode (recall that unlike a Type-II mode, a Type-I mode is canonically conjugate to a massive mode). We obtain

$$\mathcal{L} = \sqrt{g}(-2\beta v^\mu \partial_\mu \phi - \tfrac{h^{\mu\nu}}{2m}[\partial_\mu \phi \partial_\nu \phi + \partial_\mu \beta \partial_\nu \beta] - 2mC^2(x)\beta^2), \tag{5.77}$$

where $c^2 = \rho^{2/d}C^2$ is the speed of sound of the Goldstone mode (the factor of density essentially accounts for the units of $h^{\mu\nu}$). If we integrate out the massive mode β in the limit where we can neglect the dispersion (i.e. at long wavelengths), we recover the Type-I relativistic Lagrangian

$$\mathcal{L}_{\text{eff}} = \frac{\sqrt{g}}{2m}\left(\frac{(v^\mu \partial_\mu \phi)^2}{C^2} - h^{\mu\nu}\partial_\mu \phi \partial_\nu \phi\right). \tag{5.78}$$

From this, we can identify the relativistic metric $\mathcal{G}_{\mu\nu}$ by observing that this Lagrangian must be of the form in Eq. (5.6) such that

$$\sqrt{-\mathcal{G}}\mathcal{G}^{\mu\nu} = \tfrac{\sqrt{g}}{m}\left(\tfrac{v^\mu v^\nu}{C^2} - h^{\mu\nu}\right). \tag{5.79}$$

This yields an equation relating the relativistic metric to the Newton-Cartan object

and the gap of the massive mode. We find

$$\begin{aligned}\mathcal{G}_{\mu\nu} &= (mC)^{-\frac{2}{d-1}}\left(C^2 n_\mu n_\nu - h_{\mu\nu}\right),\\ \mathcal{G}^{\mu\nu} &= (mC)^{\frac{2}{d-1}}\left(\tfrac{v^\mu v^\nu}{C^2} - h^{\mu\nu}\right),\end{aligned} \tag{5.80}$$

where d is the spatial dimension. As we can see, the relativistic metric depends crucially on the potential $C(x)$.

This is helpful since, on the one hand, we can easily obtain the stress-energy tensor in the relativistic theory by varying $\delta\mathcal{G}_{\mu\nu}$. On the other hand, we can use the above formulae to connect this result to the actual stress tensor and energy current/momentum density of the non-relativistic model. In particular,

$$\begin{aligned}\delta\mathcal{G}^{\mu\nu} = (mC)^{\frac{2}{d-1}}[(v^\mu h^{\nu\lambda} + v^\nu h^{\mu\lambda} - 2\tfrac{v^\mu v^\nu}{C^2}v^\lambda)\delta n_\lambda \\ + \tfrac{1}{C^2}(v^\mu\delta^\nu_\lambda + v^\nu\delta^\mu_\lambda)\delta u^\lambda + \delta\eta^{\mu\nu}].\end{aligned} \tag{5.81}$$

Thus, we can directly relate the relativistic energy-momentum tensor $\mathcal{T}_{\mu\nu}$ to its non-relativistic counterparts by expanding

$$\delta S = \int d^{d+1}x \tfrac{1}{2}\sqrt{-\mathcal{G}}\mathcal{T}_{\mu\nu}\delta\mathcal{G}^{\mu\nu} \tag{5.82}$$

in terms of the geometric objects in the NC geometry. Doing so, we obtain

$$\begin{aligned}T^{\mu\nu} &= \tfrac{1}{m(mC)^{\frac{4}{d-1}}}(\delta^\mu_\alpha - n_\alpha v^\mu)\mathcal{T}^{\alpha\beta}(\delta^\nu_\beta - n_\beta v^\nu),\\ \epsilon^\lambda &= \tfrac{1}{m(mC)^{\frac{2}{d-1}}}v^\mu\mathcal{T}_\mu{}^\lambda,\\ p_\lambda &= -\tfrac{1}{mC^2}(\mathcal{T}_{\lambda\mu}v^\mu - v^\mu\mathcal{T}_{\mu\nu}v^\nu n_\lambda).\end{aligned} \tag{5.83}$$

where the indices on $\mathcal{T}^{\mu\nu}$ and $\mathcal{T}_\mu{}^\lambda$ are raised with $\mathcal{G}^{\mu\nu}$ while all Newton-Cartan objects use the metric $g_{\mu\nu}$. Ignoring the factors in front of these expressions, one

can think of v^ν as a timelike vector with respect to the metric $\mathcal{G}_{\mu\nu}$. In this case, v^μ is directly related to the field of the fluid flow and the object $\mathcal{E}^\lambda \propto v^\nu \mathcal{T}_\mu{}^\lambda$ is the energy current measured by an observer comoving with that flow (*not* the lab observer). By the same token $\mathcal{P}_\lambda \propto \mathcal{T}_{\lambda\nu} v^\nu$ is the momentum density measured by the comoving observer as well. Relativistically, these are strictly related $\mathcal{E}^\lambda = \mathcal{G}^{\lambda\mu}\mathcal{P}_\mu$. However, momentum is imposed by the underlying non-relativistic field theory to be orthogonal to flow $v^\lambda p_\lambda = 0$. The form of p_λ that accomplishes this includes the comoving energy density $v^\mu \mathcal{T}_{\mu\nu} v^\nu$ and subtracts it off. Lastly, $T^{\mu\nu}$ is directly related to $\mathcal{T}^{\alpha\beta}$ projected to live only on spatial slices $n_\mu T^{\mu\nu} = 0$, again as imposed by the underlying non-relativistic theory.

In effective, relativistic, analog systems, there is a preferred (lab) frame that is captured by the Newton-Cartan geometry (in particular n_μ specifies the lab frame's "clock"). This preference is hidden in the high frequency dispersion of the type-I modes and, as we have shown here, results in non-trivial momentum currents and stress-tensors.

As a particular example, a Hawking flux against the flow in an analog system should result in a real energy and momentum current away from the analog black hole. Far from the horizon (considering the effective 1+1D problem where the other two spatial dimensions are trivial) we obtain

$$\mathcal{T}_{\mu\nu} = \begin{pmatrix} \mathcal{T}_{\mathrm{H}} & -\mathcal{T}_{\mathrm{H}} \\ -\mathcal{T}_{\mathrm{H}} & \mathcal{T}_{\mathrm{H}} \end{pmatrix}, \tag{5.84}$$

for a constant $\mathcal{T}_{\mathrm{H}}$ [196] (for the radiation flowing to $+\infty$). If we apply this to the above, and assume that at $+\infty$ we have no velocity so that $v^\mu = (v^0, \mathbf{0})$ and a flat

$h^{ij} = \delta^{ij}/h_0^{1/3}$, we have

$$\begin{aligned} T^{xx} &= \tfrac{1}{m h_0^{2/3}} \mathcal{T}_{\mathrm{H}}, \\ \epsilon^{\lambda} &= \tfrac{v^0}{m} \mathcal{T}_{\mathrm{H}} \left[\tfrac{(v^0)^2}{C^2}, h_0^{-1/3}, 0, 0 \right], \\ p_{\lambda} &= \tfrac{v^0}{mC^2} \mathcal{T}_{\mathrm{H}} [0, 1, 0, 0]. \end{aligned} \tag{5.85}$$

Importantly, we see that there is a finite energy current ϵ^1 and momentum p_1 away from the horizon; there is no p_0 component due to the constraint $p_\mu v^\mu = 0$. While related to what is computed relativistically, these quantities are not exactly the same.

5.6 Discussion and Conclusions

The primary result of this work is establishing the connection between the different types of Goldstone modes and different types of analog spacetimes, as summarized in Table 5.1. This is done by revisiting the proof of the non-relativistic Goldstone theorem and allowing for the possibility of an inhomogeneous mean-field solution. We then find that the conventional Type-I Goldstone modes come equipped with an Einstein-Hilbert metric as appears in general relativity while Type-II Goldstone modes couple to a Newton-Cartan geometry. The geometry itself is determined by the spacetime dependence of symmetry-breaking mean-field—inhomogeneous symmetry breaking ultimately produces the non-trivial spacetime metric. In this work we have restricted ourselves to the case where only the overall $U(1)$ symmetry is inhomogeneously broken. This corresponds to an overall condensate flow.

Another key result is establishing the connection between quantum phase transitions and changes in the nature of the spacetime. To elucidate this, we present a simple model where the analog geometry can be tuned by a single parameter. This

drives a quantum phase transition which accompanies the transition between the Einstein-Lorentz geometry and Newton-Cartan geometry. As the phase transition is approached, the Hawking radiation produced by an event horizon changes, as encapsulated in Fig. 5.2. One key result is that the Newton-Cartan geometry exhibits no Hawking radiation, even though all fluid flows are supersonic (the group velocity of Goldstone modes vanishes at long wavelengths).

While Sec. 5.3 is a minimal theoretical model, the experimental system that most readily realizes these geometries are spin-1 condensates. In this case, for the scattering lengths a_0 and a_2 (for s-wave collisions into the spin-0 and spin-2 channels respectively), there are two phases that break the spin SU(2) symmetry: $a_0 > a_2$ gives a ferromagnetic phase with one Type-II magnon and $a_0 < a_2$ gives a polar phase (antiferromagnetic interactions) with two Type-I magnons. Upon flow, these two phases naturally realize the two different spacetimes described here. In fact, ^{7}Li, ^{41}K, and ^{87}Rb realize the ferromagnetic phase [181] with ^{87}Rb specifically already being used for Hawking-like experiments with the phonon mode [152, 154]. Additionally, ^{23}Na realizes the polar phase and critical spin superflow has been studied [197] (necessary for Hawking-like experiments). The magnon excitations in these systems can be probed by observing correlations in the spin-density, and the most basic proposal, would be to establish the vanishing Hawking radiation in the ferromagnetic phase. The progress in current spinor condensate experiments highlights that these more exotic analog spacetimes may already be in reach.

Finally, by considering the response of the Goldstone modes to variations in the analog geometries, we relate the analog stress-energy-momentum tensor in relativistic geometries directly to their non-relativistic counterpart. This is summarized by the equations below, which shows how the metric tensor in both analog spacetimes may be constructed from the underlying geometric objects of the Newton-Cartan

geometry along with an additional field $C = C(x)$:

$$\begin{aligned} g_{\mu\nu} &= n_\mu n_\nu + h_{\mu\nu}, \quad \text{Non-relativistic,} \\ \mathcal{G}_{\mu\nu} &\propto C^2 n_\mu n_\nu - h_{\mu\nu}, \quad \text{Relativistic.} \end{aligned} \tag{5.86}$$

We also provide a direct connection between the energy and momentum currents of an analog relativistic system and the more fundamental Newton-Cartan geometry which describes the lab-frame.

Within spinor Bose-Einstein condensates, there are other phenomena to include such as inhomogeneous broken non-Abelian symmetry (including textures like spiral magnetization, Bloch domain walls, and skyrmions) and synthetic gauge fields. The construction presented here also considers just the quadratic excitations, but these Goldstone modes realize more complicated nonlinear sigma models for which there is extra *intrinsic* geometry at play and would need to be incorporated into a full theory of these excitations. This new analog also raises questions of the so-called back-reaction effects of quantum fields on the corresponding analog spacetime. This has been studied in the relativistic case [22, 198], and the non-relativistic case leaves us with the tantalizing prospect of a system with a dynamical Newtonian gravity. Finally, while in this work we exclusive focused on the context of flowing spinor Bose-Einstein condensates, the phenomenon should be more general. An interesting future direction to pursue would be to try and extend these results to include more diverse platforms including electrons in solid-state systems, liquid Helium, superconductors, magnetic systems. The wide variety of systems which exhibit symmetry-breaking means there is a wide variety of systems which might exhibit this analog spacetime and its consequences.

Chapter 6: Conclusion

In this thesis we addressed a variety of interacting quantum systems by means of a description in terms of quasiparticles. In Chapters 2 and 3 we focused on BCS superconductors and their interactions with microwave cavity photons, while in Chapters 4 and 5 we turned our attention towards flowing Bose-Einstein condensates.

More specifically, in Chapter 2 we showed how microwave cavity photons interacting with the Bogoliubov quasiparticles in an enclosed superconductor can be used to drive a nonequilibrium occupation of quasiparticles. This nonequilibrium occupation can then be engineered such that it leads to an enhancement in the BCS gap. This is most easily seen for the case of a clean sample, in which case the result follows straightforwardly from the application of Fermi's Golden Rule expressed in the quasiparticle basis and the application of detailed balance.

In Chapter 3 we considered the case of cavity photons interacting with an enclosed two-dimensional BCS superconductor with competing s- and d-wave pairing instabilities. This system hosts a sub-gap collective mode (known as the Bardasis-Schrieffer mode) which is essentially an uncondensed d-wave Cooper pair atop the condensed s-wave superconducting background. We show that these Bardasis-Schrieffer modes can be treated as bosonic quasiparticles and that by driving a uniform background supercurrent they can be hybridized with the cavity photons, forming Bardasis-Schrieffer polaritons.

Then, in Chapter 4 we studied a flowing BEC which realized an analogue black hole for the Bogoliubov quasiparticles describing quantum fluctuations of the condensate. In the extreme limit of a step-like change in the condensate flow, corresponding to an analogue black hole with large surface gravity, we found that evanescent modes accompany the emitted analogue Hawking radiation. These evanescent modes be-

come pinned to the exterior of the event horizon with a length scale determined by the microscopic Lorentz invariance violation and may allow for information to propagate across the event horizon.

Finally, in Chapter 5 we considered the analogue gravity that is realized by a flowing pseudo-spin half spinor BEC. In this case, the Goldstone modes associated to the broken $SU(2)$ spin-rotation symmetry exhibit a quadratic dispersion relation and in the presence of an inhomogeneous condensate flow experiences an analogue spacetime with local Galilean invariance—the exotic Newton-Cartan spacetime. We find that the same step-like flow which exhibits Hawking radiation in the standard Lorentz-invariant analogue gravity setup emits no Hawking radiation in the Newton-Cartan spacetime, despite a nominally superluminal background flow. By adding an easy-axis anisotropy to the spin exchange interaction, we can drive system out of the analogue Newton-Cartan spacetime and into the conventional Lorentz-invariant analogue spacetime. It may be possible to observe this Newton-Cartan geometry in current-generation ultra-cold atom experiments using a pseudo-spin one Bose condensate.

Appendix A: Cavity Model

The model of the photonic sector used in this work is that of a parallel mirror cavity consisting of two conducting plates of infinite extent in the $x-y$ plane and separated by a distance L along the z axis. We solve for the electromagnetic normal modes by solving Maxwell's equations in the Coulomb gauge, assuming no electrostatic potential. We then have Ampere's law producing the equation of motion for $\mathbf{A}$

$$\left[\frac{1}{c^2}\frac{\partial^2}{\partial t^2} - \nabla^2\right]\mathbf{A} = 0 \tag{A.1}$$

which is supplemented by the Coulomb gauge constraint $\nabla \cdot \mathbf{A} = \mathbf{0}$ and boundary conditions, which are taken to be those of a perfect metal (so that the normal component of $\mathbf{B}$ and the tangential components of $\mathbf{E}$ vanish at the surface). We make the ansatz that

$$\mathbf{A}(x, y, z, t) = \frac{e^{-i\omega t + i\mathbf{q}\cdot\mathbf{r}_\perp}}{\sqrt{\text{Area}}}\vec{\epsilon}_{\mathbf{q}}(z),$$

with $\perp$ indicating the vector components in the x, y plane and Area being the normalizing area of the $x-y$ momentum summation. In this context, $\mathbf{q}$ is understood to be a vector with components only in the $x-y$ plane, and the $\perp$ will be omitted for brevity. We introduce $\vec{\epsilon}_{\mathbf{q}}(z)$ as the q-dependent polarization texture of the electromagnetic field. Due to the finite size effects in z, this is spatially varying in the z direction.

The gauge constraint then implies

$$i\mathbf{q}\cdot\vec{\epsilon}^{\perp}_{\mathbf{q}}(z) + \frac{\partial}{\partial z}\epsilon^{z}_{\mathbf{q}}(z) = 0 \tag{A.2}$$

and the boundary conditions imply that

$$\vec{\epsilon}^{\perp}_{\mathbf{q}}(z=0,L)=0. \tag{A.3}$$

These boundary conditions are compatible with a Fourier sine series, so that

$$\vec{\epsilon}^{\perp}_{\mathbf{q}}(z)\propto\sin\left(\frac{n\pi z}{L}\right).$$

with the proportionality constant being a two-component vector which can in principle depend on $\mathbf{q}$ and n. On the other hand, the z-component should have a Fourier cosine series in order to comply with boundary conditions. We see that this cosine series is related to the $\vec{\epsilon}^{\perp}(z)$ sine series by the gauge constraint, so that $\partial_z\epsilon^z(z)\propto\mathbf{q}_\perp\cdot\vec{\epsilon}^{\perp}_{\mathbf{q}}$. We thus make the ansatz

$$\vec{\epsilon}_{\mathbf{q}}(z)=\vec{\epsilon}^{\perp}_{\mathbf{q},n\alpha}\sqrt{\frac{2}{L}}\sin\left(\frac{n\pi z}{L}\right)+\epsilon^z_{\mathbf{q},n\alpha}\hat{\mathbf{e}}_z\sqrt{\frac{2}{L}}\cos\left(\frac{n\pi z}{L}\right).$$

The gauge constraint then implies

$$-\frac{n\pi}{L}\epsilon^z_{\mathbf{q},n\alpha}+i\mathbf{q}\cdot\vec{\epsilon}^{\perp}_{\mathbf{q},n\alpha}=0. \tag{A.4}$$

We therefore have only two independent degrees of freedom, determined by the in-plane components of the polarization. Often, it is convenient to choose these to lie along, and normal, to the momentum $\mathbf{q}$. Thus, we have two polarizations $\vec{\epsilon}^{\perp}_{\mathbf{q},n\alpha}$ with $\alpha=1,2$. We are free to choose the two polarization vectors to obey

$$\vec{\epsilon}_{\mathbf{q},n\alpha}\cdot\vec{\epsilon}^{*}_{\mathbf{q},n\beta}=\delta_{\alpha\beta} \tag{A.5a}$$

$$\vec{\epsilon}^{*}_{\mathbf{q},n\alpha}=\vec{\epsilon}_{-\mathbf{q},n\alpha}. \tag{A.5b}$$

We choose $\vec{\epsilon}^{\perp}_{\mathbf{q},n1}\propto\mathbf{q}\times\hat{\mathbf{e}}_z$, which is transverse to the propagation direction, and

$\vec{\epsilon}^{\perp}_{\mathbf{q},n2} \propto \mathbf{q}$ which is along the propagation direction. Normalizing and enforcing the time-reversal condition we get the polarization textures (including the z dependence)

$$\vec{\epsilon}_{\mathbf{q},n1}(z) = \frac{i\mathbf{q}\times\hat{\mathbf{e}}_z}{|\mathbf{q}|}\sqrt{\frac{2}{L}}\sin\left(\frac{n\pi z}{L}\right) \tag{A.6a}$$

$$\vec{\epsilon}_{\mathbf{q},n2}(z) = \hat{\mathbf{e}}_z\frac{|\mathbf{q}|}{\sqrt{\mathbf{q}^2+(\frac{n\pi}{L})^2}}\sqrt{\frac{2}{L}}\cos\left(\frac{n\pi z}{L}\right) - i\frac{\mathbf{q}}{|\mathbf{q}|}\frac{n\pi/L}{\sqrt{\mathbf{q}^2+(\frac{n\pi}{L})^2}}\sqrt{\frac{2}{L}}\sin\left(\frac{n\pi z}{L}\right). \tag{A.6b}$$

The second-quantized electromagnetic field admits a normal mode decomposition (in the Schrodinger picture) as

$$\hat{\mathbf{A}}(\mathbf{r}) = \sum_{\mathbf{q}n\alpha} C_{\mathbf{q}n\alpha}\left[\frac{e^{i\mathbf{q}\cdot\mathbf{r}_\perp}}{\sqrt{\text{Area}}}\hat{a}_{\mathbf{q},n\alpha}\vec{\epsilon}_{\mathbf{q},n\alpha}(z) + \text{h.c.}\right]$$

where the operators $\hat{a}_{\mathbf{q},n\alpha}$ are canonical boson annihilation operators and the coefficients C must be chosen such that A, E obey the canonical commutation relations. Incorporating the charge and enhancement factor X^2 into the effective dielectric constant we find that the constant $C = \sqrt{\frac{e^2X^2}{2\epsilon_0\omega_n(\mathbf{q})}}$ so that in full

$$\hat{\mathbf{A}}(\mathbf{r}) = \sum_{\mathbf{q}n\alpha}\sqrt{\frac{e^2X^2}{2\epsilon_0\omega_n(\mathbf{q})}}\left[\frac{e^{i\mathbf{q}\cdot\mathbf{r}_\perp}}{\sqrt{\text{Area}}}\hat{a}_{\mathbf{q},n\alpha}\vec{\epsilon}_{\mathbf{q},n\alpha}(z) + \text{h.c.}\right] \tag{A.7}$$

with the dispersion relation

$$\omega_n(\mathbf{q}) = \sqrt{\left(\frac{n\pi c}{L}\right)^2 + c^2\mathbf{q}^2}. \tag{A.8}$$

In particular, for a two dimensional sample in the $x-y$ plane located at $z = L/2$

the polarization textures projected onto the $x-y$ plane are

$$\vec{\epsilon}^{\perp}_{\mathbf{q},n1}(z=\frac{L}{2}) = \frac{i\mathbf{q}\times\hat{\mathbf{e}}_z}{|\mathbf{q}|}\sqrt{\frac{2}{L}}\sin\left(\frac{n\pi}{2}\right) \tag{A.9a}$$

$$\vec{\epsilon}^{\perp}_{\mathbf{q},n2}(z=\frac{L}{2}) = -i\frac{\mathbf{q}}{|\mathbf{q}|}\frac{n\pi/L}{\sqrt{\mathbf{q}^2+(\frac{n\pi}{L})^2}}\sqrt{\frac{2}{L}}\sin\left(\frac{n\pi}{2}\right). \tag{A.9b}$$

Since $\sin(n\pi/2)=0$ if $n=2,4,6,...$ and $(-1)^{(n-1)/2}$ for $n=1,3,5,...$ we find that only the $n=1,3,5,...$ modes couple to the sample when it is placed at the midpoint. Hence we focus on the $n=1$ mode, bearing in mind that this is a simplified model which won't be applicable in a realistic device geometry anyways.

Finally, let us comment on how to express the polarization vectors in a different choice of basis, with an intended application to the Bardasis-Schrieffer problem, in which case it is convenient to express the polarization in terms of a component parallel and perpendicular to the external supercurrent. We note that any two combinations of the two polarization functions $\vec{\epsilon}_{\mathbf{q},n\alpha}(z)$ will also satisfy the boundary conditions and gauge constraint. Therefore, we can consider the combinations

$$\begin{aligned} A\vec{\epsilon}_{\mathbf{q},n1}(z)+B\vec{\epsilon}_{\mathbf{q},n2}(z) = &\left[A\frac{i\mathbf{q}\times\hat{\mathbf{e}}_z}{|\mathbf{q}|}-iB\frac{\mathbf{q}}{|\mathbf{q}|}\frac{n\pi/L}{\sqrt{\mathbf{q}^2+(\frac{n\pi}{L})^2}}\right]\sqrt{\frac{2}{L}}\sin\left(\frac{n\pi z}{L}\right) \\ &+B\hat{\mathbf{e}}_z\frac{|\mathbf{q}|}{\sqrt{\mathbf{q}^2+(\frac{n\pi}{L})^2}}\sqrt{\frac{2}{L}}\cos\left(\frac{n\pi z}{L}\right). \end{aligned}$$

The in plane projections have x and y components at $z=L/2$ of

$$\begin{aligned} \hat{\mathbf{e}}_x\cdot\left(A\vec{\epsilon}_{\mathbf{q},n1}+B\vec{\epsilon}_{\mathbf{q},n2}\right) &= \left[A\frac{iq_y}{|\mathbf{q}|}-iB\frac{q_x}{|\mathbf{q}|}\frac{n\pi/L}{\sqrt{\mathbf{q}^2+(\frac{n\pi}{L})^2}}\right]\sqrt{\frac{2}{L}}\sin\left(\frac{n\pi}{2}\right) \\ \hat{\mathbf{e}}_y\cdot\left(A\vec{\epsilon}_{\mathbf{q},n1}+B\vec{\epsilon}_{\mathbf{q},n2}\right) &= \left[-A\frac{iq_x}{|\mathbf{q}|}-iB\frac{q_y}{|\mathbf{q}|}\frac{n\pi/L}{\sqrt{\mathbf{q}^2+(\frac{n\pi}{L})^2}}\right]\sqrt{\frac{2}{L}}\sin\left(\frac{n\pi}{2}\right). \end{aligned}$$

We would like to find a normalized set of A,B such that the projections are constant and either purely along x (e.g. the direction of the supercurrent) or y (the direction

perpendicular to the supercurrent). This gives us a linear system of equations

$$\begin{pmatrix} \frac{iq_y}{|\mathbf{q}|} & -i\frac{q_x}{|\mathbf{q}|}\frac{n\pi/L}{\sqrt{\mathbf{q}^2+(\frac{n\pi}{L})^2}} \\ -\frac{iq_x}{|\mathbf{q}|} & -i\frac{q_y}{|\mathbf{q}|}\frac{n\pi/L}{\sqrt{\mathbf{q}^2+(\frac{n\pi}{L})^2}} \end{pmatrix} \begin{pmatrix} A \\ B \end{pmatrix} \propto \begin{pmatrix} 1 \\ 0 \end{pmatrix} \text{ or } \begin{pmatrix} 0 \\ 1 \end{pmatrix}. \tag{A.10}$$

The determinant of the matrix is $\frac{n\pi/L}{\sqrt{\mathbf{q}^2+(n\pi/L)^2}} \neq 0$ and thus there is a solution to the problem. That is to say, we can choose some basis in which the polarization textures respect the orthonormality, Coulomb gauge, and time-reversal symmetry constraints, while being polarized along two fixed external axes in the $x-y$ plane.

Appendix B: Keldysh Non-Linear Sigma Model

In order to derive the correction to the quasiparticle distribution functions in the presence of disorder, we employ the Keldysh nonlinear σ model (KNLσM) as derived by Feigelman, *et. al.* [89]. This is an alternative to the Mattis-Bardeen method [88] result from the main text, and is essentially the Supplemental material from publication [35].

B.0.1 Schematic derivation of the model

We first briefly outline the derivation of the Keldysh nonlinear sigma model before describing the calculations performed in our work. For more details on the KLNσM we refer the reader to Refs. [89, 90].

The derivation of the sigma model begins with a minimally coupled BCS action on the Keldysh contour in the presence of a random impurity potential

$$S = \oint_C dt d\mathbf{x} \left[\bar{\psi} \left(i\partial_t - \hat{\epsilon} \left(-i\nabla + \frac{e}{c}\mathbf{A} \right) + \mu - V_{\text{imp}} \right) \psi + \frac{\lambda}{\nu} \bar{\psi}_\uparrow \bar{\psi}_\downarrow \psi_\downarrow \psi_\uparrow \right] \tag{B.1}$$

with $\hat{\epsilon}$ being the quasielectron energy, μ the chemical potental, ν the density of states at the Fermi surface, λ the BCS coupling strength, V_{imp} is the impurity potential. $\oint_C$ denotes integration over the Keldysh contour. One now averages over gaussian disorder which induces an effective disorder interaction in the usual manner

$$iS_{\text{dis}} = -\frac{1}{4\pi\nu\tau} \int_C dt dt' d\mathbf{x} \bar{\psi}(t)\psi(t)\bar{\psi}(t')\psi(t'). \tag{B.2}$$

The bilinears $\bar{\psi}(t)\psi(t)$ describe rapidly varying modes on the length scales of the impurities. However, the bilinears $\bar{\psi}(t)\psi(t')$ describe slowly varying degrees of freedom. Therefore a Hubbard-Stratonovich field Q dual to $\bar{\psi}(t)\psi(t')$ is introduced

to decouple the disorder interaction. The BCS interaction is also decoupled via the Hubbard-Stratonovich field Δ in the usual fashion. Coupling to the A-field is handled via the paramagnetic coupling $\mathbf{j}\cdot\mathbf{A}\approx\frac{e}{c}\mathbf{v}_F\cdot\mathbf{A}$. At this point one performs the Larkin-Ovchinnikov rotation and integrates out the fermions. This leads to an action for the Hubbard-Stratonovich fields Q and Δ

$$iS=-\frac{\pi\nu}{8\tau}\operatorname{Tr}\check{Q}^2+\operatorname{Tr}\ln\left[\check{G}^{-1}+\frac{i}{2\tau}\check{Q}-\frac{e}{c}\mathbf{v}_F\cdot\check{\mathbf{A}}+\check{\Delta}\right] \tag{B.3}$$

where G is the Bogoliubov-de Gennes Green's function. One then performs an expansion about the saddle-point solution for Q as well as a gradient expansion. One notes that the $\operatorname{Tr}Q^2$ vanishes on the soft manifold $Q^2=1$ —where we must keep in mind that the unit matrix must have the proper analyticity structure —indicating that such modes are massless. The result of these expansions along with the non-linear constraint gives the KNLσM

$$iS_{NLSM}=-\frac{\pi\nu}{8}\operatorname{Tr}\left[D\left(\hat{\partial}\check{Q}\right)^2+4i\left(i\hat{\tau}_3\partial_t\check{Q}+\check{\Delta}\check{Q}\right)\right]-i\frac{\nu}{2\lambda}\operatorname{Tr}\check{\Delta}^\dagger\hat{\gamma}^q\check{\Delta}. \tag{B.4}$$

B.0.2 Our system

We employ a slightly modified NLSM which includes coupling to a thermal bath

$$iS_{NLSM}=-\frac{\pi\nu}{8}\operatorname{Tr}\left[D\left(\hat{\partial}\check{Q}\right)^2+4i\left(i\hat{\tau}_3\partial_t\check{Q}+i\frac{\gamma}{2}\check{Q}_{\text{rel}}\check{Q}+\check{\Delta}\check{Q}\right)\right]-i\frac{\nu}{2\lambda}\operatorname{Tr}\check{\Delta}^\dagger\hat{\gamma}^q\check{\Delta} \tag{B.5}$$

where $D=v_f\tau_{\text{imp}}^2/2$ is the diffusion constant, $\nu=\nu_\uparrow+\nu_\downarrow$ is the total electronic density of states at the Fermi surface, and λ is the strength of the BCS type coupling. Tr in the above indicates a trace over all indices: both matrix and spacetime. The notation $\check{X}$ indicates a matrix in Nambu and Keldysh spaces. The matrix $\check{Q}$, describing the soft electronic degrees of freedom, is a function of position $\mathbf{r}$ and

two time coordinates t, t' and is subject to the non-linear constraint $\check{Q}^2 = \check{1}$. The photon field $\mathbf{A}$ couples to the model through the covariant derivative

$$\hat{\partial}\check{X} = \nabla\check{X} + i[\check{\mathbf{A}}, \check{X}] \tag{B.6}$$

where we have absorbed the paramagnetic coupling strength into the definition of the $\mathbf{A}$ field. All matrices in the model are 4×4 in the product of Keldysh and Nambu spaces. In what follows we employ the conventions used in Ref. kamenev. Explicitly

$$\begin{aligned} \check{Q}_{\mathrm{rel}}(\epsilon) &= \begin{pmatrix} 1 & 2F_{\mathrm{eq}}(\epsilon) \\ 0 & -1 \end{pmatrix}_K \\ \check{\mathbf{A}} &= \sum_\alpha \mathbf{a}_\alpha \hat{\gamma}^\alpha \otimes \hat{\tau}_3 \\ \check{\Delta} &= \sum_\alpha \left(\Delta_\alpha \hat{\gamma}^\alpha \otimes \hat{\tau}_+ - \Delta_\alpha^* \hat{\gamma}^\alpha \otimes \hat{\tau}_-\right) \end{aligned} \tag{B.7}$$

where the index α runs over (cl, q) and $\gamma^{\mathrm{cl}} = \sigma^0$ and $\gamma^{\mathrm{q}} = \sigma^1$ are matrices in Keldysh space. We model inelastic relaxation through a linear coupling to a bath $\hat{Q}_{\mathrm{rel}}$ with temperature T [47]. This is equivalent to the relaxation $(1/\tau)$ approximation in the kinetic equation. In particular $\gamma = \frac{1}{\tau_{\mathrm{in}}}$ is the inelastic scattering rate.

The saddlepoint equations of Eq. (B.5) for Δ_q^* and $\check{Q}$ respectively correspond to the BCS gap equation and the Usadel equation[91] for the quasiclassical Green's function $\check{Q}$. In the absence of the cavity photon field this describes the superconducting state of the electronic system without the cavity. Our strategy will be to obtain the lowest order in $\mathbf{A}$ correction to the action which is linear in Δ_q^*. This corresponds to the lowest order correction to the gap equation. In the absence of $\mathbf{A}$ the saddle point of $\check{Q}$ is

$$\hat{\partial}\left(D\check{Q}\hat{\partial}\check{Q}\right) + i\{i\hat{\tau}_3\partial_t, \check{Q}\} + i\left[i\tau_2\Delta_0 + i\frac{\gamma}{2}\check{Q}_{\mathrm{rel}}, \check{Q}\right] = 0 \tag{B.8}$$

where we have assumed Δ_{cl} to be homogenous and real. Assuming a homogeneous, steady state solution $\check{Q}_{sp}(t-t')$ we may Fourier transform to obtain

$$i\epsilon[\hat{\tau}_3, \check{Q}(\epsilon)] + i[i\tau_2\Delta_0, \check{Q}(\epsilon)] + \gamma/2\left[\check{Q}_{\rm rel}(\epsilon), \check{Q}(\epsilon)\right] = 0. \tag{B.9}$$

At the saddle point $\check{Q}$ will have the structure

$$\check{Q} = \begin{pmatrix} \hat{Q}^R & \hat{Q}^R\hat{F} - \hat{F}\hat{Q}^A \\ 0 & \hat{Q}^A \end{pmatrix}$$

as governed by fluctuation-dissipation.

B.1 Gaussian Fluctuations

Gaussian fluctuations about the saddle point can be parametrized

$$\check{Q} = \check{U}\check{V}^{-1}e^{-\check{W}/2}\hat{\sigma}_3\hat{\tau}_3 e^{\check{W}/2}\check{V}\check{U}. \tag{B.10}$$

with

$$\begin{aligned} U(\epsilon) &= \begin{pmatrix} 1 & F_{\rm eq}(\epsilon) \\ 0 & -1 \end{pmatrix}_K \hat{\tau}_0 \\ \check{V}(\epsilon) &= \begin{pmatrix} e^{\tau_1\theta/2} & 0 \\ 0 & e^{\tau_1\theta^*/2} \end{pmatrix}_K . \end{aligned} \tag{B.11}$$

Here, $\theta(\epsilon)$ is a complex angle which is determined by the Usadel equation, and satisfies $\theta(-\epsilon) = -\theta^*(\epsilon)$. The matrices U and V are a change of basis which allows us to separate the equilibrium and saddle point properties from the fluctuation effects: U describes the fluctuation dissipation relation, while V parametrizes the solution to the retarded Usadel equation. The matrix $\check{W}$ is then composed of fields multiplying the generators of the algebra which describes rotations on the soft

manifold imposed by the nonlinear constraint $\check{Q}^2 = 1$. In particular, the matrix $\check{W}$ anticommutes with $\sigma_3\tau_3$ and for $\check{W} = 0$ Eq. (B.10) reduces to the saddlepoint solution. By expanding the exponential in this parametrization we can capture the Gaussian fluctuations along the soft manifold. $\check{W}$ has 4 independent components that couple to the vector potential

$$\check{W}(\mathbf{r}, t, t') = i \begin{pmatrix} c_R(\mathbf{r}, t, t')\tau_1 & d_{cl}(\mathbf{r}, t, t')\tau_0 \\ d_q(\mathbf{r}, t, t')\tau_0 & c_A(\mathbf{r}, t, t')\tau_1 \end{pmatrix}_K , \tag{B.12}$$

the cooperon (c_R, c_A) and diffuson $(d_c l, d_q)$ fields.

We now expand Eq. (B.5) to quadratic order in the cooperon and diffuson fields c and d. Doing so we generate three types of terms. The simplest is the quadratic diffusive mode action

$$iS_{cd} = \frac{\pi\nu}{4} \int \frac{d\epsilon}{2\pi} \int \frac{d\epsilon'}{2\pi} \operatorname{tr} \left[\vec{d}_{\epsilon'\epsilon} \hat{\mathcal{D}}^{-1}_{\epsilon\epsilon'} \vec{d}_{\epsilon\epsilon'} + \vec{c}_{\epsilon'\epsilon} \hat{\mathcal{C}}^{-1}_{\epsilon\epsilon'} \vec{c}_{\epsilon\epsilon'} \right] \tag{B.13}$$

where we have defined the vector notation

$$\begin{aligned} \vec{d} &= (d^{cl}, d^q) \\ \vec{c} &= (c^R, c^A) \\ \hat{D}^{-1}_{\epsilon\epsilon'} &= \mathcal{D}^{-1}_{\epsilon'\epsilon}\sigma_+ + \mathcal{D}^{-1}_{\epsilon\epsilon'}\sigma_- \\ \hat{\mathcal{C}}^{-1}_{\epsilon\epsilon'} &= \operatorname{diag}\left([\mathcal{C}^R_{\epsilon\epsilon'}]^{-1}, [\mathcal{C}^A_{\epsilon\epsilon'}]^{-1} \right), \end{aligned} \tag{B.14}$$

and the diffuson and cooperon propagators

$$\begin{aligned}
\mathcal{D}^{-1}_{\epsilon\epsilon'} &= \mathcal{E}^R(\epsilon) + \mathcal{E}^A(\epsilon') \\
[\mathcal{C}^{R/A}]^{-1}_{\epsilon\epsilon'} &= \mathcal{E}^{R/A}(\epsilon) + \mathcal{E}^{R/A}(\epsilon') \\
\mathcal{E}^R(\epsilon) &= i\left(\epsilon + i\frac{\gamma}{2}\right)\cosh\theta_\epsilon - i\Delta\sinh\theta_\epsilon \\
\mathcal{E}^A(\epsilon) &= \left(\mathcal{E}^R(\epsilon)\right)^*.
\end{aligned} \tag{B.15}$$

At linear order we then have a coupling between diffusive modes and the gap

$$iS_{\Delta-cd} = \pi\nu\int\frac{d\epsilon}{2\pi}\left[\vec{c}_{\epsilon\epsilon}\cdot\vec{s}^c_\epsilon + \vec{d}_{\epsilon\epsilon}\hat{\sigma}_1\vec{s}^d_\epsilon\right] \tag{B.16}$$

where we have taken Δ_q to be homogeneous and real. Finally, there is a coupling of the diffusons and cooperons to the photon field

$$\pi\nu D\int\frac{d\omega}{2\pi}\mathbf{A}^\alpha_{-\omega}\cdot\mathbf{A}^\beta_\omega\int\frac{d\epsilon}{2\pi}\left[\vec{c}_{\epsilon\epsilon}\cdot\vec{r}^{c;\alpha\beta}_\epsilon + \vec{d}_{\epsilon\epsilon}\hat{\sigma}_1\vec{r}^{d;\alpha\beta}_\epsilon\right] \tag{B.17}$$

The $\vec{r}^{i;\alpha\beta}$ are matrices in the photon Keldysh space and vectors in the sense induced by Eq. B.14. They determined by the structure of the saddlepoint solution and arise from expanding to covariant derivative term in Eq. (B.5) to lowest order in the W matrix fields.

The coupling to the diffusive modes may be removed by making a shift of the fields

$$\vec{c}_{\epsilon\epsilon} \to \vec{c}_{\epsilon\epsilon} - 2\Delta^q\hat{\mathcal{C}}_{\epsilon\epsilon}\vec{s}^c_\epsilon - 2D\hat{\mathcal{C}}_{\epsilon\epsilon}\int\frac{d\omega}{2\pi}\mathbf{A}^\alpha_{-\omega}\mathbf{A}^\beta_\omega\vec{r}^{c;\alpha\beta}_\epsilon \tag{B.18}$$

$$\vec{d}_{\epsilon\epsilon} \to \vec{d}_{\epsilon\epsilon} - 2\Delta^q\hat{\mathcal{D}}_{\epsilon\epsilon}\hat{\sigma}_1\vec{s}^d_\epsilon - 2D\int\frac{d\omega}{2\pi}\mathbf{A}^\alpha_{-\omega}\mathbf{A}^\beta_\omega\hat{\mathcal{D}}_{\epsilon\epsilon}\hat{\sigma}_1\vec{r}^{d;\alpha\beta}_\epsilon. \tag{B.19}$$

This shift has three effects. The first two are to create a nonlinear term in the photon action, which we will ignore as we are not considering non-linear effects, and

to create term at second order Δ_q which we can ignore as Δ_q will be taken to 0 at the end. The important effect is that a coupling between photons and Δ_q^* is induced

$$iS_{\Delta-A} = 2\pi\nu D\Delta^q \int \frac{d\omega}{2\pi} \int \frac{d\mathbf{q}}{(2\pi)^2} \mathbf{A}^{\alpha}_{-\omega}(-\mathbf{q}) \cdot \mathbf{A}^{\beta}_{\omega}(\mathbf{q}) \int \frac{d\epsilon}{2\pi} \left[\vec{s}^{c}_{\epsilon} \hat{\mathcal{C}}_{\epsilon\epsilon} \vec{r}^{c;\alpha\beta}_{\epsilon} + \vec{s}^{d}_{\epsilon} \hat{\sigma}_1 \hat{\mathcal{D}}_{\epsilon\epsilon} \hat{\sigma}_1 \vec{r}^{d;\alpha\beta}_{\epsilon} \right]. \tag{B.20}$$

At this point we may safely integrate out the d modes and henceforth ignore them.[1]

Making the definition

$$-i\Pi^{\alpha\beta} = 2\pi\nu D\Delta^q \int \frac{d\epsilon}{2\pi} \left[\vec{s}^{c}_{\epsilon} \hat{\mathcal{C}}_{\epsilon\epsilon} \vec{r}^{c;\alpha\beta}_{\epsilon} + \vec{s}^{d}_{\epsilon} \hat{\mathcal{D}}_{\epsilon\epsilon} \vec{r}^{d;\alpha\beta}_{\epsilon} \right] \tag{B.21}$$

we can write the photon action as

$$iS_A = i \int \frac{d\omega}{2\pi} \int \frac{d\mathbf{q}}{(2\pi)^2} \mathbf{A}^{\alpha}_{-\omega,-\mathbf{q}} \left(\check{S}_0^{-1}(\omega, \mathbf{q}) - \check{\Pi}(\omega, \mathbf{q}) \right) \mathbf{A}^{\beta}_{\omega,\mathbf{q}}. \tag{B.22}$$

Integrating out $\mathbf{a}$ we obtain

$$iS = -\frac{1}{2} \operatorname{Tr} \ln \left[-i \left(\check{S}_0^{-1} - \check{\Pi} \right) \right] \approx \frac{1}{2} \operatorname{Tr} \left[\check{S}_0 \check{\Pi} \right] \tag{B.23}$$

where we have expanded to linear order in Δ_q. Since the momentum $\mathbf{q}$ appears only in S we can immediately integrate over it. Similarly we can trace over the in plane components of A. We thus define

$$\hat{D}(\omega) = \sum_{i \in \{x,y\}} \int \frac{d\mathbf{q}}{(2\pi)^2} \hat{S}^{ii}(\omega, \mathbf{q}) \tag{B.24}$$

We assume the photon modes to be governed by a density matrix which is diagonal

[1] We are free to ignore the residual coupling to Δ as the saddlepoint equation guarantees that it vanishes.

in energy. D can then be written in the usual form

$$\hat{D}(\omega) = \begin{pmatrix} N(\omega)(D^R(\omega) - D^A(\omega)) & D^R(\omega) \\ D^A(\omega) & 0 \end{pmatrix} \tag{B.25}$$

Defining $-2\pi i J(\omega) = D^R(\omega) - D^A(\omega)$ and using the analytic properties of D this can be written

$$iS = \frac{-i}{2} \int d\omega J(\omega) \left[N(\omega)\Pi_{0,0}(\omega) - (\Pi^R(\omega) - \Pi^A(\omega)) \right] \tag{B.26}$$

where we have defined $\Pi^{R/A}$ as the retarded/analytic part of $\Pi^{01/10}$. Defining

$$\nu\Delta^q \left(P^c_{\alpha\beta}(\omega) + P^d_{\alpha\beta}(\omega) \right) = -i\Pi^{\alpha\beta} \tag{B.27}$$

$$\mathcal{B}(\omega) = \frac{P^d_R(\omega) - P^d_A(\omega)}{P^d_0(\omega)} \tag{B.28}$$

with $P^0 = P_{00}$ and $P^{R/A}$ defined analogously to $\Pi^{R/A}$ the correction can be broken into two terms. The first is the equilibrium self-energy correction to to the cavity photons

$$iS^{eq}_c = \frac{\nu\Delta^q}{2} \int d\omega J(\omega) \left[\mathcal{B}(\omega) P^c_0(\omega) - (P^c_R(\omega) - P^c_A(\omega)) \right]. \tag{B.29}$$

This term should be included in the bare equilibrium result as it is a property of the equilbrium cavity-superconductor system and we therefore subtract it off henceforth. The other term

$$iS_{fluc} = \frac{\nu\Delta^q}{2} \int d\omega J(\omega)(N(\omega) - \mathcal{B}(\omega))(P^c_0(\omega) + P^d_0(\omega)) \tag{B.30}$$

is the fluctuation induced enhancement to superconductivity. This is to be compared with the correction term due to a classical monochromatic field (i.e. the original

Eliashberg effect)

$$iS = (-i\Pi_{0,0}(\omega) - i\Pi_{0,0}(-\omega))|\mathbf{A}_\omega|^2 = \nu\Delta^q(P_0(\omega)+P_0(-\omega))|\mathbf{A}_\omega|^2 \equiv \nu\Delta^q Y(\omega)|\mathbf{A}_\omega|^2. \tag{B.31}$$

Using the functional dependence of the classical Eliashberg effect on frequency $Y(\omega)$ the quantum Eliashberg effect can be written in a Fluctuation-Dissipation like form

$$iS^{\text{fluc}} = \frac{\nu\Delta^q}{2}\int_0^\infty d\omega J(\omega)(N(\omega) - \mathcal{B}(\omega))Y(\omega). \tag{B.32}$$

It should be noted that in the linearized regime P_0^d goes as γ^{-1} while P_0^c goes as γ^0. Thus, in the limit of $\gamma \to 0$ we expect the diffuson contribution to be dominant.

B.2 Gap Equation

As mentioned previously, the BCS gap equation is the saddlepoint equation of our action with respect to the source field Δ_q. Including the correction term Eq. (B.32) the gap equation then becomes

$$0 = \left.\frac{\delta iS}{\delta\Delta_q}\right|_{\Delta_q=0} = -4i\frac{\nu}{\lambda}\Delta + \frac{\pi\nu}{2}\operatorname{Tr}\hat{Q}^K\hat{\tau}_2 + \frac{\nu}{2}\int_0^\infty d\omega J(\omega)(N(\omega)-\mathcal{B}(\omega))Y(\omega) \tag{B.33}$$

We therefore define

$$\begin{aligned} F_{\text{BCS}} &= \frac{1}{\lambda} + \frac{i\pi}{8\Delta}\operatorname{Tr}\hat{Q}^K\hat{\tau}_2 \\ F_{\text{phot}} &= \frac{i\nu}{8\Delta}\int_0^\infty d\omega J(\omega)(N(\omega) - \mathcal{B}(\omega))Y(\omega) \end{aligned} \tag{B.34}$$

Which allows us to write the gap equation as $F_{\text{BCS}} = -F_{\text{phot}}$. Furthermore, F_{phot} can be broken up into a kinetic contribution F^{kin} arising from modification of the quasiparticle occupation function and a spectral contribution F^{spec} due to modification of the density of states from self energy effects, as discussed above. Most notably,

because the gap equation is linearly related to the action, the corrections to the gap equation are related to the conventional via the same fluctuation-dissipation-like relation.

B.2.1 Effective photonic spectral function

The function $J(\omega)$ can be can be calculated by relating the field $\mathbf{A}$ to the cavity mode operators $a, \bar{a}$.

Multimode Cavity

As an example of a multimode cavity we take the cavity mode Keldysh action to be given by

$$iS = i\int \frac{d\omega}{2\pi}\int \frac{d\mathbf{q}}{(2\pi)^2} a^\dagger_{q;\alpha} \underbrace{\begin{pmatrix} 0 & \omega - i\kappa - \omega_q \\ \omega + i\kappa - \omega_q & 2i\kappa N(\omega) \end{pmatrix}}_{\hat{G}^{-1}(\omega,\mathbf{q})} a_{q;\alpha}. \tag{B.35}$$

to describe a cavity coupled to the environment.[199] Using the fact that we can expression $\mathbf{A}$ in terms of a and $\bar{a}$ (in Gaussian units) as

$$\mathbf{A}_q(z) = \sqrt{\frac{2\pi c^2}{\omega_q}}\left(a_{q;\alpha}\epsilon_{\mathbf{q};\alpha}(z) + a^\dagger_{-q;\alpha}\epsilon^*_{-\mathbf{q};\alpha}(z)\right) \tag{B.36}$$

we can relate the Keldysh component of S and G

$$2S^K_{\omega,\mathbf{q};ii}(L/2, L/2) = \frac{2\pi c^2}{\omega_q}\sum_\alpha |\epsilon^i_{\mathbf{q};\alpha}(L/2)|^2\left(G^K_{-q} + G^K_q\right) \tag{B.37}$$

After some calculation we therefore find

$$J_{\mathrm{MM}}(\omega) = \int \frac{d\mathbf{q}}{(2\pi)^2}\frac{\kappa c^2}{\omega_q}\sum_\alpha \left|\epsilon_{\mathbf{q};\alpha}\left(\frac{L}{2}\right)\right|^2\left(\frac{1}{(\omega-\omega_q)^2+\kappa^2} - \frac{1}{(\omega+\omega_q)^2+\kappa^2}\right) \tag{B.38}$$

where we have used the fact that $\epsilon(L/2)$ is in plane. Now with the explicit forms of ϵ_i from the main text

$$\begin{aligned}\hat{\epsilon}_{1,\mathbf{q}}(L/2) &= -i\sqrt{\frac{2}{L}}\frac{\omega_0}{\omega_\mathbf{q}}\frac{\mathbf{q}}{|\mathbf{q}|} \\ \hat{\epsilon}_{2,\mathbf{q}}(L/2) &= \sqrt{\frac{2}{L}}\mathbf{e}_3 \times \frac{\mathbf{q}}{|\mathbf{q}|}\end{aligned} \tag{B.39}$$

we can immediately evaluate the angular integral

$$\int \frac{d\theta}{2\pi} \sum_{i\in x,y,\alpha} |\epsilon^i_{\theta,\alpha}(L/2)|^2 = \frac{2}{L}\left(1+\frac{\omega_0^2}{\omega_\mathbf{q}^2}\right). \tag{B.40}$$

We now make a change of variables from $|\mathbf{q}| \to \omega' = \omega_\mathbf{q}$. The dispersion relation $\omega_q^2 = \omega_0^2 + c^2q^2$ implies

$$\frac{qdq}{2\pi\omega'} = \frac{d\omega'}{2\pi c^2}. \tag{B.41}$$

This allows us to write J as

$$J_{\mathrm{MM}}(\omega) = \frac{2\kappa}{L}\int_{\omega_0}^{\infty} d\omega' \left(\frac{1}{(\omega-\omega')^2+\kappa^2} - \frac{1}{(\omega+\omega')^2+\kappa^2}\right)\left(1+\frac{\omega_0^2}{\omega'^2}\right). \tag{B.42}$$

This integral may be performed exactly to find

$$\begin{aligned}J_{\mathrm{MM}}(\omega) = \frac{2}{L}\Bigg[&\left(1+\omega_0^2\frac{\omega^2-\kappa^2}{(\omega^2+\kappa^2)^2}\right)\left(\tan^{-1}\frac{\omega-\omega_0}{\kappa}+\tan^{-1}\frac{\omega+\omega_0}{\kappa}\right) \\ &+\frac{\kappa\omega\omega_0^2}{\left(\omega^2+\kappa^2\right)^2}\log\left(\frac{\left((\omega-\omega_0)^2+\kappa^2\right)\left((\omega+\omega_0)^2+\kappa^2\right)}{\omega_0^4}\right)\Bigg].\end{aligned} \tag{B.43}$$

We will, however, introduce a factor X^2 into J which describes enhancement of the electron-photon coupling due to e.g. squeezing of mode volume, one factor of X coming from the enhancement of each vertex. In principle this enhancement should come from a detailed study of the structure of the photon modes. However, this physics is not captured within our simple parallel plate model and so we include the

coupling enhancement phenomenonlogically via the factor X

$$J_{\text{eff}}(\omega) = X^2 J(\omega). \tag{B.44}$$

Single mode cavity

We can also consider the effective photonic spectral function for a single mode cavity

$$iS = i \int \frac{d\omega}{2\pi} a_\alpha^\dagger(\omega) \underbrace{\begin{pmatrix} 0 & \omega - i\kappa - \omega_0 \\ \omega + i\kappa - \omega_0 & 2i\kappa N(\omega) \end{pmatrix}}_{\hat{G}^{-1}(\omega)} a_\alpha(\omega). \tag{B.45}$$

Following the steps outlined above we find that

$$J_{\text{eff;SM}}(\omega) = \frac{\kappa c^2 X}{\omega_0} \sum_\alpha \left| \epsilon_\alpha \left(\frac{L}{2} \right) \right|^2 \left(\frac{1}{(\omega - \omega_0)^2 + \kappa^2} - \frac{1}{(\omega + \omega_0)^2 + \kappa^2} \right). \tag{B.46}$$

B.2.2 Photonic corrections to the distribution function

To lowest order in $\tau_{\text{in}} = 1/\gamma$, which corresponds to taking a linearized expansion of the collision integral in the deviation of the occupation function from Fermi-Dirac, and using the fact that $J(\omega)$ is an odd function of ω we can write $F_{\text{phot}}^{\text{kin}} = F_{\text{pair}} + F_{\text{scat}}$ with the recombination contribution

$$\begin{aligned} F_{\text{pair}} = \frac{\alpha D}{\gamma c} \int_{2\Delta}^{\infty} d\omega J(\omega) \left(N(\omega) - \mathcal{B}(\omega) \right) \\ \int_{\Delta}^{\omega - \Delta} \frac{d\epsilon}{\epsilon} \left(F(\epsilon) + F(\omega - \epsilon) \right) P(\epsilon, \omega - \epsilon) \rho_{qp}(\epsilon) \rho_{qp}(\omega - \epsilon) \end{aligned} \tag{B.47}$$

and scattering contribution

$$F_{\text{scatter}} = \frac{\alpha D}{\gamma c}\int_0^\infty d\omega\,\omega J(\omega)\left(N(\omega)-\mathcal{B}(\omega)\right) \int_\Delta^\infty \frac{d\epsilon}{\epsilon(\epsilon+\omega)}\left(F(\epsilon)-F(\omega+\epsilon)\right)L(\epsilon,\omega+\epsilon)\rho_{qp}(\epsilon)\rho_{qp}(\omega+\epsilon), \quad \text{(B.48)}$$

where the fine-structure constant α appears due to reinstating the electron charge in the paramagnetic coupling which we had previously absorbed into the **A** field.

With our particular form of $J(\omega)$ ($G(w,k)$) the correction to the gap equation become

$$F_{\text{pair}} = \frac{\alpha D X^2}{c\gamma}\int_{2\Delta}^\infty d\omega J(\omega)\left(N(\omega)-\mathcal{B}(\omega)\right) \int_\Delta^{\omega-\Delta} \frac{d\epsilon}{\epsilon}\left(F(\epsilon)+F(\omega-\epsilon)\right)P(\epsilon,\omega-\epsilon)\rho_{qp}(\epsilon)\rho_{qp}(\omega-\epsilon) \quad \text{(B.49)}$$

and

$$F_{\text{scatter}} = \frac{\alpha D X^2}{c\gamma}\int_0^\infty d\omega\,\omega J(\omega)\left(N(\omega)-\mathcal{B}(\omega)\right) \int_\Delta^\infty \frac{d\epsilon}{\epsilon(\epsilon+\omega)}\left(F(\epsilon)-F(\omega+\epsilon)\right)L(\epsilon,\omega+\epsilon)\rho_{qp}(\epsilon)\rho_{qp}(\omega+\epsilon). \quad \text{(B.50)}$$

In the above we have used the definitions

$$\begin{gathered} P(\epsilon,\epsilon') = 1-\frac{\Delta^2}{\epsilon\epsilon'}, \qquad L(\epsilon,\epsilon') = 1+\frac{\Delta^2}{\epsilon\epsilon'} \\ F(\epsilon) = \tanh\frac{\epsilon}{2T}, \qquad N(\omega) = \coth\frac{\omega}{2T_p}, \qquad \mathcal{B}(\omega) = \coth\frac{\omega}{2T} \end{gathered} \quad \text{(B.51)}$$

We have assumed the photons to be at temperature T_p while the Fermions are coupled to a bath of temperature T.

The correction terms can be rewritten as

$$F_{\text{pair}} + F_{\text{scat}} = \frac{\alpha D X^2}{\gamma c} \int_\Delta^\infty d\epsilon \frac{\rho_{qp}(\epsilon)}{\epsilon} \int_0^\infty d\omega J(\omega) \left(N(\omega) - \mathcal{B}(\omega)\right)$$
$$\times \Big[\left(F(\epsilon) + F(\omega - \epsilon)\right) P(\epsilon, \omega - \epsilon) \rho_{qp}(\omega - \epsilon) \Theta(\epsilon - \Delta) \Theta(\omega - \Delta - \epsilon)$$
$$+ \left(F(\epsilon) - F(\epsilon + \omega)\right) L(\epsilon, \epsilon + \omega) \rho_{\text{qp}}(\epsilon + \omega) \Theta(\epsilon - \Delta)$$
$$+ \left(F(\epsilon - \omega) - F(\epsilon)\right) L(\epsilon - \omega, \epsilon) \rho_{\text{qp}}(\epsilon - \omega) \Theta(\epsilon - \omega - \Delta) \Big] = 2 \int_\Delta^\infty d\epsilon \frac{\rho_{qp}(\epsilon)}{\epsilon} n_1(\epsilon) \tag{B.52}$$

which allows us to move this term to the left hand side to obtain

$$\frac{1}{\lambda} - \int_\Delta^\infty d\epsilon \frac{1 - 2n_f(\epsilon) - 2n_1(\epsilon)}{\sqrt{\epsilon^2 - \Delta^2}} = 0 \tag{B.53}$$

and therefore identify the correction to the occupation function

$$n_1 = \frac{\alpha D X^2}{2\gamma c} \int_0^\infty d\omega J(\omega) \left(N(\omega) - \mathcal{B}(\omega)\right)$$
$$\times \Big[\left(F(\epsilon) + F(\omega - \epsilon)\right) P(\epsilon, \omega - \epsilon) \rho_{qp}(\omega - \epsilon) \Theta(\epsilon - \Delta) \Theta(\omega - \Delta - \epsilon)$$
$$+ \left(F(\epsilon) - F(\epsilon + \omega)\right) L(\epsilon, \epsilon + \omega) \rho_{\text{qp}}(\epsilon + \omega) \Theta(\epsilon - \Delta)$$
$$+ \left(F(\epsilon - \omega) - F(\epsilon)\right) L(\epsilon - \omega, \epsilon) \rho_{\text{qp}}(\epsilon - \omega) \Theta(\epsilon - \omega - \Delta) \Big] . \tag{B.54}$$

Defining the power spectral density of absorption $(\alpha D/c) J(\omega)$, our result can be written

$$n_1(\epsilon) = \gamma^{-1} \int_0^\infty d\omega \; S(\omega) \frac{N(\omega) - \mathcal{B}(\omega)}{2} I_\epsilon^{\text{el}}(\omega) \tag{B.55}$$

where $I_{\text{eps}}^{\text{el}}(\omega)$ is the related to the conventional Eliashberg expression [40] for a classical microwave field $\mathbf{A}_\omega$ by

$$n_1^{\text{conv.}}(\epsilon, \omega) = \frac{\alpha D |\mathbf{A}_\omega|^2}{\gamma c} I_\epsilon^{\text{el}}(\omega). \tag{B.56}$$

Appendix C: Effective Hamiltonian

Here we detail the first of two methods we used to solve for the dispersion relations depicted in Fig. 3.3 of the main text. We essentially expand the frequency-dependent dispersion of the Bardasis-Schrieffer and two photon modes and derive an effective Hamiltonian description, from which we can analytically obtain the polariton dispersions and eigenvalues. In the next section we discuss the numerical methods used to solve for the polariton dispersion directly from the hybrid inverse Green's function. In this section we will frequently employ the notation that $\int_{\mathbf{k}} \int \frac{d^2k}{(2\pi)^2}$.

As explained in the main text, we begin with the fermionic mean field model

$$S = S_{\Delta,s} + S_{\Delta,d} + S_{\text{cav}} - \sum_k \bar{\psi}_k \hat{G}_k^{-1} \psi_k + \sum_{k,q} \bar{\psi}_{k+\frac{q}{2}} \frac{1}{\sqrt{\beta \text{Vol}}} \left(\left[\frac{\mathbf{k}}{m} + \mathbf{v}_S \tau_3 \right] \cdot \mathbf{A}_q + \hat{\tau}_2 f_d(\phi_{\mathbf{k}}) d_q \right) \psi_{k-\frac{q}{2}}, \quad \text{(C.1)}$$

which has been obtained via Hubbard-Stratonovich decoupling the interaction terms in the Cooper channel and where $\hat{G}$ is the Nambu Green's function of the s-wave state. Integrating out fermions and keeping to second order in the photon and Bardasis-Schrieffer fields we obtain a description in terms of only bosonic variables

$$S_{\text{eff}} = S_d + S_A + S_{d-A}, \quad \text{(C.2)}$$

where

$$S_d = \sum_q d_{-q} \left[\frac{1}{g_d} + \int_{\mathbf{k}} f_d(\phi_{\mathbf{k}})^2 \frac{2\lambda_{\mathbf{k}}\, \delta n_{\mathbf{k}}}{(i\Omega_m)^2 - (2\lambda_{\mathbf{k}})^2} \right] d_q \tag{C.3a}$$

$$S_A = -\frac{1}{2} \sum_{q,\alpha,\beta} A_{\alpha,-q} \left[\frac{\epsilon_0}{e^2 X^2} \left((i\Omega_m)^2 - \omega_q^2 \right) \delta_{\alpha\beta} - \Pi_{\alpha\beta,q} \right] A_{\beta,q} \tag{C.3b}$$

$$S_{d-A} = i\Delta \sum_{q,\alpha} \int_{\mathbf{k}} f_d(\phi_{\mathbf{k}}) \frac{i\Omega_m\, \delta n_{\mathbf{k}}}{(i\Omega_m)^2 - (2\lambda_{\mathbf{k}})^2} \frac{\mathbf{v}_S \cdot \vec{\epsilon}_{\alpha,q}}{\lambda_{\mathbf{k}}} \left(A_{\alpha,q}\, d_{-q} - A_{\alpha,-q}\, d_q \right), \tag{C.3c}$$

and $\vec{\epsilon}_\alpha$ are the in plane components of the polarizations described in Appendix A, evaluated at $z = L/2$.

C.0.1 Bardasis-Schrieffer Sector

We begin by rewriting S_d using the mean field equation for the s-wave Δ,

$$\begin{aligned}
S_d &= \sum_q d_{-q} \left[\frac{1}{g_d} + \int_{\mathbf{k}} f_d(\phi_{\mathbf{k}})^2 \frac{\delta n_{\mathbf{k}}}{(i\Omega_m)^2 - (2\lambda_{\mathbf{k}})^2}\, 2\lambda_{\mathbf{k}} \underbrace{- \frac{1}{g_s} + \int_{\mathbf{k}} \frac{\delta n_{\mathbf{k}}}{2\lambda_{\mathbf{k}}}}_{=0} \right] d_q \\
&= \sum_q d_{-q} \left[\frac{1}{g_d} - \frac{1}{g_s} + \int_{\mathbf{k}} \frac{\delta n_{\mathbf{k}}}{2\lambda_{\mathbf{k}}} \left(\frac{(i\Omega_m)^2 + (2\lambda_{\mathbf{k}})^2 (f_d(\phi_{\mathbf{k}})^2 - 1)}{(i\Omega_m)^2 - (2\lambda_{\mathbf{k}})^2} \right) \right] d_q \\
&= \sum_q d_{-q} \left[\frac{1}{g_d} - \frac{1}{g_s} + \sum_{\mathbf{k}} \left(\frac{(i\Omega_m)^2}{2\lambda_{\mathbf{k}}} + 2\lambda_{\mathbf{k}} \cos(4\phi_{\mathbf{k}}) \right) \frac{\delta n_{\mathbf{k}}}{(i\Omega_m)^2 - (2\lambda_{\mathbf{k}})^2} \right] d_q \\
&\equiv -\frac{1}{2} \sum_q d_{-q} D^{-1}_{\mathrm{BS},q} d_q.
\end{aligned} \tag{C.4}$$

In the first line we employ the gap equation for Δ. This rewriting regulates the integration and also allows us to straightforwardly parametrize the Bardasis-Schrieffer frequency in terms of the relative strength of the s-wave and d-wave interactions. In the last line we define the BS inverse Green's function D^{-1}_{BS}. In order to change to the mode operator basis the inverse Green's function must be rewritten in a harmonic approximation. We first analytically continue the imaginary frequency to the entire complex plane, $i\Omega_m \to z \in \mathbb{C}$, then expand the inverse Green's function

to second order in z around the saddle point solution, which we identify as $\Omega_{\rm BS}$ ($D^{-1}_{\rm BS}(z=\Omega_{\rm BS},\mathbf{q})=0$), and finally restrict back to Matsubara frequency. This is simply finding the saddle point solution by the method of steepest descent. Note that because our model has no disorder, the BS frequency is real, and so the BS mode cannot decay. The result of this expansion is

$$S_d \approx -\frac{K}{2}\sum_q d_{-q}\left((i\Omega_m)^2-\Omega_{\rm BS}^2\right)d_q, \tag{C.5}$$

where the constant $K\equiv \partial^2 D^{-1}_{\rm BS}(z,\mathbf{q})/\partial z^2|_{z=\Omega_{\rm BS}}$ is a coefficient resulting from the expansion. From this form the transformation to mode operators can be performed without further difficulty:

$$S_d \to S_b = \sum_q \bar{b}_q(-i\Omega_m+\Omega_{\rm BS})b_q \quad \text{with} \quad d_q=\frac{b_q+\bar{b}_{-q}}{\sqrt{2K\Omega_{\rm BS}}}. \tag{C.6}$$

C.0.2 Photon Sector

The self-energy part of the photon action arises from

$$S_\Pi = \frac{1}{2}\,\mathrm{Tr}\left(\hat{G}\hat{\chi}\hat{G}\hat{\chi}\right) \equiv \frac{1}{2}\sum_q \mathbf{A}_{-q}\hat{\Pi}_q\mathbf{A}_q = \frac{1}{2}\sum_{q,\alpha,\beta} A_{\alpha,-q}\Pi_{\alpha\beta,q}A_{\beta,q}. \tag{C.7}$$

In the last equality, reproducing the term in the action above, the response function Π has been rewritten in the basis of cavity polarizations from the original Cartesian basis of the vector potential,

$$\Pi_{\alpha\beta,q} = \sum_{i,j}\epsilon^i_{\alpha,-\mathbf{q}}\Pi^{ij}_q\epsilon^j_{\beta,\mathbf{q}}. \tag{C.8}$$

Though the polarization basis is useful for the change to mode operators, an appropriately chosen Cartesian basis is far more convenient for the evaluation of the $\hat{\Pi}$. We choose this basis to be defined as the directions parallel and perpendicular to

the axis of the supercurrent because we know that this is the basis most relevant for the hybridization problem; only the component of $\mathbf{A}_q$ parallel to the supercurrent hybridizes with the BS mode. This can be done because there are two linearly independent polarizations which have non-zero components of the polarization in the plane (see Appendix A).

The form of $\hat{\Pi}$ can be extracted from the trace above,

$$\Pi_q^{ij} = \frac{1}{\beta}\sum_{i\varepsilon_n}\int_{\mathbf{k}} \mathrm{tr}\left[\hat{G}_{k+\frac{q}{2}}\left(v_{\mathbf{k}}^i\hat{\tau}_0 + v_S^i\hat{\tau}_3\right)\hat{G}_{k-\frac{q}{2}}\left(v_{\mathbf{k}}^j\hat{\tau}_0 + v_S^j\hat{\tau}_3\right)\right], \tag{C.9}$$

where $\hat{G}_k = \left[(i\epsilon_n - \mathbf{k}\cdot\vec{v}_S)\hat{\tau}_0 - \xi_{\mathbf{k}}^S\hat{\tau}_3 - \Delta\hat{\tau}_1\right]^{-1}$ is the Nambu Green's function. Unlike for the Bardasis-Schrieffer mode, here we keep the q dependence of the Green's functions. Upon inserting resolutions of the identity to diagonalize the Green's function with the appropriate Bogoluibov transformation, $\hat{U}_{\mathbf{k}} = \begin{pmatrix} u_{\mathbf{k}} & -v_{\mathbf{k}} \\ v_{\mathbf{k}} & u_{\mathbf{k}} \end{pmatrix}$ with $u_{\mathbf{k}}, v_{\mathbf{k}} = \sqrt{\frac{1}{2}\left(1 \pm \frac{\xi_{\mathbf{k}}^S}{\lambda_{\mathbf{k}}}\right)}$, and performing the Matsubara summation we have

$$\begin{aligned}\Pi_q^{ij} = \int \frac{d^2k}{(2\pi)^2}\sum_{\alpha,\alpha'} \frac{n_F\left(E^{\alpha'}_{\mathbf{k}-\mathbf{q}/2}\right) - n_F\left(E^{\alpha}_{\mathbf{k}+\mathbf{q}/2}\right)}{i\Omega_m - \left(E^{\alpha}_{\mathbf{k}+\mathbf{q}/2} - E^{\alpha'}_{\mathbf{k}-\mathbf{q}/2}\right)} \Big\{ & v_{\mathbf{k}}^i v_{\mathbf{k}}^j\left(\ell_{\mathbf{k},\mathbf{q}}^2\delta_{\alpha,\alpha'} - p_{\mathbf{k},\mathbf{q}}^2\delta_{\alpha,-\alpha'}\right) \\ & + v_S^i v_S^j\left(n_{\mathbf{k},\mathbf{q}}^2\delta_{\alpha,\alpha'} + m_{\mathbf{k},\mathbf{q}}^2\,\delta_{\alpha,-\alpha'}\right) \\ & + \left(v_{\mathbf{k}}^i v_S^j + v_S^i v_{\mathbf{k}}^j\right)\ell_{\mathbf{k},\mathbf{q}} n_{\mathbf{k},\mathbf{q}}\,\alpha\,\delta_{\alpha,\alpha'} \\ & + \left(v_{\mathbf{k}}^i v_S^j - v_S^i v_{\mathbf{k}}^j\right)p_{\mathbf{k},\mathbf{q}} m_{\mathbf{k},\mathbf{q}}\,\alpha\,\delta_{\alpha,-\alpha'}\Big\},\end{aligned} \tag{C.10}$$

where we have defined the superconductor coherence factors

$$\ell_{\mathbf{k},\mathbf{q}} = u_+u_- + v_+v_- \quad p_{\mathbf{k},\mathbf{q}} = u_+v_- - v_+u_- \quad n_{\mathbf{k},\mathbf{q}} = u_+u_- - v_+v_- \quad m_{\mathbf{k},\mathbf{q}} = u_+v_- + v_+u_-, \tag{C.11}$$

using the shorthand notation for the Bogoliubov amplitudes $u_\pm = u_{\mathbf{k}\pm\mathbf{q}/\mathbf{2}}$ and

$v_\pm = v_{\mathbf{k}\pm\mathbf{q}/2}$.

Analytic evaluation of this function keeping the full momentum and frequency dependence is unfeasible, so now, after analytic continuation to real frequency $i\Omega_m \to \omega + i0$, we expand to first order in the small deviation of the frequency from the cavity resonant frequency, $\delta\Omega = \omega - \omega_0 + i0$, which is the most that could be needed in the mode operator picture, and to second order in $|\mathbf{q}|$. Furthermore, we note that $v_\mathbf{k} \gg v_S$ and use this to make some further approximations, dropping terms with v_S when there is a corresponding term appearing with $v_\mathbf{k}$. We write the result of this expansion as

$$\begin{aligned}
\Pi_q^{ij} \approx\ & x_P^{10,ij}(\phi_q)\, q \left(1 - \frac{\delta\Omega}{\omega_0}\right) + x_P^{20,ij}(\phi_q)\, q^2 \\
& + \left(x_S^{00} + x_S^{01}\,\delta\Omega + x_S^{10}(\phi_q)\, q + x_S^{11}(\phi_q)\, q\,\delta\Omega + x_S^{20}(\phi_q)\, q^2\right) \delta_{ij}\delta_{i,\parallel} \\
& + \left[\left(x_{SPs}^{10,i}(\phi_q) + x_{SPa}^{10,i}(\phi_q)\right)\, q + \left(x_{SPs}^{11,i}(\phi_q) + x_{SPa}^{11,i}(\phi_q)\right)\, q\,\delta\Omega\right] \delta_{j,\parallel} \\
& \qquad + \left[\left(x_{SPs}^{20,i}(\phi_q) + x_{SPa}^{20,i}(\phi_q)\right)\, q^2\right] \delta_{j,\parallel} \\
& + \left[\left(x_{SPs}^{10,j}(\phi_q) - x_{SPa}^{10,j}(\phi_q)\right)\, q + \left(x_{SPs}^{11,j}(\phi_q) - x_{SPa}^{11,j}(\phi_q)\right)\, q\,\delta\Omega\right] \delta_{i,\parallel} \\
& \qquad + \left[\left(x_{SPs}^{20,j}(\phi_q) - x_{SPa}^{20,j}(\phi_q)\right)\, q^2\right] \delta_{i,\parallel}. \qquad \text{(C.12)}
\end{aligned}$$

The thirteen coefficients that appear in this expansion are given in Eq. (C.13). Many of them are functions of the ϕ_q, the angle $\mathbf{q}$ makes with $\vec{v}_S$. They are labeled with a subscript showing the type of vertices they arise from, P for two paramagnetic vertices $\vec{v_k}$, S for two supercurrent vertices $\vec{v}_S$, and SP for one of each. The secondary indices s and a on the SP coefficients label whether the term it is found in is symmetric or antisymmetric under exchange of the indices i and j. The superscript indices keep track of the powers of $|\mathbf{q}|$ (first index) and $\delta\Omega$ (second

index) that the coefficient multiplies.

$$x_P^{10,ij}(\phi_q) = -v_S \int_{\mathbf{k}} \frac{1}{\omega_0} N'_{\mathbf{k}} v^i_{\mathbf{k}} v^j_{\mathbf{k}} \cos\phi_q \tag{C.13a}$$

$$x_P^{20,ij}(\phi_q) = -\frac{1}{\omega_0^2} \int_{\mathbf{k}} \left[\left(\frac{\xi^S_{\mathbf{k}}}{\lambda_{\mathbf{k}}} \right)^2 N'_{\mathbf{k}} + \frac{\Delta^2}{\lambda^3_{\mathbf{k}}} \frac{\omega_0^2}{\omega_0^2 - (2\lambda_{\mathbf{k}})^2} \delta n_{\mathbf{k}} \right] v^i_{\mathbf{k}} v^j_{\mathbf{k}} \; v^2_{\mathbf{k}} \cos^2(\phi_k - \phi_q) \tag{C.13b}$$

$$x_S^{00} = 4 v_S^2 \int_{\mathbf{k}} \frac{\Delta^2}{\lambda^2_{\mathbf{k}}} \frac{\lambda_{\mathbf{k}}}{\omega_0^2 - (2\lambda_{\mathbf{k}})^2} \delta n_{\mathbf{k}} \tag{C.13c}$$

$$x_S^{01} = -2 v_S^2 \omega_0 \int_{\mathbf{k}} \frac{\Delta^2}{\lambda^2_{\mathbf{k}}} \frac{\lambda_{\mathbf{k}}}{\left[\omega_0^2 - (2\lambda_{\mathbf{k}})^2\right]^2} \delta n_{\mathbf{k}} \tag{C.13d}$$

$$x_S^{10}(\phi_q) = \omega_0 v_S^3 \int_{\mathbf{k}} \frac{\Delta^2}{\lambda^2_{\mathbf{k}}} \left[\frac{8\lambda_{\mathbf{k}}}{\left[\omega_0^2 - (2\lambda_{\mathbf{k}})^2\right]^2} \delta n_{\mathbf{k}} - \frac{1}{\omega_0^2 - (2\lambda_{\mathbf{k}})^2} N'_{\mathbf{k}} \right] \cos\phi_q \tag{C.13e}$$

$$x_S^{11}(\phi_q) = -v_S^3 \int_{\mathbf{k}} \frac{\Delta^2}{\lambda^2_{\mathbf{k}}} \left[8\lambda_{\mathbf{k}} \frac{3\omega_0^2 + (2\lambda_{\mathbf{k}})^2}{\left[\omega_0^2 - (2\lambda_{\mathbf{k}})^2\right]^3} \delta n_{\mathbf{k}} - \frac{\omega_0^2 + (2\lambda_{\mathbf{k}})^2}{\left[\omega_0^2 - (2\lambda_{\mathbf{k}})^2\right]^2} N'_{\mathbf{k}} \right] \cos\phi_q \tag{C.13f}$$

$$x_S^{20}(\phi_q) = \frac{v_S^2}{2} \int_{\mathbf{k}} \frac{\Delta^2}{\lambda^2_{\mathbf{k}}} v^2_{\mathbf{k}} \cos^2(\phi_k - \phi_q) \tag{C.13g}$$

$$\times \left[\frac{\Delta^2}{\lambda^3_{\mathbf{k}}} \frac{\omega_0^2 + (2\lambda_{\mathbf{k}})^2}{\left[\omega_0^2 - (2\lambda_{\mathbf{k}})^2\right]^2} \delta n_{\mathbf{k}} - \left(\frac{\Delta}{\lambda_{\mathbf{k}}} \right)^2 \frac{N'_{\mathbf{k}}}{\omega_0^2 - (2\lambda_{\mathbf{k}})^2} + \left(\frac{\xi^S_{\mathbf{k}}}{\lambda_{\mathbf{k}}} \right)^2 \frac{\lambda_{\mathbf{k}}}{\omega_0^2 - (2\lambda_{\mathbf{k}})^2} \delta n''_{\mathbf{k}} \right] \tag{C.13h}$$

$$x^{10,i}_{SPs}(\phi_q) = -\frac{v_S}{\omega_0}\int_{\mathbf{k}}\left(\frac{\xi^S_{\mathbf{k}}}{\lambda_{\mathbf{k}}}\right)^2 N'_{\mathbf{k}} v^i_{\mathbf{k}}\; v_{\mathbf{k}}\,\cos(\phi_k-\phi_q) \tag{C.13i}$$

$$x^{11,i}_{SPs}(\phi_q) = v_S\int_{\mathbf{k}}\left(\frac{\xi^S_{\mathbf{k}}}{\lambda_{\mathbf{k}}}\right)^2 \frac{1}{\omega_0^2} N'_{\mathbf{k}} v^i_{\mathbf{k}}\; v_{\mathbf{k}}\,\cos(\phi_k-\phi_q) \tag{C.13j}$$

$$x^{20,i}_{SPs}(\phi_q) = -v_S\int_{\mathbf{k}}\left(\frac{\xi^S_{\mathbf{k}}}{\lambda_{\mathbf{k}}}\right)^2 \frac{2}{\omega_0^2} N'_{\mathbf{k}} v^i_{\mathbf{k}}\, v_{\mathbf{k}}\,\cos(\phi_k-\phi_q)\cos\phi_q \tag{C.13k}$$

$$x^{10,i}_{SPa}(\phi_q) = \frac{v_S}{\omega_0}\int_{\mathbf{k}}\frac{\Delta^2}{\lambda^3_{\mathbf{k}}}\frac{\omega_0^2}{\omega_0^2-(2\lambda_{\mathbf{k}})^2}\delta n_{\mathbf{k}}\; v^i_{\mathbf{k}}\; v_{\mathbf{k}}\,\cos(\phi_k-\phi_q) \tag{C.13l}$$

$$x^{11,i}_{SPa}(\phi_q) = -v_S\int_{\mathbf{k}}\frac{\Delta^2}{\lambda^3_{\mathbf{k}}}\frac{\omega_0^2+(2\lambda_{\mathbf{k}})^2}{\left[\omega_0^2-(2\lambda_{\mathbf{k}})^2\right]^2}\delta n_{\mathbf{k}}\; v^i_{\mathbf{k}}\; v_{\mathbf{k}}\,\cos(\phi_k-\phi_q) \tag{C.13m}$$

$$x^{20,i}_{SPa}(\phi_q) = v_S\int_{\mathbf{k}}\frac{\Delta^2}{\lambda^3_{\mathbf{k}}}\left[\frac{\omega_0^2+(2\lambda_{\mathbf{k}})^2}{\left[\omega_0^2-(2\lambda_{\mathbf{k}})^2\right]^2}\delta n_{\mathbf{k}} - \frac{\lambda_{\mathbf{k}}}{\omega_0^2-(2\lambda_{\mathbf{k}})^2}N'_{\mathbf{k}}\right] v^i_{\mathbf{k}}\, v_{\mathbf{k}}\,\cos(\phi_k-\phi_q)\cos\phi_q \tag{C.13n}$$

In these expressions we have used the shorthand notation $\delta n_{\mathbf{k}} = n_F(E^-_{\mathbf{k}}) - n_F(E^+_{\mathbf{k}})$, $\delta n''_{\mathbf{k}} = n''_F(E^-_{\mathbf{k}}) - n''_F(E^+_{\mathbf{k}})$ and $N'_{\mathbf{k}} = n'_F(E^+_{\mathbf{k}}) + n'_F(E^-_{\mathbf{k}})$, where $n'_F(E) = \partial n_F(\epsilon)/\partial\epsilon|_{\epsilon=E}$. Because of the angular dependence inside the Fermi functions due to the Doppler shift in the energy, even the simplest of these coefficients cannot be evaluated analytically. After numerical evaluation and comparing the size of the terms in the expression for Π^{ij}_q, it so happens that only a single one of these terms is large enough to be of any importance–the constant x^{00}_S term in Eq. (C.13c), which affects just the component of $\mathbf{A}_q$ parallel to the supercurrent. This contribution to the photon action is then

$$S_\Pi = \frac{1}{2}\sum_q x^{00}_S A^\parallel_{-q} A^\parallel_q = \frac{1}{2}\sum_{q,\alpha,\beta} x^{00}_S \epsilon^\parallel_{\alpha,-\mathbf{q}}\epsilon^\parallel_{\beta,\mathbf{q}} A_{\alpha,-q}A_{\beta,q}. \tag{C.14}$$

We now change to the mode basis using the transformation defined with the empty cavity part of the action, $A_{\alpha,q} = (a_{\alpha,q} + \bar{a}_{\alpha,-q})/\sqrt{2\omega_q}$. After the usual

approximation of discarding counterrotating terms ($\bar{a}\bar{a}$ and aa) the result is

$$S_A \to S_a = \sum_{q,\alpha,\beta} \bar{a}_{\alpha,q} \left[-i\Omega_m \delta_{\alpha\beta} + \omega_{\mathbf{q}} \delta_{\alpha\beta} + x_S^{00} \frac{\epsilon^{\parallel}_{\alpha,-\mathbf{q}} \epsilon^{\parallel}_{\beta,\mathbf{q}}}{2\omega_{\mathbf{q}}} \right] a_{\beta,q}. \tag{C.15}$$

The last two terms comprise the effective photonic Hamiltonian in the polarization basis. In our approximations the transformation between modes and Cartesian components induced by the polarization vectors is unitary up to an overall constant factor, so changing back from the polarization basis to the basis defined relative to the supercurrent direction diagonalizes the Hamiltonian,

$$S_a = \sum_q \left(\bar{a}^{\parallel}_q, \bar{a}^{\perp}_q \right) \left[-i\Omega_m \hat{\mathbb{1}} + \begin{pmatrix} \omega_{\mathbf{q}} + \Pi^S_{\mathbf{q}} & 0 \\ 0 & \omega_{\mathbf{q}} \end{pmatrix} \right] \begin{pmatrix} a^{\parallel}_q \\ a^{\perp}_q \end{pmatrix}, \tag{C.16}$$

where we define the only remaining part of the photon self-energy $\Pi^S_{\mathbf{q}} = x_S^{00}/(L\,\omega_{\mathbf{q}})$.

C.0.3 Coupling Term

Finally we consider the coupling term in the action. We replace $A_{\alpha,q}$ and d_q with their definitions in terms of the mode operators $a_{\alpha,q}$ and b_q and then perform the same transformation as above, from the polarization basis back to the Cartesian supercurrent basis. We then perform an analytic continuation $i\Omega_m \to \omega + i0$ and expand around the BS frequency to lowest order (i.e. we set $\omega = \Omega_{\mathrm{BS}}$), since that is the frequency at which the BS mode and photon bands would cross and therefore where the hybridization is most important. The imaginary part of the coupling term resulting from the infinitesimal shift off the real axis identically vanishes. The result is

$$S_{d-A} \to S_{b-a} = v_S \Delta \sum_q \int_{\mathbf{k}} \sqrt{\frac{2\,\Omega_{\mathrm{BS}}}{L\,K\omega_{\mathbf{q}}}} \frac{f_d(\phi_{\mathbf{q}})}{\lambda_{\mathbf{k}}} \frac{\delta n_{\mathbf{k}}}{\Omega^2_{\mathrm{BS}} - (2\,\lambda_{\mathbf{k}})^2} \left(\bar{b}_q a^{\parallel}_q + \bar{a}^{\parallel}_q b_q \right), \tag{C.17}$$

from which we then extract the coupling matrix element $g_{\mathbf{q}}$ as in the main text. Altogether this gives the effective Hamiltonian for the coupled cavity photon-superconductor system,

$$\check{H}^{\text{eff}}_{\mathbf{q}} = \begin{pmatrix} \Omega_{\text{BS}} & g_{\mathbf{q}} & 0 \\ g_{\mathbf{q}} & \omega_{\mathbf{q}} + \Pi^S_{\mathbf{q}} & 0 \\ 0 & 0 & \omega_{\mathbf{q}} \end{pmatrix}. \tag{C.18}$$

We see that this 3×3 Hamiltonian decouples into a 2×2 block and a single state. The block describes the hybridization of the BS mode with one photon mode, and the remaining state is the decoupled "dark" photon with the empty cavity dispersion $\omega_{\mathbf{q}}$, which is unseen by the BS mode and is unaffected by the superconductor within our approximations. Since all 2×2 matrices can be trivially diagonalized, the polariton dispersion in this Hamiltonian picture can immediately be written

$$E^{(\pm)}_q = \frac{\Omega_{\text{BS}} + \omega_{\mathbf{q}} + \Pi^S_{\mathbf{q}}}{2} \pm \sqrt{\left(\frac{\Omega_{\text{BS}} - \left(\omega_{\mathbf{q}} + \Pi^S_{\mathbf{q}}\right)}{2}\right)^2 + g^2_{\mathbf{q}}}. \tag{C.19}$$

These energies have corresponding eigenstates defined through

$$\check{H}^{\text{eff}}_{\mathbf{q}} \left|E^{(\pm)}_{\mathbf{q}}\right\rangle = E^{(\pm)}_{\mathbf{q}} \left|E^{(\pm)}_{\mathbf{q}}\right\rangle, \tag{C.20}$$

which each have nontrivial overlap with both the uncoupled photon and BS states.

Appendix D: Methods for Numerical Solution

Here we detail how the direct numerical evaluation of the dispersion relation was implemented. This was used to verify that the results of the analytic model are faithful to the exact solutions determined by the poles of the bosonic Green's function.

The numerical method begins again with the effective Gaussian Matsubara action describing the coupled Bardasis-Schrieffer cavity-photon system. Schematically this is

$$S = -\frac{1}{2}\sum_{q}\begin{pmatrix} d_{-q} & \mathbf{A}_{-q}\end{pmatrix}\begin{pmatrix} D_{\mathrm{BS}}(q)^{-1} & \mathbf{g}(i\Omega_m) \\ \mathbf{g}(-i\Omega_m) & \hat{D}^{-1}_{\mathrm{phot}}\end{pmatrix}\begin{pmatrix} d_q \\ \mathbf{A}_q\end{pmatrix}, \tag{D.1}$$

where the cavity propagator $\hat{D}^{-1}_{phot} = \hat{D}^{-1}_0 - \hat{\Pi}$ includes the self energy due to the superconductor. At this stage the polariton modes can be found by solving for the frequency $z = i\Omega_m$ at which the inverse of the Green's function matrix vanishes. To do so, we numerically solve for the roots of the determinant of the inverse Green's function $\det \hat{D}^{-1}(\Omega_{\mathbf{q}i}, \mathbf{q}) = 0$. In particular the following algorithm was employed at each $\mathbf{q}$: noting that there are three roots that we are searching for

1. An interval $[\omega_l, \omega_u]$ is chosen within which to search for solutions.

2. An extremum f of $\det \hat{D}^{-1}(\Omega, \mathbf{q})$ with respect to Ω is located by finding the roots of the first derivative with respect to Ω using the Newton-Raphson method in the vicinity of the Bardasis-Schrieffer frequency Ω_{BS}.

3. The other extremum is found by searching for the root of the first derivative in the interval (ω_l, f) or (f, ω_u) as determined by the sign of the function at the endpoints. This gives us two extrema $\{f_0, f_1\}$.

4. Roots of $\det \hat{D}^{-1}(\Omega, \mathbf{q})$ are searched for using the Brent-Dekker method in the

intervals (ω_l, f_0), (f_0, f_1), and (f_1, ω_u)

Comparing the results of this procedure with the energies given in Eq. (C.19), we find that the two methods are in excellent agreement, as can be seen in the first figure of the main text.

Numerical integration and root-finding were performed using the GSL Scientific Library[200].

Appendix E: Norm of Complex Modes

Here we demonstrate that for the homogeneous system the complex momentum modes have negative norm. We begin with the unitless BdG equation

$$\left[(1+\frac{1}{2}z^2)\tau^3 + i\tau^2 + \beta z - \lambda\right] w = 0. \tag{E.1}$$

There are four roots to the characteristic equation, $z_{\pm p}$ which are the two positive norm roots, and $z_{\pm n}$ which are either negative norm and real or complex conjugate pairs. The corresponding spinors are

$$w_\nu = \frac{1}{\sqrt{|1-|h_\nu|^2|}} \begin{pmatrix} 1 \\ h_\nu \end{pmatrix} \tag{E.2}$$

where $h_\nu = \lambda - \beta z - (1+\frac{1}{2}z^2)$, as is the case for the real-momentum modes. These modes have negative norm whenever

$$|h_\nu|^2 > 1 \Rightarrow |\lambda - \beta z_\nu - (1+\frac{1}{2}z_\nu^2)|^2 > 1. \tag{E.3}$$

If we relax the constraint that $z = z_\nu$, one of the roots, we can study the regions defined by this inequality in the complex z plane, for fixed values of $\beta > 0, \lambda > 0$. We can then determine, for this β, λ, what z_ν is and see which region of the complex plane it falls in. This is depicted in Fig. E.1, for a number of different parameter values.

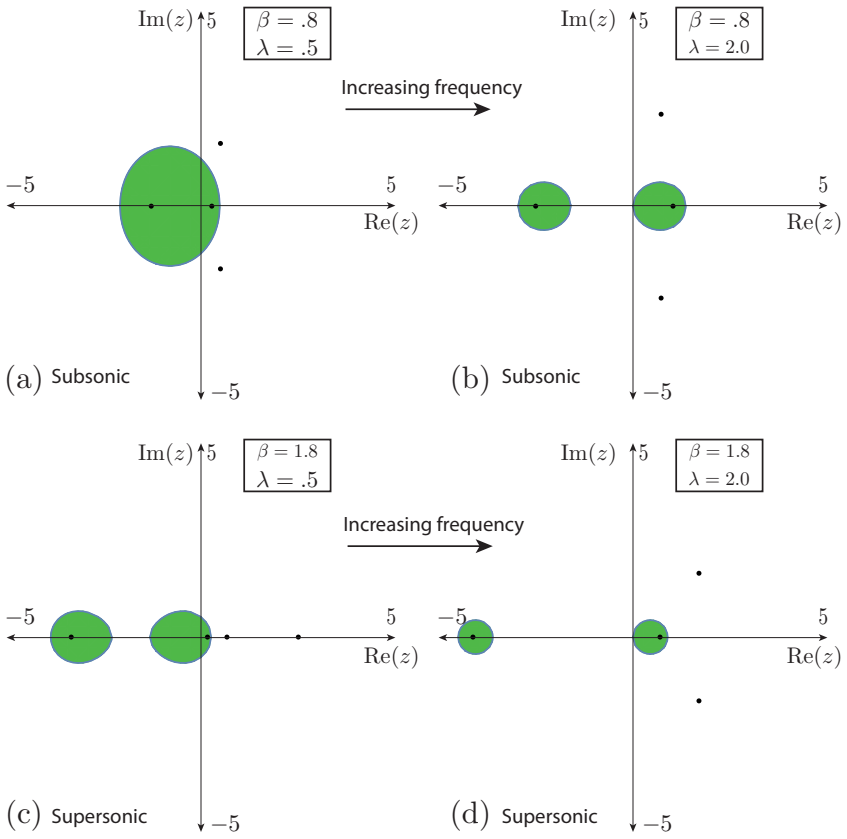

Figure E.1: Regions in the complex z (momentum) plane where the spinor has positive norm are colored green. Figures (a), (b) are for a subsonic flow at low and high frequencies, respectively. Figures (c), (d) are for a supersonic flow at low and high frequencies. Each of the four roots for the given β, λ are shown in the complex plane. Two are real and always fall in the green region (the $\pm p$ roots) while two always fall outside (the $\pm n$ roots). When the $\pm n$ momenta are not real, this shows that they still have negative norm.

Appendix F: Current and Group Velocity

Here we show that for a scattering mode the group velocity and current are equivalent. We first consider a momentum eigenmode,

$$W_{\mathbf{k}}(\mathbf{r}) = e^{i\mathbf{k}\cdot\mathbf{r}}\frac{w_{\mathbf{k}}}{\sqrt{\rho}}$$

which obeys the momentum space BdG equation

$$\left(\tau^3\left(\frac{\mathbf{k}^2}{2m}+mc^2\right)+i\tau^2mc^2+\mathbf{v}\cdot\mathbf{k}-\omega\right)w_{\mathbf{k}}=0.$$

We differentiate with respect to the wave-vector to get

$$\left(\tau^3\frac{\mathbf{k}}{m}+\mathbf{v}-\frac{\partial\omega}{\partial\mathbf{k}}\right)w_{\mathbf{k}}+\left(\tau^3\left(\frac{\mathbf{k}^2}{2m}+mc^2\right)+i\tau^2mc^2+\mathbf{v}\cdot\mathbf{k}-\omega\right)\frac{\partial w_{\mathbf{k}}}{\partial\mathbf{k}}=0. \quad \text{(F.1)}$$

We now apply $w_{\mathbf{k}}^\dagger\tau^3$ from the left and use the Hermiticity of the BdG Hamiltonian with respect to the τ^3 inner-product to eliminate the term involving $\frac{\partial w}{\partial\mathbf{k}}$. This then produces the result

$$w_{\mathbf{k}}^\dagger\tau^3w_{\mathbf{k}}\frac{\partial\omega}{\partial\mathbf{k}}=w_{\mathbf{k}}^\dagger\left[\mathbf{v}\tau^3+\frac{\mathbf{k}}{m}\right]w_{\mathbf{k}}, \quad \text{(F.2)}$$

which is the desired relation between group-velocity (LHS), and norm current (RHS). This also will potentially generalize the concept of group velocity to the evanescent modes, which still have a well-defined norm current.

Appendix G: Calculating the fluctuation Lagrangian

In this section, we put all of the algebra and Lagrangian manipulation that we left out of Section 5.2.

Our starting point is Eq. (5.1) upon substituting $\Psi = \Psi_0 + \delta\Psi$ where Ψ_0 solves the Euler-Lagrange equations Eq. (5.3) and $\delta\Psi$ can be written in terms of broken generators and massive fields Eq. (5.7).

Most of the simplifying algebra comes from $g(\hat{\sigma}\Psi, \xi) = 0$ and integration-by-parts. To facilitate the integration by parts, all equalities are be understood to be *up to a full derivative*. Furthermore, by construction the linear terms cancel, so we keep second-order terms only, indicated by $\overset{\text{fluc}}{=}$.

To deal with the term linear in derivatives, we use the object

$$f\overleftrightarrow{\partial_t}g \equiv f(\partial_t g) - (\partial_t f)g, \tag{G.1}$$

and for simplicity we sometimes replace $\partial_t f$ with $\dot{f}$ for time derivatives. We further take advantage of the Einstein summation convention (sum over indices is implied) for simplicity. The first term we investigate is

$$\begin{aligned}\tfrac{i}{2}\Psi^\dagger\overleftrightarrow{\partial_t}\Psi \overset{\text{fluc}}{=} -\tfrac{i}{2}\Psi_0^\dagger(\hat{\sigma}\overleftrightarrow{\partial_t}\hat{\sigma})\Psi_0 \\ + i(-\Psi_0^\dagger\hat{\sigma}\dot{\xi} + \xi^\dagger\dot{\hat{\sigma}}\Psi_0 + \xi^\dagger\hat{\sigma}\dot{\Psi}_0) \\ - \tfrac{i}{2}\Psi_0^\dagger\hat{\sigma}^2\dot{\Psi}_0 + \tfrac{i}{2}\dot{\Psi}_0^\dagger\hat{\sigma}^2\Psi_0.\end{aligned} \tag{G.2}$$

Performing integration-by-parts on the $\Psi_0^\dagger \hat{\sigma}\dot{\xi}$ term, we get

$$\begin{aligned}\tfrac{i}{2}\Psi^\dagger \overleftrightarrow{\partial_t}\Psi \overset{\text{fluc}}{=} -\tfrac{i}{2}\Psi_0^\dagger(\hat{\sigma}\overleftrightarrow{\partial_t}\hat{\sigma})\Psi_0 + i(\Psi_0^\dagger\dot{\hat{\sigma}}\xi + \xi^\dagger\dot{\hat{\sigma}}\Psi_0) \\ + i\dot{\Psi}_0^\dagger(\tfrac{1}{2}\hat{\sigma}^2\Psi_0 + \hat{\sigma}\xi) - i(\tfrac{1}{2}\Psi_0^\dagger\hat{\sigma}^2 - \xi^\dagger\hat{\sigma})\dot{\Psi}_0. \quad \text{(G.3)}\end{aligned}$$

The kinetic energy term takes the form

$$\begin{aligned}\partial_j\Psi^\dagger\partial_j\Psi \overset{\text{fluc}}{=} -\tfrac{1}{2}\partial_j\Psi_0^\dagger\hat{\sigma}^2\partial_j\Psi_0 - \partial_j\Psi_0^\dagger\hat{\sigma}\partial_j\hat{\sigma}\Psi_0 - \partial_j\Psi_0^\dagger\hat{\sigma}\partial_j\xi \\ - \tfrac{1}{2}\partial_j\Psi_0^\dagger\hat{\sigma}^2\partial_j\Psi_0 - \Psi_0^\dagger(\partial_j\hat{\sigma})\hat{\sigma}\partial_j\Psi_0 + \partial_j\xi^\dagger\hat{\sigma}\partial_j\Psi_0 \\ - \Psi_0^\dagger\partial_j\hat{\sigma}\partial_j\hat{\sigma}\Psi_0 + \partial_j\xi^\dagger\partial_j\xi - \Psi_0^\dagger\partial_j\hat{\sigma}\partial_j\xi + \partial_j\xi^\dagger\partial_j\hat{\sigma}\Psi_0. \quad \text{(G.4)}\end{aligned}$$

We perform integration by parts on the two instances of $-\frac{1}{2}\partial_j\Psi_0^\dagger\hat{\sigma}^2\partial_j\Psi_0$ above in opposite ways to obtain

$$\begin{aligned}\partial_j\Psi^\dagger\partial_j\Psi \overset{\text{fluc}}{=} \tfrac{1}{2}\nabla^2\Psi_0^\dagger\hat{\sigma}^2\Psi_0 - \tfrac{1}{2}\partial_j\Psi_0^\dagger\hat{\sigma}\partial_j\hat{\sigma}\Psi_0 + \tfrac{1}{2}\partial_j\Psi_0^\dagger(\partial_j\hat{\sigma})\hat{\sigma}\Psi_0 + \tfrac{1}{2}\Psi_0^\dagger\hat{\sigma}^2\nabla^2\Psi_0 \\ - \tfrac{1}{2}\Psi_0^\dagger(\partial_j\hat{\sigma})\hat{\sigma}\partial_j\Psi_0 + \tfrac{1}{2}\Psi_0^\dagger\hat{\sigma}(\partial_j\hat{\sigma})\partial_j\Psi_0 \\ - \partial_j\Psi_0^\dagger\hat{\sigma}\partial_j\xi + \partial_j\xi^\dagger\hat{\sigma}\partial_j\Psi_0 - \Psi_0^\dagger\partial_j\hat{\sigma}\partial_j\hat{\sigma}\Psi_0 + \partial_j\xi^\dagger\partial_j\xi - \Psi_0^\dagger\partial_j\hat{\sigma}\partial_j\xi + \partial_j\xi^\dagger\partial_j\hat{\sigma}\Psi_0. \quad \text{(G.5)}\end{aligned}$$

If we further use integration by parts on $-\partial_j\Psi_0^\dagger\hat{\sigma}\partial_j\xi$ and $\partial_j\xi^\dagger\hat{\sigma}\partial_j\Psi_0$, we obtain (after some reordering)

$$\begin{aligned}\partial_j\Psi^\dagger\partial_j\Psi \overset{\text{fluc}}{=} -\Psi_0^\dagger\partial_j\hat{\sigma}\partial_j\hat{\sigma}\Psi_0 - \tfrac{1}{2}\partial_j\Psi_0^\dagger\hat{\sigma}\partial_j\hat{\sigma}\Psi_0 + \tfrac{1}{2}\partial_j\Psi_0^\dagger(\partial_j\hat{\sigma})\hat{\sigma}\Psi_0 \\ - \tfrac{1}{2}\Psi_0^\dagger(\partial_j\hat{\sigma})\hat{\sigma}\partial_j\Psi_0 + \tfrac{1}{2}\Psi_0^\dagger\hat{\sigma}(\partial_j\hat{\sigma})\partial_j\Psi_0 \\ + \partial_j\xi^\dagger\partial_j\xi + \partial_j\Psi_0^\dagger\partial_j\hat{\sigma}\xi - \xi^\dagger\partial_j\hat{\sigma}\partial_j\Psi_0 - \Psi_0^\dagger\partial_j\hat{\sigma}\partial_j\xi + \partial_j\xi^\dagger\partial_j\hat{\sigma}\Psi_0 \\ + \nabla^2\Psi_0^\dagger(\tfrac{1}{2}\hat{\sigma}^2\Psi_0 + \hat{\sigma}\xi) + (\tfrac{1}{2}\Psi_0^\dagger\hat{\sigma}^2 - \hat{\sigma}\xi)\nabla^2\Psi_0. \quad \text{(G.6)}\end{aligned}$$

We observe that, along with Eq. (5.11), the equation of motion cancels the last lines in Eqs. (G.3) and (G.6) with the first line of Eq. (5.11).

All together, we can combine these equations to get the full fluctuation Lagrangian

$$\begin{aligned}\mathcal{L} \overset{\text{fluc}}{=} &-\tfrac{i}{2}\Psi_0^\dagger(\hat{\sigma}\overleftrightarrow{\partial_t}\hat{\sigma})\Psi_0 + i(\Psi_0^\dagger\dot{\hat{\sigma}}\xi + \xi^\dagger\dot{\hat{\sigma}}\Psi_0) - \tfrac{1}{2}\partial_j\Psi_0^\dagger\hat{\sigma}\partial_j\hat{\sigma}\Psi_0 + \tfrac{1}{2}\partial_j\Psi_0^\dagger(\partial_j\hat{\sigma})\hat{\sigma}\Psi_0 \\ &- \tfrac{1}{2}\Psi_0^\dagger(\partial_j\hat{\sigma})\hat{\sigma}\partial_j\Psi_0 + \tfrac{1}{2}\Psi_0^\dagger\hat{\sigma}(\partial_j\hat{\sigma})\partial_j\Psi_0 \\ &+\partial_j\xi^\dagger\partial_j\xi + \partial_j\Psi_0^\dagger\partial_j\hat{\sigma}\xi - \xi^\dagger\partial_j\hat{\sigma}\partial_j\Psi_0 - \Psi_0^\dagger\partial_j\hat{\sigma}\partial_j\xi + \partial_j\xi^\dagger\partial_j\hat{\sigma}\Psi_0 - \Psi_0^\dagger\partial_j\hat{\sigma}\partial_j\hat{\sigma}\Psi_0 + \partial_j\xi^\dagger\partial_j\xi \\ &- \frac{1}{2}\xi_a^*\left.\frac{\partial^2 V}{\partial\Psi_a^\dagger\partial\Psi_b^\dagger}\right|_0\xi_b^* - \xi_a^*\left.\frac{\partial^2 V}{\partial\Psi_a^\dagger\partial\Psi_b}\right|_0\xi_b - \frac{1}{2}\xi_a\left.\frac{\partial^2 V}{\partial\Psi_a\partial\Psi_b}\right|_0\xi_b. \end{aligned} \tag{G.7}$$

We can now expand our fluctuations in terms of their fields $\hat{\sigma}\Psi_0 = \theta_n\sigma_n\Psi_0$ and $\xi = \beta_n\xi_n$, and we obtain

$$\begin{aligned}\mathcal{L} \overset{\text{fluc}}{=} &-\tfrac{i}{2}\Psi_0^\dagger[\sigma_m,\sigma_n]\Psi_0\theta_m\partial_t\theta_n + \tfrac{1}{4m}\theta_m\partial_j\theta_n(\partial_j\Psi_0^\dagger[\sigma_m,\sigma_n]\Psi_0 - \Psi_0^\dagger[\sigma_m,\sigma_n]\partial_j\Psi_0) \\ &+i\beta_n\partial_t\theta_n(\Psi_0^\dagger\sigma_m\xi_n + \xi_n^\dagger\sigma_m\Psi_0) + \tfrac{1}{2m}\beta_m\partial_j\theta_n(\xi_m^\dagger\sigma_n\partial_j\Psi_0 - \partial_j\Psi_0^\dagger\sigma_n\xi_m + \Psi_0^\dagger\sigma_n\partial_j\xi_m - \partial_j\xi_m^\dagger\sigma_n\Psi_0) \\ &+ \tfrac{1}{2m}\Psi_0^\dagger\sigma_n\sigma_m\Psi_0\partial_j\theta_n\partial_j\theta_m \\ &+\tfrac{i}{2}\beta_m\partial_t\beta_n(\xi_m^\dagger\xi_m - \xi_n^\dagger\xi_m) + \tfrac{i}{2}\beta_n\beta_m(\xi_m^\dagger\partial_t\xi_n - \partial_t\xi_m^\dagger\xi_n) + \beta_m\partial_j\beta_n(\xi_n^\dagger\partial_j\xi_m + \partial_j\xi_m^\dagger\xi_n) \\ &-\tfrac{1}{2m}\xi_n^\dagger\xi_m\partial_j\beta_m\partial_j\beta_n - \tfrac{1}{2}\beta_n\beta_m\left[\xi_n^\dagger\left.\frac{\partial^2 V}{\partial\Psi^\dagger\partial\Psi^\dagger}\right|_0\xi_m^* + \xi_n^T\left.\frac{\partial^2 V}{\partial\Psi\partial\Psi}\right|_0\xi_m + 2\xi_m^\dagger\left.\frac{\partial^2 V}{\partial\Psi^\dagger\partial\Psi}\right|_0\xi_n\right]. \end{aligned} \tag{G.8}$$

The first three lines of Eq. (G.8) lead to the Lagrangian presented in the text Eq. (5.12) while the last two lines represent the massive modes neglected in the main text.

One can then easily check that once the full Lagrangian in Eq. (5.34) is derived that the massive modes conjugate to Goldstone modes no longer have the term that goes as $\beta_m\partial_\mu\beta_n$, only keeping the kinetic term and mass matrix (which we

diagonalize to find the type-I basis states).

Appendix H: Bogoliubov Theory for Hawking Emission

As per Eq. (5.59), the magnon field (written in terms of the complexified spinor $\Phi_3(x) = (\zeta, \zeta^*)^T$) obeys the BdG equation

$$\left[i\tau_3 \hat{D}_t + \frac{1}{2m\rho} \nabla \cdot \rho \nabla - g_3 \rho \left(\tau_0 + \tau_1 \right) \right] \Phi_3(x) = 0, \tag{H.1}$$

written in terms of the co-moving frame material derivative $\hat{D}_t = \partial_t + \mathbf{v}_s \cdot \nabla$.

Before proceeding, there are two properties of this equation that prove useful. First is the charge conjugation symmetry: if Υ solves Eq. (H.1), then so does

$$\overline{\Upsilon} \equiv \tau_1 \Upsilon^*. \tag{H.2}$$

In particular, this is important since the Nambu spinor should obey the self-conjugate property that $\Phi_3 = (\zeta, \zeta^*)^T = \overline{\Phi}_3$. Thus, it is important that this is respected by the equations of motion, which we see it is.

Furthermore, provided the density $\rho(x)$ is time independent, we can define the conserved pseudo-scalar product on the solution space

$$(\Upsilon_1, \Upsilon_2) \equiv \int d^d r \, \rho(\mathbf{r}) \Upsilon_1^\dagger(\mathbf{r}) \tau_3 \Upsilon_2(\mathbf{r}). \tag{H.3}$$

This scalar product has a number of useful features including that the charge conjugation operation changes the sign, so that

$$(\overline{\Upsilon}_1, \overline{\Upsilon}_2) = -(\Upsilon_2, \Upsilon_1). \tag{H.4}$$

We use this pseudo-inner product to define a notion of norm for solutions. Because of the τ_3, this is not the usual $L_2(\mathbb{R}^d)$ norm, and in fact is not a norm at all since it

is not positive semi-definite. There are non-trivial negative norm states which we loosely refer to as "hole-like" states, in contrast to the "particle-like" solutions with positive norm. As remarked earlier, hole-like solutions can be related to particle-like solutions by charge conjugation since if Υ has negative norm we find

$$(\Upsilon, \Upsilon) < 0 \Rightarrow (\overline{\Upsilon}, \overline{\Upsilon}) > 0.$$

To proceed further, we utilize the (assumed) time-independence of the kernel to further separate the solution $\Upsilon(x) = \Upsilon(\mathbf{r}, t)$ into energy eigenmodes

$$\Upsilon(x) = \int \frac{d\omega}{2\pi} W_\omega(\mathbf{r}) e^{-i\omega t}, \tag{H.5}$$

where $W_\omega(\mathbf{r}) = [U_\omega(\mathbf{r}), V_\omega(\mathbf{r})]^T$ is a two-component spinor which obeys the eigenvalue problem

$$\left[\omega + i\mathbf{v}_s \cdot \nabla + \frac{1}{2m\rho}\nabla \cdot \rho\nabla\tau_3 - g_3\rho\left(\tau_3 + i\tau_2\right)\right] W_\omega(\mathbf{r}) = 0. \tag{H.6}$$

We refer to [129, 141] for more details of solving this system. What is important for our discussion are the details of the dispersion relation, which are used to analyze the asymptotic scattering states at spatial infinity.

We now focus on the case of a one-dimensional homogeneous flow. In this case both the momentum k and lab-frame frequency ω are good quantum numbers and obey the standard Bogoliubov dispersion relation (using that $mc^2 = g_3\rho$) of

$$\omega = v_s k \pm \sqrt{c^2k^2 + \left(\frac{k^2}{2m}\right)^2} \equiv \omega_\pm(k), \tag{H.7}$$

where the last equality is used to define the lab frequency $\omega_\pm(k)$. At a particular frequency $\omega > 0$, we may determine which scattering states are available by finding

the real momenta k which obey $\omega = \omega_{\pm}(k)$.

Considering a step-like variation in the flow, the flow profile is as given in Eq. (5.62). For $x < 0$ and $x > 0$ the solutions to the BdG equations are still plane-waves which obey the Bogoliubov dispersion relation, albeit with different parameters ρ and v. These two dispersion relations are shown Figs. 5.3 and 5.4 for fixed values of the condensate velocities $|v_l| > |v_r|$ and densities ρ_l, ρ_r.

Instead of the lab frame, we may measure frequency with respect to the frame co-moving with the fluid flow. This is implemented by Doppler shifting to the (positive) comoving frequency

$$\Omega(k) \equiv \sqrt{c^2 k^2 + \tfrac{k^4}{4m^2}}, \tag{H.8}$$

so that $\omega_{\pm}(k) = vk \pm \Omega(k)$ (vk amounts to a Galilean boost).

For $|v| < c$ (right dispersion in Fig. 5.3), there are only two real-momenta at any positive frequency, which correspond to a right- and left-moving quasiparticle. For $|v| > c$ (left dispersion in Fig. 5.3) a new scattering channel opens whereby a wavepacket with negative free-fall frequency $[\omega_{-}(k)]$ may have positive lab-frame frequency ω.

We find the eigenfunctions for the step potential by employing matching equations at the step. These impose the continuity requirements

$$\begin{aligned} [W_\omega(x)]_{x=0^-}^{x=0^+} &= 0 \\ [\rho \partial_x W_\omega(x)]_{x=0^-}^{x=0^+} &= 0. \end{aligned} \tag{H.9}$$

Additionally, we choose them to satisfy $(W_\omega, \overline{W}_\omega) = 0$ and can be normalized such that $(W_\omega, W_\omega) > 0$ if $\omega = \omega_{+}(k)$ (positive comoving frequency) and $(W_\omega, W_\omega) < 0$ if $\omega = \omega_{-}(k)$ (negative comoving frequency).

Combining all of this, we can express the full solution in terms of positive-

frequency components only via

$$\Phi_3(x,t) = \int_0^\infty \frac{d\omega}{2\pi} \sum_\alpha \left[A(W_{\omega\alpha}) W_{\omega\alpha}(x) e^{-i\omega t} + A^*(W_{\omega\alpha}) \overline{W}_{\omega\alpha} e^{+i\omega t} \right], \tag{H.10}$$

where the $A(W_{\omega,\alpha})$ are the Fourier coefficients of the expansion and α is a set of quantum numbers which are used to label the different degenerate modes at each energy $\omega > 0$. At this point, we can second quantize the system and promote Υ to an operator. In such a case, the operator equation looks like

$$\hat{\Upsilon}(x,t) = \int_0^\infty \frac{d\omega}{2\pi} \sum_\alpha \left[a(W_{\omega\alpha}) W_{\omega\alpha}(x) e^{-i\omega t} + a^\dagger(W_{\omega\alpha}) \overline{W}_{\omega\alpha} e^{+i\omega t} \right], \tag{H.11}$$

where now $a(W_{\omega\alpha})$ are operators satisfying

$$[a(W_{\omega\alpha}), a^\dagger(W_{\omega'\alpha'})] = (W_{\omega\alpha}, W_{\omega',\alpha'}). \tag{H.12}$$

All $W_{\omega\alpha}$ are orthogonal with respect to this inner product, and so $a(W_{\omega\alpha})$ is either a creation *or* annihilation operator based on the sign of the norm.

The system may be exactly solved when the flow is homogeneous, in which case the momentum k is also a good quantum number. Assuming a solution of the form

$$W_\omega(x) = w_k e^{ikx}$$

produces the momentum space eigenvalue problem

$$\left[\omega - vk - \frac{1}{2m} k^2 \tau_3 - g_3 \rho \left(\tau_3 + i\tau_2 \right) \right] w_k = 0. \tag{H.13}$$

In principle, the momentum k depends in the energy ω, but we usually suppress this dependence for brevity.

To evaluate $(W_{\omega\alpha}, W_{\omega'\alpha'})$, we establish a couple of facts. If we let $w_k = [u_k, v_k]^T$,

then we have

$$mc^2 v_k = \left(\pm\Omega(k) - \frac{k^2}{2m} - mc^2 \right) u_k, \tag{H.14}$$

and hence

$$m^2c^4|v_k|^2 = \left\{ m^2c^4 \mp 2\Omega(k) \left[mc^2 + \frac{k^2}{2m} \mp \Omega(k) \right] \right\} |u_k|^2, \tag{H.15}$$

this relation between $|u_k|^2$ and $|v_k|^2$ allows us to evaluate

$$\begin{aligned}(W_{\omega\alpha}, W_{\omega'\alpha'}) &= \pm\Omega(k)\frac{2\rho}{m^2c^4}\left[mc^2 + \frac{k^2}{2m} \mp \Omega(k) \right] |u_k|^2 \delta_{\alpha\alpha'}\delta[k_\alpha(\omega) - k_{\alpha'}(\omega')] \\ &= \pm\Omega(k)\frac{2\rho|v_g|}{m^2c^4}\left[mc^2 + \frac{k^2}{2m} \mp \Omega(k) \right] |u_k|^2 \delta_{\alpha\alpha'}\delta(\omega - \omega').\end{aligned} \tag{H.16}$$

The term in brackets $mc^2 + \frac{k^2}{2m} - \Omega(k) > 0$, so the *sign* of the normalization depends exclusively on whether we have positive ($+\Omega(k)$) or negative ($-\Omega(k)$) comoving frequency. The terms with negative comoving frequency (or negative norm) are represented by the blue curves in Figs. 5.3 and 5.4.

We can now perform the Hawking calculation to determine the Bogoliubov transformation giving rise to excitation production. This is presented first in Fig. 5.3, where we consider a wavepacket moving away from the horizon to $+\infty$ and frequency ω, this is the Hawking mode. If we trace it back in time, it was related to a scattering process at the horizon itself, so in terms of three other positive frequency modes

$$W_{\rm H} = \alpha_R W_{R,1} + \alpha_L W_{L,2} + \beta_L \overline{W}_{L,1}, \tag{H.17}$$

where $W_{\rm H}$ includes the far propagating right-moving mode along with the evanescent near horizon solution, $W_{R,1}$ is the left-moving mode on the right, and $W_{L,(1,2)}$ are the right-moving modes on the left (counted left-to-right in Fig. 5.3). This immediately

gives us how to relate the creation operators of the out-vacuum to the in-vacuum

$$a(W_{\rm H}) = \alpha_R a(W_{R,1}) + \alpha_L a(W_{L,2}) + \beta_L a^\dagger(W_{L,1}). \tag{H.18}$$

This implies that for W_H at a particular frequency ω, we can find the number of Hawking modes leaving the horizon by considering the expectation value

$$\langle 0_{\rm in}|a(W_{\rm H})^\dagger a(W_{\rm H})|0_{\rm in}\rangle = |\beta_L|^2(W_{L,1}, W_{L,1}). \tag{H.19}$$

With the proper normalization and putting back in the dependence on frequency, the number of particles leaving the horizon at frequency ω is

$$N(\omega) = |\beta_L(\omega)|^2 \frac{(W_{L,1}(\omega), W_{L,1}(\omega))}{(W_H(\omega), W_H(\omega))}. \tag{H.20}$$

This same analysis can be done for the supersonic-to-supersonic case presented in Fig. 5.4. For lack of a better term, we call the region where there are multiple positive and negative norm channels the "super-Hawking" region. In this case, we have two modes in the Hawking process that need to be backwards scattered: one positive norm and the other negative norm. The result of the scattering process is

$$\begin{aligned} W_{\rm H} &= \beta_R \overline{W}_{R,1} + \alpha_R W_{R,2} + \beta_L \overline{W}_{L,1} + \alpha_L W_{L,2}, \\ \overline{W}_{\rm H'} &= \alpha'_R \overline{W}_{R,1} + \beta'_R W_{R,2} + \alpha'_L \overline{W}_{L,1} + \beta'_L W_{L,2}. \end{aligned} \tag{H.21}$$

These equations can be similarly related to a Bogoliubov transformation, and we can find the number of Hawking particles leaving the horizon at frequency ω by

considering

$$N(\omega) = |\beta_L(\omega)|^2 \frac{(W_{L,1}(\omega), W_{L,1}(\omega))}{(W_H(\omega), W_H(\omega))} + |\beta_R(\omega)|^2 \frac{(W_{R,1}(\omega), W_{R,1}(\omega))}{(W_H(\omega), W_H(\omega))} + |\beta'_L(\omega)|^2 \frac{(W_{L,2}(\omega), W_{L,2}(\omega))}{(W_{H'}(\omega), W_{H'}(\omega))} + |\beta'_R(\omega)|^2 \frac{(W_{R,2}(\omega), W_{R,2}(\omega))}{(W_{H'}(\omega), W_{H'}(\omega))}. \quad \text{(H.22)}$$

Despite there being more terms, there is generally less of a Hawking flux due to a decoupling of the negative and positive norm channels as we can see in Fig. 5.2.

Bibliography

[1] A. A. Abrikosov, L. P. Gorkov, and I. E. Dzyaloshinski, *Methods of Quantum Field Theory in Statistical Physics* (Dover Publications, New York, 1975).

[2] T. Holstein and H. Primakoff, "Field Dependence of the Intrinsic Domain Magnetization of a Ferromagnet", Phys. Rev. **58**, 1098 (1940).

[3] J. Bardeen, L. Cooper, and J. Schrieffer, "Theory of superconductivity", Phys. Rev. **108**, 1175–1204 (1957).

[4] N. Bogoliubov, "On a new method in the theory of superconductivity", Il Nuovo Cimento **7**, 794–805 (1958).

[5] J. Valatin, "Comments on the theory of superconductivity", Il Nuovo Cimento **7**, 843–857 (1958).

[6] P. W. Anderson, "Theory of dirty superconductors", J. Phys. Chem. Solids **11**, 26–30 (1959).

[7] Y. Nambu, "Quasi-particles and gauge invariance in the theory of superconductivity", Phys. Rev. **117**, 648–663 (1960).

[8] T. Hansson, V. Oganesyan, and S. Sondhi, "Superconductors are topologically ordered", Ann. of Phys. **313**, 497–538 (2004).

[9] P. W. Anderson, "Plasmons, Gauge Invariance, and Mass", Phys. Rev. **130**, 439–442 (1963).

[10] N. Byers and C. Yang, "Theoretical Considerations Concerning Quantized Magnetic Flux in Superconducting Cylinders", Phys. Rev. Lett. **7**, 46 (1961).

[11] D. Scalapino, S. White, and S. Zhang, "Insulator, metal, or superconductor: The criteria", Phys. Rev. B **47**, 7995 (1993).

[12] J. von Delft and D. Ralph, "Spectroscopy of discrete energy levels in ultrasmall metallic grains", Physics Reports **345**, 61–173 (2001).

[13] P. W. Anderson, "Random-Phase Approximation in the Theory of Superconductivity", Phys. Rev. **112**, 1900–1916 (1958).

[14] P. Morel and P. Anderson, "Calculation of the Superconducting State Parameters with Retarded Electron-Phonon Interaction", Phys. Rev. **125**, 1263 (1962).

[15] D. Scalapino, J. Schrieffer, and J. Wilkins, "Strong-Coupling Superconductivity. I", Phys. Rev. **148**, 263 (1966).

[16] A. Bardasis and J. R. Schrieffer, "Excitons and Plasmons in Superconductors", Phys. Rev. **121**, 1050–1062 (1961).

[17] W. G. Unruh, "Experimental Black-Hole Evaporation?", Phys. Rev. Lett. **46**, 1351–1353 (1981).

[18] L. J. Garay, J. R. Anglin, J. I. Cirac, and P. Zoller, "Sonic Analog of Gravitational Black Holes in Bose-Einstein Condensates", Phys. Rev. Lett. **85**, 4643–4647 (2000).

[19]L. J. Garay, J. R. Anglin, J. I. Cirac, and P. Zoller, "Sonic black holes in dilute Bose-Einstein condensates", Phys. Rev. A **63**, 023611 (2001).

[20]C. Barceló, S. Liberati, and M. Visser, "Analogue Gravity", Living Rev. Relativ. **14**, 3 (2011).

[21]M. Stone, "Acoustic energy and momentum in a moving medium", Phys. Rev. E **62**, 1341–1350 (2000).

[22]Keser, A.C. and Galitski, V., "Analogue stochastic gravity in strongly-interacting Bose–Einstein condensates", Ann. Phys. **395**, 84–111 (2018).

[23]J. Bekenstein, "Generalized second law of thermodynamics in black-hole physics", Phys. Rev. D **9**, 3292–3300 (1974).

[24]S. W. Hawking, "Black hole explosions?", Nature **248**, 30–31 (1974).

[25]S. Hawking, "Particle Creation by Black Holes", Commun. Math. Phys. **43**, 199–220 (1975).

[26]H. Watanabe and H. Murayama, "Unified Description of Nambu-Goldstone Bosons without Lorentz Invariance", Phys. Rev. Lett. **108**, 251602 (2012).

[27]Y. Hidaka, "Counting Rule for Nambu-Goldstone Modes in Nonrelativistic Systems", Phys. Rev. Lett. **110**, 091601 (2013).

[28]E. Cartan, "Sur Les Variétés à Connexion Affine et La Théorie de La Relativité Généralisée (Première Partie)", Ann. Sci. Ec. Norm. Sup. **40**, 325–412 (1923).

[29]E. Cartan, "Sur Les Variétés à Connexion Affine, et La Théorie de La Relativité Généralisée (Première Partie) (Suite)", Ann. Sci. Ec. Norm. Sup. **41**, 1–25 (1924).

[30]K. Jensen, "On the coupling of Galilean-invariant field theories to curved spacetime", SciPost Phys. **5**, 011 (2018).

[31]J. M. Luttinger, "Theory of Thermal Transport Coefficients", Phys. Rev. **135**, A1505–A1514 (1964).

[32]A. Gromov and A. G. Abanov, "Thermal Hall Effect and Geometry with Torsion", Phys. Rev. Lett. **114**, 016802 (2015).

[33]M. Geracie, D. T. Son, C. Wu, and S.-F. Wu, "Spacetime Symmetries of the Quantum Hall Effect", Phys. Rev. D **91**, 45030 (2015).

[34]D. T. Son, "Newton-Cartan Geometry and the Quantum Hall Effect", (2013), arXiv:1306.0638.

[35]J. B. Curtis, Z. M. Raines, A. A. Allocca, M. Hafezi, and V. M. Galitski, "Cavity Quantum Eliashberg Enhancement of Superconductivity", Phys. Rev. Lett. **122**, 167002 (2019), arXiv:1805.01482.

[36]A. F. G. Wyatt, V. M. Dmitriev, W. S. Moore, and F. W. Sheard, "Microwave-Enhanced Critical Supercurrents in Constricted Tin Films", Phys. Rev. Lett. **16**, 1166–1169 (1966).

[37]A. H. Dayem and J. J. Wiegand, "Behavior of Thin-Film Superconducting Bridges in a Microwave Field", Phys. Rev. **155**, 419–428 (1967).

[38]G. M. Eliashberg, "Film Superconductivity Stimulated by a High-Frequency Field", JETP Lett. **11**, 114–116 (1970).

[39]B. I. Ivlev and G. M. Eliashberg, "Influence of nonequilibrium excitations on the properties of a superconducting films in a high-frequency field", JETP Lett. **13**, 333–336 (1971).

[40]B. I. Ivlev, S. G. Lisitsyn, and G. M. Eliashberg, "Nonequilibrium Excitations in Superconductors in High-Frequency Fields", J. Low Temp. Phys. **10** (1973).

[41]T. M. Klapwijk, J. N. van den Bergh, and J. E. Mooij, "Radiation-stimulated superconductivity", J. Low Temp. Phys. **26**, 385–405 (1977).

[42]A. Schmid, "Stability of Radiation-Stimulated Superconductivity", Phys. Rev. Lett. **38** (1977).

[43]A. Schmid, "SUPERCONDUCTORS OUT OF THERMAL EQUILIBRIUM", Le J. Phys. Colloq. **39**, C6–1360–C6–1367 (1978).

[44]J.-J. Chang and D. J. Scalapino, "Nonequilibrium superconductivity", J. Low Temp. Phys. **31**, 1–32 (1978).

[45]A. Robertson and V. M. Galitski, "Nonequilibrium enhancement of Cooper pairing in cold fermion systems", Phys. Rev. A **80** (2009).

[46]A. Robertson, V. M. Galitski, and G. Refael, "Dynamic Stimulation of Quantum Coherence in Systems of Lattice Bosons", Phys. Rev. Lett. **106**, 165701 (2011).

[47]K. S. Tikhonov, M. A. Skvortsov, and T. M. Klapwijk, "Superconductivity in the presence of microwaves: Full phase diagram", Phys. Rev. B **97**, 184516 (2018).

[48]T. Klapwijk and P. de Visser, "The discovery, disappearance and re-emergence of radiation-stimulated superconductivity", Ann. Phys. **417**, 168104 (2020).

[49]A. Zong et al., "Evidence for topological defects in a photoinduced phase transition", Nat. Phys. **15**, 27–31 (2019).

[50]A. Kogar et al., "Light-induced charge density wave in $LaTe_3$", Nat. Phys. **16**, 159–163 (2020).

[51]R. Matsunaga et al., "Higgs Amplitude Mode in the BCS Superconductors $Nb_{1-x}Ti_xN$ Induced by Terahertz Pulse Excitation", Phys. Rev. Lett. **111**, 057002 (2013).

[52]A. F. Kemper, M. A. Sentef, B. Moritz, J. K. Freericks, and T. P. Devereaux, "Direct observation of Higgs mode oscillations in the pump-probe photoemission spectra of electron-phonon mediated superconductors", Phys. Rev. B **92**, 224517 (2015).

[53]K. Katsumi et al., "Higgs Mode in the *d*-Wave Superconductor $Bi_2Sr_2CaCu_2O_{8+x}$ Driven by an Intense Terahertz Pulse", Phys. Rev. Lett. **120** (2018).

[54]M. Buzzi et al., *Higgs-mediated optical amplification in a non-equilibrium superconductor*, 2019, arXiv:1908.10879 [supr-con].

[55]R. Mankowsky et al., "Nonlinear lattice dynamics as a basis for enhanced superconductivity in $YBa_2Cu_3O_{6.5}$", Nature **516**, 71–73 (2014).

[56]M. Först et al., "Femtosecond x rays link melting of charge-density wave correlations and light-enhanced coherent transport in $YBa_2Cu_3O_{6.6}$", Phys. Rev. B **90**, 184514 (2014).

[57]M. Mitrano et al., "Possible light-induced superconductivity in K_3C_{60} at high temperature", Nature **530**, 461–464 (2016).

[58]A. Cavalleri, "Photo-induced superconductivity", Contemp. Phys. **59**, 31–46 (2018).

[59]Z. M. Raines, V. G. Stanev, and V. M. Galitski, "Enhancement of superconductivity via periodic modulation in a three-dimensional model of cuprates", Phys. Rev. B **91**, 184506 (2015).

[60]A. A. Patel and A. Eberlein, "Light-induced enhancement of superconductivity via melting of competing bond-density wave order in underdoped cuprates", Phys. Rev. B **93**, 195139 (2016).

[61]M. A. Sentef, A. F. Kemper, A. Georges, and C. Kollath, "Theory of light-enhanced phonon-mediated superconductivity", Phys. Rev. B **93**, 144506 (2016), arXiv:1505.07575.

[62]Y. Murakami, N. Tsuji, M. Eckstein, and P. Werner, "Nonequilibrium steady states and transient dynamics of conventional superconductors under phonon driving", Phys. Rev. B **96** (2017).

[63]A. Komnik and M. Thorwart, "BCS theory of driven superconductivity", Eur. Phys. J. B **89**, 244 (2016).

[64]M. Knap, M. Babadi, G. Refael, I. Martin, and E. Demler, "Dynamical Cooper pairing in nonequilibrium electron-phonon systems", Phys. Rev. B **94**, 214504 (2016).

[65]J.-i. Okamoto, A. Cavalleri, and L. Mathey, "Theory of Enhanced Interlayer Tunneling in Optically Driven High-Tc Superconductors", Phys. Rev. Lett. **117**, 227001 (2016).

[66]M. Kim, Y. Nomura, M. Ferrero, P. Seth, O. Parcollet, and A. Georges, "Enhancing superconductivity in A_3C_{60} fullerides", Phys. Rev. B **94**, 155152 (2016), eprint: 1606.05796.

[67]M. Babadi, M. Knap, I. Martin, G. Refael, and E. Demler, "Theory of parametrically amplified electron-phonon superconductivity", Phys. Rev. B **96** (2017).

[68]Y. Z. Chou, Y. Liao, and M. S. Foster, "Twisting Anderson pseudospins with light: Quench dynamics in terahertz-pumped BCS superconductors", Phys. Rev. B **95**, 1–14 (2017), arXiv:1611.07089.

[69]D. M. Kennes, E. Y. Wilner, D. R. Reichman, and A. J. Millis, "Transient superconductivity from electronic squeezing of optically pumped phonons", Nat. Phys. **13**, 479–483 (2017).

[70]M. A. Sentef, A. Tokuno, A. Georges, and C. Kollath, "Theory of Laser-Controlled Competing Superconducting and Charge Orders", Phys. Rev. Lett. **118**, 087002 (2017).

[71]G. Chiriacò, A. J. Millis, and I. L. Aleiner, "Transient superconductivity without superconductivity", Phys. Rev. B **98**, 1–5 (2018), eprint: 1806.06645.

[72]Y. Lemonik and A. Mitra, "Quench dynamics of superconducting fluctuations and optical conductivity in a disordered system", Phys. Rev. B **98**, 214514 (2018).

[73]M. H. Michael, A. von Hoegen, M. Fechner, M. Först, A. Cavalleri, and E. Demler, *Parametric resonance of Josephson plasma waves: A theory for optically amplified interlayer superconductivity in* $YBa_2Cu_3O_{6+x}$, Apr. 2020, arXiv:2004.13049 [supr-con].

[74]P. W. Anderson, "Coherent Excited States in the Theory of Superconductivity: Gauge Invariance and the Meissner Effect", Phys. Rev. **110**, 827–835 (1958).

[75]L. Ioffe and A. Larkin, "Gapless fermions and gauge fields in dielectrics", Phys. Rev. B **39** (1989).

[76]J. Polchinski, "Low-energy dynamics of the spinon-gauge system", Nuclear Physics B **422**, 617–633 (1994).

[77]P. Lee, N. Nagaosa, and X. Wen, "Doping a mott insulator: physics of high-temperature superconductivity", Rev. Mod. Phys. **78**, 17–85 (2006).

[78]P. A. Lee, "Amperean Pairing and the Pseudogap Phase of Cuprate Superconductors", Phys. Rev. X **4**, 031017 (2014).

[79]C. Cohen-Tannoudji, J. Dupont-Roc, and G. Grynberg, *Photons and Atoms: Introduction to Quantum Electrodynamics* (Wiley, 1997).

[80]E. Purcell, H. Torrey, and R. Pound, "Resonance Absorption by Nuclear Magnetic Moments in a Solid", Phys. Rev. **69**, 37–38 (1946).

[81]R. H. Dicke, "Coherence in Spontaneous Radiation Processes", Phys. Rev. **93**, 99–110 (1954).

[82]E. Jaynes and F. Cummings, "Comparison of quantum and semiclassical radiation theories with application to the beam maser", Proc. IEEE **51**, 89–109 (1963).

[83]G. Baskaran, *Superradiant Superconductivity*, 2012, arXiv:1211.4567 [cond-mat.supr-con].

[84]T. W. Ebbesen, "Hybrid Light-Matter States in a Molecular and Material Science Perspective", Acc. Chem. Res. **49** (2016).

[85]H. Deng, G. Weihs, C. Santori, J. Bloch, and Y. Yamamoto, "Condensation of Semiconductor Microcavity Exciton Polaritons", Science **298**, 199–202 (2002).

[86]J. Kasprzak et al., "Bose-Einstein condensation of exciton polaritons", Nature **443**, 409–414 (2006).

[87]T. Byrnes, N. Y. Kim, and Y. Yamamoto, "Exciton–polariton condensates", Nat. Phys. **10**, 803–813 (2014).

[88]D. C. Mattis and J. Bardeen, "Theory of the Anomalous Skin Effect in Normal and Superconducting Metals", Phys. Rev. **111**, 412–417 (1958).

[89]M. V. Feigel'man, A. Larkin, and M. A. Skvortsov, "Keldysh action for disordered superconductors", Phys. Rev. B **61**, 12361 (2000).

[90]A. Kamenev, *Field Theory of Non-Equilibrium Systems* (Cambridge University Press, Cambridge, 2011).

[91]K. D. Usadel, "Generalized Diffusion Equation for Superconducting Alloys", Phys. Rev. Lett. **25**, 507–509 (1970).

[92]A. Blais, R.-S. Huang, A. Wallraff, S. M. Girvin, and R. J. Schoelkopf, "Cavity quantum electrodynamics for superconducting electrical circuits: An architecture for quantum computation", Phys. Rev. A **69**, 062320 (2004).

[93]G. Scalari et al., "Ultrastrong Coupling of the Cyclotron Transition of a 2D Electron Gas to a THz Metamaterial", Science **335**, 1323–1326 (2012).

[94]C. Maissen et al., "Ultrastrong coupling in the near field of complementary split-ring resonators", Phys. Rev. B **90**, 205309 (2014).

[95]M. Malerba et al., "Towards strong light-matter coupling at the single-resonator level with sub-wavelength mid-infrared nano-antennas", Appl. Phys. Lett. **109**, 21111 (2016).

[96]A. Bayer et al., "Terahertz Light–Matter Interaction beyond Unity Coupling Strength", Nano Lett. **17**, 6340–6344 (2017).

[97]M. A. Sentef, M. Ruggenthaler, and A. Rubio, "Cavity quantum-electrodynamical polaritonically enhanced electron-phonon coupling and its influence on superconductivity", Sci. Adv. **4**, eaau6969 (2018).

[98]A. A. Allocca, Z. M. Raines, J. B. Curtis, and V. M. Galitski, "Cavity superconductor-polaritons", Phys. Rev. B **99**, 020504 (2019), arXiv:arXiv:1807.06601v1.

[99]G. Mazza and A. Georges, "Superradiant Quantum Materials", Phys. Rev. Lett. **122**, 017401 (2019), arXiv:1804.08534.

[100]F. Schlawin, A. Cavalleri, and D. Jaksch, "Cavity-Mediated Electron-Photon Superconductivity", Phys. Rev. Lett. **122**, 133602 (2019), arXiv:1804.07142.

[101]I. Carusotto and C. Ciuti, "Quantum fluids of light", Rev. Mod. Phys. **85**, 299–366 (2013).

[102]J. J. Hopfield, "Theory of the Contribution of Excitons to the Complex Dielectric Constant of Crystals", Phys. Rev. **112**, 1555–1567 (1958).

[103]C. Weisbuch, M. Nishioka, A. Ishikawa, and Y. Arakawa, "Observation of the coupled exciton-photon mode splitting in a semiconductor quantum microcavity", Phys. Rev. Lett. **69**, 3314–3317 (1992).

[104]E. Wertz et al., "Spontaneous formation and optical manipulation of extended polariton condensates", Nat. Phys. **6**, 860 (2010).

[105]F. Li et al., "From Excitonic to Photonic Polariton Condensate in a ZnO-Based Microcavity", Phys. Rev. Lett. **110**, 196406 (2013).

[106]Y. Sun et al., "Bose-Einstein Condensation of Long-Lifetime Polaritons in Thermal Equilibrium", Phys. Rev. Lett. **118**, 016602 (2017).

[107]A. Kavokin, G. Malpuech, and M. Glazov, "Optical Spin Hall Effect", Phys. Rev. Lett. **95**, 136601 (2005).

[108]C. Leyder et al., "Observation of the optical spin Hall effect", Nat. Phys. **3**, 628–631 (2007).

[109]T. Jacqmin et al., "Direct Observation of Dirac Cones and a Flatband in a Honeycomb Lattice for Polaritons", Phys. Rev. Lett. **112**, 116402 (2014).

[110]C. E. Whittaker et al., "Exciton Polaritons in a Two-Dimensional Lieb Lattice with Spin-Orbit Coupling", Phys. Rev. Lett. **120**, 097401 (2018).

[111]H. S. Nguyen et al., "Acoustic Black Hole in a Stationary Hydrodynamic Flow of Microcavity Polaritons", Phys. Rev. Lett. **114**, 036402 (2015).

[112]F. Baboux et al., "Measuring topological invariants from generalized edge states in polaritonic quasicrystals", Phys. Rev. B **95**, 161114 (2017).

[113]F. P. Laussy, A. V. Kavokin, and I. A. Shelykh, "Exciton-Polariton Mediated Superconductivity", Phys. Rev. Lett. **104**, 106402 (2010).

[114]O. Cotleţ, S. Zeytinoğlu, M. Sigrist, E. Demler, and A. Imamoğlu, "Superconductivity and other collective phenomena in a hybrid Bose-Fermi mixture formed by a polariton condensate and an electron system in two dimensions", Phys. Rev. B **93**, 054510 (2016).

[115]F. Kretzschmar et al., "Raman-Scattering Detection of Nearly Degenerate *s*-Wave and *d*-Wave Pairing Channels in Iron-Based $Ba_{0.6}K_{0.4}Fe_2As_2$ and $Rb_{0.8}Fe_{1.6}Se_2$ Superconductors", Phys. Rev. Lett. **110**, 187002 (2013).

[116]T. Böhm et al., "Balancing Act: Evidence for a Strong Subdominant *d*-Wave Pairing Channel in $Ba_{0.6}K_{0.4}Fe_2As_2$", Phys. Rev. X **4**, 041046 (2014).

[117]D. Jost et al., "Indication of subdominant d-wave interaction in superconducting $CaKFe_4As_4$", Phys. Rev. B **98**, 020504 (2018), arXiv:1805.12034.

[118]S. Maiti, T. A. Maier, T. Böhm, R. Hackl, and P. J. Hirschfeld, "Probing the Pairing Interaction and Multiple Bardasis-Schrieffer Modes Using Raman Spectroscopy", Phys. Rev. Lett. **117**, 257001 (2016).

[119]S. Maiti and P. J. Hirschfeld, "Collective modes in superconductors with competing *s*- and *d*-wave interactions", Phys. Rev. B **92**, 094506 (2015).

[120]A. Altland and B. Simons, *Condensed Matter Field Theory*, 2nd (Cambridge University Press, New York, 2010), p. 786.

[121]A. Moor, A. F. Volkov, and K. B. Efetov, "Amplitude Higgs Mode and Admittance in Superconductors with a Moving Condensate", Phys. Rev. Lett. **118**, 047001 (2017).

[122]M. M. Qazilbash et al., "Electronic correlations in the iron pnictides", Nat. Phys. **5**, 647 (2009).

[123]N. Barišić, D. Wu, M. Dressel, L. J. Li, G. H. Cao, and Z. A. Xu, "Electrodynamics of electron-doped iron pnictide superconductors: Normal-state properties", Phys. Rev. B **82**, 054518 (2010).

[124]D. C. Johnston, "The puzzle of high temperature superconductivity in layered iron pnictides and chalcogenides", Adv. Phys. **59**, 803–1061 (2010).

[125]V. Cvetkovic and O. Vafek, "Space group symmetry, spin-orbit coupling, and the low-energy effective Hamiltonian for iron-based superconductors", Phys. Rev. B **88**, 134510 (2013).

[126]E. F. Talantsev and J. L. Tallon, "Universal self-field critical current for thin-film superconductors", Nat. Commun. **6**, 7820 (2015).

[127]S. J. Singh et al., "Ultrahigh critical current densities, the vortex phase diagram, and the effect of granularity of the stoichiometric high-T_c superconductor $CaKFe_4As_4$", Phys. Rev. Mater. **2**, 074802 (2018).

[128]K. A. Musaelian, J. Betouras, A. V. Chubukov, and R. Joynt, "Mixed-symmetry superconductivity in two-dimensional fermi liquids", Phys. Rev. B **53**, 3598–3603 (1996).

[129]J. Curtis, G. Refael, and V. Galitski, "Evanescent modes and step-like acoustic black holes", Ann. Phys. **407**, 148–165 (2019), arXiv:1801.01607.

[130]C. Bambi, "Astrophysical Black Holes: A Compact Pedagogical Review", Ann. Phys. **530**, 1700430 (2018).

[131]S. B. Giddings, "Astronomical tests for quantum black hole structure", Nat. Astron. **1**, 0067 (2017), arXiv:1703.03387.

[132]L. Susskind, "The paradox of quantum black holes", Nat. Phys. **2** (2006).

[133]A. Almheiri, D. Marolf, J. Polchinski, and J. Sully, "Black holes: complementarity or firewalls?", J. High Energy Phys. **2013**, 62 (2013).

[134]G. Volovik, *The Universe in a Helium Droplet* (Oxford University Press, Oxford, 2009).

[135]C. Barceló, S. Liberati, and M. Visser, "Analogue gravity from Bose-Einstein condensates", Class. Quantum Gravity **18**, 1137–1156 (2001).

[136]T. A. Jacobson and G. E. Volovik, "Event Horizons and Ergoregions in ^{3}He", Phys. Rev. D **58**, 64021 (1998).

[137]G. E. Volovik, "The Topology of the Quantum Vacuum", in *Lect. notes phys.* Vol. 870, edited by D. Faccio, F. Belgiorno, S. Cacciatori, V. Gorini, and S. Liberati (Springer, 2013), pp. 343–383.

[138]P. O. Fedichev and U. R. Fischer, "Gibbons-Hawking Effect in the Sonic de Sitter Space-Time of an Expanding Bose-Einstein-Condensed Gas", Phys. Rev. Lett. **91**, 240407 (2003).

[139]U. R. Fischer and R. Schützhold, "Quantum simulation of cosmic inflation in two-component Bose-Einstein condensates", Phys. Rev. A **70**, 063615 (2004).

[140]R. Schützhold, M. Uhlmann, Y. Xu, and U. R. Fischer, "Sweeping from the Superfluid to the Mott Phase in the Bose-Hubbard Model", Phys. Rev. Lett. **97**, 200601 (2006).

[141]J. Macher and R. Parentani, "Black-hole radiation in Bose-Einstein condensates", Phys. Rev. A **80**, 043601 (2009).

[142]S.-Y. Chä and U. R. Fischer, "Probing the Scale Invariance of the Inflationary Power Spectrum in Expanding Quasi-Two-Dimensional Dipolar Condensates", Phys. Rev. Lett. **118**, 130404 (2017).

[143]F. Bemani, R. Roknizadeh, and M. Naderi, "Quantum simulation of discrete space-time by the Bose-Hubbard model: From analog acoustic black hole to quantum phase transition", Annals of Physics **388**, 186–196 (2018).

[144]D. Sels and E. Demler, "Thermal radiation and dissipative phase transition in a BEC with local loss", Ann. Phys. **412**, 168021 (2020), eprint: 1809.10516.

[145]S. Eckel, A. Kumar, T. Jacobson, I. B. Spielman, and G. K. Campbell, "A Rapidly Expanding Bose-Einstein Condensate: An Expanding Universe in the Lab", Phys. Rev. X **8**, 021021 (2018).

[146]R. Schützhold and W. G. Unruh, "Hawking Radiation in an Electromagnetic Waveguide?", Phys. Rev. Lett. **95**, 031301 (2005).

[147]G. Jannes et al., "Hawking Radiation and the Boomerang Behavior of Massive Modes near a Horizon", Phys. Rev. D **83**, 104028 (2011).

[148]A. Roldan-Molina, A. S. Nunez, and R. A. Duine, "Magnonic black holes", Phys. Rev. Lett. **118**, 061301 (2017).

[149]U. Leonhardt and P. Piwnicki, "Relativistic Effects of Light in Moving Media with Extremely Low Group Velocity", Phys. Rev. Lett. **84**, 822–825 (2000).

[150]J. Drori, Y. Rosenberg, D. Bermudez, Y. Silberberg, and U. Leonhardt, "Observation of Stimulated Hawking Radiation in an Optical Analogue", Phys. Rev. Lett. **122**, 010404 (2019).

[151]L.-P. Euvé, F. Michel, R. Parentani, T. G. Philbin, and G. Rousseaux, "Observation of Noise Correlated by the Hawking Effect in a Water Tank", Phys. Rev. Lett. **117**, 121301 (2016).

[152]J. Steinhauer, "Observation of self-amplifying Hawking radiation in an analogue black-hole laser", Nat. Phys. **10**, 864–869 (2014).

[153]Y.-H. Wang, T. Jacobson, M. Edwards, and C. W. Clark, "Mechanism of stimulated Hawking radiation in a laboratory Bose-Einstein condensate", Phys. Rev. A **96** (2017), arXiv:1605.01027.

[154]J. Steinhauer, "Observation of quantum Hawking radiation and its entanglement in an analogue black hole", Nat. Phys. **12**, 959–965 (2016).

[155]R. Balbinot, A. Fabbri, S. Fagnocchi, A. Recati, and I. Carusotto, "Nonlocal density correlations as a signature of Hawking radiation from acoustic black holes", Phys. Rev. A **78**, 021603 (2008).

[156]F. Franchini and V. E. Kravtsov, "Horizon in Random Matrix Theory, the Hawking Radiation, and Flow of Cold Atoms", Phys. Rev. Lett. **103**, 166401 (2009), arXiv:arXiv:0905.3533v2.

[157]P.-É. Larré, A. Recati, I. Carusotto, and N. Pavloff, "Quantum fluctuations around black hole horizons in Bose-Einstein condensates", Phys. Rev. A **85**, 013621 (2012).

[158]J. Macher and R. Parentani, "Black/white hole radiation from dispersive theories", Phys. Rev. D **79**, 124008 (2009).

[159]S. Finazzi and R. Parentani, "Black hole lasers in Bose–Einstein condensates", New J. Phys. **12**, 095015 (2010).

[160]C. Mayoral, A. Fabbri, and M. Rinaldi, "Steplike discontinuities in Bose-Einstein condensates and Hawking radiation: Dispersion effects", Phys. Rev. D **83**, 124047 (2011).

[161]I. Zapata, M. Albert, R. Parentani, and F. Sols, "Resonant Hawking radiation in Bose–Einstein condensates", New J. Phys. **13**, 063048 (2011).

[162]S. Corley and T. Jacobson, "Hawking spectrum and high frequency dispersion", Phys. Rev. D **54**, 1568–1586 (1996).

[163]S. Corley, "Computing the spectrum of black hole radiation in the presence of high frequency dispersion: An analytical approach", Phys. Rev. D **57**, 6280–6291 (1998).

[164]S. Corley and T. Jacobson, "Black hole lasers", Phys. Rev. D **59**, 124011 (1999), arXiv:9806203v3.

[165]T. Jacobson and D. Mattingly, "Hawking radiation on a falling lattice", Phys. Rev. D **61** (1999).

[166]R. Schützhold and W. G. Unruh, "Hawking radiation with dispersion versus breakdown of the WKB approximation", Phys. Rev. D **88**, 124009 (2013), arXiv:arXiv:1308.2159v1.

[167]U. R. Fischer, R. Schützhold, and M. Uhlmann, "Bogoliubov theory of quantum correlations in the time-dependent Bose-Hubbard model", Phys. Rev. A **77**, 043615 (2008).

[168]D. Bermudez and U. Leonhardt, "Resonant Hawking radiation as an instability", Class. Quantum Grav. **36** (2018).

[169]U. Leonhardt, T. Kiss, and P. Ohberg, "Bogoliubov theory of the Hawking effect in Bose Einstein condensates", J. Opt. B Quantum Semiclassical Opt. **5**, S42–S49 (2003).

[170]A. Recati, N. Pavloff, and I. Carusotto, "Bogoliubov theory of acoustic Hawking radiation in Bose-Einstein condensates", Phys. Rev. A **80**, 043603 (2009).

[171]P.-É. Larré and N. Pavloff, "Hawking radiation in a two-component Bose-Einstein condensate", Europhysics Lett. **103**, 60001 (2013).

[172]Y. Castin, "Bose-Einstein Condensates in Atomic Gases: Simple Theoretical Results", in *Coherent atomic matter waves*, Vol. 72, edited by R. Kaiser, C. Westbrook, and F. David (Springer, Berlin, Heidelberg, 2001).

[173]U. Leonhardt, T. Kiss, and P. Ohberg, "Theory of elementary excitations in unstable Bose-Einstein condensates and the instability of sonic horizons", Phys. Rev. A **67** (2003).

[174]T. Jacobson, "Introduction to Quantum Fields in Curved Spacetime and the Hawking Effect", in *Lect. quantum gravity. ser. cent. estud. cient.* Edited by A. Gomberoff and D. Marolf (Springer US, Boston, MA, 2005).

[175]Y. Kagan, D. L. Kovrizhin, and L. A. Maksimov, "Anomalous Tunneling of Phonon Excitations between Two Bose-Einstein Condensates", Phys. Rev. Lett. **90**, 130402 (2003).

[176]I. Amado, B. Sundborg, L. Thorlacius, and N. Wintergerst, "Black holes from large N singlet models", J. High Energy Phys. **2018**, 75 (2018).

[177]P. Hořava, "Quantum gravity at a Lifshitz point", Phys. Rev. D **79**, 084008 (2009).

[178]J. H. Wilson, J. B. Curtis, and V. M. Galitski, *Analogue spacetimes from nonrelativistic Goldstone modes in spinor condensates*, Jan. 2020, arXiv:2001.05496 [quant-gas].

[179]G. Volovik, "Black hole and hawking radiation by type-II Weyl fermions", J.E.T.P. Lett. **104**, 645–648 (2016).

[180]Y. Kedem, E. J. Bergholtz, and F. Wilczek, *Black and White Holes at Material Junctions*, Jan. 2020, arXiv:2001.02625.

[181]D. M. Stamper-Kurn and M. Ueda, "Spinor Bose gases: Symmetries, magnetism, and quantum dynamics", Rev. Mod. Phys. **85**, 1191–1244 (2013).

[182]H. P. Künzle, "Galilei and Lorentz Structures on Space-Time: Comparison of the Corresponding Geometry and Physics", Ann. Inst. Henri Poincaré **17**, 337–362 (1972).

[183]B. Bradlyn and N. Read, "Low-Energy Effective Theory in the Bulk for Transport in a Topological Phase", Phys. Rev. B **91**, 125303 (2015).

[184]M. H. Christensen, J. Hartong, N. A. Obers, and B. Rollier, "Boundary stress-energy tensor and Newton-Cartan geometry in Lifshitz holography", J. High Energy Phys. **2014**, 57 (2014).

[185]M. H. Christensen, J. Hartong, N. A. Obers, and B. Rollier, "Torsional Newton-Cartan geometry and Lifshitz holography", Phys. Rev. D **89**, 061901 (2014).

[186]J. Hartong and N. A. Obers, "Hořava-Lifshitz gravity from dynamical Newton-Cartan geometry", J. High Energy Phys. **2015**, 155 (2015).

[187]M. Taylor, "Lifshitz Holography", Class. Quantum Grav. **33**, 33001 (2016).

[188]R. Barnett, D. Podolsky, and G. Refael, "Geometrical Approach to Hydrodynamics and Low-Energy Excitations of Spinor Condensates", Phys. Rev. B **80**, 24420 (2009), arXiv:arXiv:0903.1863v2.

[189]N. D. Mermin and H. Wagner, "Absence of Ferromagnetism or Antiferromagnetism in One- or Two-Dimensional Isotropic Heisenberg Models", Phys. Rev. Lett. **17**, 1133–1136 (1966).

[190]P. C. Hohenberg, "Existence of Long-Range Order in One and Two Dimensions", Phys. Rev. **158**, 383–386 (1967).

[191]S. Coleman, "There Are No Goldstone Bosons in Two Dimensions", Comm. Math. Phys. **31**, 259–264 (1973).

[192]E. Bergshoeff, A. Chatzistavrakidis, L. Romano, and J. Rosseel, "Newton-Cartan gravity and torsion", J. High Energy Phys. **2017**, 194 (2017).

[193]T.-L. Ho, "Spinor Bose Condensates in Optical Traps", Phys. Rev. Lett. **81**, 742–745 (1998).

[194]T. Ohmi and K. Machida, "Bose-Einstein Condensation with Internal Degrees of Freedom in Alkali Atom Gases", J. Phys. Soc. Japan **67**, 1822–1825 (1998).

[195]Y. Liao and V. Galitski, "Drag viscosity of metals and its connection to Coulomb drag", Phys. Rev. B **101**, 195106 (2020), arXiv:1912.08227.

[196]P. C. W. Davies, S. A. Fulling, and W. G. Unruh, "Energy-momentum tensor near an evaporating black hole", Phys. Rev. D **13**, 2720–2723 (1976).

[197]J. H. Kim, S. W. Seo, and Y. Shin, "Critical Spin Superflow in a Spinor Bose-Einstein Condensate", Phys. Rev. Lett. **119**, 185302 (2017).

[198]U. R. Fischer, "Dynamical Aspects of Analogue Gravity: The Backreaction of Quantum Fluctuations in Dilute Bose-Einstein Condensates", in *Quantum analogues: from phase transitions to black holes and cosmology*, Vol. 718, edited by W. G. Unruh and R. Schützhold, Lecture Notes in Physics (Springer, Berlin, Heidelberg, 2007), pp. 93–113.

[199]L. Sieberer, M. Buchhold, and S. Diehl, "Keldysh Field Theory for Driven Open Quantum Systems", Reports Prog. Phys. **79** (2016).

[200]M. Galassi and B. Gough, *GNU Scientific Library: Reference Manual*, GNU manual (Network Theory, 2009).